University of Alberta

MODELING GREENHOUSE GAS EXCHANGE IN AN AGRICULTURAL FIELD AND A NATURAL GRASSLAND

BY

TAO LI

A thesis submitted to the Faculty of Graduate Studies and Research in partial fulfillment of the requirements for the degree of

Doctor of Philosophy

in

Soil Science

Department of Renewable Resources

Edmonton, Alberta

Spring, 2005

Abstract

N_2O accounts for 6% of the radiative forcing caused by global greenhouse gases, but the estimates of N_2O emissions using Intergovernmental Panel on Climate Change (IPCC) Tier 1 methodology may have larger than 62% of uncertainty. The temporal and spatial variation of site-specific N_2O emissions results in the uncertainty, however, it is not considered in IPCC Tier 1 and cannot be measured by current field measurement techniques. This study was intended to develop a scientifically defensible methodology to account for these variations under diverse agricultural practices, and to contribute to the development of an IPCC Tier 2 methodology.

The site-specific N_2O emissions over the hummocky landscape have been addressed by modeling technique through combining *ecosys* and landscape soil property predictor (*LSPP*) with GIS in this study. The dynamics of climate, soil water content and soil temperature resulted in temporal variation of 83%, 99%, and 51% in the modeled hourly, seasonal and annual N_2O emissions, respectively. Spatial heterogeneity in soil organic carbon, organic nitrogen, mineral nitrogen (NH_4^+ and NO_3^-) and water contents, soil temperature, and topography resulted in spatial variation ranging from 88% to 341% in the modeled annual N_2O emissions. Modeled N_2O emissions decreased from upper to lower slopes under wet conditions, but increased under dry conditions. "Hot spots" (localized area of very high N_2O emissions) switched to "cold spots" (localized area of very lower N_2O emissions) when relative water-filled porosity rose above 0.6 – 0.7. Zero tillage, manure fertilizer, permanent grassland or fallow reduced modeled annual N_2O emissions from 18% up to 41% in comparison with conventional crop and land management. Total N_2O emissions summarized from grid cells that fully represented site-

specific N_2O emissions were 18% lower than the estimation of IPPC Tier 1 for a wheat-barley-canola field during 2000 to 2002.

CO_2 is another key greenhouse gas, the estimation of which can be improved by modeling. The modeled carbon gain of semi-arid natural grassland will be 28 g C m^{-2} y^{-1} during the next 100 years under changing climate. This grassland would be a sink of greenhouse gases with large carbon sequestration and less N_2O emissions.

Acknowledgements

This research was supported by grants from the Canadian Agri-Food Research Council to RFG and colleagues and from the Natural Sciences and Engineering Research Council (NSERC) to RFG and LBF. This project and my studies could not have been completed without the assistance from many people.

First of all, I am grateful to my supervisor, Dr. Robert F. Grant, for the great assistance and guidance he has provided to me over the years. He acted as my academic resources throughout each stage of this project. My appreciation is extended to other members of committee – Dr. Keith Paustian, Dr. Ross W. Wein, Dr. Vincent L. St. Louis and Dr. Glen W. Armstrong – for their support and constructive suggestions.

I have to specially thank Mr. Tom W. Goddard, Mr. Len Kryzanowski, and staff in their research groups, for providing the detailed field measurement data and assistance with the collection of field samples at the Viking site. I must also thank Sean McGinn and Hugh McLean at the Lethbridge Research Centre for providing meteorological data, Dr. Lawrence B. Flanagan, Peter Carlson, Linda Wever, Francine May, Bruce Johnson and Andrew Howton for providing excellent field and lab assistance at Lethbridge. I could not have done the model runs, validations and sensitivity analyses without these data. Thanks to the staff of the Department of Renewable Resources, University of Alberta – Mrs. Sandy Nakashima for managing and supporting my graduate studies, Mr. Clive Figueiredo and Mrs. Monica Molina-Ayala for the analysis of soil samples, and to members of our research group – Dr. Muhammad Akbar, Guanwen Zhang, Kimlin Metivier, Johnny Montenegro-Ballestero, and Dimitre Dimitrov for the suggestions and encouragement during the completion of this thesis.

Finally, I am most grateful to my wife and daughter, for their love, support and encouragement year by year. Now that my graduate studies are coming to an end, and a new chapter of my life will begin, I know I will always remember the impressive, pleasurable period that I spent at the beautiful campus of University of Alberta. I am very happy that I have gained so much of knowledge and mage so many friends while studying here.

TABLE OF CONTENTS

Chapter 1: General Introduction.....1
1.1 Spatial and temporal variation of N_2O emissions.....1
1.2 Detection of the temporal and spatial variation in N_2O emissions.....3
1.3 Mathematical models for simulating N_2O emissions.....4
1.4 Soil properties for modeling landscape N_2O emissions.....6
1.5 Agricultural practices affecting N_2O emissions.....7
1.6 Scaling up N_2O emissions.....8
1.7 Objectives and contents.....9
References.....10

Chapter 2: The Prediction of Soil Properties by a Digital Terrain Model and Sensitivity of N_2O Emissions to Uncertainties of Predicted Soil Properties.....20
2.1 Introduction.....20
2.2 Study site and field methods.....23
2.2.1 Study site.....23
2.2.2 Field sampling and laboratory analysis of soil properties.....24
2.2.3 Calculating terrain attributes.....25
2.3 Methods.....33
2.3.1 Prediction models of soil properties.....33
2.3.1.1 Stepwise multiple linear model (SMLR).....33
2.3.1.2 Artificial neural network (ANN).....34
2.3.1.3 Inverse distance weight (IDW).....35
2.3.2 Validation of prediction models.....36
2.3.2.1 Predictions of soil properties in validation dataset.....36
2.3.2.2 Statistical analysis of model validation.....36
2.3.3 Data management.....37
2.3.4 Sensitivities of N_2O emissions to uncertainties of soil properties.....38
2.3.4.1 Allocation of soil properties.....38
2.3.4.2 Simulation of N_2O missions.....39
2.3.4.3 Assessing sensitivities of modeled N_2O emissions.....39
2.4 Results.....40
2.4.1 Relationships between terrain attributes and measured soil properties.....40
2.4.2 Validation of SMLR, ANN and IDW models.....42
2.4.3 Prediction functions of SMLR.....45
2.4.4 Sensitivities of modeled N_2O emissions to uncertainties of predicted soil properties.....47
2.5 Discussion.....48
2.5.1 Terrain attributes, soil formation and soil properties.....48
2.5.2 Predictive capability of SMLR, ANN and IDW.....51
2.5.3 Sensitivities of N_2O emissions to uncertainties of soil properties.....53
2.6 Conclusions.....55
References.....56
Appendix 2.1: Stepwise multiple linear regression algorithm.....63

Appendix 2.2: Equations of Artificial Neural Network (ANN).....65
Appendix 2.3: The interface of Landscape Soil Property Predictor (LSPP).....67

Chapter 3: Modeling Landscape Effects on N_2O Emissions in a Hummocky Agricultural Field.....69
3.1 Introduction.....69
3.2 Modeling N_2O emissions in landscapes.....72
3.2.1 Modeling water transport.....72
3.2.1.1 Surface water movement.....72
3.2.1.2 Subsurface water flow.....72
3.2.2 Solute Transport.....73
3.2.2.1 Surface transport.....73
3.2.2.2 Subsurface transport.....73
3.2.3 Gas Exchange.....73
3.2.4 N_2O production.....74
3.2.4.1 Denitrification.....74
3.2.4.2 Nitrification.....75
3.2.5 Architecture of *3D-Ecosys-GIS* Model.....75
3.3 Study site.....76
3.4 Field Measurement of N_2O Emission.....77
3.5 Model Experiment.....78
3.6 Results.....79
3.6.1 Measured and modeled N_2O fluxes at the landscape scale.....79
3.6.2 Temporal variation of N_2O emissions across landscape.....87
3.6.3 Spatial variation of N_2O emissions across landscape.....88
3.6.3.1 Spatial variation of modeled soil water, solute and N_2O emissions along a slope transect.....88
3.6.3.2 Spatial variation of modeled daily N_2O emissions.....89
3.6.3.3 Spatial variation of modeled annual N_2O emissions.....96
3.6.4 The relationship between modeled N_2O emissions and terrain attributes....97
3.7 Discussion.....100
3.7.1 The reliability of modeled N_2O fluxes.....100
3.7.2 Temporal variation of modeled N_2O emissions.....102
3.7.3 Spatial variations of modeled N_2O emissions.....103
3.7.4 Relation of temporal and spatial variation in N_2O emissions to N_2O inventory.....104
3.8 Conclusions.....105
References.....106
Appendix 3.1: The main equations and variables for simulating of landscape N_2O emissions in the *3D-Ecosys-GIS*.....113
Appendix 3.2: The interface of *3D-Ecosys-GIS*.....117

Chapter 4: The Effects of Land and Cropping Management on N_2O Emissions in a Hummocky Agricultural Landscape.....119
4.1 Introduction.....119
4.2 Methods.....122

4.2.1 Study site....122
4.2.2 Land and cropping management scenarios....123
4.2.3 Scaling up N_2O emissions to field scale....125
4.2.4 Model runs and evaluation....126
4.3 Results and discussion....127
4.3.1 Effects of tillage on N_2O emissions....127
4.3.2 Effects of fertilizer on N_2O emissions....131
4.3.3 Effects of rotation on N_2O emissions....135
4.3.3.1 Effects of conversion from grassland to cropping on N_2O emissions....136
4.3.3.2 Effects of fallow on N_2O emissions....139
4.3.3.3 Effects of continuous grassland versus cropping on N_2O emissions....139
4.3.4 Scaling N_2O emissions up to field scale....140
4.4 Conclusions....143
References....144
Appendix 4.1: Equation for estimates of N_2O emissions by IPCC method....150
Appendix 4.2: The annual N_2O emissions in the entire study site estimated by the regression function of terrain attributes and modeled N_2O emissions of four sub sites....151

Chapter 5: Climate Impact on Net Ecosystem Productivity of a Semi-arid Natural Grassland: Modeling and Measurement....152
5.1 Introduction....152
5.2 Methods....154
5.2.1 Model Description....154
5.2.1.1 Energy exchange....154
5.2.1.2 Water Relations....154
5.2.1.3 CO_2 fixation....155
5.2.1.4 Autotrophic respiration....156
5.2.1.5 Heterotrophic respiration....156
5.2.1.5.1 Decomposition....156
5.2.1.5.2 Microbial growth....157
5.2.2 Field Experiment....158
5.2.2.1 Description of study site....158
5.2.2.2 Measurement energy and CO_2 fluxes....159
5.2.3 Model Experiment....160
5.2.3.1 Testing CO_2 and energy fluxes under current climate....160
5.2.3.2 Predicting changes in NEP during climate change....161
5.3 Results....162
5.3.1 Soil Water Content....162
5.3.2 Diurnal Variation in Energy and CO_2 Fluxes....162
5.3.2.1 Energy Fluxes....162
5.3.2.2 CO_2 Fluxes....165
5.3.3 Modeled vs. Measured Energy and CO_2 Fluxes....165
5.3.3.1 Energy Fluxes....165

5.3.3.2 CO_2 Fluxes.....166
5.3.4 Daily Net Ecosystem Productivity.....166
5.3.5 Annual Net Ecosystem Productivity.....168
5.3.6 Century-Scale Net Ecosystem Productivity.....171
5.4 Discussion.....173
5.5 Conclusions.....176
References.....177

Chapter 6: Review, General Conclusions and Discussion.....183
References.....188

List of Tables

Table 1.1: The coefficients of spatial variation (CSV – the ratio (%) of standard deviation to mean of emissions over a spatial scale) in N_2O emissions reported in the literature.....2

Table 2.1: Mean and coefficient of spatial variation [CSV – ratio (%) of standard deviation to mean over landscape] of measured soil properties in a hummocky agricultural landscape.....24

Table 2.2: Terrain attributes used for predictions of soil properties in the study site at Viking, Alberta, Canada.....25

Table 2.3: The combinations of soil properties to be allocated for testing sensitivity of N_2O emissions to uncertainties of predicted soil properties in the hummocky agricultural landscape at Viking, Alberta, Canada.....39

Table 2.4: Pearson correlation (R) between measured soil properties and their localized TAs that derived from DEM of the hummocky landscape at Viking, Alberta, Canada.....41

Table 2.5: Validation results of measured versus predicted soil properties for three model methods ($R^2 = 0.26$ at $P \leq 0.05$).....44

Table 2.6: The prediction functions of individual soil property derived by SMLR from 42 data combinations in calibration dataset.....45-46

Table 2.7: Uncertainties (%) of predicted soil properties from validation of SMLR with measured soil properties.....47

Table 2.8: The uncertainties of total N_2O emission in the sub site F1 (3.23 ha.) caused by uncertainties of soil properties 48

Table 2.9: The uncertainties or differences found in current measurement or estimation methods from literature.....54

Table 3.1: Statistical results from log-transformed regressions of measured on modeled N_2O fluxes ($\mu g\ N\ m^{-2}\ h^{-1}$).....86

Table 3.2: The coefficients of variation (CV, %) in log-transformed values and mean of measured and modeled N_2O fluxes for measured emission events at top, middle slopes, foot slopes and depressions in the hummocky agricultural landscape at Viking, Alberta, Canada, in 2000, 2001 and 2002.....86

Table 3.3: Temporal variation of modeled hourly N_2O fluxes ($\mu g\ N\ m^2\ h^{-1}$) for all sub sites in the three years in the hummocky landscape at Viking, Alberta, Canada.....87

Table 3.4: The Spatial variation of modeled daily N_2O emissions and of soil NH_4^+ and NO_3^- contents, and of soil daily relative water-filled porosity (RWFP) and temperature (ST) in the upper 20 cm soil zone during 3 daily emissions events (E1, E2, E3) over four sub sites (F1, F2, F3 and F4) in the hummocky agricultural landscape.....95

Table 3.5: Spatial variation of annual N_2O emissions in the four sub sites (F1, F2, F3 and F4) in the hummocky agricultural landscape at Viking, Alberta, Canada, in 2000, 2001 and 2002.....97

Table 3.6: The Pearson correlation (R) between annual N_2O emissions and terrain attributes in the hummocky agricultural landscape at Viking, Alberta, Canada in 2000, 2001, 2002.....100

Table 4.1: The scenarios and their cropping, tillage and fertilizer managements for which N_2O emissions were simulated in the hummocky agricultural landscape at Viking, Alberta, Canada.....124

Table 4.2: Annual N_2O emissions and spatial variations under different tillage management at the hummocky agricultural landscape at Viking, Alberta, Canada, in 2000, 2001 and 2002.....127

Table 4.3: The key factors explaining differences of N_2O emissions among conventional (CT), reduced (RT) and no (NT) tillage.....128

Table 4.4: Annual N_2O emissions, spatial variations and emission factors under chemical (CF), manure (MF), double chemical (DCF) and no (NF) fertilizer management in the hummocky agricultural landscape at Viking, Alberta, Canada, in 2000, 2001 and 2002.....132

Table 4.5: Annual N_2O emissions and spatial variations under wheat-barley -canola (WBC), wheat-fallow (WF), wheat-wheat-fallow (WWF), continuous wheat (CW), continuous hay (CH) and hay-hay-hay-wheat -wheat-wheat (HHHWWW) in the hummocky agricultural landscape at Viking, Alberta, Canada, in 2000, 2001 and 2002.....136

Table 4.6: Total N_2O emission in the entire study field (76.6 ha) derived by different scaling up methods.....141

Table 5.1: Properties of the Orthic Brown Chernozem at Lethbridge, Alberta. Soil texture, organic matter content and pH of A (0 to 9 cm) and B horizons (9 to 25 cm) were measured at the field site, and those of lower layers were extracted from AGRASID (http://www.agric.gov.ab.ca /agdex/000/agrasid. Html) θ_{FC}, θ_{WP}, ρ_b and K_{sat} were calculated from soil texture (Saxton et al., 1986).....161

Table 5.2: The climate change scenario developed from results of the Canadian Regional Climate Model (CRCM-II) for the Lethbridge area.....162

Table 5.3: Regression of modeled on measured hourly energy and CO_2 fluxes in 1998, 1999 and 2000. Model outputs in the 58th, 59th and 60th year of a 110 year model run were used in the regression analysis.....166

Table 5.4: The C balance of grassland calculated from gap-filled eddy covariance fluxes and modelled in 1998, 1999 and 2000. Positive values indicate C gain from atmosphere, negative values indicate C loss to atmosphere.....169

Table 5.5. Average annual C transfers during last ten years following 100 years under current (1991-2000) vs. changed (Table 5.2) climates.....172

List of Figures

Figure 2.1: The study site, soil profile locations and sub site of sensitive study of N_2O emissions in east center of Alberta, Canada (53°05'N, 111°47'W).....23

Figure 2.2: The terrain attribute maps of the whole study site.....30–31

Figure 2.3: The slope shape described in plan and profile curvature.....31

Figure 2.4: The distributions of terrain attributes derived from the entire study site.....32

Figure 2.5: The architecture of artificial neural network (ANN).....35

Figure 2.6: The data flow diagram accompanying landscape soil property predictor (LSPP).....37

Figure 2.7: The distribution of error ratio calculated by Eq. 2.6 for all predicted cases in the validation.....43

Figure 2.8: Soil properties estimated by SMLR for thickness (a), pH (g), and sand (c), silt (e), total organic carbon (i) and total organic nitrogen (k) contents in A horizon, and thickness (b), pH (h), sand (g), silt (f), total organic carbon (j) and total organic nitrogen (l) contents in B horizon in the hummocky landscape at Viking, Alberta, Canada.....50–51

Figure 3.1: The architecture of *3D-Ecosys-GIS* model 76

Figure 3.2: The study site, observation transects and sub sites at Viking, Alberta, Canada (53°05'N, 111°47'W).....77

Figure 3.3: The measured (dot) and modeled (line) N_2O fluxes at top, middle slope and foot slope in sub site F2 in the hummocky agricultural landscape at Viking, Alberta, Canada in 2000.....80

Figure 3.4: The measured (dot) and modeled (line) N_2O fluxes at top, middle slope and foot slope in sub site F2 in the hummocky agricultural landscape at Viking, Alberta, Canada in 2001.....81

Figure 3.5: The measured (dot) and modeled (line) N2O fluxes at top, middle slope and foot slope in sub site F2 in the hummocky agricultural landscape at Viking, Alberta, Canada in 2002.....82

Figure 3.6: The measured (dots) and modeled (solid line) N2O fluxes, rainfall (vertical bars), and relative water-filled porosity (RWFP, long-dash line) and soil temperature (dot line) in upper 20 cm zone at (b) foot slope in sub site F2, and (a) top and (c) depression in sub site F4 in the hummocky agricultural landscape at Viking, Alberta, Canada, in 2000, 2001, 2002.....83

Figure 3.7: The relationships of measured and modeled N_2O fluxes at different landscape positions in four measuring transects in sub sites F1, F2, F3 and F4 in the hummocky agricultural landscape at Viking, Alberta, Canada, in 2000, 2001 and 2002.....85

Figure 3.8: The changes of (a) elevation, (b) rainfall, (c) relative water-filled

porosity (RWFP) in the upper 20 cm soil zone, (d) NH_4^+, (e) NO_3^- and (f) N_2O emission on a hill slope transect from June 30 to July 8 2000. Numbers in lines indicate the days from June 30 2000.....90–91

Figure 3.9: The soil RWFPs during three N_2O emission events (E1: June 13 2000; E2: 19 June 2001; and E3: 28 May 2002) on the four sub sites (F1, F2, F3 and F4) in the hummocky agricultural landscape at Viking, Alberta, Canada.....93

Figure 3.10: The N_2O emission (mg N m^{-2} d^{-1}) during three N_2o emission events (E1: June 13 2000; E2: 19 June 2001; and E3: 28 May 2002) on the four sub sites (F1, F2, F3 and F4) in the hummocky agricultural landscape at Viking, Alberta, Canada.....94

Figure 3.11: The annual N_2O emissions (g N m^{-2}) in the four sub sites (F1, F2, F3 and F4) in the hummocky agricultural landscape at Viking, Alberta, Canada, in 2000, 2001 and 2002.....98

Figure 4.1: The study site, chamber locations and sub sites at Viking, Alberta, Canada (53°05'N, 111°47'W).....122

Figure 4.2: The dynamics of soil total organic nitrogen (TON) and NO_3^- contents, daily RWFP and N_2O emissions under conventional tillage (CT), reduced tillage (RT) and no-tillage (NT) in the hummocky agricultural landscape at Viking, Alberta, Canada, in 200, 2001, 2002.....129

Figure 4.3: An expanded graph from Fig. 4.2d to show the differences of N_2O emission in a period of 2000 under conventional (CT, black solid line), reduced (RT, dots) and no (NT, long dash line) tillage.....130

Figure 4.4: The dynamics of soil total organic nitrogen (TON) and NO_3^- contents, daily RWFP and daily N_2O emissions under chemical fertilizer (CF), double chemical fertilizer (DCF, no-fertilizer (NF) and cattle manure (MF) in the hummocky agricultural landscape at Viking, Alberta, Canada, in 2000, 2001, 2002.....133

Figure 4.5: The dynamics of soil total organic nitrogen (TON) and NO_3^- contents, daily RWFP and daily N_2O emissions under wheat-barley-canola (WBC), wheat-wheat-fallow (WWF), wheat-fallow (WF), continuous wheat (CW), hay-hay-hay-wheat-wheat-wheat (HHHWWW) and continuous hay (CH) in the hummocky agricultural landscape at Viking, Alberta, Canada, in 200, 2001, 2002. Fertilizer was indicated if it was applicable.....137–138

Figure 5.1: Measured (symbol) and modelled (line) soil moistures. Dash dot line indicates the permanent wilting point (17 % in vol. in 1998, 18% in 1999 and 2000). The depths for comparing measured and simulated data were 10 cm in 1998, 15 cm in 1999 and 2000.....163

Figure 5.2: Measured (symbols) and modelled (lines) latent heat flux (LE) and sensible heat flux (H) from days 177 to 182 and 225 to 230 during 1998 to 2000. Negative values indicate upward fluxes.....164

Figure 5.3: Measured (symbol) and modeled (line) net ecosystem CO_2 flux from days 177 to 182 and 225 to 230 during 1998 to 2000. Negative values indicate upward fluxes....167

Figure 5.4: Measured (symbol) and modeled (line) daily net carbon exchange during 1998 to 2000. Negative values indicate C loss....168

Figure 5.5: Measured (symbol) and modelled (line) above-ground C during 1998 to 2000....170

Figure 5.6: Soil carbon change under current climate and climate change scenarios. The climate change scenarios were developed from the results of the Canadian Regional Climate Model (CRCM-II V3.5) nested with CGCM2 outputs from the GHG+A transient simulation under scenario "IS92a"....173

Chapter 1: General Introduction

Global warming, which occurs due to increasing greenhouse gas concentrations in the atmosphere, is part of the large challenge of sustainable development. N_2O currently accounts for 6 percent of greenhouse gases that caused global warming (IPCC Third Assessment Report, 2001). Kroeze et al. (1999) estimated that total global N_2O emissions were about 17.6 Tg N in 1994. Approximately 9.7 Tg N (55%) of the total arose from natural terrestrial and aquatic systems, and approximately 7.9 Tg N (45%) came from anthro-pogenic sources. The contribution of agriculture to the global N_2O source was about 35% (International Fertilizer Industry Association and FAO Report, 2001). Mosier and Kroeze (2000) estimated agricultural emissions increased from about 1.5 Tg N_2O-N y^{-1} in 1900, to 2.9 Tg N y^{-1} in 1950, to 6.2 Tg N y^{-1} in 1994 and will increase to 9.1 Tg N y^{-1} in 2020. However, Brown et al. (2002) and Lim et al. (1999) reported that the uncertainty of current N_2O inventory (IPPC guidelines, 1997) was larger than 62% in agricultural soils, which was beyond the reduction targets in the Kyoto Protocol for most countries (Monni et al., 2004). This uncertainty mainly resulted from the large temporal and spatial variability of N_2O fluxes (Flessa et al., 2002; Scott et al., 1999). Site specific conditions, such as soil properties, crop and soil management, and climate, also elicit large differences of N_2O emissions (Beauchamp, 1997). Current N_2O inventory (e.g. IPCC tier 1 methodology) uses single emission factor (1.25% of N input in Canada, Olsen et al. 2003) which summarized from numerous field experiment, but it does not account for the temporal and spatial variation and the effects of site specific conditions on N_2O emissions. Therefore, current N_2O inventories must be improved to fully consider the large spatial and temporal variability and site specifications so that the uncertainty in estimation of N_2O emission can be minimized.

1.1 Spatial and temporal variation of N_2O emissions

The coefficients of spatial variation (CSV – the ratio (%) of standard deviation to mean of emissions over a spatial scale) in N_2O emissions have be found to vary between 21% and 500% (Table 1.1). Pennock and Corre (2001) reported that N_2O emissions were significantly higher at foot slopes than at shoulders or midslopes, and that total emissions

increased positively with nitrogen fertilizing rate, and Corre et al. (1999) measured that N_2O emissions at foot slopes were one to ten times higher than those at shoulder slopes in an agricultural soil in a glacial hummocky landscape in central Saskatchewan, Canada. Van Kessel et al. (1993) showed that denitrification rates were significantly higher at low landscape positions than at high landscape positions. Corre et al. (1996), van Kessel et al. (1993), and Pennock et al. (1992) have demonstrated that soil moisture is the dominant control on the rate of N_2O emissions and that soil moisture is often higher at lower positions in a given landscape. Florinsky et al. (2003) also found that differences in N_2O emissions were affected by differences in accumulation of soil moisture and organic matter due to the local topography. Large temporal variations of N_2O emissions have also been attributed to soil thawing and freezing cycles, differences of plant residues, crop species, fluctuations of soil water and temperature, and dynamics of mineral nitrogen (NH_4^+ and NO_3^-) (Flessa et al., 2002; Chao, et al., 2000; Röver et al., 1999; Williams et al., 1999; Kaiser et al., 1998). In agricultural soils, N availability and soil moisture are the major controls on temporal variations of N_2O emissions (Weitz et al., 2001; Paul and Clark, 1996).

Table 1.1: The coefficients of spatial variation (CSV – the ratio (%) of standard deviation to mean of emissions over a spatial scale) in N_2O emissions reported in the literature.

Author	CSV (%)	Spatial scale	Type of ecosystem
Mosier et al. (1981, 1982)	> 60		
Bremner et al. (1979)	50	100 m^2	
Matthias et al. (1980)	31 – 168	100 m^2	
Folorunso and Rolston (1984)	282 – 379	1 – 2 m apart	
Yamulki et al. (1995)	24 – 57	1 – 2 m apart	Wheat field
Grant and Pattey (2003)	30 -180	< 500 m	Fertilized agricultural fields
Choudhary et al. (2002)	119		Arable land, permanent pasture
Mahmood et al. (1998)	> 200		
Lemke et al. (1998)	< 92	Provincial scale	Agricultural soil
Williams et al. (1999)	21 – 286		Permanent pasture
Röver et al. (1999)	100 – 500		Arable soil
Kaiser et al. (1996)			
Myrold (1988)			

Coefficients of temporal variation (CTV – the ratio (%) of standard deviation to mean of fluxes over a time period) in N_2O emissions during growing seasons have been found to be larger than 150% (Thornton et al., 1996; Flessa et al., 1995). The temporal variation of seasonal N_2O emissions was large, with fluxes ranging from 0 to 1100 mg m^{-2} h^{-1} measured by automatic chambers in potato fields of Germany (Flessa et al., 2002). Water-filled porosity and soil temperature respectively explained 40% and 75% of this large temporal variability. In southern Taiwan, China, Chao et al. (2000) measured the mean CTVs of seasonal N_2O emissions in various agro-ecosystems to be from 36.3% to 130.9% for paddy soil, from 14.8% to 17.6% for upland soil, from 16.8% to 17.9% for orchard soil, and from 24.9 to 25.5% for hardwood forest soil. Diurnal N_2O fluxes varied from 16.1 μg N m^{-2} h^{-1} to 412.0 μg N m^{-2} h^{-1} in a banana orchard (Chao et al., 2000). Through field measurements in a permanent pasture near Grange-over-Sands, Cumbria, UK, Williams et al. (1999) found that the diurnal variation of N_2O emissions followed that of soil temperature at 10 cm depth, with N_2O emissions peaking in late afternoon, and that fertilizer coinciding with rainfall caused large N_2O emissions. They measured that the seasonal N_2O emissions varied from 0.05 mg N m^{-2} d^{-1} to 16.8 mg N m^{-2} d^{-1}. Kaiser et al. (1998) measured the CTV of annual N_2O emissions between 136% and 192% over spring barley, sugar beet and winter wheat fields at Timmerlah near Braunschweig, Lower Saxony, Germany. The large spatial and temporal variability of N_2O emissions suggests a complex response to small environmental changes associated with landscape and time. Therefore, aggregation of plot-scale emission measurements to regional scales should be based upon sub-daily measurements at representative landscape positions, rather than upon less frequent measurements at individual sites as is currently done (Grant and Pattey, 2003). Aggregation needs to very localized to account for site-specific environmental factors (Beauchamp, 1997). In addition, the identification of areas in which N_2O emissions are high in regional scales is essential for the implementation of N_2O emission mitigation strategies (Bareth, 2001).

1.2 Detection of the temporal and spatial variation in N_2O emissions

Currently, accurate measurement of N_2O emissions at field scale is difficult because of their great spatial and temporal variability. Measurements of N_2O emissions fall into two

main categories: surface chamber and micrometeorological techniques (International Fertilizer Industry Association and FAO Report, 2001). Surface chamber techniques are the most widely used technique for measuring N_2O emissions at small spatial scales (< 1 m^2). The advantages of surface chamber measurements are low cost and easy utilization, and they are well adapted to addressing spatial variation in N_2O emissions. However, it is difficult for surface chambers to capture the temporal variability of N_2O emissions because of low measurement frequency (Bouwman, 1996; Blackmer et al., 1982). Flessa et al. (2002) developed an automated system for near-continuous, long-term measurements to track temporal variation, but the high cost and complicated installation reduced the possibility to address spatial variations by setting up this kind of chamber at different landscape positions. The temporal variability of N_2O emissions may be better measured by micro-meteorological techniques (Wagner-Riddle et al., 1996). These techniques have low spatial resolution because the upwind fetch distance ranges from 20 to 200 m, and uncertainties in flux assessment are mainly due to spatial heterogeneity of N_2O within the fetch (Laville et al., 1999). Micrometeorological techniques are therefore well adapted to provide long-term estimations of N_2O emissions at the landscape scale, but have limited ability to resolve topographic and treatment effects on N_2O emissions. Presently, no measurement methods are available to address the temporal and spatial variations of N_2O emission simultaneously. Mathematical models, which incorporate the biological, chemical and physical processes of N_2O emissions and can be calibrated by measured data, may provide a methodology to address the spatial and temporal variability of N_2O emissions (Grant and Pattey, 2003).

1.3 Mathematical models for simulating N_2O emissions

A few ecosystem models have the ability to simulate N_2O emissions. DNDC (DeNitrification-DeComposition), a process-oriented simulation model of carbon (C) and nitrogen (N) biogeochemistry in agricultural ecosystems and an integrated one-dimensional model of field-level C and N dynamics in soil-vegetation systems, was developed to assess N_2O, NO, N_2, NH_3 and CO_2 emissions from agricultural soils in daily time step (Li, 2000; Li et al., 1992). The model contains climate, crop growth, decomposition and denitrification sub-models. It has the ability to simulate the magnitude

and seasonal trends of N_2O emissions at a regional scale (Brown et al., 2002; Li et al., 1996, 2001) and at a plot scale (Xu-Ri et al., 2003). N_2O is produced in nitrification and denitrification processes. The concentration of NH_4^+ from decomposition of organic matter controls nitrification. A constant fraction (0.002) of nitrification is allocated to N_2O. N_2O from denitrification is a function of soluble C, soil temperature, soil pH, N-substrate availability, soil moisture and denitrifier biomass.

CENTURY, a multicompartmental ecosystem model developed to simulate long-term changes in soil organic C and N, nutrient cycling, and plant production for the soil-plant ecosystem, can simulate long-term nitrogen gases emissions at a regional scale on monthly time step (Liu et al., 2000; Parton et al., 1988, 1996; Robertson, 1989). The DAYCENT (Del Grosso et al., 2001; Kelly et al., 2000; Parton et al., 1998), a new version of CENTURY, simulates exchanges of C, nutrients (N, P, S), and gases (CO_2, CH_4, N_2O, NO_x, N_2) among the atmosphere, soil and plants on a daily time step. DAYCENT includes sub-models for plant productivity, decomposition of dead plant material and soil organic matter, soil water and temperature dynamics, and trace gas fluxes under different land uses (Del Grosso et al., 2002). The N_2O emission is a fraction of total N gas flux (N_2+N_2O) which is a function of soil water effects on denitrification, on the minimum rate of NO_3^- and a soil respiration. Fractions of N_2 and N_2O are calculated according to effects of soil NO_3, respiration rate and water, respectively.

These one-dimensional (vertical direction) models have the ability to simulate the temporal and spatial (coarse scale) variations in N_2O emissions and the effects of land use, vegetation and management on N_2O emissions. However, these models do not simulate the energy and mass exchanges among adjacent grid cells and cannot represent the spatial heterogeneities of soil properties that vary associated with landscape topography. Therefore, these models are unable to simulate spatial variations of N_2O emissions at a landscape level.

Ecosys can be used to estimate energy, CO_2, N_2O, CH_4, and nutrient exchange under current or projected climates (Li et al., 2004; Grant, 2001, 1999, 1997, 1995a, 1995b; Grant and Nalder, 2000; Grant and Pattey, 1999; Grant et al., 2001a, 2001b, 2001c, 1999a, 1999b, 1998, 1995a, 1995b 1993a, 1993b, 1993c). It is three dimensional ecosystem model including *X* and *Y* for horizontal coordinates, and *Z* for elevation.

Theoretically, it has the ability to simulate the spatial and temporal variations of energy, carbon and trace greenhouse gases exchange (Grant and Pattey, 2003) on hourly time step and at any spatial scale. To represent the temporal and spatial variation of N_2O emissions, *Ecosys* requires topographically referenced soil properties and field management data at a fine scale (meters to tens meters).

1.4 Soil properties for modeling landscape N_2O emissions

Topographically referenced soil properties at the fine scale are not routinely practical. Doing detailed soil sampling and laboratory analysis is difficult because of the high cost and large time requirement. However, during the last two decades, soil properties have been predicted from correlations between soil properties and various soil forming factors, such as vegetation, management practices, parent material, topography, and climate (McBratney et al., 2003; Park and Vlek, 2002). The predictions are based on the assumption that each soil property has a unique spatial distribution over the landscape due to differences in geochemical and geomorphological mobilities of soil materials, and also to differential responses of soil properties to given pedological and ecological processes of soil formation (Huggett, 1975; Park and Vlek, 2002). Among these factors of soil formation, the terrain attributes, which quantitatively describe the topography and can be easily derived from digital elevation maps, are most often used as key predictors of soil properties (McBratney et al., 2003; Bishop and McBratney, 2001; McBratney et al., 2000). However, uncertainties are always associated with predicted soil properties (Bui and Moran, 2003; McBratney et al., 2002; Chiles and Delfiner, 1999; Deutsch and Journel, 1998; Goovaerts, 1997; Cressie, 1993; Isaaks and Srivastava, 1990), although they have been already used for detailed soil mapping (Mueller and Pierce, 2003; Florinsky and Arlashina, 1998; Lexer and Honninger, 1998) and ecosystem management (Booltink, et al., 2001; Garcia, et al., 2000; Gessler et al., 2000; Stafford, 2000). The uncertainties in predicted soil properties would propagate uncertainties in N_2O emissions when these soil properties are used to initialize ecosystem models to simulate N_2O emissions. The magnitude of these uncertainties in N_2O emissions will determine whether or not the predicted soil properties can be used to simulate N_2O emissions. So far, such a study has not be conducted. Current N_2O inventory (IPCC guidelines) will be improved if

the predicted soil properties can be used to initialize ecosystem models to represent the temporal and spatial variation of N_2O emissions.

1.5 Agricultural practices affecting N_2O emissions

The factors in the IPCC guidelines were summarized from numerous experiments and observations and for all agricultural soils, regardless of variations in soil and crop management and climate. Field measurements have indicated that crop rotation, tillage and fertilizer type strongly affect N_2O emissions, but the effects were not consistent. Jacinthe and Dick (1997) measured 50% and 23% higher N_2O emissions respectively in a continuous corn and corn-soybean rotation field than in a corn-soybean/wheat-hairy vetch rotation in fine loamy and silt soil at Piketon, OH, USA, using a chamber technique. The low carbon to nitrogen ratio (C:N) of crop residues contributed to higher N_2O emissions (Kaiser et al., 1998). Lemke et al. (1999) measured higher N_2O emissions in a fallow field than in a crop field in the Alberta parkland region, Canada. Mogge et al. (1999) and Choudhary et al. (2002) found that grassland always had lower N_2O emissions than did crop fields. Harrison and Webb (2001) found that nitrate-nitrogen fertilizer caused greater N_2O emissions in comparison with ammonium sulfate under wet conditions, while urea generally caused greater N_2O emissions than ammonium-nitrogen fertilizers unless soil was dry and soil temperature was low. Christensen (1983) measured higher N_2O emissions in an organically fertilized field than in a chemically fertilized field under the same N fertilizer rate. However, Lemke et al. (1999) estimated lower N_2O emissions in manured field (total N 90 kg ha^{-1} and C:N $\approx$ 24:1) than in an urea-fertilized field (56 kg N ha^{-1}) according to chamber measurements. Choudhary et al. (2002), Ball et al. (1999) and Aulakh et al. (1984) found that N_2O emissions were higher in no-tillage than in conventional tillage. In contrast, Lemke et al. (1999) measured that N_2O emissions were generally lower in no-tillage than conventional (intensive) tillage, in the Alberta parkland region, Canada. These conflicting conclusions may be the result of the large spatial variation of N_2O emissions (Table 1.1) at different measurement locations of field experimental treatments. Mathematical modeling can provide a well-constrained test to ensure that the differences in N_2O emissions among different management scenarios arise

only from specified management factors. Therefore, modeling techniques may provide a method to clarify the effects of crop rotation, tillage and fertilizer on N_2O emissions.

1.6 Scaling up N_2O emissions

As described above, because of the strong spatial and temporal variations of N_2O emissions, the heterogeneities of soil properties over landscapes, and the disadvantages of current measuring methods, accurately measuring or estimating N_2O emissions at landscape, regional, provincial and national scales is difficult. The aggregation of landscape N_2O emissions to longer time scales (e.g. seasonal, annual, decade), may be based on the possibility of a strong relation of emissions to 'average' biophysical conditions (International Fertilizer Industry Association and FAO Report, 2001). However, to obtain reliable 'average' biophysical conditions will be a difficult task because of the large variations in environmental conditions at different time scales.

A few models have the ability to calculate the field or regional N_2O emissions (such as DNDC, CENTURY) based on the hypothesis that the N_2O emissions are same if the vegetation, soil type and management are the same or similar at concerning scale. However, this hypothesis may be incorrect because Grant and Patty (2003) demonstrated that small environmental changes associated with landscape and time series may cause large changes in N_2O emissions. Sozanska et al. (2002) used field measurements to establish a multiple regression model between N_2O emissions and the factors affecting them. This model was then coupled with a GIS framework to estimate regional and national N_2O emissions. This model accounted for the effects of land use, soil temperature, soil water content, soil C content and N input on N_2O emissions. It provided a simple method for estimating N_2O emissions, but was constrained by the accuracy of measurements of soil temperature and soil water content which varied with landscape position. Minor differences in only one of the measurement sites used in model calibration can cause major shifts in the model's correlation coefficient (Bouwman et al., 1993). Freibauer (2003) reported that errors from regression models which were used to estimate regional to continental N_2O emissions from agricultural soils in Europe were from 30% to 100%.

Currently, the national and provincial N_2O emissions are estimated using the IPCC guidelines (Olsen et al., 2003; Mosier et al., 1999). However, in order to minimize the uncertainties, more acute models should account for the temporal and spatial variations of N_2O emissions and the site-specific effects of crop and soil management and climate. So far, the crucial problem of scaling up N_2O emissions from micro-sites to plot (fine) scales (micrometeorological and chamber measurements, and modeling results) to coarse scales (field or landscape, regional, provincial and national scales) remains unsolved. Mathematical modeling may provide a solution to this problem if the model can handle large and complex input and output information at a coarse scale.

1.7 Objectives and contents

The objectives of this study were to develop a methodology for estimating N_2O emissions at the landscape and field scales as well as to clarify the effects of cropping, tillage and fertilizer on N_2O emissions. This study included following components. Firstly, a digital terrain model was developed to predict soil properties at a fine scale. Secondly, the capability of *ecosys* was extended to handle complex input and output information in map format, in which *ecosys* was integrated into a GIS framework. The new version of *ecosys*, named *3D-Ecosys-GIS*, provided a platform to simulate the temporal and spatial variation of N_2O emissions based on physical, chemical and biological processes of N_2O production and emissions. Thirdly, the effects of crop rotation, tillage and fertilizer on N_2O emissions were studied at the landscape scale using *3D-Ecosys-GIS*, and a few methods for scaling up N_2O emissions from plot or landscape scale to field scale were tested.

While a general introduction has been given in this chapter, the remainder of this thesis consists of following five chapters. Chapter 2 discusses the prediction of soil properties at fine scale and the possibility of using predicted soil properties as input data to simulate landscape N_2O emissions. Chapter 3 describes the modeling technique and the temporal and spatial variation of landscape N_2O emissions. Chapter 4 discusses the effects of crop rotation, tillage and fertilizer on N_2O emissions at landscape level and the N_2O emissions at the field scale. Chapter 5 describes the impact of climate change on net

CO_2 exchange of natural grassland over next 100 years. Chapter 6 gives the general review, discussion and conclusions.

References

Aulakh, M.S. and Rennie, D.A., 1984. Nitrogen transformations with special reference to gaseous N losses from zero-tilled soils of Saskatchewan, Canada. Soil & Tillage Research. 7(1-2):157–171.

Ball, B.C., Scott, A., Parker, J.P., 1999. Field N_2O, CO_2 and CH_4 fluxes in relation to tillage compaction and soil quality in Scotland. Soil & Tillage Research. 53(1):29–39.

Bareth, G., 2001. Soil-land-use-system approach to estimate nitrous oxide emissions from agricultural soils. Nutrient Cycling in Agroecosystems. 60(1):219–234.

Beauchamp, E.G., 1997. Nitrous oxide emission from agricultural soils. Can. J. Soil Sci. 77:113–123.

Bishop, T.F.A. and McBratney, A.B., 2001. A comparison of prediction methods for the creation of field-extent soil property maps. Geoderma. 105:93–111.

Blackmer, A.M., Robbins, S.G., Bremner, J.M., 1982. Diurnal variability in rate of emission of nitrous oxide from soils. Soil Science Society of America Journal. 46:937–942.

Booltink, H.W.G., van Alphen, B.J., Batchelor, W.D., Paz, J.O, Stoorvogel, J.J., Vargas, R., 2001. Tools for optimizing management of spatially-variable fields. 70:445–476.

Bouwman, A.F., 1996. Direct emission of nitrous oxide from agricultural soils. Nutrient Cycling in Agroecosystems. 46:53–70.

Bouwman, A.F., Fung, I., Matthews, E., John, J., 1993. Global analysis of the potential for N_2O production in natural soils. Global Biogeochemical Cycles. 7:557–597.

Bremner, J.M., Robbins, S.G., Blackmer, A.M., 1979. Seasonal variability in emission of nitrous-oxide from soil. Geophysical Research Letters. 7(9):641–644.

Brown, L., Syed,B., Jarvis, S. C., Sneath, R. W., Phillips, V. R., Goulding, K. W. T., Li., C., 2002. Development and application of a mechanistic model to estimate emission of nitrous oxide from UK agriculture. Atmospheric Environmen. 36(6):917–928.

Bui, E.N. and Moran, C.J., 2003. A strategy to fill gaps in soil survey over large spatial extents: an example from the Murray–Darling basin of Australia. Geoderma. 111(1-2):21–44.

Chao, C.C., Young, C.C., Wang, Y.P., Chao, W.L., 2000. Daily and seasonal nitrous oxide fluxes in soils from hardwood forest and different agroecosystems of Taiwan. Chemosphere: Global Change Science. 2:77–84.

Chiles, J.P., Delfiner, P., 1999. Geostatistics: Modeling Spatial Uncertainty. Wiley, New York.

Choudhary, M.A., Akramkhanov, A., Saggar, S., 2002. Nitrous oxide emission from a New Zealand cropped soil: tillage effects, spatial and seasonal variability. Agriculture, Ecosystems and Environment. 93:33–43.

Christensen, S., 1983. Nitrous oxide emission from soil under permanent grass: seasonal and diurnal functions as influenced by manuring and fertilization. Soil Biol. Biochem. 15(5):531–536.

Clemens, J., Schillinger, M.P., Goldbach, H., Huwe, B., 1999. Spatial variability of N2O emissions and soil parameters of an arable silt loam—a field study. Biology and Fertility of Soils. 28:403–406.

Corre, M.D.; Pennock, D.J.; Van Kessel, C.; Elliott, D.K.; 1999. Estimation of annual nitrous oxide emissions from a transitional grassland-forest region in Saskatchewan, Canada. Biogeochemistry. 44(1):29–49.

Corre, M.D.; Van Kessel, C.; Pennock, D.J., 1996. Landscape and seasonal patterns of nitrous oxide emissions in a semiarid region. Soil Sci. Soc. Am. J. 60:1806–1815.

Cressie, N.A., 1993. Statistics for Spatial Data. Wiley, New York.

Del Grosso, S.J., Ojima, D.S., Parton, W.J., Mosier, A.R., Peterson G., Schimel, D.S., 2002. Simulated effects of dryland cropping intensification on soil organic matter and greenhouse gas exchanges using the DAYCENT ecosystem model, Environmental Pollution. 116(1):S75–S83.

Del Grosso, S.J., Parton, W.J., Mosier, A.R., Hartman, M.D., Brenner, J., Ojima, D.S., Schimel, D.S., 2001. Simulated interaction of carbon dynamics and nitrogen trace gas fluxes using the DAYCENT model. In: Schaffer, M., Ma, L., Hansen, S. (Eds.),

Modeling Carbon and Nitrogen Dynamics for Soil Management. CRC Press, Boca Raton, FL, 303–332.

Deutsch, C.V. and Journel, A.G., 1998. GSLIB: Geostatistical Software Library and User's Guide. Oxford University. Press, New York.

Flessa, H., Do¨rsch, P., Beese, F., 1995. Seasonal variation of N2O and CH4 fluxes in differently managed arable soils in southern Germany. Journal of Geophysical Research. 100:23115–23124.

Flessa, H., Ruser, R., Schilling, R., Loftfield, N., Munch, J.C., Kaiser, E.A., Beese, F., 2002. N_2O and CH_4 fluxes in potato fields: automated measurement, management effects and temporal variation. Geoderma. 105(3-4):307–325.

Florinsky, I.V. and Arlashina, H.A., 1998. Quantitative topographic analysis of gilgai soil morphology. Geoderma. 82:359–380.

Florinsky, I.V., McMahon, S., Burton, D.L., 2003. Topographic control of soil microbial activity: a case study of denitrifiers. Geoderma. 119(1-2):33–53.

Folorunso, O.A. and Rolston, D.E., 1984. Spatial variability of field-measured denitrification gas fluxes. Soil-Sci. Soc. Am. J. 48:1214–1219.

Freibauer, A., 2003. Regionalised inventory of biogenic greenhouse gas emissions from European agriculture. European Journal of Agronomy. 19:135–160.

Garcia, P.J.D., Olson, K.R., Lang, J.M., 2000. Predicting corn and soybean productivity for Illinois soils. Agricultural System. 64(3):151–170.

Gessler, P.E., Chawwick, O.A., Chamran, F., Althouse, L., Holmes, K., 2000. Modeling soil-landscape and ecosystem properties using terrain attributes. Soil Sci. Soc. Am. J. 64(6):2046–2056.

Goovaerts, P., 1997. Geostatistics for natural resources evaluation. Oxford Univ. Press, New York.

Grant, R. F. and Pattey, E., 2003. Modelling variability in N_2O emissions from fertilized agricultural fields. Soil Biology and Biochemistry. 35(2):225–243.

Grant, R.F. and Nalder, I.A., 2000. Climate change effects on net carbon exchange of a boreal aspen-hazelnut forest: estimates from the ecosystem model ecosys. Global Change Biology. 6(2):183–200.

Grant, R.F. and Pattey, E., 1999. Mathematical modelling of nitrous oxide emissions from an agricultural field during spring thaw. Global Biogeochemical Cycles. 13:679–694.

Grant, R.F., 1995a. Dynamics of energy, water, carbon and nitrogen in agricultural ecosystems: simulation and experimental validation. Ecological Modeling. 81(1-3): 169–181.

Grant, R.F., 1995b. Mathematical modelling of nitrous oxide evolution during nitrification. Soil Biol. Biochem. 27:1117–1125.

Grant, R.F., 1997. Changes in soil organic matter under different tillage and rotation: mathematical modeling in ECOSYS. Soil Science Society of America Journal. 61(4): 1159–1175.

Grant, R.F., 1999. Simulation of methanotrophy in the mathematical model ecosys. Soil Biol. Biochem. 31:287–297.

Grant, R.F., 2001. A review of the Canadian ecosystem model ecosys. In: Shaffer, M., (Ed.), Modeling Carbon and Nitrogen Dynamics for Soil Management. CRC Press, Boca Raton, 175–264.

Grant, R.F., Black, T.A., Hartog, G. den, Berry, J.A., Neumann, H.H., Blanken, P.D., Yang, P.C., Russell, C., Nalder, I.A., den Hartog, G., 1999a. Diurnal and annual exchanges of mass and energy between an aspen-hazelnut forest and the atmosphere: testing the mathematical model ECOSYS with data from the BOREAS experiment. Journal of Geophysical Research. 104(D22):27699–27717.

Grant, R.F., Jarvis, P.G., Massheder, J.M., Hale, S.E., Moncrieff, J.B., Rayment, M., Scott, S.L., Berry, J.A., 2001a. Controls on carbon and energy exchange by a black spruce-moss ecosystem: testing the mathematical model Ecosys with data from the BOREAS experiment. Glob. Biogeochem. cycles. 15(1):129–147.

Grant, R.F., Juma N.G., Robertson, J.A., Izaurralde, R.C., McGill, W.B., 2001b. Long-term changes in soil carbon under different fertilizer, manure, and rotation: testing the mathematical model ecosys with data from the Breton plots. Soil Sci. Soc. Am. j. 65(1):205–214.

Grant, R.F., Juma, N.G., McGill, W.B., 1993c. Simulation of carbon and nitrogen transformations in soils. I: mineralization. Soil Biology & Biochemistry. 25:1317–1329.

Grant, R.F., Kimball, B.A., Brooks, T.J, Wall, G.W., Pinter Jr, P.J., Hunsaker, D.J., Adamsen, F.J., Lamorte, R.L., Leavitt, S.W., Thompson, T.L., Matthias, A.D., 2001c. Modeling Interactions among carbon dioxide, nitrogen, and climate on energy exchange of wheat in a free air carbon dioxide experiment. Agronomy Journal. 93: 638–649.

Grant, R.F., Nyborg, M., Laidlaw, J., 1993a. Evolution of nitrous oxide from soil: I. Model development. Soil Sci. 156:259–265.

Grant, R.F., Nyborg, M., Laidlaw, J., 1993b. Evolution of nitrous oxide from soil: II. Experimental results and model testing. Soil Sci. 156:266–277.

Grant, R.F., Izaurralde, R.C., Nyborg, M., Malhi, S.S., Solberg, E.D, Jans-Hammermeister, D., Stewart, B.A., 1998. Modeling tillage and surface residue effects on soil C storage under ambient vs. elevated CO2 and temperature in ECOSYS. In: Soil processes and the carbon cycle. (Ed. Lal, R., Kimble, J.M., Follett, R.F.). CRC Press Inc.; Boca Raton; USA. 527-547.

Grant, R.F., Wall, G.W., Kimball, B.A., Frumau, K.F.A., Pinter, P.J.Jr, Hunsaker, D.J., Lamorte, R.L., 1999b. Crop water relations under different CO_2 and irrigation: testing of ECOSYS with the free air CO_2 enrichment (FACE) experiment. Agricultural and Forest Meteorology. 95:27–51.

Harrison, R. and Webb, J., 2001. A review of the effect of N fertilizer type on gaseous emissions. Advances in Agronomy. 73:65-108.

Huggett, R.J., 1975. Soil landscape systems: A model of soil genesis. Geoderma. 13:1-22.

Intergovernmental Panel on Climate Change (IPCC), Climate Change 2001: The Scientific Basis: Contribution of Working Group I to the Third Assessment Report of the Intergovernmental Panel on Climate Change, 881 pp., Cambridge Univ. Press, New York, 2001.

Intergovernmental Panel on Climate Change (IPCC), Organization for Economic Cooperation and Development (OECD) and International Energy Agency (IEA),

Revised 1996 IPCC Guidelines for National Greenhouse Gas Inventories, Organ. for Econ. Coop. Dev., Paris, 1997.

International Fertilizer Industry Association, Food and Agriculture Organization of the United Nations, 2001. Global estimates of gaseous emissions of NH_3, NO and N_2O from agricultural land.

Isaaks, E.H., and Srivastava, R.M., 1990. An Introduction to Applied Geostatistics. Oxford Univ. Press, New York.

Jacinthe, P.A. and Dick, W.A., 1997. Soil management and nitrous oxide emissions from cultivated fields in southern Ohio. Soil and Tillage Research. 41(3-4):221–235.

Kaiser, E.A., Kohrs, K., Küchke, E., Schnug, E., Heinemeyer, O., Munch, J.C., 1998. Nitrous oxide release from arable soil: importance of N fertilization, crops and temporal variation. Soil Biol. Biochem. 30(12):1553–1563.

Kelly, R.H., Parton, W.J., Hartman, M.D., Stretch, L.K., Ojima, D.S., Schimel, D.S., 2000. Intra and interannual variability of ecosystem processes in shortgrass steppe. Journal of Geophysical Research: Atmospheres. 105:20093–20100.

Kroeze, C., Mosier, A.R., Bouwman, L., 1999. Closing the global N2O budget: a retrospective analysis 1500-1994. Global Biogeochemical Cycles. 13:1-8.

Laville, P., Jambert, C., Cellier, P., Delmas, R., 1999. Nitrous oxide fluxes from a fertilised maize crop using micrometeorological and chamber methods. Agricultural and Forest Meteorology. 96(1-3):19-38.

Lemke, R.L., Izaurralde, R.C., Malhi, S.S., Arshad, M.A., Nyborg, M., 1998. Nitrous oxide emission from agricultural soils of the Boreal and parkland regions of Allberta. Soil Sci. Soc., Am. J. 62:1096–1102.

Lemke, R.L., Izaurralde, R.C., Nyborg, M., Solberg, E.D., 1999. Tillage and N source influnce soil-emitted nitrous oxide in the Alberta Parkland region. Canadian Journal of Soil Science. 79(1):15–24.

Lexer, M.J., and Honninger, K., 1998. Estimating physical soil parameters for sample plots of large-scale forest inventories. Forest Ecology and Management. 111: 231-247.

Li, C., 2000. Modeling trace gas emissions from agricultural ecosystems. Nutrient Cycling in Agroecosystems. 58:259–276.

Li, C., Frolking, S., Frolking, T.A., 1992. A model of nitrous oxide evolution from soil driven by rainfall events. 1. Model structure and sensitivity. Journal of Geophysical Research. 97:9759–9776.

Li, C., Narayanan, V., Harriss, R., 1996. Model estimates of nitrous oxide emissions from agricultural lands in the United States. Global Biogeochemical Cycles. 10:297–306.

Li, T., Grant, R.F., Flanagan, L.B., 2004. Climate impact on net ecosystem productivity of a semi-arid natural grassland: modeling and measurement. Agricultural and Forest Meteorology. 126:99–116.

Lim, B., Bioleau, P., Bonduki, Y., van Amstel, A.R., Janssen, L.H.J.M., Olivier, J.G.J., Kroeze, C., 1999. Improving the quality of national greenhouse gas inventories. Environmental Sciences and Policy. 2:335–346.

Liu, S.G., Reiners, W.A., Keller, M., Schimel, D.S., 2000. Simulation of nitrous oxide and nitric oxide emissions from tropical primary forests in the Costa Rican Atlantic Zone, Environmental Modelling and Software. 15(8).727–743.

Mahmood, T., Ali, R., Malik, K.A., Shamsi, S.R.A., 1998. Nitrous oxide emissions from an irrigated sandy-clay loam cropped to maize and wheat. Biological Fertilizer Soils. 27:189–196.

Matthhias, A.D., Blackmer, A.M., Brenmner, J.M., 1980. A simple chamber technique for field measurement of emission of nitrous-oxide from soils. Journal of Environmental Quality. 9(2):251–256.

McBratney, A.B., Odeh, I.O.A., Bishop, T.F.A, Dunbar, M.S., Shatar, T.M., 2000. An overview of pedometric techniques for use in soil survey, Geoderma. 97(3-4):293-327.

McBratney, A.B., Mendonca Santos, M.L., Minasny, B., 2003. On digital soil mapping. Geoderma. 117(1-2):3–52.

Mogge, B., Kaiser, E.A., Munch, J.C., 1999. Nitrous oxide emissions and denitrification N-losses from agricultural soils in the Bornhoved Lake region: influence of organic fertilizers and land-use. Soil Boilogy and Biochemistry. 31:1245–1252.

Monni, S., Syri, S., Savolainen, I., 2004. Uncertainties of the Finnish greenhouse gas emission inventory. Environmental Science & Policy. 7:87–98.

Mosier, A. and Kroeze, C., 2000. Potential impact on the global atmospheric N_2O budget of the increased nitrogen input required to meet future global food demands, Chemosphere - Global Change Science. 2(3-4):465–473.

Mosier, A., Kroeze, C., Nevison, C., Oenema, O., Seitzinger, S., van Cleemput, O., 1999. An overview of the revised 1999 IPCC guidelines for national greenhouse gas inventory methodology for nitrous oxide from agriculture. Environment Science & Policy, 2, 325–333.

Mosier, A.R. and Hutchinson, G.L., 1981. Nitrous-oxide emissions from cropped fields. Journal of Environmental Quality. 10(2):169–173.

Mosier, A.R., Hutchinson, G.L., Sabey, B.R., et al., 1982. Nitrous-oxide emissions from barley plots treated with ammonium-nitrate or sewage-sludge. Journal of Environmental Quaility. 11(1):78–81.

Mosier, A.R., Stillwell, M., Parton, W.J. et al., 1981. Nitrous-oxide emissions from a native shortgrass prairie. Soil Sci. Soc. Am. J. 45(3):617–619.

Mueller and Pierce, 2003. Soil carbon maps: Enhancing spatial estimates with simple terrain attributes at multiple scales. Soil Sci. Soc. Am. J. 67:258–267.

Myrold, D.D., 1988. Denitrification in rye-grass and winter wheat cropping systems of western Oregon. Soil Science Society of America Journal. 52:412–416.

Olsen, K., Wellisch, M., Bioleau, P., Blain, D., et al., 2003. Canada's greenhouse gas inventory (1990 – 2001). ISBN 0-662-35106-1, Environment Canada.

Park, S.J. and Vlek, L.G., 2002. Prediction of three-demensional soil spatial variability: a comparison of three environmental correlation techniques. Geoderma. 109:117–140.

Parton, W.J., Hartman, M.D., Ojima, D.S., Schimel, D.S., 1998. DAYCENT: its land surface submodel: description and testing. Global Planetary Change. 19:35–48.

Parton, W.J., Mosier, A.R., Ojima, D.S., Valentine, D.W., Schimel, D.S., Weier, K., Kulmala, A.E., 1996. Generalized model for N2 and N2O production from nitrification and denitrification. Global Biogeochem. Cycles. 10:401–412.

Parton, W.J., Mosier, A.R., Schimel, D.S., 1988. Rates and pathways of nitrous oxide production in a shortgrass steppe. Biogeochemistry. 6:45–58.

Paul, E.A.; and Clark, F.E., 1996. Soil microbiology and biochemistry. Second edition, Academic Press.

Pennock, D.J. and Corre, M.D., 2001. Development and application of landform segmentation procedures, Soil and Tillage Research. 58(3-4):151–162.

Pennock, D.J.; van Kessel, C.; Farrell, R.E.; Sutherland, R.A., 1992. Landscape-scale variations in denitrifcation. Soil Sci. Soc. Am. J. 56:770–776.

Robertson, G.P., 1989. Nitrification and denitrification in humid tropical ecosystems: potential control on nitrogen retention. In: Proctor, J. (Ed.), Mineral Nutrients in Tropical Forest and Savanna Ecosystems. Blackwell Scientific Publishers, Oxford, UK, 55–69.

Röver, M., Heinemeyer, O., Munch, J.C., Kaiser, E.A., 1999. Spatial heterogeneity within the plough layer: high variability of N_2O emission rates. Soil Biology and Biochemistry. 31(2):167–173.

Scott, A., Crichton, I., Ball, B.C., 1999. Long-term monitoring of soil gas fluxes with closed chambers using automated and manual systems. J. Environ. Qual. 28:1637–1643.

Sozanska, M., Skiba, U., Metcalfe, S., 2002. Developing an inventory of N_2O emissions from British soils. Atmospheric Environment. 36(6):987–998.

Stafford, J.V., 2000. Implementing precision agriculture in the 21st century. J. Agric. Engng. Res. 76:267–275.

Thornton, F.C., Bock, B.R., Tyler, D.D., 1996. Soil emissions of nitric oxide and nitrous oxide from injected anhydrous ammonium and urea. Journal of Environmental Quality. 25:1378–1384.

Van Kessel, C.; Pennock, D.J.; Farell, R.E., 1993. Seasonal variations in denitrifcation and nitrous evolution at the landscape scale. Soil Sci. Soc. Am. J. 57:988–995.

Wagner-Riddle, C., Thurtell, G.W., King, K.M., Kidd, G.E., Beauchamp, E.G., 1996. Nitrous oxide and carbon dioxide fluxes from a bare soil using a micrometeorological approach. Journal of Environmental Quality. 25:898–907.

Weitz, A.M., Linder, E., Frolking, S., Crill, P.M., Keller, M., 2001. N_2O emissions from humid tropical agricultural soils: effects of soil moisture, texture and nitrogen availability. Soil Biology and Biochemistry. 33(7-8):1077–1093.

Williams, D.Li., Ineson, P., Coward, P.A., 1999. Temporal variations in nitrous oxide fluxes from urine-affected grassland. Soil Biology and Biochemistry. 31(5):1999, 779–788.

Xu-Ri, Wang, M., Wang, Y., 2003. Using a modified DNDC model to estimate N_2O fluxes from semi-arid grassland in China, Soil Biology and Biochemistry. 35(4):615–620.

Yamulki, S., Goulding, K.W.T., Webster, C.P., Harrison, R.M., 1995. Studies on no and N_2O fluxes from a wheat field. Atmospheric Environment. 29(14):1627–1635.

Chapter 2: The Prediction of Soil Properties by a Digital Terrain Model and Sensitivity of N_2O Emissions to Uncertainties of Predicted Soil Properties

2.1 Introduction

There has been increasing interest in obtaining detailed information on spatial variation in soil properties with growing adoption of precision agriculture (Booltink, et al., 2001; Stafford, 2000), and fine scale soil maps (Zhu et al. 2004; Mueller and Pierce, 2003; Florinsky and Arlashina, 1998; Lexer and Honninger, 1998). This information is also needed for simulating landscape spatial variations in greenhouse gas emissions (Grant and Pattey, 2003), soil water retention (Romano and Palladino, 2002), crop yield (Garcia et al., 2000), and ecosystem productivity (Gessler et al., 2000). Detailed soil sampling and laboratory analyses are rarely possible because of high cost and time requirements. Many attempts have been made to establish correlations between soil properties and more readily available information, about vegetation, management practice, parent material, and topography (Park and Vlek, 2002). Many such correlations, which are used to extend sparse and expensive soil measurements, have been studied in the last two decades (McBratney et al., 2003; Bishop and McBratney, 2001; McBratney et al., 2000). The Scorpan model, which was developed from Jenny's (1941) famous equation, uses soil properties, climate, vegetation, terrain attributes, landscape position, parent material, and history or age of land as predictors of soil properties. Scorpan has been widely used although earlier research did not involve all the predictors in this equation (McBratney et al., 2003).

Prediction methods based on Scorpan can be classified into three groups (Bishop and McBratney, 2001). First, statistical methods are used to establish the correlations between land surface information and soil properties, then soil properties can be predicted by multiple linear regression (Bishop and McBratney, 2001; Ryan et al., 2000), regression tree (Park and Vlek, 2002), artificial neural networks (Park and Vlek, 2002; McBratney et al., 2000; Zhu, 2000), fuzzy-logic (Carre and Girard, 2002; MacMillan et al., 2000; Zhu and Band, 1994), or Bayesian rules (Lilburne et al., 1998). Second, geostatistical methods

such as ordinary kriging (Oberthur et al. 1999), kriging and co-kriging (Chaplot et al., 2000; Knotters et al., 1995; Odeh et al. 1994, 1995) are widely used in some models for mapping soil properties. Third, hybrid methods involve the integration of statistical and geostatistical methods. Regression-kriging adds the kriged residual values to regression predictions (Odeh et al., 1995, Bishop and McBratney, 2001). Kriging with external drift uses the local mean of the target variables and performs simple kriging on the residuals (Goovearts, 1999; Bishop and McBratney, 2001). Most of these methods use terrain attributes, land use and coverage types, which can be easily derived from topographical maps and remote sensing data, to build the prediction function.

The selection of predictors in Scorpan strongly depends on the soil properties that need to be estimated. Terrain attributes are one of the most frequently used predictors. The accuracy with which soil properties have been predicted has varied greatly with different terrain attributes used as predictors, so the key to predicting soil properties more accurately is the selection of appropriate terrain attributes rather than prediction methods (Park and Burt, 2002).

Terrain attributes are indicators of microtopographic characteristics. Microtopography influences the spatial distribution of soil moisture, pH, salts and free ions (Kovda et al., 1992), and hence soil formation (Buol et al., 1973). Therefore, terrain attributes provide a general knowledge of spatial patterns associated with the redistribution of water, solute and sediment in vertical and lateral directions through the landscape. Water is a fundamental factor of soil formation. Where soil water conditions are favorable, such as at concave slopes and water accumulating areas, pedogenic processes are active because soil water accelerates rates of soil physical, chemical and biological processes. Terrain attributes are found to influence almost all soil formation processes and are therefore related to soil water content (Oztas et al., 2003; Pennock and Corre, 2001; Gobin et al., 2000; Florinsky et al., 1998; Osher and Buol, 1998; King et al., 1994; Odeh et al., 1991) and nutrient content, hence to plant growth and community type (Oztas et al., 2003), microbial activities (Florinsky et al., 2003), nutrient accumulation and transformation, mass and energy transport, lateral and vertical redistribution of soil material (Kachanoski and Carter, 1999), and physical and chemical weathering. These soil formation processes result in different soil properties including horizon thicknesss (Gessler et al., 1995;

Kachanoski et al., 1985a, b; Bell et al., 1994; Moore et al., 1993; Carter and Ciolkosz, 1991; Pennock et al., 1987), soil texture (Osher and Buol, 1998; King et al., 1994; Odeh et al., 1991), pH, organic matter contents (Oztas et al., 2003; Pennock and Corre, 2001; Wang et al., 2001; Osher and Buol, 1998; Moore et al., 1993), and nitrogen (Wang et al., 2001) and other nutrients (Wang et al., 2001; Moore et al., 1993; Carter and Ciolkosz, 1991; Martz and de Jong, 1990). Spatial differences in mobility of water, solutes and sediment, and differential responses of soil materials to pedological and ecological processes arising from these differences in mobility, result in spatial variation of soil over a landscape (Park and Vlek, 2002; Huggett, 1975), and soil properties can be estimated based on relationships between terrain attributes and soil properties (McBratney et al., 2003). The estimated soil properties can be used for detailed soil mapping (Zhu et al. 2004; Mueller and Pierce, 2003; Florinsky and Arlashina, 1998; Lexer and Honninger, 1998) and ecosystem management (Booltink, et al., 2001; Garcia, et al., 2000; Gessler et al., 2000; Stafford, 2000) although with some uncertainty (Bui and Moran, 2003; McBratney et al., 2002; Chiles and Delfiner, 1999; Deutsch and Journel, 1998; Goovaerts, 1997; Cressie, 1993; Isaaks and Srivastava, 1990).

If soil N_2O emissions are calculated from the estimated soil properties with their uncertainties, the sensitivities of N_2O emissions to these uncertainties will determine whether these estimations can be used for modeling N_2O emissions. If the estimated soil properties can be used to estimate N_2O emission, the large temporal and spatial variability of N_2O emissions can be captured simultaneously in landscape, field and regional scales with a combination of detailed soil properties and mathematical modeling (Grant and Pattey, 2003). Large temporal and spatial variations of N_2O flux rates are a main source of error in estimating cumulative N_2O fluxes from cultivated soils (Flessa et al., 2002; Scott et al., 1999). Current measurement methods, such as micrometeorology and chamber techniques, have difficulty in catching the temporal and spatial variability simultaneously. These methods also have uncertainties in flux measurements and therefore large cumulative errors in N_2O emissions (Flessa et al., 2002; Laville et al., 1999; Brumme and Beese 1992). Therefore, the combination of detailed soil properties and mathematical modeling may provide more accurate estimation of N_2O emissions. However, the magnitude of the uncertainty in N_2O emissions that results from the

uncertainty of soil properties is unclear. The propagation of uncertainties in N_2O emissions from uncertainties of soil properties will determine the usefulness of the mathematic modeling technique to address the temporal and spatial variability of N_2O emissions, in obtaining reliable estimations of N_2O emissions in landscape, field, regional, and even national scales.

The objectives of this study were (1) to investigate the ability to predict soil properties from terrain attributes in agricultural land with hummocky topography in a western Canadian prairie, and (2) to investigate the sensitivity of N_2O emissions to uncertainties of soil properties, then to determine whether or not the estimated soil properties can be used to simulate landscape N_2O emissions.

2.2 Study site and field methods

2.2.1 Study site

The study site (Fig. 2.1) is a 76 ha field representative of the black soil region in the aspen parkland ecoregion in east-central Alberta, near Viking, Alberta, Canada. Average precipitation was 359 mm, and average air temperature was 2.8 °C from 1996 to 2002. This site has hummocky topography with a moderate slope (10-13%) and elevation difference of less than 12 m. It is representative of hummocky glaciated landscapes in the western prairies of Canada. Black Chernozemic soils are the dominant soil type. The site is under a conventional cultivation system with a wheat-barley-canola crop rotation fertilized with 86, 13, 76 kg N ha^{-1}, respectively. The entire site was stratified into 10×10 m grid cells for predicting soil properties. One sub site F1 (3.23 ha. Fig. 2.1) was selected from the entire site for testing sensitivity of N_2O emissions to predicted soil properties. The difference of elevation within F1 was less than 8 m.

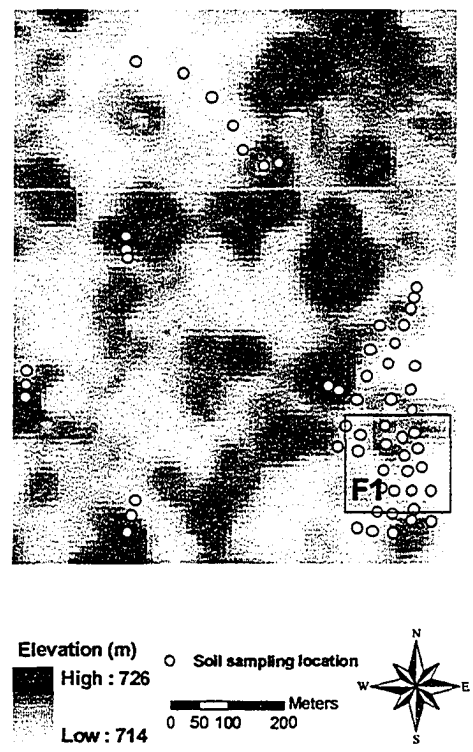

Figure 2.1: The study site, soil profile locations and sub site of sensitivity study of N_2O emissions in east center of Alberta, Canada (53°05'N, 111°47'W).

2.2.2 Field sampling and laboratory analysis of soil properties

Three to five soil samples were collected from each of 57 soil profiles that were 50-100 cm deep and represented different landscape types in the study site. The geographic position of each soil profile was recorded by a global positioning system (Garmin GPS-III plus with accuracy 1 to 5 meters for position, Garmin International Inc. Olathe, KS, USA), and thicknesses of A and B horizons were measured on soil profile core. About 1 kg of composite soil sample was taken from each of A, B and C horizons in each profile. Soil samples were analyzed for clay, silt and sand contents, pH, and total organic carbon (TOC) and total organic nitrogen (TON). Soil samples were air-dried and ground to pass through a 2 mm sieve. Soil texture was analyzed using sedimentation hydrometer methods. Water-based (2:1 in water to soil) pH was measured with an electronic meter. TOC was measured by a 6N HCl acidification in a tin container followed by Dumas combustion protocol. TON was analyzed by Carlo-Erba, NA-1550 N+C Elemental analyser following the Dumas combustion protocol.

In the hummocky agricultural landscape, the spatial variations of soil properties were from 11% to 64% for 20 soil properties (Table 2.1). Over the landscape, soil texture was similar in A, B and C horizons, and pH increased from surface to deeper soil horizons. TOC and TON were found mainly in the A horizon, and concentration reduced to one third in the B horizons and one sixth in the C horizons. This large variation in soil properties was used for model calibration and validation.

Table 2.1: Mean and coefficient of spatial variation (CSV – ratio (%) of standard deviation to mean over landscape) of measured soil properties in a hummocky agricultural landscape.

Horizon	Item	Thickness	Texture (%)			Chemical Properties		
		(cm)	Clay	Silt	Sand	pH	TOC (g C/kg)	TON (mg N/kg)
A	M ± SD[§]	24 ± 13	21 ± 4	33 ± 7	46 ± 7	6.1 ± 0.7	35 ± 13	3108 ± 1057
	CV	54	19	21	15	11	37	34
B	M ± SD	35 ± 16	26 ± 5	32 ± 8	42 ± 9	6.9 ± 0.8	11 ± 7	1149 ± 609
	CV	46	19	25	21	12	64	53
C	M ± SD	--	23 ± 6	34 ± 8	43 ± 8	8.0 ± 0.9	6 ± 2	577 ± 242
	CV	--	26	24	19	11	33	42

[§]: "M" and SD indicates the average and standard deviation of measured soil properties over landscape.

2.2.3 Calculating terrain attributes

A digital elevation map (DEM) was generated at a 10-meter resolution in ArcGIS 8.2 (from ESRI, 2002) by kriging interpolation from field data measured by a high accuracy differential global positioning system (GPS). Terrain attributes (TA) were calculated by ArcGIS 8.2 and Terrain Analysis Using Digital Elevation Models 2.0 (TauDEM. Tarbonton, 2002) from DEM. Twelve terrain attributes described below were used as predictors for soil properties in this study (Table 2.2).

Table 2.2: Terrain attributes used for predictions of soil properties in the study site at Viking, Alberta, Canada.

Terrain attribute		Description	Source or reference
RE	Relative elevation (m)	Elevation difference between grid cell and mean of entire field.	
AS	Aspect (Degree in clockwise from north)	Direction of steepest slope.	Shary et al., 2002
SP	Slope (%)	Slope percentage.	Shary et al., 2002
CA	Catachment Area (m^2)	Total upslope area to each grid cell.	Shary et al., 2002
SCA	Special catachment area (m^2 m^{-1})	CA per unit contour width.	TauDEM. Tarboton, 2002
TUL	Total upslope length (m)	Total length of upslope flow paths terminating at each grid cell.	TauDEM. Tarboton, 2002
LUL	Longest upslope length (m)	Length of the longest upslope flow path terminating at each grid cell.	TauDEM. Tarboton, 2002
IWI	Inverse Wetness Index (m m^{-3})	The ratio of slope to catchment area. (IWI=SP'/CA). SP' is slope in m m^{-1}.	TauDEM. Tarboton, 2002
SPI	Stream Power Index (m^3 m^{-1})	SPI = SP*CA.	Florinsky et al., 2002; Moore et al., 1991
PLC	Plan curvature (Degree m^{-1})	Curvature along contour line.	Shary et al., 2002
PFC	Profile curvature (Degree m^{-1})	Vertical curvature along slope profile.	Shary et al., 2002
TCI	Terrain Complexity Index (dimensionless)	TCI = PFC'*$\log_{10}$(SCA). PFC' is elevation difference of each grid to surrounding grid cells in 3 by 3 moving windows.	Park et al., 2001.

Relative elevation (RE) (Table 2.2) is the difference between elevation of a local grid cell and the mean elevation of the entire field (Fig. 2.2a). REs exercise significant influence over the spatial distribution of soil properties in agricultural landscapes

(MacMillan et al., 2000; Brubaker et al., 1993; Miller et al., 1985). Grid cells with negative RE are likely to be downslope, and hence accumulating water and sediments and to develop thicker and more fertile soil layers. Grid cells with a positive RE are likely to be upslope, and hence sources of water and sediments and to develop thinner and poorer soil layers. The REs were normally distributed in the whole site, but lower areas (RE < 0) were slightly larger than upper areas (RE > 0) (Fig. 2.4a).

Aspect (AS) (Table 2.2) determines the intensity of accepting radiation. It affects evapotranspiration, snow accumulation and melting (Florinsky and Arlashina, 1998; Young, 1972), and indicates the direction of water movement on slopes and thereby the soil spatial distribution. Areas with an AS of 0° – 90° and 270° – 360° (north facing) will receive less radiation energy. These areas were found mainly on hummocky slopes (Fig. 2.2b). All depression areas had greater exposure to radiation with an AS of 90° – 270° (south face). Degree classes of AS occurred at almost equivalent proportions in the entire study site (Fig. 2.4b). This study site is therefore a typical hummocky landscape.

Slope (SP) (Table 2.2) is positively related to flow velocity, and hence erosive power of runoff (Wischmeier and Smith, 1978). Larger SP induces greater flow velocity (Manning's equation, Eq. 2.1) and larger sediment transport capacity of surface flow (Eq. 2.2), so that erosion which is the product of flow volume and transport capacity increases strongly with slope (Morgan et al., 1998a, b). Therefore, the higher the SP, the thinner the A Horizon is at upper slopes in comparison with that at lower slopes. The distribution of SP in the study site corresponds to the RE map (Fig. 2.2a and 2.2c). Higher SPs occur only on the hummocky slopes, and foot slopes possess moderate SPs (Fig. 2.2c). SPs of most grid cells are smaller than 8% (Fig. 2.4c).

$$u = (S^{\frac{1}{2}} r^{\frac{2}{3}}) / n \qquad (2.1)$$

Where u is the velocity of overland flow (cm s^{-1}), S is the slope (cm cm^{-1}), r is the hydraulic radius (cm), and n is Manning's surface roughness ($cm^{-1/3}$ s).

$$TC = c(uS - 0.4)^{\eta} \qquad (2.2)$$

Where TC is the sediment transport capacity of overland flow (g cm^{-3} water), and c and η are experimentally-derived coefficients depending on soil particle size.

Catchment area (CA) (Table 2.2) measures the upslope source area of water, sediment and nutrients for each grid cell. The large CAs occur at foot slopes and depressions, and largest CAs are found mainly in the main flow path network (Fig. 2.2d). The number of grid cells decreases exponentially from small to large CAs, and almost half of all grid cells in the entire site have CAs that include only their own local cell areas ($10\times10 = 100$ m^2) (Fig. 2.4d). **Special catchment area (SCA)** (Table 2.2) indicates the ratio of upslope source area to contour width of a grid cell. Larger SCAs exist at foot slopes and convergences, but smaller SCAs occur at depressions, top slopes and summits because of their larger contour width or smaller upslope source area (Fig. 2.2e). One-third of grid cells have a 10 $m^2 m^{-1}$ SCA, but no grid cell has a SCA about 5 m^2 m^{-1} (Fig. 2.4e). Large CA or SCA values indicate a large collection area of water and sediments, therefore, thick and fine soil layers with high nutrient and water contents are more likely to develop.

Total upslope length (TUL) and **longest upslope length (LUL)** (Table 2.2) are the lengths of up-stream flow paths of water into a local grid cell, and indicate the distance covering which suspended sediment flows to the grid cell, and also indirectly indicate the source area of water and sediment. Grid cells with larger values of TUL and LUL are more likely to accumulate water and sediment or to suffer strong water erosion because of greater detachment along longer flow paths with higher runoff velocity. These grid cells will likely receive fewer coarse soil particles suspended in water because flow distance is longer and coarse particles settle rapidly during overland flow, resulting in a finer soil texture, relatively higher nutrient and water contents, and thicker soil layers. Large values of TUL and LUL always occur at foot slopes and depressions (Fig. 2.2f and 2.2g). Their distributions over the entire site coincide with the distribution of CA (Fig. 2.2d, 2.2f, and 2.2g). Large LUL and TUL are found in the main flow path network, therefore water, solutes and sediment accumulate at lower landscapes where LUL and TUL are large below hummocky hills. However, more than 80% of grid cells in the study site have small TUL and LUL values (Fig. 2.4f and 2.4g), and a few grid cells have large TUL and LUL values as shown in Fig. 2.2f and 2.2g.

Inverse Wetness Index (IWI) (Table 2.2) is the ratio of slope to catchment area (CA). IWI indicates the time and amount of water and sediment that will stay in a grid

cell (Fig. 2.3). Therefore, IWI relates to surface soil water content and sediment deposition in an opposite way to how the wetness index relates (Park and Burt, 2002; Gomez-Plaza et al., 2001). In grid cells with smaller IWI, more sediment is deposited on the surface and more water infiltrates into deeper soil layers. Biological processes of soil formation in these cells are active because of better soil water conditions. As a result, a finer and thicker soil is developed. Because CAs are large at depressional and foot slope areas and the IWIs are therefore low (Fig. 2.2h), water and sediment will stay at foot slopes and depressions for long times. With small CAs and shallow slopes at summits, the low IWIs mean less sediment deposits and lower soil water contents. Large IWIs occur at middle to top slopes because of steep slopes. These areas are the most important source areas of water and sediment as was found in ^{137}Cs research conducted on hummocky landscapes (Pennock, 2003). Almost half of grid cells in the study site have IWI near zero, and the number of grid cells decreases exponentially from low to high IWIs (Fig. 2.4h).

Stream Power Index (SPI) (Table 2.2), which is the product of SP and CA, is the potential erosive power of overland water flows (Florinsky and Arlashina, 1998; Moore et al., 1991). A grid cell with larger SPI likely has coarser soil texture, a thinner surface soil layer, and lower water and nutrient contents due to strong water erosion. Large SPIs occur at lower slopes because CAs are quite large and slopes are moderate (Fig. 2.2i), therefore, strong erosion generally happens at lower slopes. Erosion would be less at summits and depressions because SPIs are very small with almost no slope. The number of grid cells decreases exponentially from low to high SPI values (Fig. 2.4i). More than half of grid cells have SPI near zero. Large SPI indicating likelihood of strong erosion happens only in less than 5% grid cells in the study site.

Plan Curvature (PLC) (Table 2.2) is the rate at which slope changes in the general contour direction and indicates flow convergence or divergence across the dominant slope (Fig. 2.3). Flows diverge when PLC > 0, and flows converge when PLC < 0. When PLC is negative, surface flow is accelerated, increasing erosion and resulting in thinner and coarser soil layers. When PLC is positive, surface flow is decelerated, and erosion decreases and sediment is deposited. Therefore, soil layers are thicker and texture is finer. The irregular distributions of divergent and convergent grid cells reflect the characteris-

tics of a hummocky landscape (Fig. 2.2j). The highest PLCs occur mainly in summits and foot slopes, while the lowest PLCs exist mainly at the upper slopes and convergences (Fig. 2.2j). However, similar proportions of divergence and convergence areas imply a complex topographic landscape (Fig. 2.4j).

Profile curvature (PFC) (Table 2.2) is rate at which slope changes in the direction of the dominant flow path. A negative PFC indicates a concave slope (micro-valley), while a positive one is a convex slope (micro-hill) (Minasny and McBratney, 2001). PFC indicates accelerating or decelerating flow along convex or concave slopes (Shary et al., 2002; Fig. 2.3). Generally, erosion occurs at convex slopes (PFC > 0), while deposition occurs at concave slopes (PFC < 0). As a result, surface soil layers are thinner, textures are coarser, and nutrient and water contents are lower at convexities than at concavities. Convexities exist mainly at upper slopes and saddles, and the highest PFCs are at top slopes (Fig. 2.2k). Concavities occur at lower slopes and depressions, and the lowest PFCs exist mainly at foot slopes (Fig. 2.2k). Concavities and convexities have the same proportion in the study site (Fig. 2.4k).

Topographic complexity index (TCI) (dimensionless, Table 2.2) indicates three-dimensional micro-terrain shapes within a given influencing radius at a grid cell. TCI estimates the sedimentation and transport capacities of overland flow (Park et al., 2001). Positive and negative TCIs are found in gilgai microrelief (Breemen and Buurman, 2002). Positive TCI means that the elevation of the grid cell is lower than those of surrounding grid cells (the gilgai depressions), so that the grid cell acts as a sink of water and soil materials, and has stronger eluviation, shrinking and swelling processes, which lead to the formation of a thick, fine surface soil layer, and high water and nutrient contents. Negative TCI means that the elevation of the grid cell is higher than those of surrounding grid cells (the gilgai mounds), so that the grid cell acts as a source of water and soil materials, and has weaker shrinking and swelling processes, which result in a thin and coarse surface soil layer and low water and nutrient contents (Breemen and Buurman, 2002). The similar proportion of positive and negative TCIs in the study site (Fig. 2.4l) indicates that the number of grid cells which will be sources and sinks of water and soil material is similar from a three-dimensional topographic view. Foot slopes and upper slopes are the main sink and source areas, respectively (Fig. 2.2l).

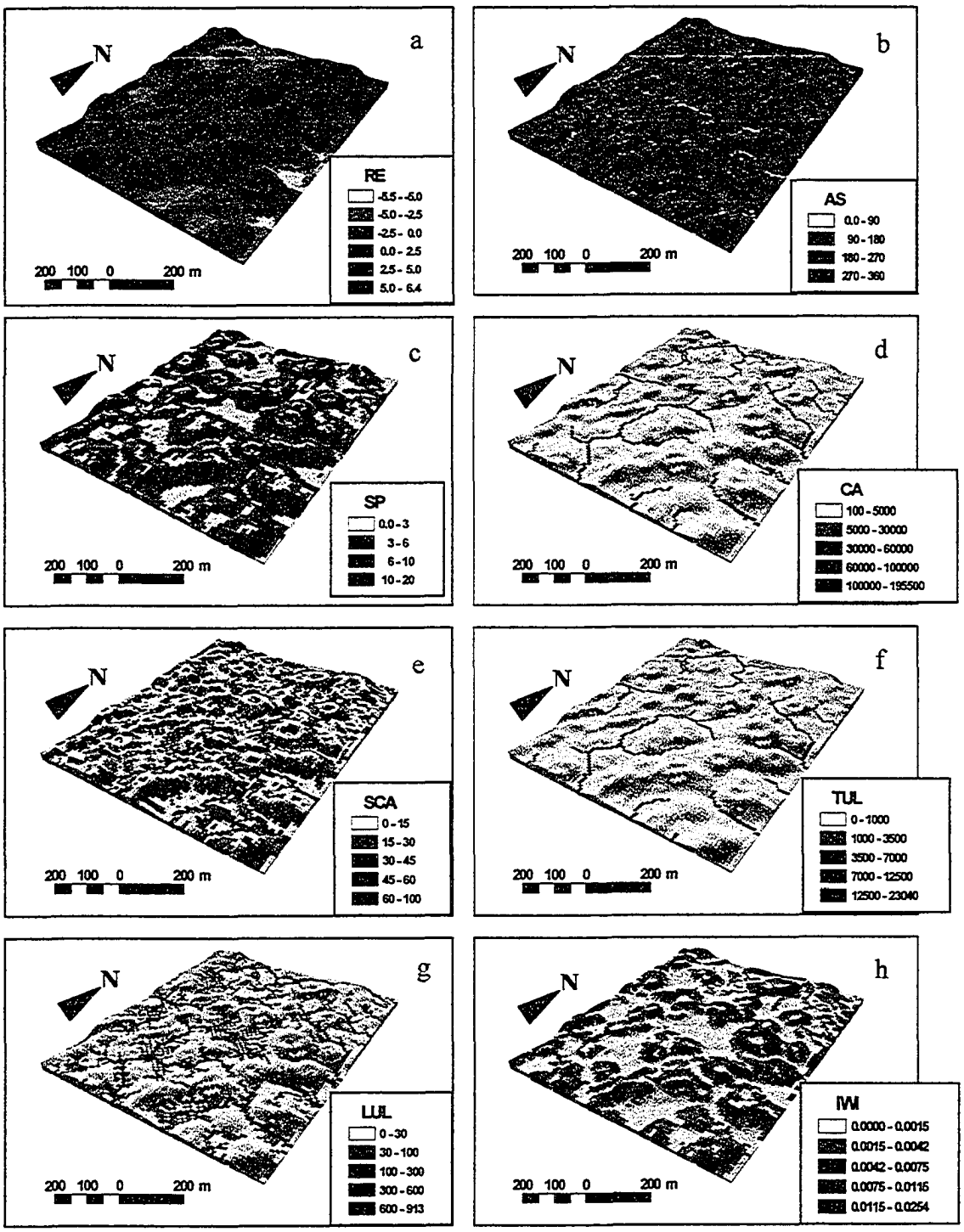

(Continued on next page)

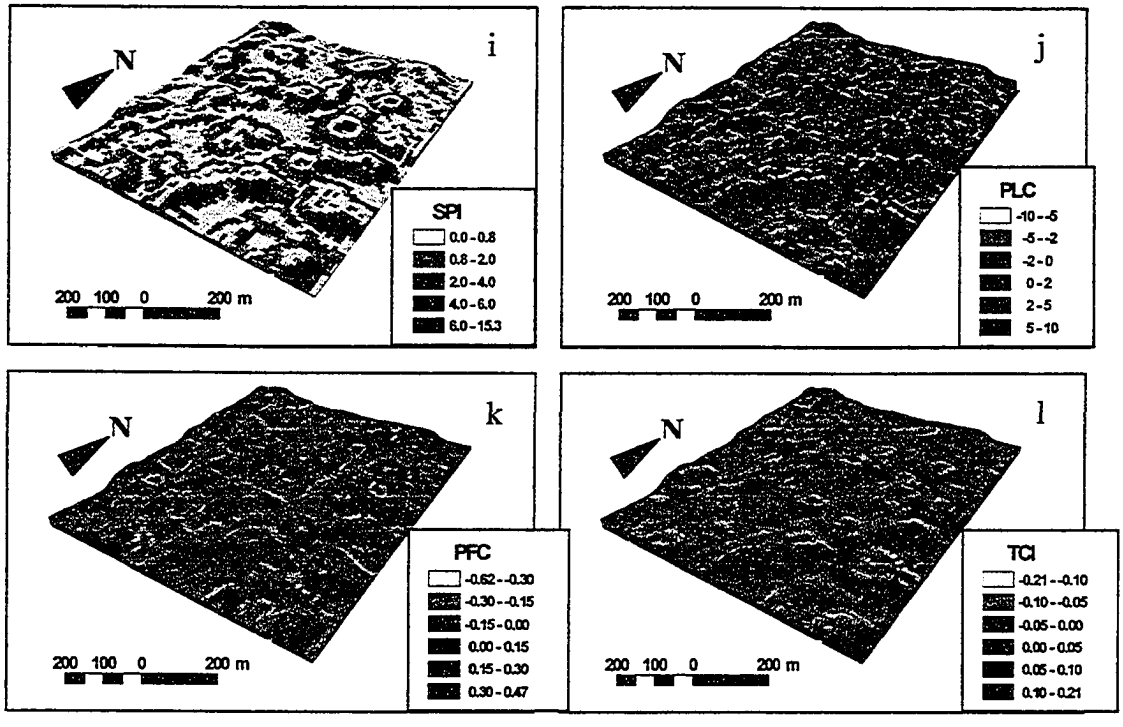

Figure 2.2: The terrain attribute maps of the whole study site. The units are m for RE, TUL and LUL; degree for AS; % for SP; m^2 for CA; $m^2 m^{-1}$ for SCA; m m^{-3} for IWI; $m^3 m^{-1}$ for SPI; degree m^{-1} for PLC and PFC; and no unit for TCI.

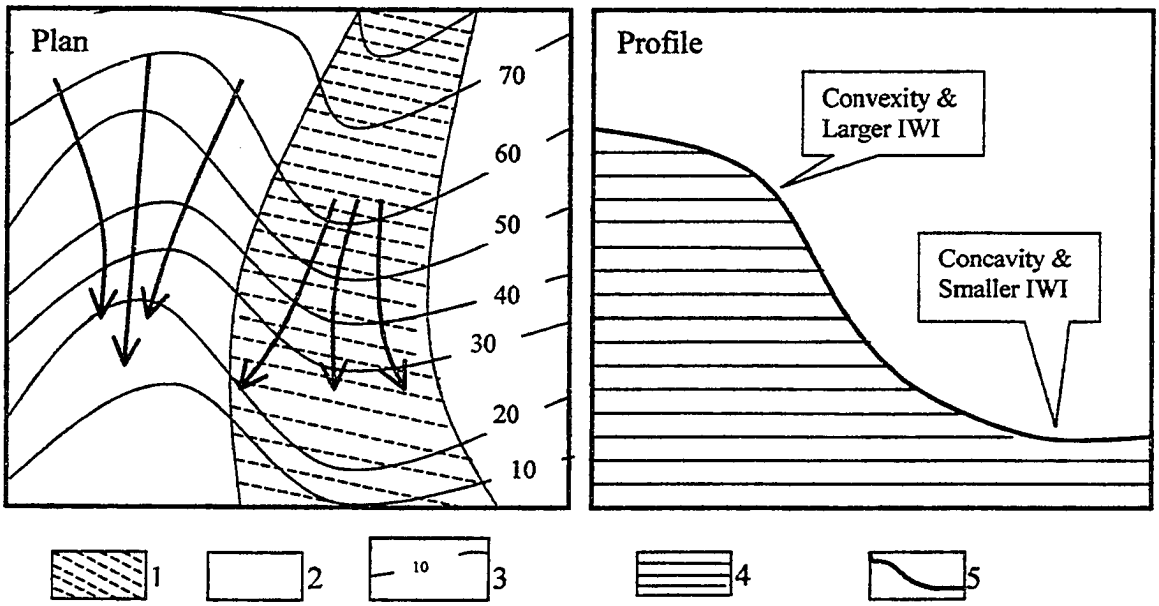

Figure 2.3: The slope shape described in plan and profile curvature. 1 – divergence area, 2 – convergence area, 3 – contour lines, 4 – soil body, 5 – soil surface.

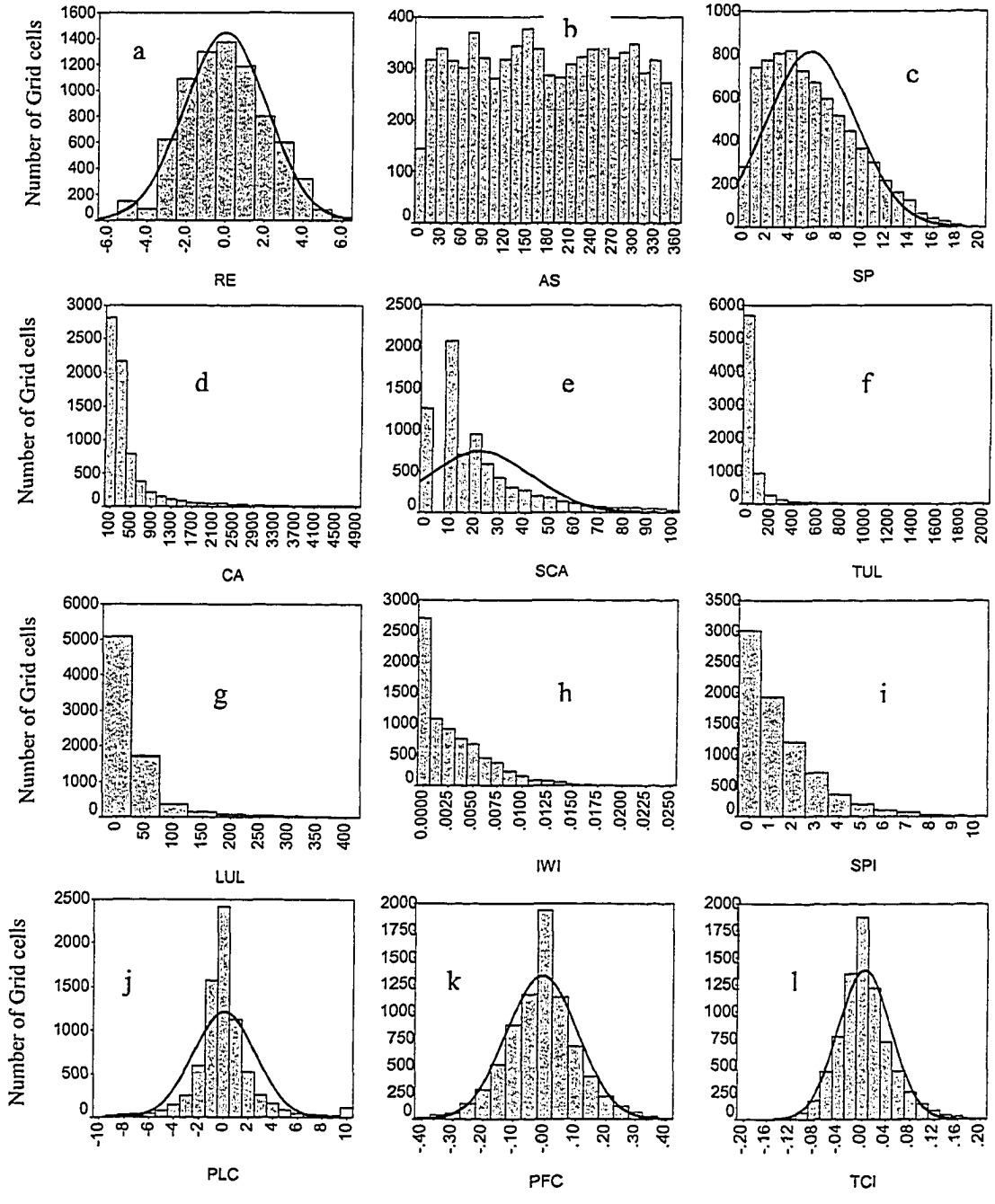

Figure 2.4: The distributions of terrain attributes derived from whole study site. The total amount of grid cells were 7663 with grid cell size 10×10 meters. The units are m for RE, TUL and LUL; degree for AS; % for SP; m^2 for CA; $m^2\ m^{-1}$ for SCA; m m^{-3} for IWI; $m^3\ m^{-1}$ for SPI; degree m^{-1} for PLC and PFC; and no unit for TCI.

The preceding terrain attributes were chosen to build correlations between landscape topographic conditions and soil properties because the current hummocky landscape was developed from glacial till through the processes of water and soil redistributions.

2.3 Methods

2.3.1 Prediction models of soil properties

Stepwise multiple linear model (SMLR), artificial neural network (ANN) and inverse distance weight (IDW) are the common methods used to predict soil properties based on terrain attributes (TAs) (Park and Vlek, 2002; Bishop and McBratney, 2001; McBratney et al., 2000; Ryan et al., 2000; Zhu, 2000). These three methods were used to predict soil properties in a hummocky agricultural landscape at Viking, Alberta, Canada, and the predictions were assessed by independent validation.

Data for horizon thickness (excluding for the C horizon), soil texture, total organic carbon and nitrogen contents, and soil pH in A, B and C horizons in randomly selected 57 soil profiles (Table 2.1) were randomly split into two sub datasets. The calibration dataset consisted of 42 soil profiles used to derive the linear prediction functions in SMLR, to generate the neural network in the ANN, or to perform IDW interpolation in ArcGIS. The independent validation sub dataset consisting of the remaining 15 soil profiles was used to validate the SMLR, ANN or IDW models. During validation and prediction processes, the best two functions of texture were directly used to estimate two of silt, clay and sand contents, and third one depended on the estimated two and was subtracted from 100.

2.3.1.1 Stepwise multiple linear model (SMLR)

A multiple linear regression function was developed for each soil property in each horizon (Table 2.1) by relating 12 TAs (x) to each soil property (y) in each of the 42 soil profiles in the calibration dataset using forward stepwise multiple linear regression methods. The TAs for the grid cells in which the 42 soil profiles in the calibration dataset were located were added into and removed from a multiple linear regression equation to develop the function with the highest correlation and lowest root mean square of error between each predicted and measured soil property. A FORTRAN algorithm was developed to perform this calibration process (Appendix 2.1). This process was repeated for each soil property presented in Table 2.1 to develop 20 different SMLR functions. The advantage of the SMLR was that the non-significant TAs were eliminated from prediction functions, so the predictions of unknown points in soil properties were simplified.

2.3.1.2 Artificial neural network (ANN)

The ANN used in this paper is a multiple layer, back propagation neural network with one hidden layer of 5 nodes and one node in the output layer (Fig. 2.5). Each node in the input layer was one of the 12 TAs, and input values of which were normalized from 0 to 1. The node in the output layer was the predicted soil property of which was also normalized from 0 to 1. The values of each node in the hidden layer (H_j) resulted from a hyperbolic tangent function (for non-linear relationship) transformation of the products (x_j) of input values in the input layer (I_i) and a weighting factor between input and hidden layers ($R_{i,j}$) (Appendix 2.2: Eqs. A2.1 and A2.2). The output value (Y_o) resulted from a hyperbolic tangent function transformation of the products (x_o) of values in the hidden layer (H_j) and a weighting factor between hidden and output layers ($R_{j,o}$) (Eqs. A2.3 and A2.4). The sum of squared errors (E^t) between predicted and measured soil properties and weighting factors (W^t) at a training iteration (t) were respectively calculated from Eqs. A2.5 and A2.6. Each weight-ing factor ($R_{i,j}$ and $R_{j,o}$) was reassigned by Eq. A2.7 for the next iteration. The learning rate (α) and momentum (β) for controlling the convergence rate to final results were fixed (Eq. A2.7).

The calibration dataset was divided into two parts. The internal training data with randomly 85% of input data combinations (e.g. 35 combinations) in the calibration dataset were used to derive the weight factor array (Fig. 2.5), called the neural network topography by following Eqs. A2.1 to A2.7. The remaining calibration data (7 data combinations) were used to test the neural network topography. This process was called the internal test. In this process, the I_i (Eq. A2.1) layer was replaced by normalized terrain attributes of the internal test grid cells to get predicted Y'(soil properties) (Eqs. A2.1 to A2.4), then the root mean square error (*RMSE*) was calculated by comparing predicted values with normalized measurements (Eq. A2.8) before reassigning the weighting factors. After reassigning all weighting factors by Eqs. A2.5 to A2.7, the internal training and testing processes were repeated until one of following three conditions was achieved. 1) *RMSE* in the internal test reached an acceptably low value (normally, *RMSE* $\leq$ 1% or 5% of mean of normalized measurements of soil property), 2) *RMSE* was not improved with further iteration, 3) Training reached a set maximum number of iterations (200000).

The calibration processes of ANN were repeated for each soil property in each horizon (Table 2.1) to get 20 different neural network topographies. When the final neural network topography was used to predict soil properties, the Y' was denormalized by the same function used to normalize values of soil properties used in developing the neural network topography.

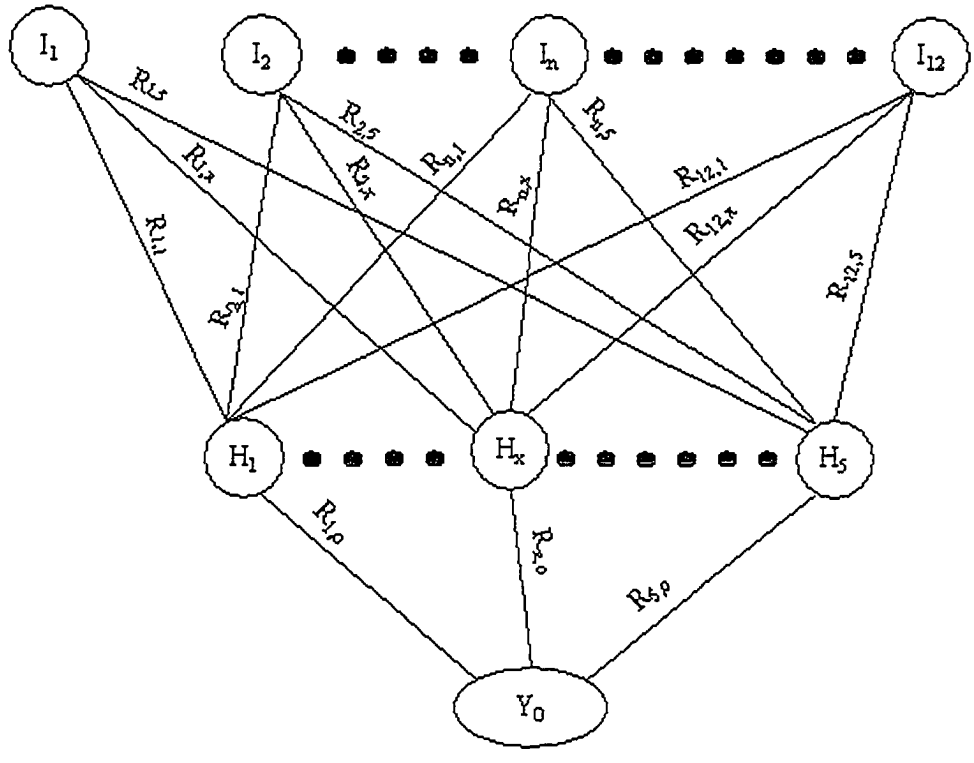

Figure 2.5: The architecture of artificial neural network (ANN). I_1, I_2, to I_{12} are the input layer of 12 terrain attributes. H_1 to H_5 are the nodes of hidden layer. Y_o is a single node of output layer. R is the weighting rate from one layer to next layer.

2.3.1.3 Inverse distance weight (IDW)

IDW is a spatial surface interpolating function of ArcGIS 8.2. The basic assumption of IDW is that things that are close to one another are more alike than those that are farther apart. IDW assumes that each measured point has a local influence that diminishes with distance. IDW will estimate the soil properties of a grid cell by using its surrounding grid cells at which the soil properties have already been measured. Those soil properties measured closest to the grid cell will have more influence on the predicted value than will those farther away. The interpolation was repeated for each soil property in Table 2.1.

2.3.2 Validation of prediction models

The predicting capabilities of SMLR, ANN and IDW were evaluated through independent validations after the regression functions (SMLR) and neural network topographies (ANN) were obtained, and interpolations (IDW) had been done for all soil properties in Table 2.1. All soil properties in the validation dataset predicted by derived SMLR functions or neural network topographies in ANN, and interpolation in IDW. These validations were then evaluated through statistical test.

2.3.2.1 Predictions of soil properties in validation dataset

In SMLR, the TAs from each data combination in the validation dataset replaced corresponding TAs in the regression function for each soil property (Table 2.1) to calculate 15 predicted values for each soil property, which were compared with measured values.

In ANN, the TAs associated with each soil property (Table 2.1) in the validation dataset replaced the corresponding TAs in the input layer of neural network topography to calculate predicted values through Eqs. A2.1 to A2.4 (Appendix 2.2), which were compared with measured values.

In IDW, interpolated soil property values for the 15 profiles in the validation dataset were compared with measured values.

2.3.2.2 Statistical analysis of model validation

Pearson correlation in SPSS statistical software was used to study the relationships between individual TAs and soil properties. Correlations (R^2), normalized mean square error (NMSE) and mean absolute error (MAE) between predicted and measured soil properties in the validation dataset (Eqs. 2.3, 2.4 and 2.5, Park and Vlek, 2002; Gobin et al., 2001) were used to evaluate SMLR, ANN and IDW models. In equations 2.3 to 2.5, n represented the validating dataset size (15), O and P were the measured and predicted values respectively, while $\overline{O}$ and $\overline{P}$ were the means of measured and predicted values respectively, s^2 was the variance of a measured soil property. The R^2 and NMSE allowed for a direct comparison of model performance for different soil properties. The *MAE* and *NMSE* represented the absolute and relative uncertainty of model prediction. The error

ratio (*ER*) calculated for each soil property in each profile (Eq. 2.6) evaluated the probability of different error classes over all soil properties in the validation dataset under SMLR, ANN and IDW by using the histogram method in SPSS.

$$R^2 = \frac{(\sum_{i=1}^{n}(O_i-\overline{O})(P_i-\overline{P}))^2}{(\sum_{i=1}^{n}(O_i-\overline{O})^2)(\sum_{i=1}^{n}(P_i-\overline{P})^2)} \quad (2.3)$$

$$NMSE = \frac{\frac{1}{n}\sum_{i=1}^{n}(O_i-P_i)^2}{s^2} \quad (2.4)$$

$$MAE = \frac{1}{n}\sum_{i=1}^{n}\frac{abs(O_i-P_i)}{O_i} \quad (2.5)$$

$$ER = \frac{O_i-P_i}{O_i} \quad (2.6)$$

2.3.3 Data management

Because input and output datasets were large and impossible to manage manually, the Landscape Soil Property Predictor (LSPP) was developed to perform data management, including calibration of SMLR and ANN models, and prediction of soil properties for specific landscape locations and the entire site with calibrated SMLR and ANN models (Fig. 2.6). IDW was a geostatistical model, for which interpolation could be done in ArcGIS 8.2, therefore it was not integrated into LSPP. The TAs were calculated in ArcGIS and TauDEM, and the results were integrated into text (*.txt), database (*.dbf) or comma delimited (*.csv) files. Output files were represented in a dbf format. The dbf file could be converted into a map format (Appendix 2.3A and 2.3C). LSPP included a main interface (Appendix 2.3A) for file management, a function interface (Appendix 2.3B) for performing calibration and validation of SMLR and ANN, and a mapping interface (Appendix 2.3C) for converting text data into a map.

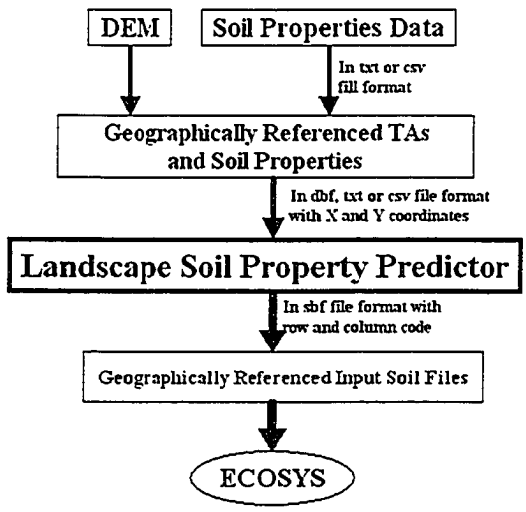

Figure 2.6: The data flow diagram accompanying landscape soil property predictor (LSPP).

2.3.4 Sensitivities of N_2O emissions to uncertainties of soil properties

A sensitivity analysis of N_2O emissions to uncertainties in soil properties was conducted to determine whether the soil properties predicted by LSPP were accurate enough to simulate landscape N_2O emissions. *3D-Ecosys-GIS* (refer to Chapter 3 for details) was used to simulate N_2O emissions over the sub site F1 (Fig. 2.1). *Ecosys*, which is the core of *3D-Ecosys-GIS*, is a three-dimensional biological, biochemical and physical process model, which has the capability to simulate landscape N_2O emission (Grant and Pattey, 2003; Grant et al., 1993a, 1993b). Predicted soil properties varying within uncertainty ranges (See 2.3.4.1) were used to initialize the *3D-Ecosys-GIS* model. Sensitivities of landscape N_2O emissions to uncertainties of predicted soil properties were evaluated by comparing the differences of modeled N_2O emissions from different allocations of soil properties to grid cells within ranges of uncertainty established during LSPP validation (Fig. 2.1).

2.3.4.1 Allocation of soil properties

The uncertainty of each soil property was defined as the standard deviation of ER (Eq. 2.6) between predicted and measured soil properties in the validation dataset. For each grid cell of 323 grid cells in sub site F1, horizon thickness, soil texture, and total organic carbon and nitrogen contents in A and B horizons were randomly allocated within their uncertainties according to combinations in Table 2.3 (e.g. predicted values ± random values within uncertainty). Twelve combinations (Table 2.3) were used to identify the soil properties to which N_2O emissions were the most sensitive. Emissions from these combinations were compared with those from a control combination (CC) which directly used predicted soil properties without any changes. In the *3D-Ecosys-GIS*, uncertainties in soil texture affected soil hydraulic properties, thus soil water content and gas diffusivity, and thereby N_2O emissions. Uncertainties in TOC and TON affected available sources of carbon oxidation, nitrogen mineralization, nitrification and denitrification. Uncertainties in horizon thick-ness affected total amount of TOC, TON and air-filled porosity. Considering that the generation and emission of N_2O often occurs in upper 10 cm soil layers (Payne, 1991), the uncertainties in soil properties of the C horizon were not included in this study. Soil pH was excluded in this study because of its

small spatial variation (Table 2.1). Uncertainties of TOC and TON coincided because measured soil organic C:N ratios varied little through the landscape.

Table 2.3: The combinations of soil properties to be allocated for testing sensitivity of N_2O emissions to uncertainties of predicted soil properties in the hummocky agricultural landscape at Viking, Alberta, Canada. + indicates the soil property was included in a combination of predicted values ± random uncertainties.

Combination code¶	Horizon A				Horizon B			
	Thickness	Texture	TOC	TON	Thickness	Texture	TOC	TON
CC								
ABHTCN	+	+	+	+	+	+	+	+
ABH	+				+			
ABT		+				+		
ABCN			+	+			+	+
AHTCN	+	+	+	+				
AH	+							
AT		+						
ACN			+	+				
BHTCN					+	+	+	+
BH					+			
BT						+		
BCN							+	+

¶ : The letter A and B indicate horizon A and B respectively, H is the horizon thickness, T is the soil texture, and CN is TOC and TON. CC is control combination in which soil property data is taken directly from prediction results.

2.3.4.2 Simulation of N_2O missions

Only one model run for each combination in Table 2.3 was started on January 1, 1999, and ended on December 31, 2001 because of the limitation of computation facility. Except for soil properties, all other inputs of *3D-Ecosys-GIS* including soil and crop management, and hourly climate data were the same for all runs. The crops were canola in the very wet year 1999 (500 mm precip. vs. average of 359 mm), wheat in the wet year 2000 (451 mm precip. > average), and barley in the normal year 2001 (332 mm precip. ≈ average). The outputs in 1999 were not used in the following assessment, in order to exclude the effects of initialized inorganic nitrogen contents on N_2O emissions.

2.3.4.3 Assessing sensitivities of modeled N_2O emissions

The modeled annual N_2O emissions of sub site F1 (3.23 ha. in Fig. 2.1) in the wet year 2000 and the normal year 2001 were used to assess sensitivities of N_2O emissions to

uncertainties of soil properties. Uncertainties of N_2O emissions (*ER* in %) were calculated from Eq. 2.6, where O_i and P_i were the annual N_2O emissions of sub site F1 from CC and one of the combinations in Table 2.3, respectively. The uncertainties of N_2O emissions were evaluated by comparing them with the uncertainties of current measure-ment methods reviewed from literature. Predicted soil properties from LSPP could be used to simulate landscape N_2O emissions, unless these sensitivities were greater than the uncertainties in current measurement methods.

2.4 Results

2.4.1 Relationships between terrain attributes and measured soil properties

In the A horizon, decreases of PFC from convexities (PFC > 0) to concavities (PFC < 0) were associated with increased horizon thickness, silt, TOC and TON contents, and with decreased clay content (Table 2.4). Decreases of PLC from divergences (PLC > 0) to convergences (PLC < 0) were associated with decreased horizon thickness, silt, TOC and TON contents, and with increased clay and sand contents and soil pH. Decreases of RE from upper to lower positions were associated with increased horizon thickness, silt, TOC and TON contents, and with decreased clay content. When SP increased from shallow to steep, silt content and soil pH decreased. With larger CA and TCI, and longer TUL and LUL, clay content declined, but silt, TOC and TON contents rose. Moreover, horizon thickness increased, and sand content and soil pH decreased with longer LUL. With higher TCI, horizons were thicker and soil pH was lower. When IWI increased, horizon thickness, silt, TOC and TON contents decreased, but clay content increased. These relationships between TAs and soil properties were similar in the B and C horizons, but were less pronounced. These relationships were consistent with the expectations described for these TAs in 2.2.3.

The correlations between TAs and soil properties were also consistent with those found in other research (Oztas et al., 2003; Wang et al., 2001; Osher and Buol, 1998; Gessler et al., 1995; Bell et al., 1994; King et al., 1994; Moore et al., 1993; Carter and Ciolkosz, 1991; Odeh et al., 1991; Martz and de Jong, 1990; Kachanoski et al., 1985a, b), especially on hummocky landscapes over glacial till as in this study (Pennock and Corre, 2001; Pennock et al., 1987). These relationships are frequently found, but may vary with

Table 2.4: Pearson correlation (R) between measured soil properties and their local TAs derived from a DEM of the hummocky landscape at Viking, Alberta, Canada.

Terrain Attributes[§]	Thickness of Horizon	Texture			Chemical Properties		
		Clay	Silt	Sand	pH	TOC	TON
		Horizon A					
Profile curvature (PFC)	-0.52**	0.40**	-0.40**	0.15	0.22&	-0.62**	-0.60**
Plan curvature (PLC)	0.64**	-0.34*	0.55**	-0.34*	-0.33*	0.58**	0.59**
Relative elevation (RE)	-0.51**	0.50**	-0.32*	0.02	0.24&	-0.60**	-0.59**
Slope (SP)	-0.13	0.07	-0.30*	0.24&	-0.35**	-0.18	-0.16
Aspect (AS)	-0.06	-0.09	0.02	0.04	-0.05	-0.09	-0.11
Catchment area (CA)	0.19	-0.28*	0.45*	-0.26&	-0.19	0.38**	0.39**
Total upslope length (TUL)	0.19	-0.28*	0.44**	-0.25&	-0.18	0.38**	0.39**
Longest upslope length (LUL)	0.43**	-0.29*	0.55**	-0.36**	-0.27*	0.52**	0.53**
Special catchment area (SCA)	-0.10	0.02	-0.24&	0.21	-0.09	-0.01	-0.02
Terrain complex index (TCI)	0.57**	-0.37**	0.39**	-0.17	-0.27&	0.68**	0.66**
Stream power index (SPI)	-0.10	0.01	-0.24&	0.21	-0.22&	-0.04	-0.02
Inverse wetness index (IWI)	-0.55**	0.40**	-0.46**	0.21	0.15	-0.62**	-0.60**
		Horizon B					
Profile curvature (PFC)	-0.15	0.08	-0.37**	0.28**	0.34*	-0.33*	-0.34**
Plan curvature (PLC)	0.19	0.13	0.41**	-0.44**	-0.43**	0.38**	0.47**
Relative elevation (RE)	-0.39**	-0.20	-0.14	0.32*	0.09	0.03	-0.01
Slope (SP)	0.47**	-0.12	-0.28*	0.29*	-0.21	-0.27&	-0.32*
Aspect (AS)	-0.07	-0.23&	0.03	0.07	-0.05	-0.04	-0.06
Catchment area (CA)	0.02	0.06	0.17	-0.21	-0.34**	-0.01	0.00
Total upslope length (TUL)	0.02	0.06	0.16	-0.20	-0.34**	-0.01	-0.01
Longest upslope length (LUL)	0.11	0.23&	0.30*	-0.44**	-0.39**	0.06	0.09
Special catchment area (SCA)	0.18	0.03	-0.17	0.13	0.14	-0.15	-0.14
Terrain complex index (TCI)	0.16	-0.01	0.39**	-0.39**	-0.48**	0.42**	0.44**
Stream power index (SPI)	0.42**	-0.03	-0.21	0.20	-0.05	-0.23&	-0.24&
Inverse wetness index (IWI)	-0.14	-0.17	-0.22&	0.37**	0.26&	-0.28*	-0.31*
		Horizon C					
Profile curvature (PFC)		0.16	0.05	0.26&	0.32*	0.22&	0.04
Plan curvature (PLC)		-0.42**	-0.1	-0.39**	-0.46**	-0.21	-0.09
Relative elevation (RE)		0.43**	0.11	0.30*	0.34**	0.32*	0.16
Slope (SP)		0.01	-0.19	-0.02	-0.06	-0.21	0.18
Aspect (AS)		0.32*	0.30*	0.13	0.19	0.21	0.28*
Catchment area (CA)		-0.15	-0.10	-0.32*	-0.36**	-0.13	-0.09
Total upslope length (TUL)		-0.14	-0.10	-0.32*	-0.36**	-0.13	-0.08
Longest upslope length (LUL)		-0.32*	-0.21	-0.45**	-0.51**	-0.22&	-0.10
Special catchment area (SCA)		-0.04	-0.09	0.06	0.04	-0.11	-0.01
Terrain complex index (TCI)		-0.31*	-0.09	-0.38**	-0.44**	-0.25&	-0.13
Stream power index (SPI)		-0.07	-0.18	-0.01	-0.06	-0.23&	0.05
Inverse wetness index (IWI)		0.31*	0.07	0.29*	0.34**	0.22&	0.10

**: Significance level 0.01; *: Significance level 0.05; &: Significance level 0.10. [§]: For abbreviations of terrain attributes, see Table 2.2. "AS" was transformed by cosine function.

the environment, geomorphology and pedology in different landscapes. Therefore, soil properties could be predicted from TAs, but the prediction functions and TAs to be used in these functions would vary according to local morphological, pedological and environmental conditions. In the hummocky agricultural landscape, landscape position which was indicated by RE, macro and micro slope shape (PFC, PLC and TCI), and the TAs that described water and sediment movement (TUL, LUL, CA and IWI) were the most important predictors of soil properties. PLC was the most consistent predictor across all soil properties in the A and B horizons.

In some cases, however, relationships between TAs and soil properties were contrary to the expected relationships described in 2.2.3. For example, SP and SPI were positively related to thickness of the B horizon. Some TAs were found not to be useful predictors of soil properties. SCA was not significantly related to any soil properties, therefore, they would not be important predictors of soil properties in the hummocky agricultural landscape at Viking (Table 2.4). SPI was significantly related only to thick-ness of the B horizon, but was not an important TA for other soil properties. AS was only positively and significantly related to TON and clay and silt contents of the C horizon, therefore, it was important for the prediction of these soil properties. In addition, no apparent predictors existed among all the TAs for clay content of the B horizon, and the silt and TON contents of the C horizon.

Some TAs, such as PFC in the B horizon, and PFC, RE and IWI in the C horizon positively correlated to soil pH while CA and TUL in the B and C horizons negatively correlated to soil pH. This implies the pH of deeper soil horizons was easier to predict by TAs than that of upper horizons. These TAs determined the amount of water and solute collection and the vertical translocation of salt and free ions, especially the basic cations, hence the concentration of soil solution, thereby the soil pH (Kovda et al., 1992). The relationships of TOC and TON to TAs were same in A, B and C horizons. Topography weakly influenced the TOC and TON of the C horizon mainly because of very low TOC and TON (Table 2.1).

2.4.2 Validation of SMLR, ANN and IDW models

Table 2.5 presents the results of independent validation for predicted versus measured soil properties in the validation dataset (15 data combinations). Each of the three models (SMLR, ANN and IDW) described earlier can partially explain variation in individual soil properties in the landscape. Predicted results for the A horizon were generally in better agreement with measured values than were those for the B and C horizons.

Soil properties predicted by SMLR, except sand content in the A horizon and TON and TOC in the C horizon, were significantly correlated to measured values ($R^2 \geq R^2_{critical} = 0.26$ at $P \leq 0.05$) with quite low bias (*MAE* < 0.4, Eq. 2.5). Variances of prediction errors were smaller than variances of measured values (*NMSE* < 1, Eq. 2.4). The error ratios (*ER*, Eq. 2.6) of 300 cases (20 soil properties × 15 soil profiles) predicted by SMLR were nearly normally distributed (Fig. 2.7a). Soil properties estimated by SMLR were within 25% of measured soil properties in 80% of cases. The standard deviation of *ER* (uncertainties for all cases) ranged from –39% to 25% of measured soil properties.

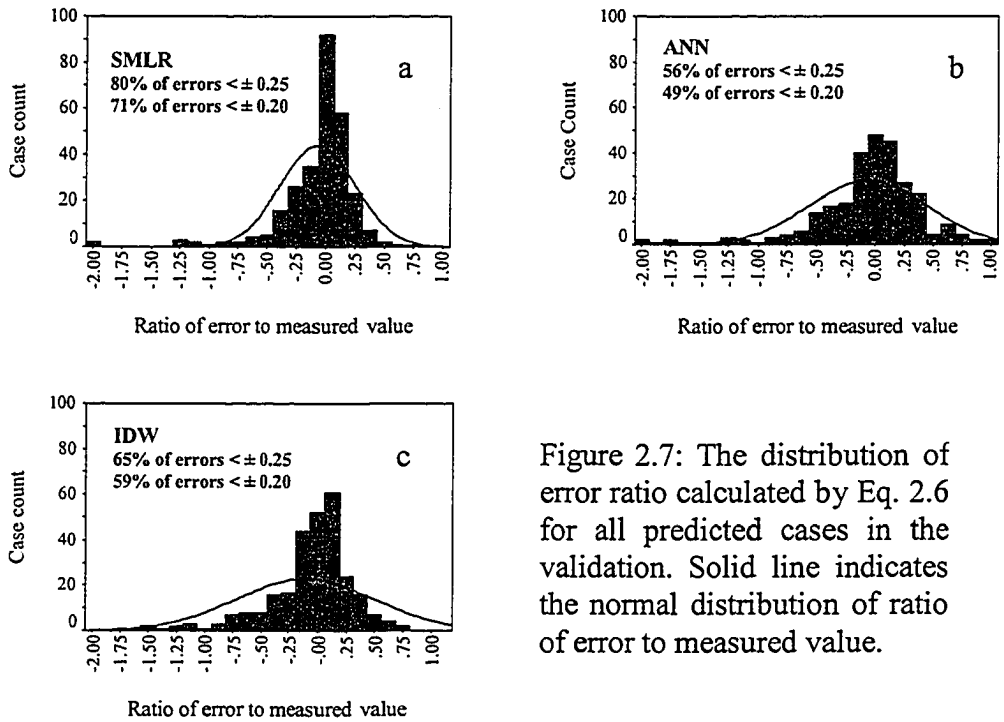

Figure 2.7: The distribution of error ratio calculated by Eq. 2.6 for all predicted cases in the validation. Solid line indicates the normal distribution of ratio of error to measured value.

All soil properties of the A horizon predicted by ANN, except clay content, were significantly correlated with measured values ($R^2 \geq 0.26$, Table 2.5). The predicted thickness, texture and TOC of the B horizon, and texture and pH of the C horizon were

also significantly correlated with measured values. However, *NMSE* and *MAE* from ANN were larger than those from SMLR. ANN predicted 56% of soil properties within 25% of the measured values and the *ER* had a nearly normal distribution. Predicted uncertainties were from –56% to 44% of measured soil properties (Fig. 2.7b).

Table 2.5: Validation results of measured versus predicted soil properties for three model methods ($R^2 = 0.26$ at $P \leq 0.05$).

Methods			SMLR			ANN			IDW		
Items			R^2	MAE	NMSE	R^2	MAE	NMSE	R^2	MAE	NMSE
Horizon A	Horizon Thickness		0.64	0.25	0.23	0.67	0.40	0.63	0.29	0.49	0.12
	Texture	Clay	0.58	0.13	0.18	0.15	0.22	0.67	0.57	0.15	0.13
		Silt	0.29	0.11	0.68	0.58	0.22	2.48	0.27	0.15	0.80
		Sand	0.11	0.08	0.28	0.26	0.22	7.01	0.60	0.08	0.62
	Chemical Properties	pH	0.35	0.06	0.39	0.36	0.09	1.05	0.04	0.09	0.51
		TOC	0.76	0.17	0.26	0.66	0.31	0.69	0.21	0.49	0.39
		TON	0.73	0.16	0.31	0.76	0.25	0.93	0.26	0.44	0.40
Horizon B	Horizon Thickness		0.38	0.38	0.34	0.16	0.70	2.12	0.22	0.76	0.66
	Texture	Clay	0.29	0.14	0.22	0.33	0.24	1.51	0.18	0.17	0.32
		Silt	0.38	0.22	0.09	0.37	0.25	0.69	0.21	0.27	0.11
		Sand	0.42	0.21	0.20	0.35	0.28	0.83	0.18	0.28	0.14
	Chemical Properties	pH	0.45	0.08	0.26	0.14	0.13	0.57	0.25	0.13	0.23
		TOC	0.26	0.28	0.39	0.32	0.35	3.44	0.13	0.42	0.74
		TON	0.35	0.23	0.98	0.07	0.49	3.78	0.26	0.38	0.93
Horizon C	Texture	Clay	0.28	0.24	0.07	0.16	0.34	0.07	0.30	0.26	0.14
		Silt	0.38	0.11	0.90	0.52	0.33	1.40	0.11	0.12	0.14
		Sand	0.42	0.11	0.05	0.20	0.27	0.88	0.01	0.17	0.07
	Chemical Properties	pH	0.72	0.05	0.01	0.75	0.17	0.55	0.25	0.14	0.06
		TOC	0.24	0.23	0.17	0.00	0.55	2.50	0.16	0.16	0.29
		TON	0.04	0.74	1.35	0.10	0.40	1.14	0.32	0.60	23.36

Predictions by IDW in thickness, soil texture and TON in the A horizon, TON in the B horizon, and clay and TON contents in the C horizon, were significantly correlated with measured values ($R^2 \geq 0.26$, Table 2.5), but not strongly. *NMSE* and *MAE* of IDW were similar to those of SMLR. IDW predicted 65% of soil properties within 25% of the measured values, and *ER* also had a nearly normal distribution with uncertainties from -72% to +50% (Fig. 2.7c).

In summary, SMLR was the best method to predict soil properties using a small calibration dataset (42 data combinations). IDW had a low predicting ability, especially when IDW predicted soil properties of grid cells which were outside the spatial range of

those of the training data. ANN had poor predicting ability because of the limitation of the small calibration dataset size in this study. The left skew of the *ER* distribution implied that SMLR, ANN and IDW overestimated soil properties, sometimes by as much as two times (Fig. 2.7) according to Eq. 2.6.

2.4.3 Prediction functions of SMLR

The correlations (R^2) of prediction functions derived by SMLR were lower than 0.78 (Table 2.6), although the prediction results of SMLR were the best of the three predicting methods in this study. The prediction functions of TOC and TON in the C horizon were not good enough for prediction, resulting in the poor predictions for these two soil properties (Table 2.5).

Most of the terrain attributes that were significantly related to soil properties in Table 2.4 are presented in the corresponding prediction functions in Table 2.6 as predictors. The relationships between individual terrain attributes and soil properties were the same in both tables. However, some terrain attributes, which also affected the soil properties significantly as shown in Table 2.4, were not included in the prediction functions in Table 2.6. For instance, CA was not included in the prediction functions for silt content and TOC of the A horizon, and the LUL was not included in the prediction for pH of the A horizon. These terrain attributes were excluded because they were highly correlated with other terrain attributes in the prediction functions.

Table 2.6: The prediction functions of individual soil property derived by SMLR from 42 data combinations in calibration dataset.

Terrain Attributes[§]	Thickness of Horizon (cm)	Texture			Chemical Properties		
		Clay (%)	Silt (%)	Sand (%)	pH (%)	TOC (g/kg)	TON (mg/kg)
		Horizon A					
Intercept	25.85	18.45	35.00	46.01	6.71	40.61	3556.11
Profile curvature (PFC)	-10.12	5.99	-18.03			-10.96	-828.83
Plan curvature (PLC)	1.16		0.61	-0.45	-0.07	0.60	58.39
Relative elevation (RE)	-1.25	0.85	0.04			-1.84	-142.28
Slope (SP)			-0.35		-0.07		
Aspect (AS)							
Catchment area (CA)							1.17
Total upslope length (TUL)			0.11			0.13	9.87
Longest upslope length (LUL)	0.16		0.09	0.01		0.02	1.88
Special catchment area (SCA)							

Terrain complex index (TCI)	8.74	-2.69	0.02			75.29	5947.28
Stream power index (SPI)				0.54			
Inverse wetness index (IWI)	-361.31	82.61	-18.34	35.82		-78.40	-505.33
R^2	0.65	0.43	0.54	0.13	0.42	0.78	0.76
se	7.18	3.10	4.47	5.71	0.54	7.31	629.49
p	<0.01	<0.05	<0.01	>0.05	<0.01	<0.01	<0.01
			Horizon B				
Intercept	33.17	28.39	31.01	41.73	7.36	13.95	1412.58
Profile curvature (PFC)		11.92	-24.68	0.53	1.31		
Plan curvature (PLC)			0.65	-0.27	-0.06	0.38	46.55
Relative elevation (RE)	-3.08						
Slope (SP)	1.19	-0.16	-0.71	0.69			-28.04
Aspect (AS)							
Catchment area (CA)					-0.0004		
Total upslope length (TUL)							
Longest upslope length (LUL)		0.13		-0.24			
Special catchment area (SCA)							
Terrain complex index (TCI)		-19.57	37.80	-25.03	-5.11	52.39	4762.63
Stream power index (SPI)	4.89						
Inverse wetness index (IWI)			1269.66			-206.93	-7271.91
R^2	0.50	0.44	0.39	0.51	0.53	0.48	0.50
se	11.45	4.44	6.50	6.26	0.58	4.95	476.62
p	<0.01	<0.05	<0.01	<0.01	<0.01	<0.01	<0.01
			Horizon C				
Intercept		20.558	37.36	41.08	8.78	6.43	758.23
Profile curvature (PFC)					1.11	2.59	-2007.36
Plan curvature (PLC)		-0.84		-0.02	-0.08	0.07	44.51
Relative elevation (RE)		1.29		0.53	0.05	0.26	72.52
Slope (SP)			-1.07			-0.16	32.03
Aspect (AS)		3.97	8.15				1.09
Catchment area (CA)				-0.00005		-0.01	-2.65
Total upslope length (TUL)				-0.33		0.06	21.45
Longest upslope length (LUL)		-0.02	-0.06	-0.10	-0.01	0.06	14.06
Special catchment area (SCA)						0.03	-2.15
Terrain complex index (TCI)				-62.08	-5.26	1.12	-7553.19
Stream power index (SPI)						-0.35	
Inverse wetness index (IWI)		159.97			1.40	124.86	
R^2		0.39	0.39	0.42	0.66	0.15	0.07
se		5.29	5.74	6.45	0.54	2.13	742.79
p		<0.01	<0.05	<0.01	0.00	>0.05	>0.05

[§]: For abbreviations of terrain attributes, see Table 2.2. "AS" was transformed by cosine function. "se" was the standard error of prediction functions. "p" was the significance level.

Almost all terrain attributes were included in the prediction functions for TOC and TON of the C horizon (Table2.6), because no terrain attribute was significantly related to

TOC and TON of the C horizon (Table 2.4) and SMLR could not identify significant predictors among the terrain attributes. As a result, the lower significance level of prediction functions implied that the TOC and TON of the C horizon could not be predicted well (Table 2.5).

2.4.4 Sensitivities of modeled N_2O emissions to uncertainties of predicted soil properties

Because the best predictions of soil properties in LSPP were achieved by SMLR (Table 2.5 and Fig. 2.7), soil properties and their uncertainties (Table 2.7) predicted by SMLR were used to evaluate the sensitivities of N_2O emissions to uncertainties of soil properties. The uncertainty of each predicted soil property was calculated as described in section 2.3.4.1.

Table 2.7: Uncertainties (%) of predicted soil properties from validation of SMLR with measured soil properties.

Horizon	Thickness	Sand content	Silt content	TOC	TON
A	39	6	11	21	20
B	32	19	27	36	32

Note: The uncertainty of clay content was not presented in this table because the clay content was not necessary input in the *3D-Ecosys-GIS*.

Adding the uncertainties to soil properties generally lowered the modeled total N_2O emissions of the sub site F1 (Fig. 2.1), but adding the uncertainties to TOC and TON in the B horizon caused an increase (BCN, Table 2.8). The uncertainties of soil properties caused less than 16% uncertainty in modeled N_2O emission of F1. There were no obvious differences in the uncertainties of N_2O emissions in the wet (2000) and normal (2001) years. The uncertainties in TOC and TON of the A horizon (ACN combination, Table 2.3) resulted in the largest uncertainty of modeled N_2O emissions. The uncertainties in horizon thickness and soil texture resulted in small uncertainties in modeled N_2O emission. The effects of uncertainties of horizon thickness and soil texture in total N_2O emissions were offset by those of TOC and TON over the landscape, because the uncertainties of modeled N_2O emissions from ABHTCN and AHTCN were similar to those from ABCN and ACN respectively (Table 2.8).

Table 2.8: The uncertainties of total N_2O emission in the sub site F1 (3.23 ha.) caused by uncertainties of soil properties.

Combination[§]	Changes to CC from (%)		
	2000	2001	Average
CC	0.00	0.00	0.00
ABHTCN	-3.97	-3.16	-3.63
ABH	-1.32	-0.50	-0.97
ABT	-5.46	-4.71	-5.14
ABCN	-4.25	-3.36	-3.88
AHTCN	-15.45	-14.94	-15.24
AH	-1.15	0.00	-0.66
AT	-0.89	-0.05	-0.54
ACN	-15.60	-15.21	-15.44
BHTCN	-4.77	-4.39	-4.61
BH	-1.76	-1.19	-1.52
BT	-0.27	-0.31	-0.29
BCN	0.20	0.36	0.27

[§]: For abbreviations of combinations, see Table 2.3.

2.5 Discussion

2.5.1 Terrain attributes, soil formation and soil properties

The significant relationships of TAs to soil properties (Table 2.4) suggested that TAs governed the redistribution of water, solute and sediment. AS and RE controlled the direction of the redistribution. SP, PFC and PLC changed the speed of water movement resulting in the redistribution of sediment. PFC, PLC, TCI and CA determined locations of erosion or deposition and their extent through changes in speed and amount of surface flow (Eqs. 2.1 and 2.2). IWI and TCI determined the magnitude of illuviation and eluviation. As a result, soil formation was affected as described in 2.2.3, resulting in the heterogeneities of soil properties. A few ^{137}Cs measurements conducted in Black Chernozem soils in a similar hummocky glacial till landscape at Saskatchewan, Canada, had found that the redistribution of water, solute and sediment in hill slopes in the hummocky agricultural landscape resulted in the spatial differences of soil properties (Pennock et al., 1999, 1994; Pennock and De Jong, 1991, 1987). Large net losses from soil erosion changed to small net losses or net gains from deposition as PFC decreased from convexities to concavities, PLC decreased from divergences to convergences, CA increased from upper slopes to lower slopes, and SP decreased from steep slopes to

shallow slopes (Pennock and De Jong, 1991, 1987). As a result, depth of the A horizon, soil organic matter and total organic nitrogen contents increased, soil pH decreased and soil texture was finer (Pennock et al., 1999, 1994). Similar relationships between TAs and soil properties were found in this study although most of the correlation coefficients were lower than 0.6 (Table 2.4). However, different correlations between individual TAs and soil properties (Table 2.4) implied complex effects of TAs on soil formation. Therefore, no general function could be used to estimate different soil properties, or even the same soil properties in different soil horizons as others have found (Park and Vlek, 2002; Bishop and McBratney, 2001; McBratney et al., 2000; Ryan et al., 2000; Zhu, 2000).

The results of SMLR predicted by the functions in Table 2.6 showed that coarser soil changed to finer and thickness of the A horizon increased from upper to lower slopes (Fig. 2.8a). These results were consistent with conclusions from ^{137}Cs studies conducted by Zebarth et al. (2002) on a hummocky podzolic landscape in New Brunswick, Canada, and by Pennock et al. (1994) on a Chernozemic soil in a hummocky glacial till landscape in Saskatchewan, Canada. Associated with sediment redistribution, TOC and TON contents increased from upper to lower slopes, and pH decreased. Active surface and subsurface transport (e.g. surface runoff, and vertical and lateral water movement in subsurface soil) selectively removed fine soil particles. Silt and clay with solute were eroded from upper slopes and deposited at concave (PFC < 0) and foot slope areas (PFC < 0, large CA, small SP and IWI) (Figs. 2.2 and 2.8e and f) due to the decrease in velocity of runoff with decreased SP (Eqs. 2.1 and 2.2). Eluviation at positions with large CA, very small IWI and positive TCI resulted in higher clay or silt contents in the B horizon than in the A horizon, and smaller differences of TOC and TON between the A and B horizons (Table 2.1, Figs. 2.2 and 2.8i, j, k and l). Eluviation leached solute and basic cations to deeper horizons, resulting in the increases of predicted and measured pH values (predicted (and measured) average pH = 6.1 (6.1) in the A horizon < 6.9 (6.9) in the B horizon < 7.9 (7.5) in the C horizon; Fig. 2.8g and h). This eluviation was demonstrated by field measurements in a similar landscape and soil type to this study at

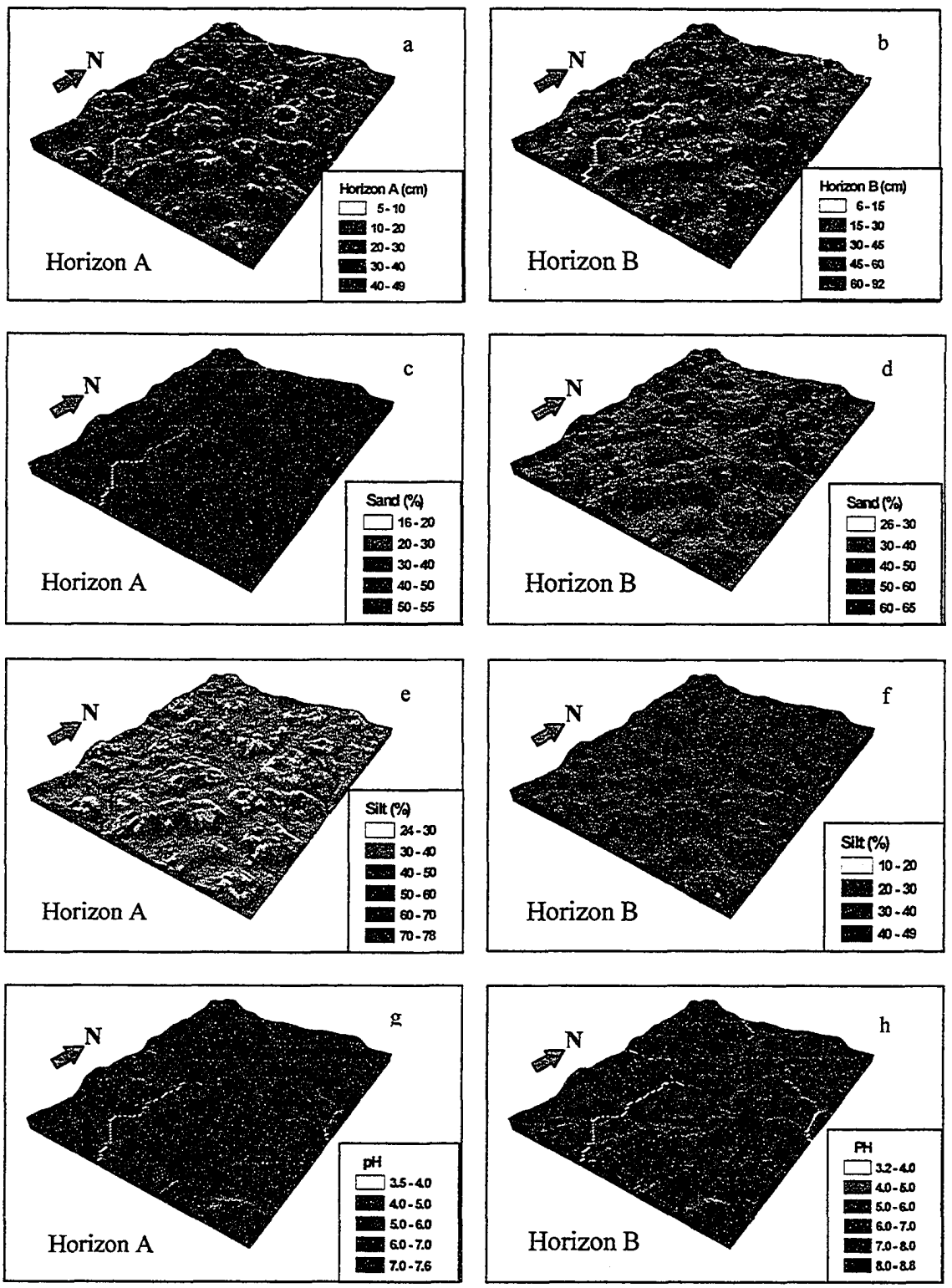

(Continued on next page)

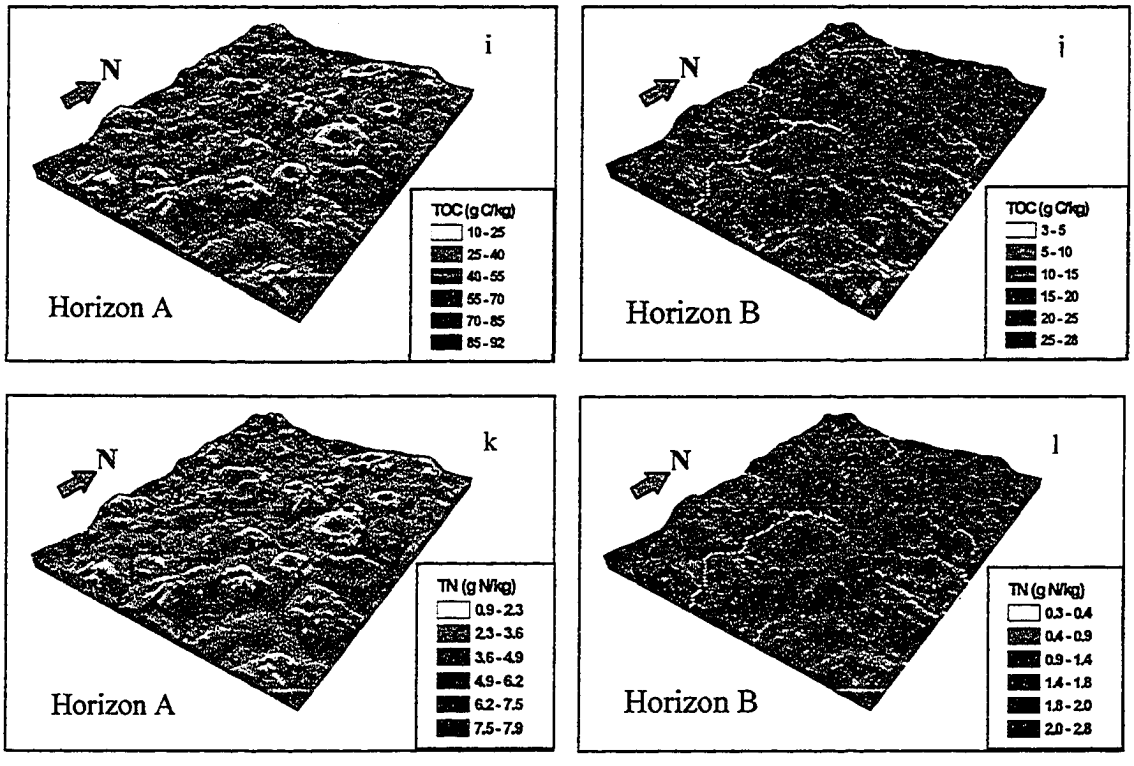

Figure 2.8: Soil properties estimated by SMLR for thickness (a), pH (g), and sand (c), silt (e), total organic carbon (i) and total organic nitrogen (k) contents in A horizon, and thickness (b), pH (h), sand (g), silt (f), total organic carbon (j) and total organic nitrogen (l) contents in B horizon in the hummocky landscape at Viking, Alberta, Canada.

Saskatchewan, Canada (Pennock et al., 1994). At lower slopes, the thicker A horizon and stronger eluviation with large CA and TCI, and negative PFC reduced capillary rise, weakening the effects of carbonate on pH. Strong water leaching at lower slopes also lowered soil pH.

2.5.2 Predictive capability of SMLR, ANN and IDW

IDW as an interpolating method was not good enough to derive soil properties based on a few measured data points on the hummocky landscape (Table 2.5, Fig. 2.7) because of the great variation of the topography. ANN, the nonlinear adaptive model, predicted soil properties less successfully because of its strong dependency on size (35 data combinations) and quality of the training dataset. If the training dataset was too small or did not represent all variations of TAs and soil properties in the study site, the prediction

would be poor. Except for a few surface soil properties, the nonlinear functions derived by ANN could not predict soil properties reliably in this study, as was also found by Park and Vlek (2002). SMLR proved to be a more effective method to describe the spatial variations of soil properties in this hummocky agricultural landscape at Viking, Alberta, Canada.

Validation (Table 2.5) indicated that soil properties, except for TON and TOC of horizon C and sand content of the A horizon, had clear correlations with TAs that could be described using a linear statistical model. MAEs from SMLR for all soil properties in this study (25%) were comparable with those of a soil inference system method for pH, soil texture and TOC (4% to 69% in Tables 4, 5 and 6, McBratney et al. 2002). These MAEs were less than uncertainties from multiple linear regression and cokriging-regression methods for soil moisture, residual phosphorus, solum thickness, depth to calcium carbonate and organic carbon content in a Canadian Black Chernozemic soil in a glacial till landscape in Manitoba (~38% in Florinsky et al., 2002). Uncertainties of less than 25% in 80% of predicted soil properties (Fig. 2.7a) were consistent with the results of Moore et al. (1993). Some uncertainty may be attributed to the different spatial scales of the TAs and the measured soil properties. TAs represented the average status in 10×10 m grid cells while soil properties were measured in area of 0.5×0.5 m. The uncertainties in the representation of topography generated during the production of the DEM (Goovaerts, 2001) would induce accompanying uncertainty within TAs. These two sources of uncertainty from different resolutions and generation of the DEM resulted in the low coefficients between predicted and measured values (Table 2.5) and some high uncertainties (Table 2.7). With significant correlations (R^2) and lower biases (MAE and NMSE) (Table 2.5) in comparing predicted soil properties with measured values, the predictions of SMLR were reliable for horizon thickness, texture, pH and TOC and TON in the A, B and C horizons, except for TOC and TON of the C horizon, and could be used to produce detailed soil information maps and for further detailed ecosystem research.

Attempts to predict soil properties from linear regression functions of TAs achieved varying degrees of success. Generally, the predictive capability of regression models was the greatest in the A horizon and less in the deeper soil layers (average $R^2 = 0.54$ in the A horizon > 0.46 in the B horizon > 0.38 in the C horizon, Table 2.5) because of the higher

correlation between TAs and soil properties of the A horizon (Table 2.4). The TAs would have affected the surface movement of water, solute and sediment much more than vertical and lateral subsurface movement of water, solutes and soil particles during soil formation. Spatial variations of soil properties resulted mainly from active surface runoff, and differentiation of soil properties into different horizons resulted from eluviation and illuviation processes. The variations of soil properties were related to the three-dimensional arrangement of slope geometry and soil development (Park and Burt, 2002 and 1999). The predicted and measured results (Fig. 2.8 and Table 2.1) supported the basic assumption that the functional correlation between soil properties and landform geometry arose from the downslope hydraulic gradient that controlled water movement (Huggett, 1975; Moore et al., 1993).

2.5.3 Sensitivities of N_2O emissions to uncertainties of soil properties

The random changes of soil properties within 39% (Table 2.7) of predicted values caused less than 16% uncertainty in modeled N_2O emissions from the sub site F1 (Table 2.8). These uncertainties of modeled N_2O emissions were smaller than the uncertainties of N_2O fluxes measured by chamber and were similar to those measured by micro-meteorological methods (Laville et al., 1999; Table 2.9), and slightly smaller than the differences in N_2O emissions measured by chambers with different measuring frequent-cies (Table 2.9; Flessa et al., 2002; Crill et al., 2000; Scott et al., 1999; Brumme and Beese, 1992). These uncertainties of modeled N_2O emissions were comparable to or even smaller than the differences among different measurement methods (Christensen et al., 1996; Table 2.9), and smaller than uncertainties of estimates for regional N_2O emissions by IPCC and regression methods that are based on soil N, fertilizer, texture, etc. (Table 2.9, Brown et al., 2001; Freibauer, 2003). However, the sensitivity of modeled N_2O emissions to uncertainties of soil properties differed among soil properties (Table 2.8).

Uncertainties of soil properties in the A horizon caused large uncertainties in modeled N_2O emissions (Table 2.8). Payne (1991) summarized from numerous N isotope research that denitrification generally occurred in the upper 10 cm soil layer. In the sub site F1, average thickness of the A horizon was 23 cm, and minimum thickness of the A horizon

Table 2.9: The uncertainties or differences found in current measurement or estimation methods from literature

Methods	Uncertainty or difference	Measurement frequency	Compared to measurement	Field condition	References
Chamber	±40% ~ 50%	These were uncertainties for measured fluxes from measurement methods		Heavy fertilized maize field	Laville et al., 1999
Eddy covariance	±27%				
Gradient estimates	±18%				
Fourier transform infrared spectrometers (FTIR)	±6.4%				Walsh et al., 1997
Chamber	+40%	Weekly	1 meas. /9 hours	Fertilized potato	Flessa et al., 2002
	-32% ~ -56%	Monthly			
	+6% ~ +49%	Weekly	5 meas./day	Beech	Brumme and Beese, 1992
	-40%	Every 3 days	4 meas./day	Grassland	Scott et al., 1999
	+20%	Daily	4 meas./day	Papaya	Crill et al., 2000
	+40%	Per 2.5 days			
IPCC estimates	> ±62%				Brown et al. 2001
Regression estimates	±29% ~ 64%	For European agricultural soil based on soil N, texture, fertilizer, etc.			Freibauer A., 2003
0.008 m^2 closed chamber	-20%	1 meas./day	0.125 m^2 chamber and 1 meas./day		Christensen et al., 1996
0.140 m^2 open flow chamber	-6%	9~24meas./day			
Gradient FTIR	-26%	8~24meas./day			
Gradient TDL, MPI[a]	< 1%	1 meas./day			
Gradient TDL, ITE[a]	+61%	1 meas./day			
Eddy covariance TDL, MPI	+31%	2~11meas./day			
Eddy covariance TDL, ITE	+55%	8-24meas./day			
Conditional sampling TDL, ITE	+88%	1 meas./day			
Conditional sampling FTIR	+145%	1 meas./day			

[a]: Tunable diode laser spectroscopy (TDL). MPI and ITE indicated the different equipment producer and with different mast closer.

was 8 cm. Therefore, uncertainties of soil properties in the B horizon caused very small uncertainties in modeled N_2O emissions.

The uncertainties of TOC and TON caused the largest uncertainty of modeled N_2O emissions (Table 2.8). Concurrent changes in TOC and TON also meant concurrent changes in the amount of substrates for carbon oxidation and nitrogen mineralization, hence in the demand for electron acceptors and the production of NH_4^+ and NO_3^-. Therefore, the changes of TOC and TON directly affected N_2O production and had stronger effects on uncertainty of N_2O emissions than did other tested soil properties.

In summary, the uncertainties of soil properties predicted by SMLR in LSPP based on the topographic terrain attributes caused uncertainties in modeled N_2O emissions (Table 2.8). The uncertainties of TOC and TON were the main reasons for uncertainties of modeled N_2O emissions. However, these uncertainties in modeled N_2O emissions compared well with the uncertainties found in current measuring and estimating methods (Table 2.9). The soil properties predicted by SMLR in LSPP could be used as soil property inputs of *3D-Ecosys-GIS* to simulate landscape N_2O emission.

2.6 Conclusions

The landscape position, slope shape such as concavity, convexity, convergence and divergence, and factors that describe the redistribution of water, solute and sediment such as upslope stream length, catchment area, micro topographic complex index and inverse wetness index, were the most important predictors of soil properties in the hummocky agricultural landscape. The results of SMLR were more accurate than those of the pure GIS interpolation method – Inverse Distance Weight (IDW), and were more efficient than the complex nonlinear method – Artificial Neural Network (ANN). Uncertainties of SMLR predictions were 20% to 39% for horizon thickness, less than 30% for soil texture, pH, total organic carbon and nitrogen contents, and increased with depth of soil layers.

When the soil properties predicted by SMLR in LSPP were used to initialize ecosystem model (*3D-Ecosys-GIS*) to simulate landscape N_2O emissions, uncertainties in predicted soil properties up to 39% caused uncertainties in modeled annual N_2O emissions of entire landscape up to 16%. Landscape N_2O emissions were most sensitive to uncertainties of total organic carbon and nitrogen contents. These uncertainties of N_2O

emissions were comparable to or even smaller than the uncertainties of N_2O emissions in current field measurement techniques (chamber and micrometeorological (+ TDL) methods) or estimations such as IPCC inventory. Therefore, the soil properties predicted by SMLR in LSPP could be used to initialize an ecosystem model for simulating landscape N_2O emissions. It would then be very useful to improve the estimate of N_2O emissions by accounting for temporal and spatial variation caused by spatial heterogeneities of site specific conditions.

References

Bell, J.C., Thompson, J.A., Butler, C.A., McSweeney, K., 1994. Modeling soil genesis from a landscape perspective. In: Etchevers B., J.D. (Ed). Transactions of the 15th World Congress of Soil Science. Acepulco, Mexico, July 1994. 6A. The International Society of Soil Science and the Mexican Society of Soil Science, Mexico. 179–195.

Bishop, T.F.A. and McBratney, A.B., 2001. A comparison of prediction methods for the creation of field-extent soil property maps. Geoderma. 105: 93–111.

Booltink, H.W.G., van Alphen, B.J., Batchelor, W.D., Paz, J.O, Stoorvogel, J.J., Vargas, R., 2001. Tools for optimizing management of spatially-variable fields. Agricultural Systems. 70(2-3): 445–476.

Breemen, N.van and Buurman, P., 2002. Soil formation (2nd edition). Kluwer Academic Publisher, The Netherlands. pp245–255.

Brown, L., Brown, S.A., Jarvis, S.C., Syed, B., Goulding, K.W.T., Phillips, V.R., Sneath, R.W., Pain, B.F., 2001. An inventory of nitrous oxide emissions from agriculture in the UK using the IPCC methodology: emission estimate, uncertainty and sensitivity analysis. Atmospheric Environment. 35(8):1439–1449.

Brubaker, S.C., Jones, A.J., Lewis, D.T., Frank, K., 1993. Soil properties associated with landscape position. Soil. Sci. Soc. Amer. J. 57(1):235–239.

Brumme, R., Beese, F., 1992. Effect of liming and nitrogen fertilization on emissions of CO_2 and N_2O from a temperate forest. J. Geophys. Res. 97:12851–12858.

Bui, E.N. and Moran, C.J., 2003. A strategy to fill gaps in soil survey over large spatial extents: an example from the Murray–Darling basin of Australia. Geoderma. 111:21–44.

Buol, S.W., Hole, F.D., McCracen, R.T., 1973. Soil genesis and classification. The Iowa State University Press, Ames. pp360.

Carre, F. and Girard, M.C., 2002. Quantitative mapping of soil types based on regression kriging of taxonomic distances with landform and land cover attributes. Geoderma. 110:241– 263.

Carter, B.J. and Ciolkosz, E.J., 1991. Slope gradient and aspect effects on soil developed from sandstone in Pennsylvania. Geoderma. 49:199–213.

Chaplot, V., Walter, C., Curmi, P., 2000. Improving soil hydromorphy prediction according to DEM resolution and available pedological data. Geoderma. 97:405–422.

Chiles, J.P. and Delfiner, P., 1999. Geostatistics: Modeling Spatial Uncertainty. Wiley, New York.

Christensen, S, Ambus, P., Arah, J.R.M, Clayton, H., Galle, B., Griffith, D.W.T., Hargreaves, K.J., Klemedtsson, L., Lind, A.M., Maag, M., Scott, A., Skiba, U., Smith, K.A., Welling, M., Wlenhold, F.G., 1996. Nitrous oxide emission from an agricultural field: Comparison between measurements by flux chamber and micrometerological techniques. Atmospheric Environment. 30:4183–4190.

Cressie, N.A., 1993. Statistics for Spatial Data. Wiley, New York.

Crill, P.M., Keller, M., Weitz, A., Grauel, B., Veldkamp, E., 2000. Intensive field measurements of nitrous oxide emissions from a tropical agricultural soil. Global Biogeochemical Cycles. 14(1):85–95.

Deutsch, C.V. and Journel, A.G., 1998. GSLIB: Geostatistical Software Library and User's Guide. Oxford University. Press, New York.

Flessa, H., Ruser, R., Schilling, R., Loftfield, N., Munch, J.C., Kaiser, E.A., Beese, F., 2002. N_2O and CH_4 fluxes in potato fields: automated measurement, management effects and temporal variation. Geoderma. 105(3-4):307–325.

Florinsky, I. V., Eilers, R. G., Manning, G. R., and Fuller, L. G., 2002. Prediction of soil properties by digital terrain modelling. Environmental Modelling & Software. 17(3):295–311.

Florinsky, I.V. and Arlashina, H.A., 1998. Quantitative topographic analysis of gilgai soil morphology. Geoderma. 82:359–380.

Florinsky, I.V., McMahon, S., Burton, D.L., 2003. Topographic control of soil microbial activity: a case study of denitrifiers. Geoderma. 119:33–53.

Freibauer, A., 2003. Regionalised inventory of biogenic greenhouse gas emissions from European agriculture. European Journal of Agronomy. 19(2):135–160.

Garcia, P.J.D., Olson, K.R., Lang, J.M., 2000. Predicting corn and soybean productivity for Illinois soils. Agricultural Systems. 64(3):151–170.

Gessler, P.E., Chadwick, O.A., Chamran, F., Althouse, L., Holmes, K., 2000. Modeling soil-landscape and ecosystem properties using terrain attributes. Soil Sci. Soc. Am. J. 64(6):2046–2056.

Gessler, P.E., Moore, I.D., McKenzie, N.J., Ryan, P.J., 1995. Soil-landscape modeling and spatial prediction of soil attributes. International Journal of Geographical Information Systems. 9:421–432.

Gobin, A., Campling, P., Feyen, J., 2001. Soil-landscape modelling to quantify spatial variability of soil texture. Phys. Chem. Earth (B). 26(1):41–45.

Gomez_Plaza, A., Martinez-Mena, M., Albaladejo, J., Castillo, V.M., 2001. Factors regulating spatial distribution of soil water content in small semiarid catchments. Journal of Hydrology. 253:211–226.

Goovaerts, P., 1997. Geostatistics for Natural Resources Evaluation. Oxford Univ. Press, New York.

Goovaerts, P., 1999. Geostatistics in soil science: state-of-the-art and perspectives. Geoderma. 89:1–45.

Goovaerts, P., 2001. Geostatistical modelling of uncertainty in soil science. Geoderma. 103:3–26.

Grant, R. F. and Pattey, E., 2003. Modelling variability in N_2O emissions from fertilized agricultural fields. Soil Biology and Biochemistry. 35(2): 225–243.

Grant, R.F., 1995. Dynamics of energy, water, carbon and nitrogen in agricultural ecosystems: simulation and experimental validation. Ecological Modeling. 81(1-3): 169–181.

Grant, R.F., Nyborg M., Laidlaw, J., 1993a. Evolution of nitrous oxide from soil: I. Model development. Soil Sci. 156:259–265.

Grant, R.F., Nyborg, M., Laidlaw, J., 1993b. Evolution of nitrous oxide from soil: II. Experimental results and model testing. Soil Sci. 156:266–277.

Huggett, R.J., 1975. Soil landscape systems: A model of soil genesis. Geoderma.13:1–22.

Isaaks, E.H., and Srivastava, R.M., 1990. An Introduction to Applied Geostatistics. Oxford Univ. Press, New York.

Jenny, H., 1941. Factors of soil formation, a system of quantitative pedology. McGraw-Hill, New York.

Kachanoski, R.G. and Carter M.R., 1999. Landscape position and soil redistribution under three soil types and land use practices in Prince Edward Island, Soil and Tillage Research. 51(3-4):211–217.

Kachanoski, R.G., de Jong, E., Rolston, D.E., 1985b. Spatial and spectral relationship of soil properties and microtopography: I. Density and thickness of A horizon. Soil Sci. Soc. Am. J. 49:812–816.

Kachanoski, R.G., Rolston, D.E., de Jong, E., 1985a. Spatial and spectral relationship of soil properties and microtopography: I. Density and thickness of A horizon. Soil Sci. Soc. Am. J. 49:804–812.

King, D., Bourennane, H., Daroussin, J., Isambert, M., 1994. Spatial distribution of loamy soils related to topography in a smooth relief region. In: Etchevers B., J.D. (Ed), Transactions of the 15th World Congress of Soil Science. Acapulo, Mexico. July, 1994. 6B. Intl. Soc. Soil Sci. Mexican Soc. Soil Sci. Mexico. 320–321.

Knotters, M., Brus, D.J., Oude Voshaar, J.H., 1995. A comparison of kriging, co-kriging and kriging combined with regression for spatial interpolation of horizon depth with censored observations. Geoderma. 67:227–246.

Kovda, T.V., Morgun, Y.G., Alekseyeva, T.V., 1992. Development of gilgai soil cover in cental Ciscaucasia. Eurasian Soil Sci. 24:28–45.

Laville, P., Jambert, C., Cellier P., Delmas, R., 1999. Nitrous oxide fluxes from a fertilised maize crop using micrometeorological and chamber methods. Agricultural and Forest Meteorology. 96(1-3):19–38.

Lexer, M.J., and Honninger, K., 1998. Estimating physical soil parameters for sample plots of large-scale forest inventories. Forest Ecology and Management. 111:231–247.

Lilburne, L., Hewitt, A., McIntosh, P. Lynn, I., 1998. GIS-driven models of soil properties in the high country of the south island. 10th Colloquium of the spatial information research center, University of Otago, New Zealand. 173–180.

MacMillan, R.A., Pettapiece, W.W., Nolan, S.C., Goddard, T.W., 2000. A generic procedure for automatically segmenting landforms into landform elements using DEMs, heuristic rules and fuzzy logic. Fuzzy Sets and Systems. 113:81–100.

Martz, L.W. and de Jong, E., 1990. Natural radionuclides in the soil of a small agricultural basin in the Canadian Praires and their association with topography, soil properties and erosion. Catena. 17:85–96.

McBratney, A.B, Minasny, B., Cattle, S.R., Vervoort, R.W., 2002. From pedotransfer functions to soil inference systems. Geoderma. 109(1-2):41–73.

McBratney, A.B., Mendonca Santos, M.L., Minasny, B., 2003. On digital soil mapping. Geoderma.117(1-2):3–52.

McBratney, A.B., Odeh, I.O.A., Bishop, T.F.A, Dunbar, M.S., Shatar, T.M., 2000. An overview of pedometric techniques for use in soil survey, Geoderma. 97(3-4):293-327.

Miller, J.J., Acton, D.F., St. Arnaud, R.J., 1985. The effect of groundwater on soil formation in a morainal landscape in Saskatchewan. Can. J. Soil Sci. 65:293–307.

Minasny, B. and McBratney, A.B., 2001. A rudimentary mechanistic model for soil formation and landscape development, II. A two-dimensional model incorporating chemical weathering. Geoderma. 103:161–179.

Moore, I.D., Gessler, P.E., Nielsen, G.A., Peterson, G.A., 1993. Soil attribute prediction using terrain analysis. Soil Sci. Soc. Am. J. 57: 443–452.

Moore, I.D., Grayson, R.B., Ladson, A.R., 1991. Digital terrain modelling; a review of hydrological, geomorphological and biological applications. Hydrol. Proc. 5:3–30.

Morgan, R.P.C., Quinton, J.N., Smith, R.E., Govers, G., Poesen, J.W.A., Auerswald, K., Chisci, G., Torri, D. and Styczen, M.E. 1998a. The European Soil Erosion Model (EUROSEM): a dynamic approach for predicting sediment transport from fields and small catchments. Earth Surface Processes and Landforms. 23:527–544.

Morgan, R.P.C., Quinton, J.N., Smith, R.E., Govers, G., Poesen, J.W.A., Auerswald, K., Chisci, G., Torri, D., Styczen, M.E. and Folly, A.J.V. 1998b. The European Soil

Erosion Model (EUROSEM): documentation and user guide v. 3.6. Silsoe College, Cranfield University, Silsoe, Bedford, U.K.

Mueller, T. and Pierce, F., 2003. Soil carbon maps: Enhancing spatial estimates with simple terrain attributes at multiple scales. Soil Sci. Soc. Am. J. 67:258–267.

Oberthur, T., Goovaerts, P., Dobermann, A., 1999. Mapping soil texture classes using field texturing, particle size distribution and local knowledge by both conventional and geostatistical methods. European Journal of Soil Science. 50:457– 479.

Odeh, I.O.A., Chittleborough, D.J., McBratney, A.B., 1991. Elucidation of soil-landform interrelationships by canonical ordination analysis. Geoderma. 49:1–32.

Odeh, I.O.A., McBratney, A.B., Chittleborough, D.J., 1994. Spatial prediction of soil properties from landform terrain attributes derived from a digital elevation model. Geoderma. 63:197–214.

Odeh, I.O.A., McBratney, A.B., Chittleborough, D.J., 1995. Further results on prediction of soil properties from terrain attributes: heterotopic cokriging and regression-kriging. Geoderma. 67:215–225.

Osher, L.J. and Buol, S.W., 1998. Relationship of soil properties to parent material and landscape position in eastern Madre de Dios Peru. Geoderma. 83:143–166.

Oztas, T., Koc, A., Comakli, B., 2003. Changes in vegetation and soil properties along a slope on overgrazed and eroded rangelands. Journal of Arid Environments. 55(1):93–100.

Park, S.J. and Burt, T.P., 2002. Identification and characterization of pedogeomorphological processes on a hill slope. Soil Sci. Soc. Am. J. 66:1897–1910.

Park, S.J. and Vlek, L.G., 2002. Prediction of three-demensional soil spatial variability: a comparison of three environmental correlation techniques. Geoderma. 109: 117–140.

Park, S.J. and Burt, T.P., 1999. Identification of throughflow using the distribution of secondary iron oxides in soils. Geoderma. 93(1-2):61–84.

Park, S.J., McSweeney, K., Lowery, B., 2001. Identification of the spatial distribution of soils using a process-based terrain characterization. Geoderma. 103:249–272.

Payne, W.J., 1991. A review of methods for field measurements of denitrification. Forest Ecology and Management. 44(1):5–14.

Pennock, D.J., 2003. Terrain attributes, landform segmentation, and soil redistribution. Soil & Tillage Research. 69(1):15–26.

Pennock, D.J. and Corre, M.D., 2001. Development and application of landform segmentation procedures, Soil and Tillage Research. 58(3-4):151–162.

Pennock, D.J., McCann, B.L., DeJong, E., Lemmen, D.S., 1999. Effects of soil redistribution on soil properties in a cultivated Solonetzic-Chernozemic landscape of Southwestern Saskatchewan. Canadian Journal of Soil Science. 79(4):593–601.

Pennock, D.J., Anderson, D.W., De Jong, E., 1994. Landscape-scale changes in indicators of soil quality due to cultivation in Saskatchewan, Canada. Geoderma. 64:1–19.

Pennock, D.J. and De Jong, E., 1991. Spatial pattern of soil redistribution in boroll landscape, southern Saskatchewan. Canadian Journal of Soil Science. 150:867–873.

Pennock, D.J. and De Jong, E., 1987. The influence of slope curvature on soil erosion and deposition in hummocky terrain. Soil Sci. 144:209–217.

Pennock, D.J., Zebarth, B.J., de Jong, E., 1987. Landform classification and soil distribution in hummocky terrain Saskatchewan, Canada. Geoderma. 40:297–315.

Romano, N. and Palladino, M., 2002. Prediction of soil water retention using soil physical data and terrain attributes. J. Hydrol. 265(1-4):56–75.

Ryan, P.J., McKenzie, N.J., O'Connell, D., Loughhead, A.N., Leppert, P.M., Jacquier, D., Ashton, L., 2000. Integrating forest soils information across scales: spatial prediction of soil properties under Australian forests. Forest Ecology and Management. 138:139–157.

Scott, A., Crichton, I., Ball, B.C., 1999. Long-term monitoring of soil gas fluxes with closed chambers using automated and manual systems. J. Environ. Qual. 28:1637–1643.

Shary, P.A., Sharaya, L.S., Mitusov, A.V., 2002. Fundamental quantitative methods of land surface analysis. Geoderma. 107:1–32.

Simmons, F.W., Cassel, D.K., Daniels, R.B., 1989. Landscape and soil property effects on corn grain yield response to tillage. Soil Sci. Soc. Am. J. 53 (2):534–539.

Stafford, J.V., 2000. Implementing precision agriculture in the 21st century. J. Agric. Eng.. Res. 76:267–275.

Tarboton D.G., 2002. Terrain Analysis Using Digital Elevation Models (TauDEM). http://moose.cee.usu.edu/taudem/taudem.html.

Walsh, C.P., Bell, W., Gradiner, T., Swann, N., Woods, P., Notholt, J., Schutt, H., Galle, B., Arlander, W., Mellqvist, J., 1997. An uncertainty budget for ground-based fourier transform infrared column measurement of HCl, HF, N_2O, and HNO_3 deduced from results of side by side instrument intercomparisons. Journal of Geophysical Research. 102(D7):8867–8873.

Wang, J., Fu, B., Qiu, Y., Chen, L.D., 2001. Soil nutrients in relation to land use and landscape position in a semi-arid small catchment on the loess plateau in China, Journal of Arid Environments. 48(4):537–550.

Wischmeier, W.H. and Smith, D.D., 1978. Predicting rainfall erosion losses, a guide to conservation planning. Agr. Handbook. No. 537. USDA, Washington, 58.

Young, A., 1972. Slopes. Oliver and Boyd, Edinburgh. 288.

Zebarth, B.J., Rees, H., Walsh, J., Chow, L., Pennock, D.J., 2002. Soil variation within a hummocky podzlic landscape under intensive potato production. Geoderma. 110:19–33.

Zhu, A.X. and Band, L.E., 1994. A knowledge-based approach to data integration for soil mapping. Canadian Journal of Remote Sensing. 20:408–418.

Zhu, A.X., 2000. Mapping soil landscape as spatial continua: the neural network approach. Water Resources Research. 36:663–667.

Zhu, J., Cristine, L.S.M., Norman J.M., Yue. W, Lowery, B., 2004. Combined mapping of soil properties using a multi-scale tree-structured spatial model. Geoderma. 118(3-4):321–334.

Appendix 2.1: Stepwise multiple linear regression algorithm

```
cccccccccccccccccccccccccccccccccccccccccccccccccccccccccccccccc
C Forward stepwise multiple linear regression
C algorithm developed by Tao Li, June 12, 2003
C Input file:
C **************************************************************
C  Line 1:         NVAR (number of variables), OBS (number of data combinations)
C  Line 2:  the integer number for each variable use as "1" for independent
C                  variables or "-1" for dependent variable or "0" for non-useful variables
C  Line 3 to Line n present x and y data.
C **************************************************************
```

```
C  NOTE: The input file must be text format with fixed name as "temptxt"
CCCCCCCCCCCCCCCCCCCCCCCCCCCCCCCCCCCCCCCCCCCCCCCCCCCCCCCCCCCCCCCCCCCC
    PROGRAM SMLR_FORWARD
     USE MSIMSLSD
     USE MSFLIB
     INTEGER   LDCOEF, LDCOV, LDCOVS, NVAR, I1, I, J,
   &               IFRQ, IGRP, IWT, LDX, LDXMEA, NCOL, NGROUP,
   &               NROW, NRMISS, IDO
    INTEGER   NI(1)

     PARAMETER  (IFRQ=0, IGRP=0, IWT=0, NGROUP=1, LDXMEA=1,
  &                IDO=3)
     INTEGER   IEND, INVOKE, IPRINT, ISTEP, NFORCE, NOBS, NSTEP
     INTEGER,ALLOCATABLE::LEVEL(:), IND(:)
     REAL(8)   AOV(13), TOL, PIN, POUT, B0, SWT(1)
     REAL(8),ALLOCATABLE:: COEF(:,:), COVS(:,:), HIST(:), SCALE(:)’
  &                SWEPT(:), X(:,:), D(:), OB(:), XVAL(:,:),COV(:,:), DIF(:),XMEAN(:,:)
     INTEGER,ALLOCATABLE::IWK(:)
     OPEN(UNIT=10,FILE='temptxt',STATUS='OLD')
     READ(10,*)NVAR,NOBS
     ALLOCATE(LEVEL(NVAR))
     LDCOEF=NVAR
     LDCOV=NVAR
     LDCOVS=NVAR
     LDX=NOBS
     NROW=NOBS
     NCOL=NVAR
    ALLOCATE(D(NVAR),OB(NVAR),XVAL(NVAR, NGROUP),DIF(NVAR),
   &      X(NOBS,NVAR),IND(NVAR),COEF(LDCOEF,5),COV(LDCOV,NVAR),
   &      COVS(LDCOVS,NVAR),HIST(NVAR),SCALE(NVAR),SWEPT(NVAR),
   &      IWK(2*NVAR),XMEAN(LDXMEA,NVAR))
C         !! read patterns from file !!
C
     READ(10,*)(LEVEL(I1),I1=1,NVAR)
C         !! read X1, X2, ... Xn, Y data
     READ(10,*)((X(I,J), J = 1, NVAR),I=1, NOBS)
     CLOSE(10)
     DO I=1, NVAR
     IND(I)=I
     ENDDO
     NI(1)=NOBS

     CALL DC2VPL (IDO, NROW, NVAR, NCOL, X, LDX, IND, IFRQ,
   &               IWT, NGROUP, IGRP, NI, SWT, XMEAN, LDXMEA, COV,
   &               LDCOV, NRMISS, D, OB, XVAL, DIF)

    INVOKE = 0
    NFORCE = 0
    NSTEP  = -1
    ISTEP  = 1
    PIN    = 0.20
    POUT   = 0.25
    TOL    = 100.0*DMACH(4)
    IPRINT = 1
    CALL DR2TEP (INVOKE, NVAR, COV, LDCOV, LEVEL, NFORCE, NSTEP,
   &          ISTEP, NOBS, PIN, POUT, TOL, IPRINT, SCALE, HIST,
```

```
&          IEND, AOV, COEF, LDCOEF, COVS, LDCOVS,SWEPT,IWK)
 B0=XMEAN(1,NVAR)
 DO 5 I = 1, (NVAR-1)
 IF(HIST(I).GT.0.0)THEN
 B0=B0-XMEAN(1,I)*COEF(I,1)
 J=J+1
 XMEAN(1,J)=XMEAN(1,I)
 ENDIF
5 CONTINUE

      OPEN(UNIT=6,FILE='TESTOUT')
      WRITE(6,6) AOV(11)
      WRITE(6,7) AOV(12)
      WRITE(6,8) AOV(10)
      WRITE(6,9) AOV(9)

6     FORMAT('R-Squared ', F10.6)
7     FORMAT('Adjusted R2 ', F10.6)
8     FORMAT('P-Value ', F10.6)
9     FORMAT('F-stats ', F10.6)
      WRITE(6,10) AOV(13)

      WRITE(6,20) B0
10    FORMAT( 'Standard Error ',F8.4)
20    FORMAT( 'INTERCEPT ',F10.4)
    DO I1=1,NVAR
      IF(SWEPT(I1).GT.0)THEN
      WRITE(6,30) I1,COEF(I1,1)
      ENDIF
30    FORMAT(I5,F10.4)
      ENDDO
      CLOSE(6)
      OPEN(UNIT=7,FILE='TESTOUT2')
      DO I1=1,NVAR
      IF(SWEPT(I1).GT.0)THEN
      WRITE(7,40) I1
      ENDIF
40    FORMAT(I5)
      ENDDO
      CLOSE(7)

    END PROGRAM SMLR_FORWARD
```

Appendix 2.2: Equations of Artificial Neural Network (ANN).

Equations:

$$x_j = \sum_{i=1}^{n} R_{i,j} I_i \qquad \text{(A2.1)}$$

$$H_j = \frac{e^{x_j} - e^{-x_j}}{e^{x_j} + e^{-x_j}} \qquad \text{(A2.2)}$$

$$x_o = \sum_{j=1}^{q} R_{j,o} H_j \qquad \text{(A2.3)}$$

$$Y_o = \frac{e^{x_o} - e^{-x_o}}{e^{x_o} + e^{-x_o}} \quad \text{(A2.4)}$$

$$E^t = \sum_{k=1}^{m} (Y_k^{'} - Y_k^t)^2 \quad \text{(A2.5)}$$

$$W^t = \sum_{i=1}^{n} \sum_{j=1}^{q} R_{i,j}^t + \sum_{j=1}^{q} \sum_{o=1}^{p} R_{j,o}^t \quad \text{(A2.6)}$$

$$R_{i,j}^{t+1} = R_{i,j}^t + \alpha \frac{\partial E}{\partial W} + \beta (R_{i,j}^t - R_{i,j}^{t-1}) \quad \text{(A2.7)}$$

$$RMSE = \sqrt{(\sum_{r=1}^{s} (Y_r^{'} - Y_r^t)^2) / s} \quad \text{(A2.8)}$$

Superscripts and subscripts:

n: number of variables in input layer (n = 12 in this study).
q: number of variables in hidden layer (q = 5 in this study).
p: number of variables in output layer (p = 1 in this study).
i: i^{th} variable in input layer.
j: j^{th} variable in hidden layer.
o: o^{th} variable in output layer.
m: number of interior training data pairs (k = 35 in this study).
k: k^{th} data pair in interior training data pairs.
s: number of interior testing data pairs (s = 7 in this study).
r: r^{th} data pair in interior testing data pairs.
t: training loop.

Variables:

x: temporary value for hyperbolic tangent normalization.
R: weighting ratio from current layer to next layer.
I: value in input layer (normalized TA).
H: temperate value in hidden layer.
Y: the predicted value in output layer (normalized soil property).
Y': the normalized value of measured soil property.
E: total square error between predicted and measured values.
W: total of weighting rate.
∂E: the difference of E between loop t and t-1.
∂W: the difference of W between loop t and t-1.
α: the learning rate (from 0 to 1).
β: the momentum rate (from 0 to 1).
RMSE: root of mean square error in interior test.

Appendix 2.3: The interface of Landscape Soil Property Predictor (LSPP).

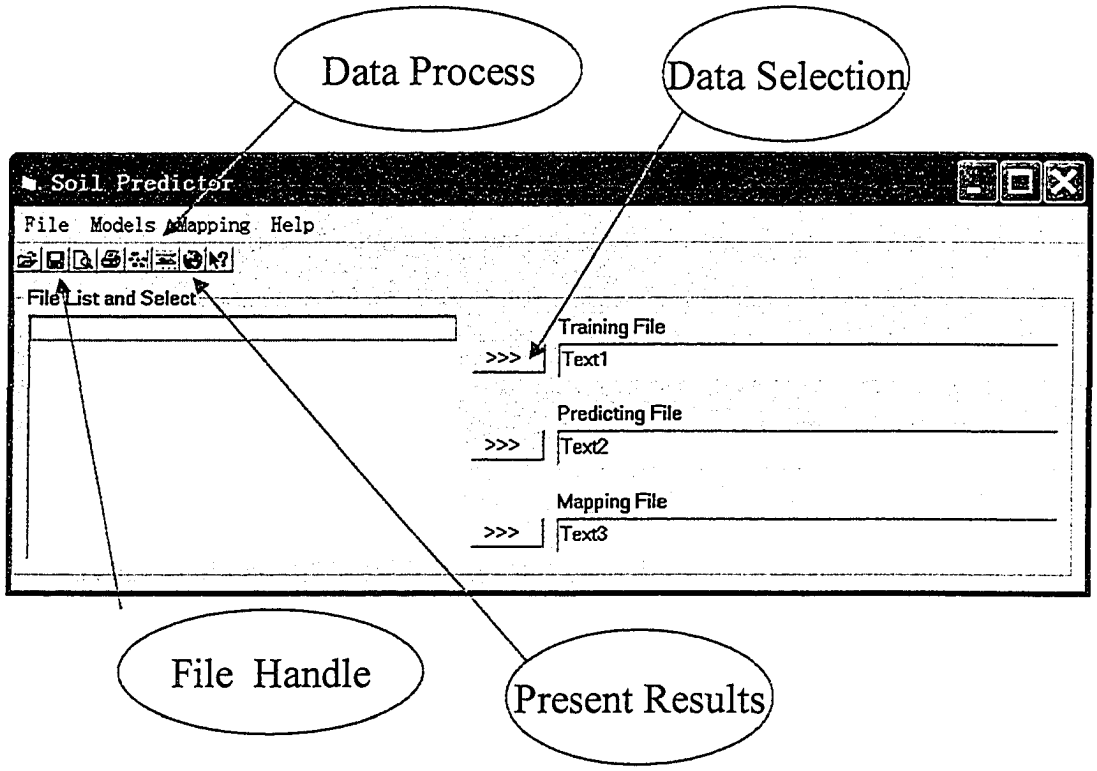

Appendix 2.3A: The main interface of LSPP.

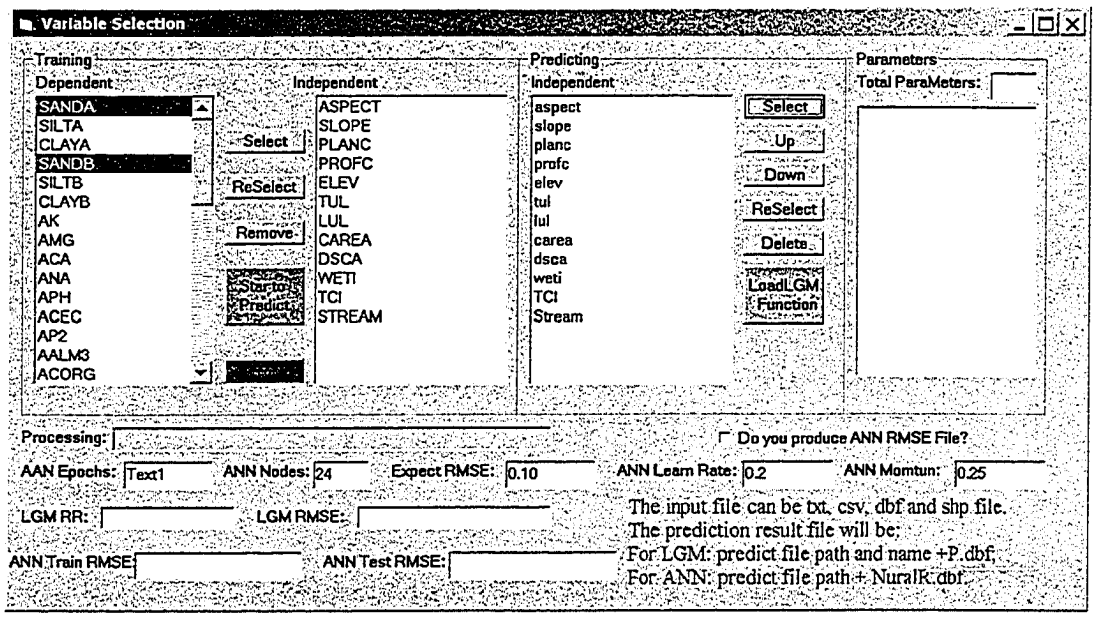

Figure 2.3B: The function interface of LSPP.

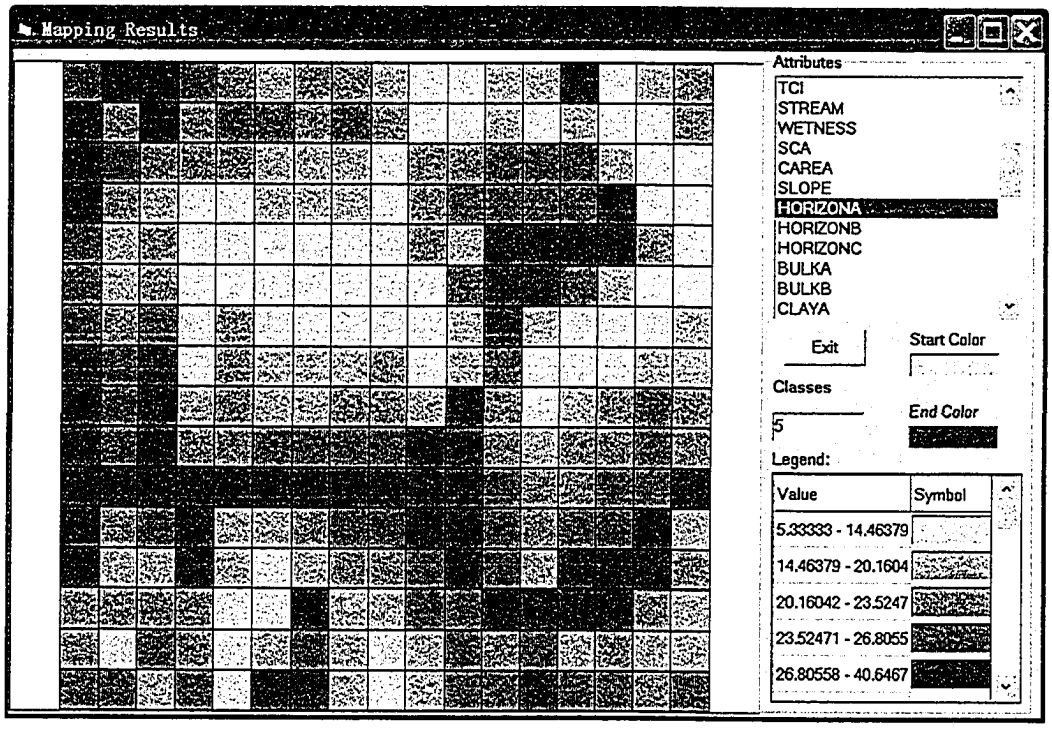

Appendix 2.3C: The mapping interface of LSPP.

Chapter 3: Modeling Landscape Effects on N_2O Emissions in a Hummocky Agricultural Field

3.1 Introduction

N_2O accounts for 6 percent of radiative forcing that cause global warming (IPCC Third Assessment Report, 2001). Global N_2O emissions were 17.7 Tg N per year, of which 4.2 Tg N (24% of the total) came from agricultural soil in 1998 (IPCC, 2001). In Canada, agriculture contributed 8.3% of 670 Mt CO_2 equivalent greenhouse gas emissions in 2001, of which N_2O emission accounted for 60% (Olsen et al., 2003). Currently, global and national N_2O emissions are estimated from the IPCC guidelines (1997), which are summarized from limited data sets. The guidelines do not account for the site-specific effects of topography, climate, soil properties, cropping and soil management, and the large temporal and spatial variations in N_2O emissions. Uncertainty in estimates of N_2O emissions by the IPPC guidelines might be 70% to 80% in arable soil at national scle (Lim et al., 1999). This uncertainty is much higher than the current reduction target (about 20%) in the Kyoto Protocol. Large temporal and spatial variations of N_2O fluxes have been a main source of error in estimating cumulative N_2O fluxes from arable soils (Flessa et al., 2002; Scott et al., 1999). Therefore, a new inventory method that considers site-specific effects and large temporal and spatial variation is necessary to provide more accurate estimates of N_2O emissions.

Spatial variation of N_2O emissions is generally larger than 100% in spatial scales of meters to hundreds of meters. Pennock and Corre (2001) reported that N_2O emissions were significantly higher at footslopes than at shoulders or midslopes, and that total emission increased with nitrogen fertilizing rate. Corre et al. (1999) measured that N_2O emissions were one to ten times higher at foot slopes than at shoulder slopes in an agricultural soil in central Saskatchewan. Van Kessel et al. (1993) showed that denitrification rates were significantly higher at low landscape positions than at high landscape positions. Choudhary et al. (2002) reported the mean coefficient of spatial variation in N_2O emission was 119% on conventional and no-tillage agricultural systems, and permanent pasture in New Zealand. The large-scale spatial variability in N_2O emission might be up to 92% in the

agricultural soils of the boreal and parkland regions of Alberta, Canada (Lemke et al., 1998). Williams et al. (1999) found that the coefficients of spatial variability in N_2O emission ranged from 21% to 286% in a permanent pasture in UK. Röver et al. (1999), Kaiser et al. (1996), Myrold (1988) and Folorunso and Rolston (1984) reported the coefficients of spatial variation in N_2O emission were 100% to 500% in arable soil. In addition, Weitz et al. (2001), Corre et al. (1996), van Kessel et al. (1993), and Pennock et al. (1992) have demonstrated that soil moisture is the dominant control on N_2O fluxes, and that soil moisture often increased as they moved downhill in a given landscape. N availability would be another factor controlling N_2O emissions (Weitz et al., 2001; Paul and Clark, 1996).

However, finding complete descriptions of the effects of landscape patterns, especially long-term effects, on N_2O emission is difficult. As well as having large spatial variability, N_2O emissions also have large temporal variability. Flessa et al. (2002) used an automatic chamber system to measure N_2O fluxes (4 measurements per day) in potato fields in Germany. They found that temporal variation of the seasonal N_2O emission was large with flux rates ranging from 0 to 1100 $\mu g\ m^{-2}\ h^{-1}$. Water filled porosity and soil temperature explained 40% and 75% of the large temporal variability, respectively. In Taiwan, Chao et al. (2000) found that temporal coefficients of seasonal variation in N_2O production measured by chamber 1 to 6 times per day were 36–131%, 19–18%, 17–18%, and 25–26% for paddy soil, upland soil, orchard soil, and hardwood forest soil, respectively, and that diurnal N_2O flux measurements varied from 16.1 $\mu g\ N\ m^{-2}\ h^{-1}$ to 412.0 $\mu g\ N\ m^{-2}\ h^{-1}$ in a banana orchard. Through field measurements with a continuous monitoring flow-through system in a permanent pasture near Grange-over-Sands, Cumbria, UK, Williams et al. (1999) found that the diurnal variation of N_2O emission followed that of soil temperature at 10 cm depth, with N_2O production peaking in late afternoon. They also found that large N_2O emissions occurred when fertilizer coincided with rainfall. They measured seasonal N_2O fluxes that varied from 0.05 $mg\ N\ m^{-2}\ d^{-1}$ to 16.8 $mg\ N\ m^{-2}\ d^{-1}$. Kaiser et al. (1998) measured coefficients of temporal variation in N_2O fluxes that ranged between 136% and 192% over spring barley, sugar beet and winter wheat fields in Germany. Large temporal variation of N_2O emissions were caused by daily, seasonal and annual changes of climate, soil thawing and freezing cycles, differences in plant residues, crop species, the

fluctuations of soil water and temperature, and fertilizer effects on the dynamics of nitrification (NH_4^+) and denitrification (NO_3^-) (Flessa et al., 2002; Chao, et al., 2000; Röver et al., 1999; Williams et al. 1999; Kaiser et al., 1998). However, the large temporal variations of N_2O emission have been mostly assessed by infrequent chamber measurements.

The disadvantages of current field measurement techniques (micrometeorology and chamber) constraine the complete characterization of the large temporal variation, especially diurnal variation, as well as spatial variation in landscape. Chamber methods can be used to detect spatial variation, but have difficulty in measuring temporal variation unless automated. Micrometeorological methods can be used to measure temporal variation, but cannot resolve spatial variation in landscapes because their footprint areas are generally larger than 1 ha. Therefore, no measurement techniques have been available to assess temporal and spatial variations simultaneously. Ecosystem modeling would be the most useful method to address the large temporal and spatial variation of N_2O emissions if it could be combined with a geographic information system (GIS), and information about spatial variation of soil properties in landscapes.

To represent the effects of landscape heterogeneity on N_2O emissions in ecosystem models, the physical, chemical and biological processes that drive N_2O emissions, must be described in three dimensions. *Ecosys* is an ecosystem model that simulates water, solute and gas transport, and their effects on plant and microbial transformation of carbon (C) and nitrogen (N) (Li et al, 2004; Grant et al. 2001a, 2001b, 2001c, 1999a, 1999b, 1998, 1995a, 1995b; Grant and Nalder, 2000; Grant, 1999, 1997, 1995). When water transport causes O_2 deficiency, the shortage of electron acceptors for carbon oxidation is met through a series of denitrification processes from which N_2O is generated (Grant and Pattey, 2003).

In summary, no clear description of the magnitude and variation of N_2O emissions from a landscape is available. Landscape effects on temporal and spatial variations of N_2O emissions must be clarified to provide methods to improve estimates of N_2O emissions used in current national inventories. This chapter describes the integrated model of *ecosys* and GIS (*3D-Ecosys-GIS*), and its application in modeling landscape effects on the temporal and spatial variations of N_2O emissions.

3.2 Modeling N_2O emission in landscapes

In *ecosys*, three-dimensional water, solute and gas transport is simulated to determine spatial variation in the physical environment controlling N_2O emissions in landscapes. Horizon thickness, soil texture, total organic carbon and nitrogen contents and pH were the main soil properties in this study that were considered to cause the spatial variation in N_2O emissions. The calculation of water, solute and gas flows are described below with reference to equations in Appendix 3.1. To represent the spatial variations of soil properties and topography to *3D-Ecosys-GIS*, the landscape was divided into square grid cells in x (W–E) and y (N–S) directions, and soil was stratified into a number of soil layers in the z (vertical) direction.

3.2.1 Modeling water transport

3.2.1.1 Surface water movement

Runoff of surface water is generated when rainfall exceeds the sum of soil infiltration capacity, surface storage and plant interception. Surface water flow (Q_w, $m^3\ m^{-2}\ h^{-1}$) of each landscape position (grid cell in a watershed) in x (W–E) and y (N–S) directions is calculated by the Manning equation (Eq. A3.1, Morgan et al., 1998a, b). The slope (S) in Eq. A3.1 is calculated from the elevation difference of the ground surface plus depth of mobile surface water (d) between adjacent grid cells. The d in Eq. A3.1 is the positive difference between depth of surface water plus ice thickness and the maximum depth of surface storage per unit area. The maximum depth of surface storage is calculated from surface roughness and S according to Shaffer and Larson (1987) based on the assumption of triangular rills. The Manning's roughness coefficient (n, Eq. A3.1) is calculated from microtopographic roughness and particle size (soil texture) according to Morgan et al. (1998b). Surface flows (Q_w) in easterly and southerly directions are assigned positive values, and Q_w in westerly and northerly directions are assigned negative values.

3.2.1.2 Subsurface water flow

Water movement in subsurface soil is governed by a three-dimensional Richards' Equation (Eq. A3.3) (Kutilek and Nielsen, 1994; Somma et al., 1998; Sharma et al., 1987) for each x, y and z direction in a soil layer of a grid cell in the landscape.

When water moves through unsaturated soil, the hydraulic conductivity $K(\theta)$ is the geometric mean of those in the zones from and to which water is moving (Eq. A3.3). $\partial\Psi_i$ and ∂Z_{dt} are the differences of soil water potential (MPa) and distance (m) in the zones from and to which water is moving. Ψ is total water potential (MPa), which is sum of matric, gravitational and osmotic potentials.

When water moves in saturated soil, Eq. A3.3 is formulated as a three-dimensional Green-Ampt equation. The $K(\theta)$ equals saturated hydraulic conductivity (K_s). $\partial\psi_i$ and ∂Z_{dt} are the differences of soil water potential and distance in the saturated zone behind the wetting front and those in the unsaturated zone ahead of the wetting front.

3.2.2 Solute Transport

3.2.2.1 Surface transport

For each x, y position (grid cell) in a landscape, solute transport Q_{sj} (g m^{-2} h^{-1}) in x and y directions across the soil surface (Eq. A3.4) is calculated for each solute j from surface water flow Q_w (Eq. A3.1) and surface solute concentration (Eq. A3.5). The concentration of each solute by which transport is driven is generated from precipitation-dissolution, ion exchange, biological transformation and ion pairing reactions, and from the mixing of solute between water in the top-surface layer (depth = 0.005 – 0.01 m) and the surface water above.

3.2.2.2 Subsurface transport

A three-dimensional convection-dispersion equation (Eq. A3.6) (Kasteel et al., 2000; El-Sadek et al., 1999; Somma et al., 1998; Su, 1997; Yang et al., 1997) is used to calculate the subsurface transport flux of each solute through each landscape position x, y and z. In each x, y and z, the sink or source term U_n is negative when solute is added, and positive when solute removed from the soil solution through transformation, desorption, dissolution, ion exchange and ion pairing reactions, fertilizer, and uptake or release by root, mycorrhizae (Grant, 1998) and microbial communities.

3.2.3 Gas Exchange

Three-dimensional gas convection-diffusion equation (Eqs. A3.7 and A3.8) (Cousin et

al., 1999) is used to simulate transport of each gas k including O_2 and N_2O. N_2O is generated through **N_2O production** processes (see 3.2.4) that are directly and indirectly affected by soil water, nutrient contents and soil temperature. The gas exchange between gaseous and aqueous phases (E_k, Eq. A3.9) maintains the dynamic equilibrium of gases in soil gaseous and aqueous phases. The biological term U_{gk} (Eq. A3.8) is assigned a positive value when the gas is consumed by biological processes, and assigned a negative value when the gas is generated through biological processes.

Gas exchange processes within the soil and between the soil surface and atmosphere are very sensitive to soil water content. As soil water content increases, air-filled porosity (θ_g in Eq. A3.10) decreases, sharply reducing gaseous diffusivity (D_{gk}, Eq. A3.10), and hence gas concentration G_{gk} (Eqs. A3.7). Thus this change decreases aqueous gas concentration (G_{wk}, Eq. A3.8) through Eq. A3.9. In the case of O_2, the supply of O_2 for biological uptake (U_{gk}, Eq. A3.8) decreases rapidly, forcing the use of other electron acceptors that drive denitrification processes, sequentially generating NO_2^-, N_2O, and eventually N_2 (see 3.2.4).

There is also a complex sensitivity of gas exchange to soil temperature in the model. An increase in soil temperature causes a decrease in gas solubility (f_{sk} in Eqs. A3.9 and A3.12), and so decreases aqueous gas concentration G_{wk} (Eqs. A3.8 and A3.9). An increase in soil temperature also raises biological consumption (e.g. U_{gO2} in Eq. A3.8) further decreasing G_{wk}. These decreases are only partially offset by an increase of gaseous and aqueous diffusivity with soil temperature (f_g and f_w in Eqs, A3.10 and A3.11).

The sensitivity of gas exchange to soil water and temperature can result in sharp changes O_2 supply, and hence in N_2O production through denitrification and nitrification with comparatively small changes in soil water and temperature.

3.2.4 N_2O production

3.2.4.1 Denitrification

The oxidation of soil carbon by all aerobic heterotrophs (Eq. A3.15) develops a demand for electron acceptors (R'_{O2}, Eq. A3.16) met preferentially by aqueous O_2. The consequent reduction of aqueous O_2 (R_{O2}, Eq. A3.17) drives the transport of O_2 between the atmosphere and the soil depending on aerodynamic boundary layer conductance and soil gaseous diffusivity (Eqs. A3.7 and A3.10), and to a lesser extent dispersion-diffusion in

water (Eq. A3.8). If the reduction of O_2 (R_{O2}, Eq. A3.17 = U_{gk} in Eq. A3.8) is smaller than demand (R'_{O2}, Eqs. A3.16), the demand for electron acceptors unmet by O_2 (R_e, Eq. A3.18) can be met by NO_3^- (Eq. A3.19), NO_2^- (Eq. A3.20), and N_2O (Eq. A3.21) reduction, sequentially increasing the production of NO_2^-, N_2O and N_2 (Grant, 2001, 1995b; Grant et al., 1993a, 1993b). Aqueous N_2O is thus competitively generated and consumed by NO_2^- and N_2O reduction, with net production being the difference between Eqs. A3.20 and A3.21. The parameters of 0.0625, 7 and 2 in Eqs. A3.17 to A3.20 convert O_2 (g) to electron (mol), electron (mol) to NO_x-N (g) and NO_2^--N (g) to N_2O-N (g). The temperature sensitivity of heterotrophic oxidation (f_t in Eq. A3.15) is an Arrhenius function of soil temperature (Eq. A3.22).

3.2.4.2 Nitrification

N_2O can also be generated through the reduction of NO_2^- by ammonium oxidizers during nitrification. The oxidation of NH_4^+ by aerobic-autotrophic ammonium oxidizers (Eq. A3.23) develops a demand for O_2 (R'_{O2n}, Eq. A3.24). The actual reduction of O_2 is limited by the concentration of O_2 at the surface of ammonium oxidizers (R_{O2n}, Eq. A3.25) which is controlled by transport (Eqs. A3.7 and A3.8) and dissolution (Eq. A3.9) processes. As O_2 availability decreases, the deficiency of electron acceptors for NH_4^+ oxidation (Eq. A3.26) is met by NO_2^- generated in nitrification. The reduction of NO_2^- generates N_2O (Eq. A3.27). The sensitivity of N_2O production from nitrification is mainly controlled by gas exchange (Eqs. A3.7 to A3.14), and by O_2 demand of NH_4^+ oxidation affected by soil temperature through an Arrhenius function (Eq. A3.22). The production of N_2O by this mechanism is usually a small fraction of ammonium oxidized, because $[O_{2n}]$ is usually much larger than K_{O2n} in Eq. A3.25.

3.2.5 Architecture of *3D-Ecosys-GIS* Model

At a landscape scale, *ecosys* can model hundreds of grid cells, and each grid cell has its own terrain attributes, soil properties, crops and soil management practices. Manually handling the information and editing the input files of *ecosys* for hundreds of grid cells is difficult. A link program was developed to integrate the three dimensional *ecosys* into a GIS framework which handles inputs for all grid cells, enabling *ecosys* to simulate

landscape N_2O emission (Fig. 3.1). The integrated model is named *3D-Ecosys-GIS* (see the interface in appendix 3.2) as a sub version of *ecosys*. The communications between the GIS and link programs and between the link program and *3D-ecosys* are maps and text files, respectively.

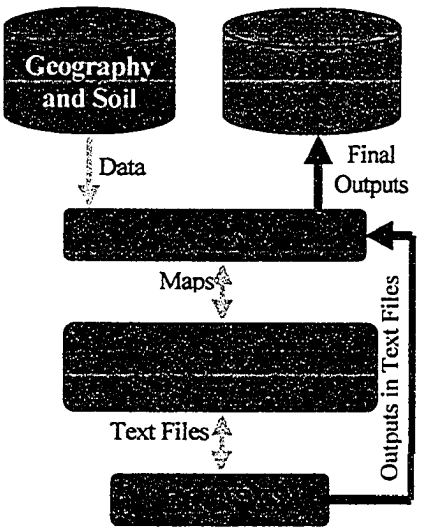

Figure 3.1: The architecture of *3D-Ecosys-GIS* model.

A digital elevation map (DEM) was derived in the GIS for the landscape being studied from global positioning system (GPS) data (Fig. 3.1). The GIS suggested the minimum size of grid cells for which topographic attributes could be derived according to the density of measured points in the GPS data. This minimum size was then increased as required for landscape analysis while retaining at least 3 grid cells within typical slope lengths. Terrain attributes (Chapter 2) were derived from the DEM by functions and extensions of GIS software.

The Landscape Soil Property Predictor (LSPP) was used to estimate properties of soil profiles at fine scale from limited measurements of soil profile properties and from terrain attributes derived in the GIS (Fig. 3.1, see details in Chapter 2).

The linkage program (Fig. 3.1) consisted of input and output file handlers. The input file handler stratified grid cells to have the same number of soil layers, and generated text input files in the format required by *3D-ecosys* for a sample watershed in the landscape derived from the DEM in GIS. The output file handler converted text files from *3D-ecosys* into GIS maps of N_2O emissions.

3.3 Study site

The study site (Fig. 3.2) is a 76.6 ha. field representative of the black soil region in the aspen parkland ecoregion near Viking, Alberta, Canada. Average precipitation was 359 mm, and average air temperature was 2.8 °C during 1996 to 2002. The site has a hummocky topography with a moderate slope (10% to 13%). The elevation of the site varies between 714 m and 726 m. The field is dominated by black chernozemic soils. The field was cultivated conventionally with a wheat, barley and canola crop rotation fertilized

with 86, 13, and 76 kg N ha^{-1}, respectively, and cropping management using precision agriculture.

3.4 Field Measurement of N_2O Emission

Four field observation transects were marked out in 1997 (Fig. 3.2) to measure N_2O fluxes by the static chamber method. Four measurement locations along each transect represented top, middle, and foot slopes and depressional areas. Field measurements of N_2O emissions were performed for these transects by research staff of Tom W. Goddard's group in Alberta Agriculture, Food and Rural Development.

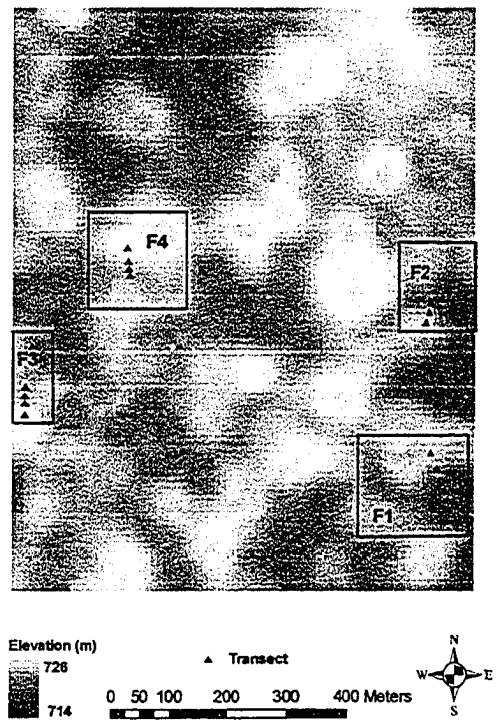

Figure 3.2: The study site, observation transects and sub sites at Viking, Alberta, Canada (53°05'N, 111°47'W).

Rectangular plexiglass chambers were used on the upland portions of these transects. The chambers were 0.1 m^2 in area and had 10 liter headspace capacity. In the depressional areas, cylindrical chambers 15 cm in diameter were used to minimize plant disturbance (Sprout and Goddard, 2003). The upland chambers were removed and replaced after seeding and harvesting operations. At sampling times flat lids were placed on the chambers and held in place with heavy duty rubber bands. After 30 minutes an air sample was removed from the chamber with a 20 cc syringe and placed in a 10 ml container for storage and transport. Samples were taken approximately twice a week during peak times at spring thaw in March and after high rainfall events from May to July. Otherwise, samples were taken about once per week until August, then once every two weeks, and then once a month in the late fall and winter. The actual sample dates depended on spring thaw and rainfall events. Samples were always taken between 13:00 and 14:00 of local time.

N_2O was measured with a gas chromatograph (model 3400, Varian Instrument Company, Walnut Creek, California, USA) equipped with a Ni63 electron capture detector and a ten port 2 position valve and valve actuator (Valco Valve # ET4C10UWE, Valco

Instruments Company, Houston, Texas, USA). Separation of N_2O from other air components was achieved by using a pre-column (Porapak N, 80/100 mesh, 0.45m x 1/8" OD x 2mm ID stainless steel, Chrompack #ML3256) followed by an analytical column (Hayesep D, 80/100 mesh, 1.8m x 1/8"OD x 2mm ID, Chrompack #PDP3206). The pre-column was backflushed 30 seconds after injection to prevent water and sulphur components from entering the analytical column. The retention time for N_2O was approximately 1.6 minutes at a flow rate of 20 ml/min of argon/methane (90:10% by volume) and an oven temperature of 60 °C. The detector was held at 300°C. Standards and samples were manually injected into the 1 ml sample loop using plastic luer type syringes. The instrument was standardized across a range of 0.29–6.86 ppm N_2O by injecting custom gas mixtures (Praxair Specialty Gasses, Edmonton, AB) at full strength and at specific dilutions with high purity nitrogen. Star Chromatography Workstation software (version 3.3, Varian Instrument Company, Walnut Creek, California, USA) was used for data processing.

3.5 Model Experiment

Computational constraints prevented simulation of N_2O emission for the entire study site at 10 meters resolution (7763 grid cells) with the *3D-Ecosys-GIS* model. Simulation was limited to four sub sites (F1, F2, F3 and F4 in Fig. 3.2). Each sub site included one complete mini-watershed around one observation transect. These sub sites were represented in *3D-Ecosys-GIS* as a matrix with 10×10 meters resolution, resolved into rows x (W–E) and columns y (N–S). Measurement locations along each transect were identified by column and row numbers in each sub site. Some locations were at boundaries of two adjacent grid cells, or at the intersection of four adjacent grid cells. Therefore, averaged model values of adjacent grid cells were used to compare with measurements at these locations. Plant residue carbon was initialized from the outputs of an initializing model run for one grid cell over 50 years. Crop and soil management in these four sub sites followed that reported for the field.

The model was run for each sub site starting on January 1, 1997 and ending December 31, 2002. Hourly climate data from 1997 to 2002 from a meteorological station at Viking were used in all simulation runs. The crops were wheat in 1997, barley in 1998, canola in

1999, wheat in 2000 (precipitation = 451 mm), barley in 2001 (precip. = 332 mm) and canola in 2002 (Precip. = 221 mm). The outputs in 1997, 1998 and 1999 were not used to evaluate the effects of landscape on N_2O emissions to allow inorganic nitrogen in the model to become independent from initialized values. The modeled hourly N_2O emissions were compared with measured data to validate the *3D-Ecosys-GIS* model.

3.6 Results

3.6.1 Measured and modeled N_2O fluxes at the landscape scale

Modeled N_2O fluxes varied from 0 to 3600 μg N m^{-2} h^{-1}, while measured N_2O fluxes varied between 0 and 300 μg N m^{-2} h^{-1} (Figs. 3.3, 3.4, 3.5 and 3.6). In the example transect in sub site F2, modeled N_2O fluxes decreased from wet through normal to dry years (Fig. 3.3, 3.4 and 3.5). Modeled N_2O fluxes decreased from top through middle to foot slopes in the wet year (2000; precip. 451 mm >> average precip. 359 mm) (Fig. 3.3b, c and d) while they increased in the dry year (2002; 221 mm << average precip.) (Fig. 3.5b, c and d). However, fluxes were lower at middle slope than at top and foot slopes in the normal year (2001; precip. 332 mm ≈ average precip.) (Fig. 3.4b, c and d).

Modeled N_2O fluxes were very sensitive to change in soil water content. Much of the variation of modeled N_2O fluxes resulted from small changes in relative water-filled porosity (RWFP). Increasing RWFP decreased air-filled porosity (θ_g, Eq. A3.10), which causes large reductions of gas diffusivity when θ_g declined below threshold values (D_g, Eq. A3.10). Reduction of D_g slowed replenishment of O_2 (U_{gk}, R_{O2} and R_{O2n}, Eqs. A3.8, A3.17 and A3.25), and so raised the unmet demand for electron acceptors (R_e and R_{en}, Eqs. A3.18 and A3.26), causing large increases of N_2O fluxes (Eqs. A3.19 to A3.21, and A3.27; Figs. 3.3, 3.4, 3.5 and 3.6). For instance, increases in RWFP of only 0.02 and 0.06 caused N_2O fluxes to raise by about 1600 μg N m^{-2} h^{-1} on days 148 to 149 and by 3400 μg N m^{-2} h^{-1} on days 162 to 165 in 2000 (Fig. 3.6a). Similarly, an increase in RWFP of 0.07 to 0.08 increased N_2O fluxes by 400 μg N m^{-2} h^{-1} on days 153 to 155 in 2001 (Fig. 3.6b) and by 140 μg N m^{-2} h^{-1} on days 199 to 200 in 2002 (Fig. 3.6c). Thus the time course of modeled emissions was more characteristic of a threshold response to changes in θ_g, rather than a continuous one.

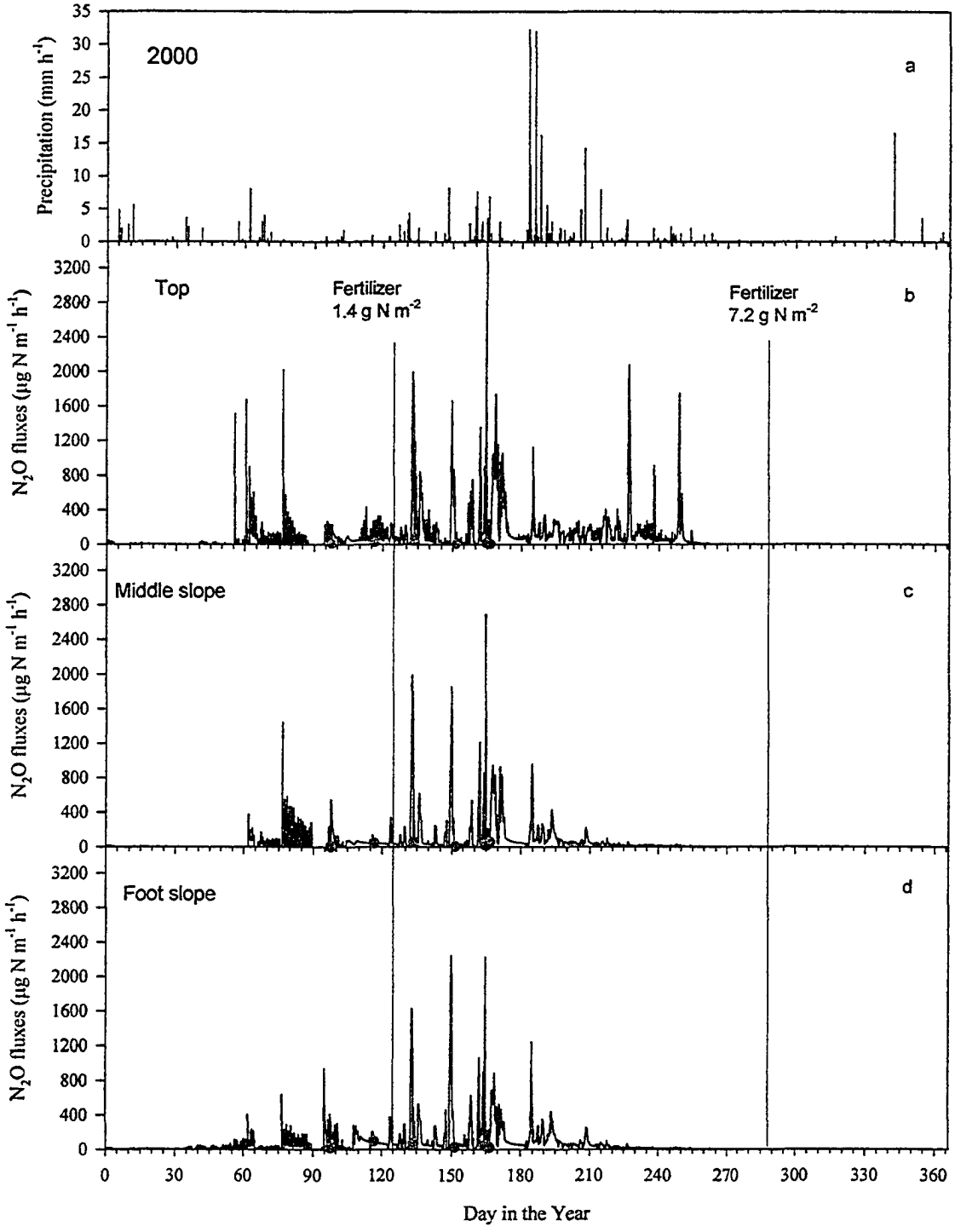

Figure 3.3: The measured (dot) and modeled (line) N_2O fluxes at top, middle and foot slopes in sub site F2 in the hummocky agricultural landscape at Viking, Alberta, Canada in 2000.

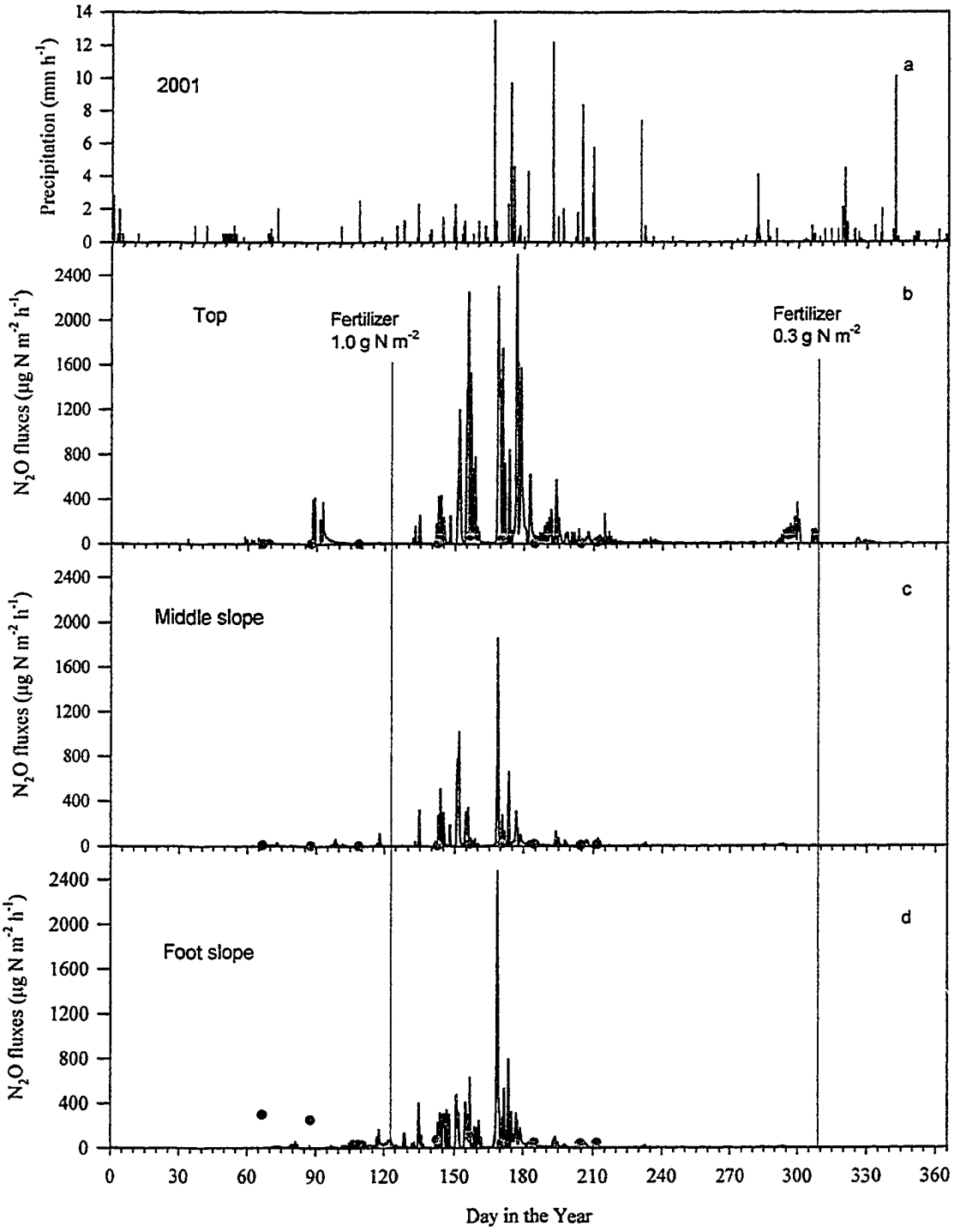

Figure 3.4: The measured (dot) and modeled (line) N_2O fluxes at top, middle and foot slopes in sub site F2 in the hummocky agricultural landscape at Viking, Alberta, Canada in 2001.

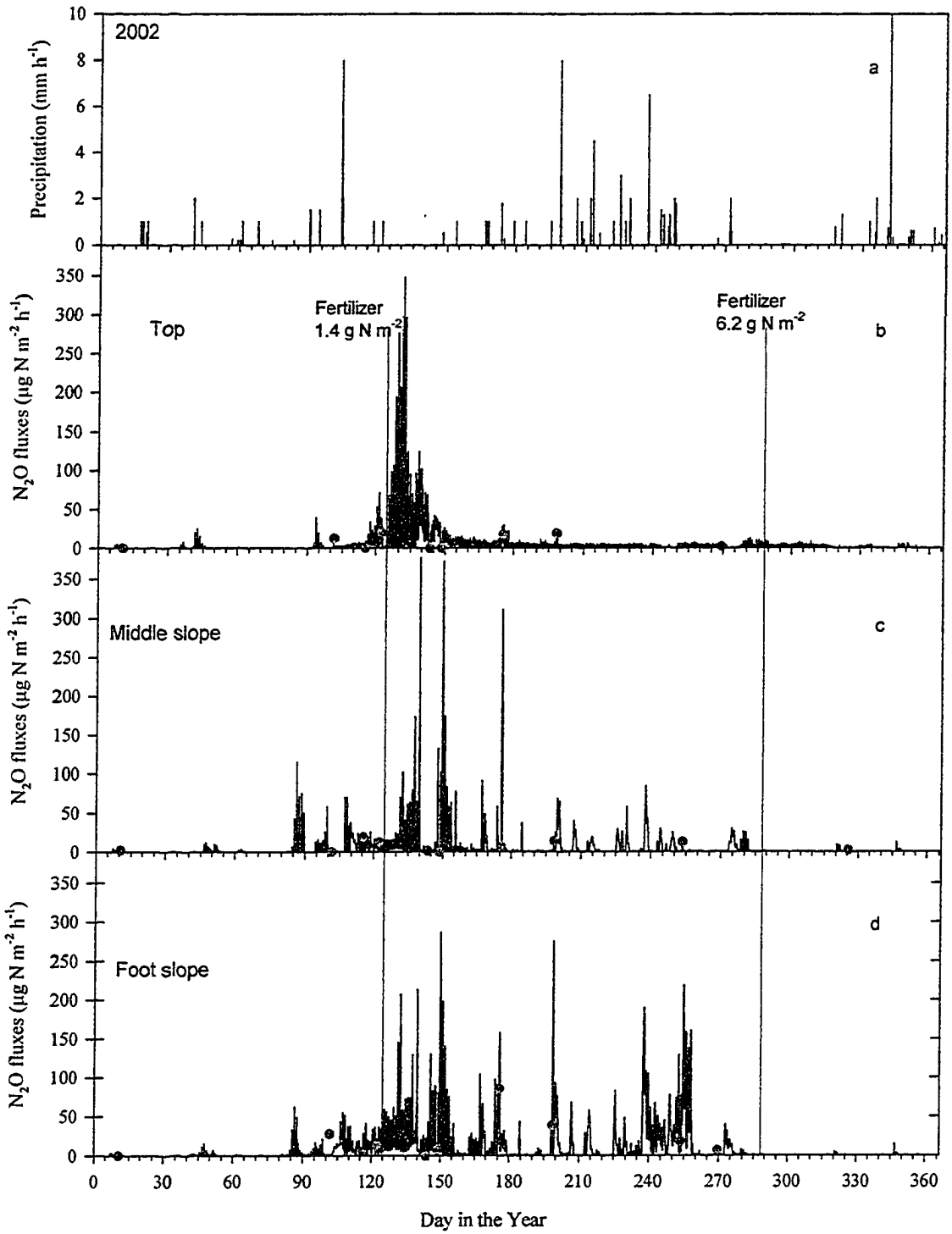

Figure 3.5: The measured (dot) and modeled (line) N_2O fluxes at top, middle and foot slopes in sub site F2 in the hummocky agricultural landscape at Viking, Alberta, Canada in 2002.

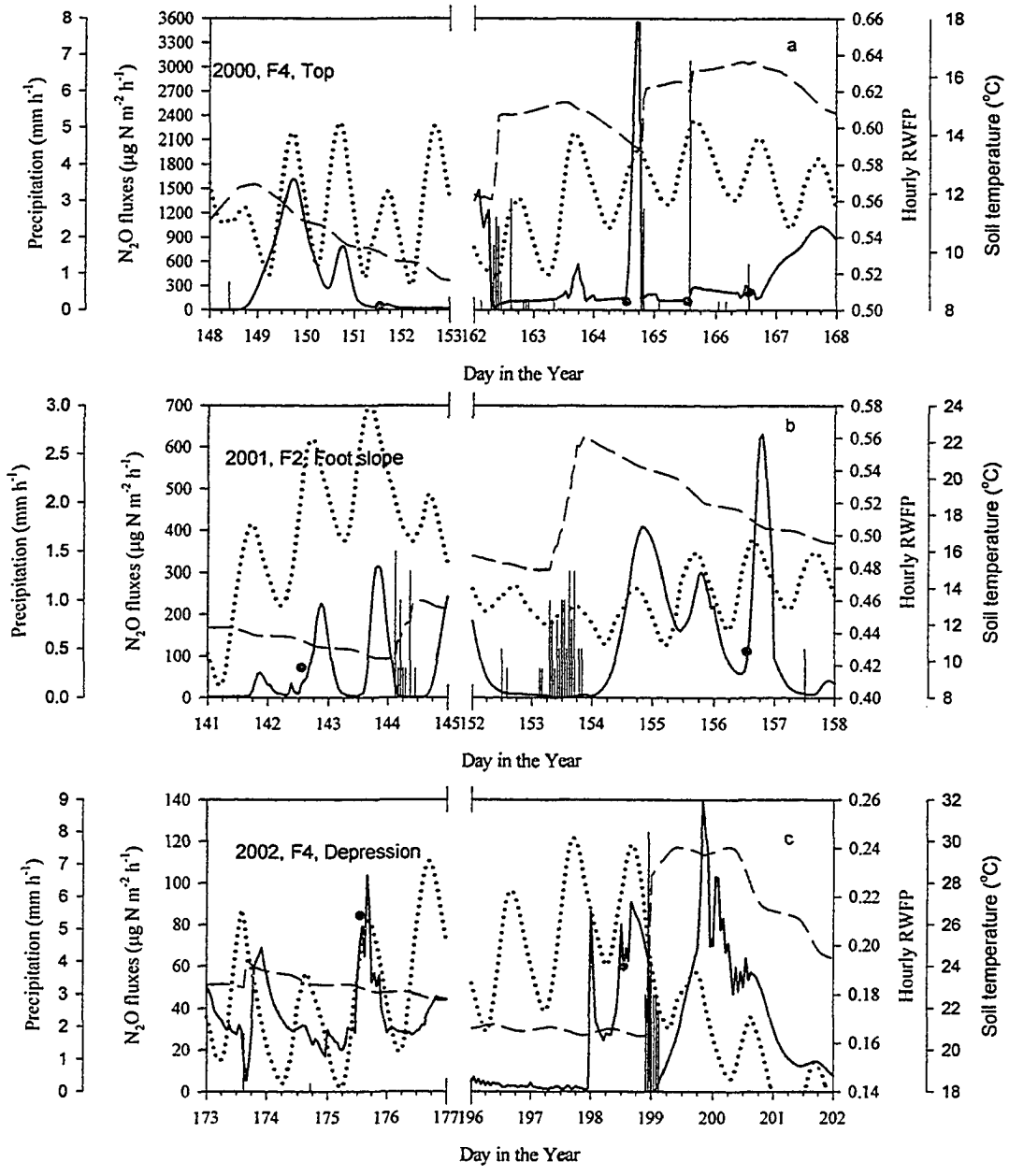

Figure 3.6: The measured (dots) and modeled (solid line) N_2O fluxes, rainfall (vertical bars), and relative water-filled porosity (RWFP, long-dash line) and soil temperature (dot line) in upper 20 cm zone at (b) foot slope in sub site F2, and (a) top and (c) depression in sub site F4 in the hummocky agricultural landscape at Viking, Alberta, Canada, in 2000, 2001, 2002.

Modeled N_2O emissions responded sharply to diurnal changes in soil temperature. Most of modeled peak N_2O emissions occurred during the late afternoon to early night following the peak of the average soil temperature in the upper 20 cm soil zone (Fig. 3.6). Peak soil temperatures occurred later than did peak air temperatures because thermal conductivity of

soil was lower than that of air. As soil temperatures increased during the day, microbial activities developed higher O_2 demand (R'_{O2}, Eqs. A3.15 and A3.16; R'_{O2n} Eqs. A3.23 and A3.24) through an Arrhenius function (Eq. A3.22). The replenishment of O_2 was decreased at the same time because of decreasing O_2 solubility in warmer soil (Eqs. A3.9 and A3.12), so that rising deficiency of O_2 (($R'_{O2} - R_{O2}$) and ($R'_{O2n} - R_{O2n}$)) and the consequent demand for electron acceptors (R_e and R_{en}, Eqs. A3.17 and A3.26) produced large N_2O emissions in warmer soil (Eqs. A3.19 to A3.20, and A3.27). For example, large N_2O fluxes on days 149 to 150 in 2000 (Fig. 3.6a), 142 to 144 in 2001 (Fig. 3.6b), and 175 to 176 in 2002 (Fig. 3.6c) were caused by increases of soil temperature in the upper 20 cm soil zone.

Rapid changes in modeled N_2O fluxes caused by small changes in soil water and temperature complicated comparisons with measured fluxes. For example, during selected periods in Fig. 3.6, measured N_2O fluxes were 110 and 120 μg N m^{-2} h^{-1} in 2000, 111 μg N m^{-2} h^{-1} in 2001, and 56 μg N m^{-2} h^{-1} in 2002. Measured N_2O fluxes did not show the large temporal variation of modeled N_2O fluxes (Fig. 3.3, 3.4, 3.5 and 3.6). However, measured and modeled N_2O fluxes matched each other very well at the time of the measurements.

The correlations between modeled and measured hourly N_2O fluxes were highly significant in 2000, 2001 and 2002 (Table 3.1). Modeled results explained variation of measured N_2O fluxes very well in the wet year ($R^2 = 0.87$ in 2000), but less well in the normal ($R^2 = 0.40$ in 2001) and dry years ($R^2 = 0.37$ in 2002) when variation in fluxes was smaller. The model generally overestimated N_2O fluxes in the three years, i.e. *b* in Table 3.1 was smaller than 1 (Tables 3.1 and 3.2, Fig. 3.7). Measured and modeled N_2O fluxes from the wet year were larger and much closer to the 1:1 line than were those in the normal and dry years (Fig. 3.7). The smaller correlations (R^2, Table 3.1) and large scatter from the 1:1 line in the normal and dry years probably resulted from smaller variation in measured values with most measured N_2O fluxes being smaller than 75 μg N m^{-2} h^{-1} (Fig. 3.7b and c).

The averaged measured and modeled N_2O fluxes from the four transects decreased from tops through middle slopes to foot slopes in the wet year, but were in reverse order in the dry year (Table 3.2). Both measured and modeled N_2O fluxes larger than 75 μg N m^{-2} h^{-1}

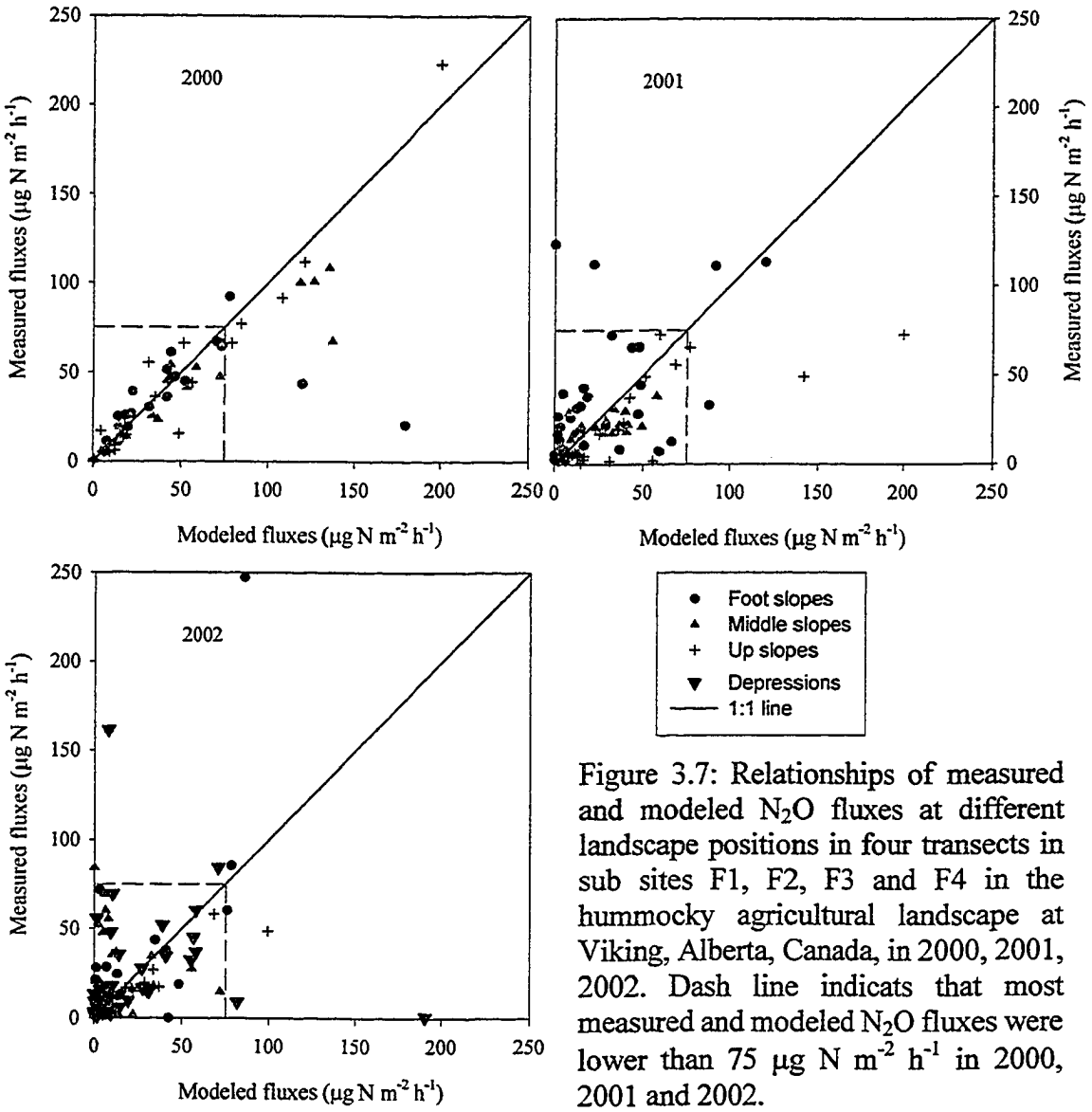

Figure 3.7: Relationships of measured and modeled N_2O fluxes at different landscape positions in four transects in sub sites F1, F2, F3 and F4 in the hummocky agricultural landscape at Viking, Alberta, Canada, in 2000, 2001, 2002. Dash line indicats that most measured and modeled N_2O fluxes were lower than 75 μg N m^{-2} h^{-1} in 2000, 2001 and 2002.

mainly occurred at tops and middle slopes in the wet year, and at foot slopes and depressions in the normal and dry years (Fig. 3.7 and Table 3.2). The coefficients of spatial variation (CSV – the ratio (%) of standard deviation to mean of non-zero N_2O fluxes across landscape) in measured and modeled N_2O fluxes were similar (Table 3.2, Fig. 3.7).

The ratio of standard differences between measured and modeled N_2O fluxes (SD) to the means of measured N_2O fluxes (RSD) varied annually between 120% and 170% in the three years (Table 3.1). The RSDs were in the ranges of coefficients of variation (CV) in measured N_2O fluxes at each landscape position among the four transects (Fig. 3.2) (taking landscape positions as treatments and transects as replications) (18% ~ 183%, Table 3.2).

The ranges of CVs for measured and modeled N_2O fluxes were pronounced, although CVs varied among measured events (Table 3.2). Modeled and measured N_2O fluxes both decreased with precipitation, but were not related to fertilizer application rate (Tables 3.1 and 3.2).

Table 3.1: Statistical results from log-transformed regressions of measured on modeled N_2O fluxes (μg N m^{-2} h^{-1}). Sig.: significance level. SD was standard differences between modeled and measured values. RSD was the ratio of SD to measured mean. a ± se was the regression intercept and its standard error, and b ± se was the regression slope and its standard error.

Year	Data pairs[§]	Precipitation (mm)	Fertilizer (g N m^{-2})	R^2	Sig.	SD (μg N m^{-2} h^{-1})	RSD (%)	a ± se	b ± se
2000	60	451	8.6	0.87	<0.001	51	150	0.44 ± 0.16	0.84 ± 0.04
2001	81	332	1.3	0.40	<0.001	27	123	1.25 ± 0.23	0.55 ± 0.08
2002	103	221	7.6	0.37	<0.001	27	169	1.39 ± 0.18	0.52 ± 0.07

[§]: The statistical analysis was performed from non-zero data pairs.

Table 3.2: The coefficients of variation (CV) in log-transformed values and mean of measured and modeled N_2O fluxes for measured emission events at top, middle and foot slopes and depressions in the hummocky agricultural landscape at Viking, Alberta, Canada, in 2000, 2001 and 2002.

	Tops		Middle slopes		Foot slopes		Depressions		Coefficient of spatial variation (%)[¶]
	CV range[§] (%)	Mean[‡] (μg N m^{-2} h^{-1})	CV Range (%)	Mean (μg N m^{-2} h^{-1})	CV range (%)	Mean (μg N m^{-2} h^{-1})	CV Range (%)	Mean (μg N m^{-2} h^{-1})	
				Measured N_2O fluxes					
2000	60 ~ 162	40	33 ~ 84	32	18 ~ 133	30	--	--	93
2001	48 ~ 168	16	18 ~ 81	13	36 ~ 126	38	--	--	147
2002	72 ~ 178	8	67 ~ 183	13	48 ~ 169	21	62 ~ 139	23	133
				Modeled N_2O fluxes					
2000	48 ~ 126	55	38 ~ 103	49	9 ~ 133	46	--	--	84
2001	53 ~ 173	28	27 ~ 81	25	41 ~ 166	47	--	--	124
2002	40 ~ 190	13	37 ~ 179	18	42 ~ 186	26	77 ~ 181	30	148

[§]: Zero values were removed before log-transformation. CV indicated coefficient of variation of a measured or modeled N_2O emission event taking landscape positions as treatments and measurement transects as replications.

[‡]: The mean of modeled fluxes came from the N_2O fluxes that corresponded to those in the measured emission events.

[¶]: Coefficient of spatial variation in measured N_2O fluxes was developed from non-zero measurement data. Coefficient of spatial variation of modeled N_2O fluxes was calculated from the modeled values that corresponded to those in the measured emission events.

In summary, modeled N_2O fluxes were comparable with measured values in

coefficients of variation and spatial patterns in the hummocky agricultural landscape. Modeled N_2O emissions of *3D-Ecosys-GIS* could therefore represent the field N_2O emissions.

3.6.2 Temporal variation of N_2O emissions across landscape

Total area of the four sub sites was 12% (9 ha.) of the entire study site (F1, F2, F3 and F4 in Fig. 3.1). Across the hummocky agricultural landscape, average hourly N_2O fluxes for the whole year declined by one-third from the wet year to the dry year (Table 3.3). The coefficient of temporal variation (CTV – ratio (%) of standard deviation to mean of log-transformed non-zero N_2O fluxes at one site over time) in modeled hourly N_2O fluxes was higher in the dry year than those in the normal and wet year (97% vs. 81% and 73%). Modeled hourly N_2O fluxes reached 2569 $\mu g\ N\ m^{-2}\ h^{-1}$ in the wet year, but 16% of that rate in the dry year (Table 3.3).

Table 3.3: Temporal variation of modeled hourly N_2O fluxes ($\mu g\ N\ m^2\ h^{-1}$) for all sub sites[‡] in the three years in the hummocky landscape at Viking, Alberta, Canada.

Year	Annual total ($g\ N\ m^{-2}$)[‡]	Average hourly flux ($\mu g\ N\ m^2\ h^{-1}$)	CTV (%)[§]	Maximum flux ($\mu g\ N\ m^2\ h^{-1}$)
2000	0.56	64	73	2569
2001	0.38	43	81	1684
2002	0.18	21	97	410
In 3 years	1.12	43	83	2569

[§]: The coefficient of temporal variation (CTV) was calculated from log-transformed values of modeled N_2O fluxes.
[‡]: This is average values of all model grid cells excluded those from boundary grid cells.

Most modeled emissions occurred between seeding (spring fertilizer) to grain filling (May 4 to July 30), contributing 76% and 74% of annual N_2O emissions in 2000 and 2001 (Figs. 3.3 to 3.5). Periods of greatest N_2O emissions coincided with those of precipitation. Emissions remained larger during May and June than during the rest of in 2002 even though precipitation during this period was only 19% of the annual total (Fig. 3.5). With substrates (mineral N) for nitrification and denitrification provided by spring fertilizer (early May, Figs. 3.3 to 3.5) and mineralization during this period, large N_2O emissions occurred after any effective rainfall that could cause transient O_2 deficiency. Before May, lower soil temperature caused lower demand for O_2 and hence electron acceptors, lowering N_2O emissions (Figs. 3.3 to 3.5, Eqs. A3.15 to A3.21). After July 30, mineral N was

depleted by crop uptake resulting in lower N_2O emissions. The fall fertilizer did not affect N_2O emissions in the late fall and winter (Figs. 3.3 to 3.5). If precipitation was high in winter and spring, such as in 2000 (Fig. 3.3a), fall fertilizer application considerably increased the N_2O emissions in the following spring (Fig. 3.3b, c and d). The spring fertilizer application might continuously raise N_2O emissions through the growing season until fall fertilizer application (Fig. 3.5c and d).

As the precipitation declined from 451 mm in 2000, through 322 mm in 2001, to 221 mm in 2002, modeled annual N_2O emission declined from 0.56 g N m^{-2}, through 0.38 g N m^{-2}, to 0.18 g N m^{-2}. The large decrease of annual N_2O emission resulted mainly from the decrease of precipitation during the main emission period (Fig. 3.5a).

3.6.3 Spatial variation of N_2O emissions across landscape

3.6.3.1 Spatial variation of modeled soil water, solute and N_2O emissions along a slope transect

A hill slope in the hummocky agricultural landscape was randomly selected from sub site F2 to study the changes in soil water content in the upper 20 cm soil zone that controlled variation in N_2O emissions. This hill slope included top, backslope (concavity with small catchment area), midslope, foot slope (concavity with large catchment area) and flat area (Fig. 3.8a), with a horizontal distance of 100 meters encompassing 10 grid cells. From June 30 to July 8, 2000, total rainfall was 122.7 mm including four big rainfall events on July 1 (32.8 mm), July 2 (24.1 mm), July 4 (37.6 mm) and July 6 (24.4 mm) (Fig. 3.8b). All data for this study were abstracted from the model run for sub site F2.

On the first day (June 30), the relative water-filled porosity (RWFP) in the upper 20 cm soil zone increased from upper slope to lower slope, and was slightly higher at concavities and at foot slopes (Fig. 3.8c). The spatial patterns of NH_4^+ (Fig. 3.8d) and NO_3^- (Fig. 3.8e) contents in soil were similar to that of RWFP (Fig. 3.8c). N_2O emissions were less than 2 mg N m^{-2} d^{-1} on top, backslope and midslope (Fig. 3.8g). N_2O emission was about 6 mg N m^{-2} d^{-1} at the foot slope (Fig. 3.8f) with higher RWFP (Fig. 3.8c).

Rainfall from July 1 to 6 (Fig. 3.8b) caused increases in RWFP (Fig. 3.8c). Runoff flowed to and accumulated at concavities (back and foot slopes at 20 to 30 m and at 70 to 80 m of horizontal distance in Fig. 3.8a) (Eqs. A3.1 and A3.2), resulting in larger increases

of RWFP and NH_4^+ during the study period (Fig. 3.8c and d). The increase of NH_4^+ might have resulted from (1) water blocking the surface soil resulting in shortage of O_2, reducing nitrification (Eq. A3.25), and (2) surface transport of solute accompanying surface runoff resulting in larger increases at backslopes and footslopes (Eqs. A3.4 and A3.5). The NO_3^- content decreased with the increase of soil water on the rainy days (Fig. 3.8e) probably from less replenishment through nitrification, from consumption through denitrification and very small amount of leaching. The decrease of NO_3^- was less at lower slopes than at upper slopes because NO_3^- was transported from upper slopes to lower slopes with surface and subsurface water flow (Eqs. A3.4 to A3.6) partially offsetting the decrease of NO_3^- described above during the rainy days. The N_2O emissions increased during the first 4 days with the rise in RWFP, then decreased during the following two days as RWFP rose further causing lower gas diffusivity (Fig. 3.8c and f, Eq. A3.10). On July 3, the threshold value of RWFP to N_2O emission remarkably increased the emission over the slope (Fig. 3.8c and f).

During the two days after rain events, RWFP decreased because water was removed by evapotranspiration and drained to deeper soil layers and to adjacent grid cells through subsurface downhill flow (Eq. A3.3). Air-filled porosity increased which restored gaseous pathways through the soil surface and caused rapid increase of gas diffusion (Eqs. A3.7 and A3.10). Consequently, accumulated N_2O production from previous days was rapidly released to the atmosphere (day 9, Fig. 3.8f). The lower RWFP resulted in lower N_2O emissions on slopes. A RWFP of about 0.6 resulted in N_2O emission of about 60 mg N m^{-2} d^{-1} at the foot slope (Day 9, Fig. 3.8f). When RWFPs were 0.6 – 0.7 at the foot slope (days 5–8, Fig. 3.8c), N_2O emissions were 20 to 40 mg m^{-2} d^{-1} lower (Fig. 3.8f). These results demonstrated how the large spatial and temporal variations of N_2O emissions arose in the model (e.g. in Tables 3.2 and 3.3).

3.6.3.2 Spatial variation of modeled daily N_2O emission

Three events were used to study the spatial variability of modeled RWFP and associated N_2O emissions in the hummocky agricultural landscape (Figs. 3.9 and 3.10). N_2O emission events on 13 June 2000 (E1), 19 June 2001 (E2) and 28 May 2002 (E3) were the largest at most grid cells in the four sub sites (F1, F2 F3 and F4, Fig. 3.2) in each of the three years. For event one (E1), precipitation during the week before the event was 45.6 mm, including

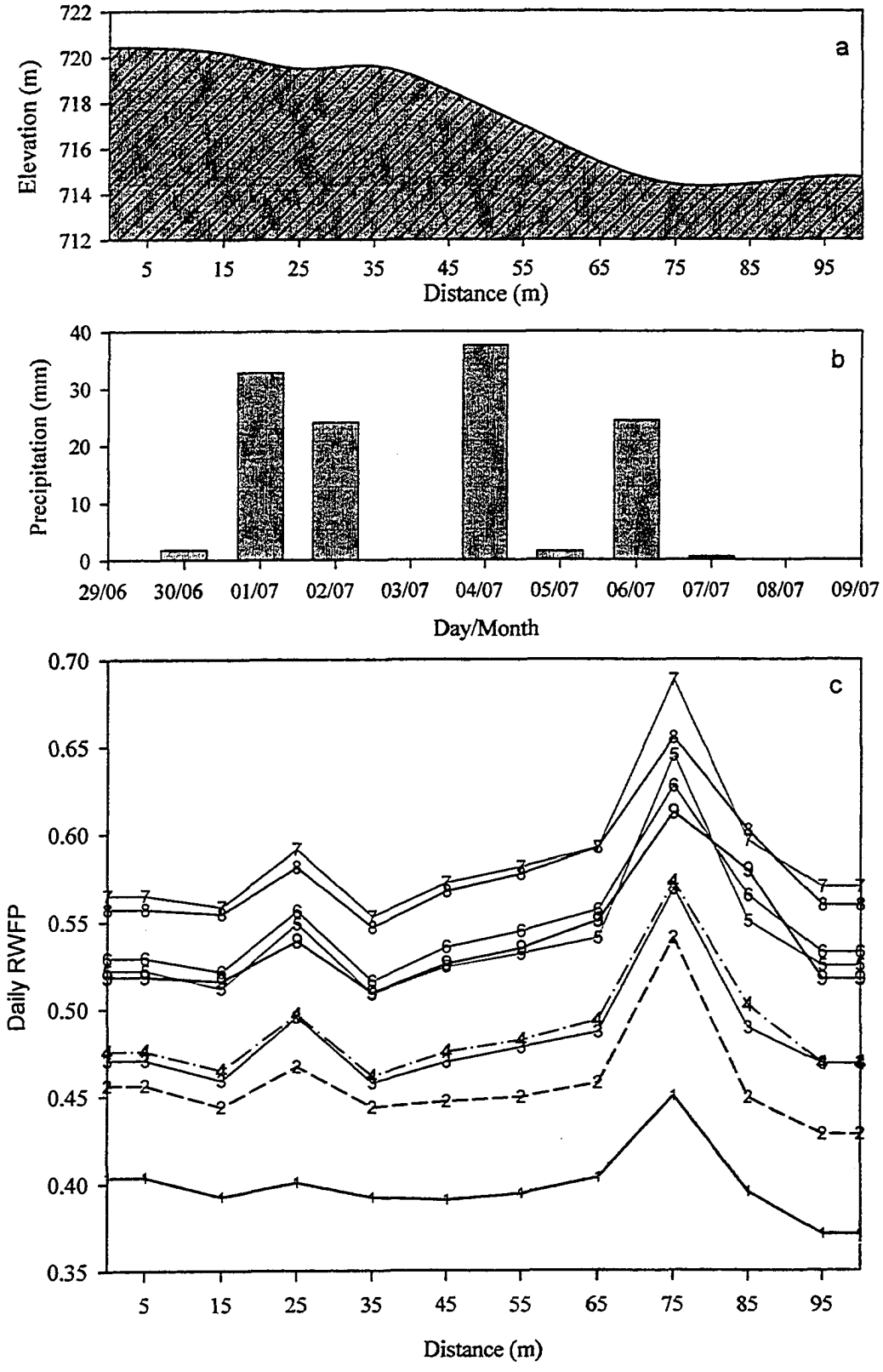

(Continued on next page)

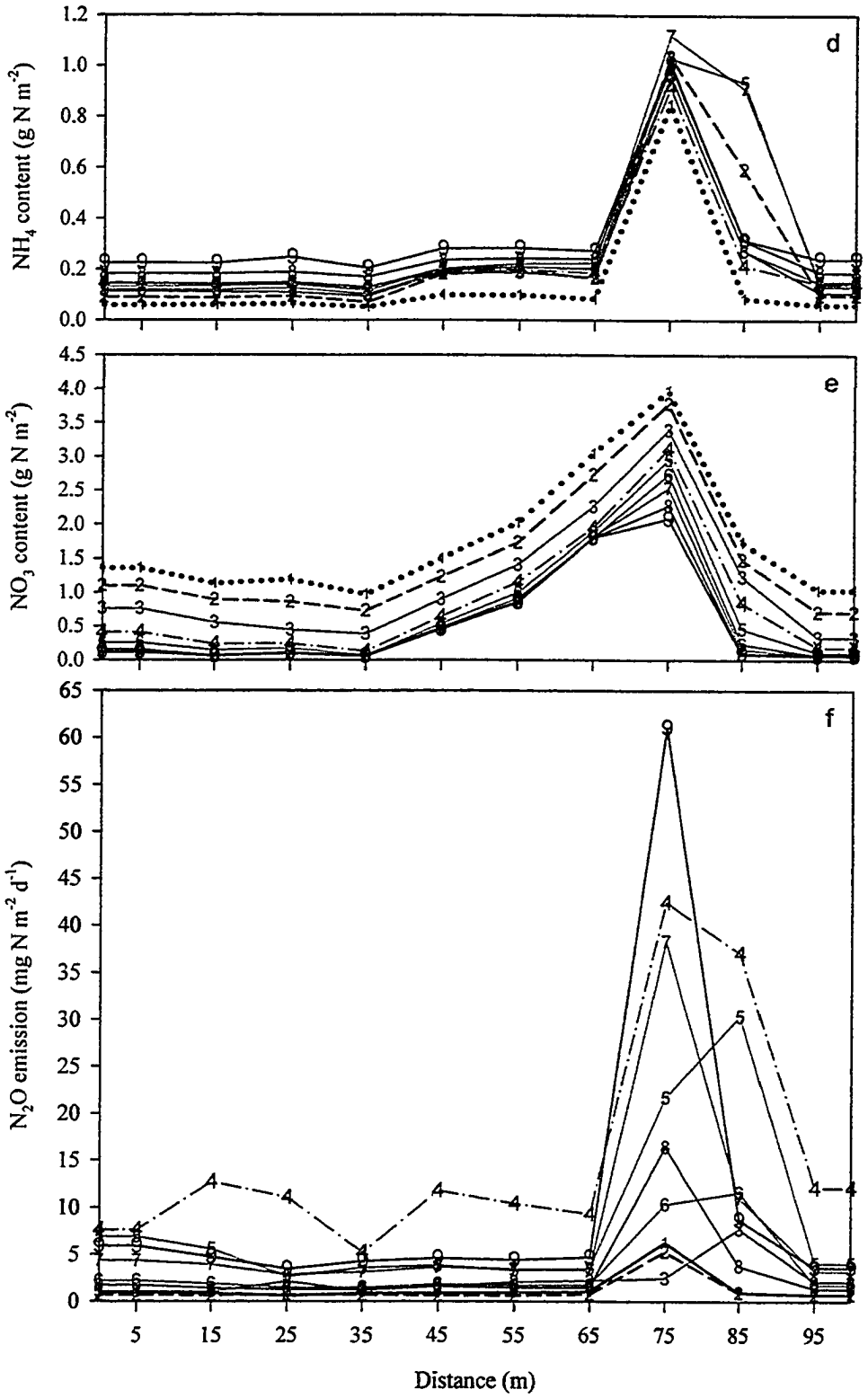

Figure 3.8: The changes of (a) elevation, (b) rainfall, (c) relative water-filled porosity (RWFP) in the upper 20 cm soil zone, (d) NH_4^+, (e) NO_3^- and (f) N_2O emissions on a hill slope transect from June 30 to July 8 2000. Numbers on lines indicate the days from June 30 2000.

6.4 mm during the day of event and a maximum daily precipitation of 13.7 mm. For event two (E2), precipitation during the week before the event was 28.3 mm, including a large rainfall of 25.7 mm 3 days before the event day. For event three (E3), no precipitation occurred during the week before the event.

Continuous rainfall before E1 elevated RWFPs to be higher than 0.6 over the landscape. As discussed in 3.6.3.1, surface and subsurface water flow (Eqs. A3.1 to A3.3) resulted in further increase of RWFP at lower slopes and depressions, although the differences among RWFPs might be less than 0.1 (Fig. 3.9a, d, g and j). Associated with the spatial variation of RWFP, modeled daily N_2O emissions were generally higher at upper slopes than those at lower slopes (Fig. 3.10a, d, g and j). The daily N_2O emissions were lower than 1 mg N m^{-2} at "cold spots" in depressional areas (indicate by locations "1" in Fig. 3.10a, and "2" in Fig. 3.10 j). The higher RWFP at lower slopes and depressions greatly decreased gas diffusivity (D_g, Eq. A3.10) causing a strong deficiency of O_2 and hence a strong demand for electron acceptors (R_e and R_{en}, Eqs. A3.18 and A3.26), forcing denitrification to the terminal stage (N_2, Eq. A3.21) to supply enough electron acceptors, and thereby reducing N_2O production (Figs. 3.8c, f, 3.10a, d, g and j). Spatial variation of 9% in RWFP resulted in spatial variation of 102% in daily N_2O emissions (Table 3.4). The redistribution of solute through surface and subsurface flow (Eqs. A3.4 to A3.6) resulted in large spatial variations in NH_4^+ and NO_3^- (Table 3.4, Fig. 3.8d and e), contributing to the large spatial variation in daily N_2O emissions.

During E2, modeled maximum N_2O emission of 142 mg N m^{-2} d^{-1} in the landscape was lower than that during E1 (151 g N m^{-2} d^{-1}). However, the coefficient of spatial variations in daily N_2O emissions increased to 142% with the increased spatial variation of modeled RWFP (Table 3.4). The subsurface movement of water during 3 days after a large rainfall event increased the differences of modeled RWFP between upper and lower slopes (Figs. 3.8c f, 3.9b and k). The modeled RWFPs were higher than 0.4 at most grid cells in the landscape, and 0.05 to 0.35 higher at lower slopes, convergences and depressions than at upper slopes (Fig. 3.9b, e, h and k). Modeled N_2O emissions were 2 to 30 mg N m^{-2} d^{-1} higher at tops and foot slopes than at midslopes in sub site F1, F2, and F3 (Fig. 3.9b, e, and h), but they were about 20 mg N m^{-2} d^{-1} higher at upper slopes than at "cold spots" at depressional areas in F1 and F4 ("1" in Fig. 3.10b , "2" in Fig. 3.10k).

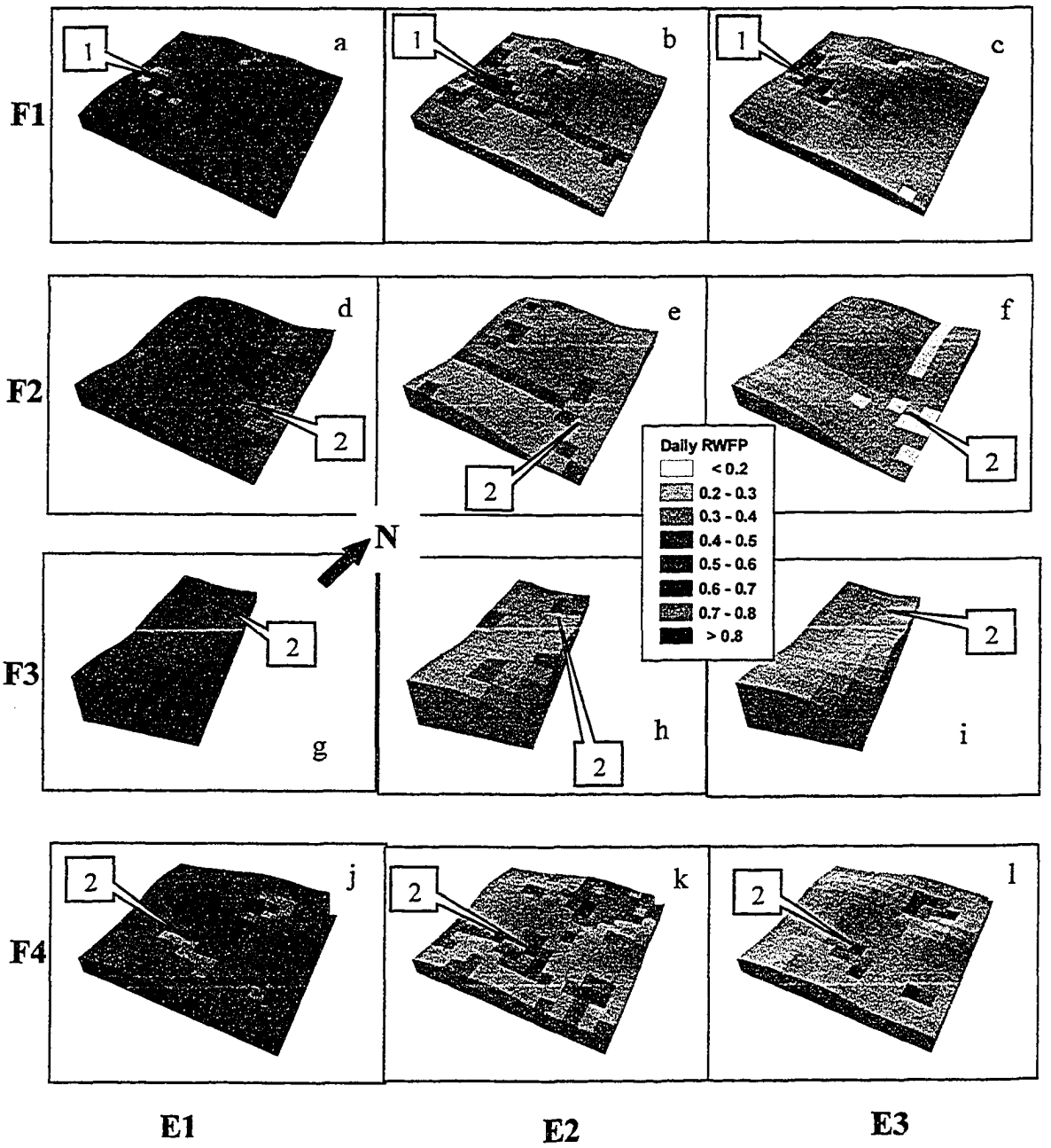

Figure 3.9: The soil RWFPs during three N_2O emission events (E1: June 13 2000; E2: 19 June 2001; and E3: 28 May 2002) on the four sub sites (F1, F2, F3 and F4) in the hummocky agricultural landscape at Viking, Alberta, Canada. 1 indicates a grid cell with continuously low emission. 2 indicates grid cell that changed between low and high emissions.

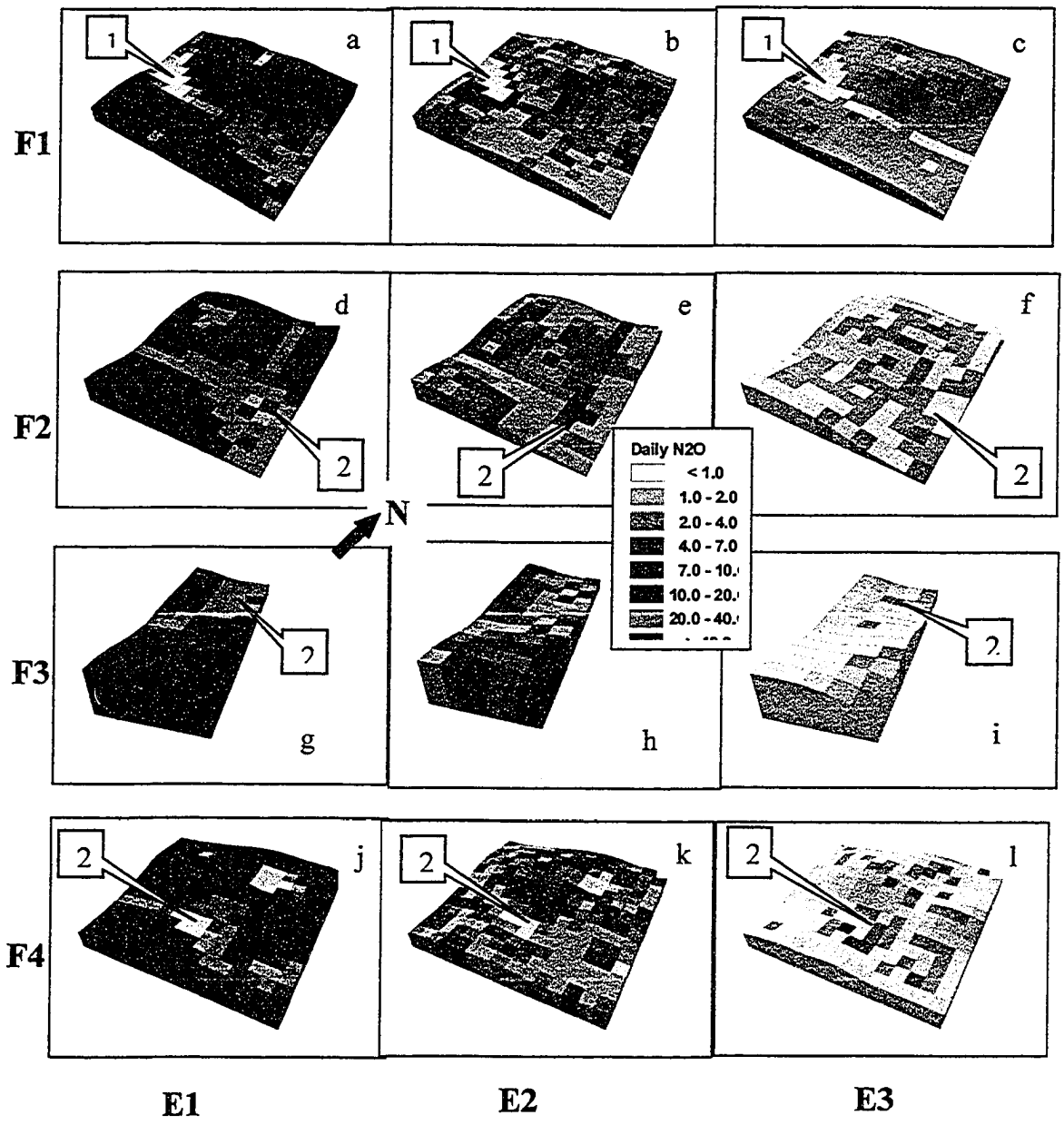

Figure 3.10: The N_2O emission (mg N m^{-2} d^{-1}) during three N_2O emission events (E1: June 13 2000; E2: 19 June 2001; and E3: 28 May 2002) on the four sub sites (F1, F2, F3 and F4) in the hummocky agricultural landscape at Viking, Alberta, Canada. 1 indicates a grid cell with continuously low emission. 2 indicates a grid cell that changed between low and high emissions.

Table 3.4: The spatial variation of modeled daily N_2O emissions and of soil NH_4^+ and NO_3^- contents, and of soil daily relative water-filled porosity (RWFP) and temperature (ST) in the upper 20 cm soil zone during 3 daily emissions events (E1, E2, E3) over four sub sites (F1, F2, F3 and F4) in the hummocky agricultural landscape.

	N_2O (mg N m^{-2} d^{-1})	RWFP[c]	ST (°C)	NH_4^+ (g N m^{-2})	NO_3^- (g N m^{-2})
	Spatial variation of daily event on 13 June 2000 (E1)				
Mean[a]	26.9	0.62	12.2	0.5	5.1
CSV (%)[b]	102	9	2	376	75
Max[a]	150.8	0.85	14.2	17.5	68.1
Min[a]	0.0	0.36	11.0	0.0	0.0
	Spatial variation of daily event on 19 June 2001 (E2)				
Mean	10.8	0.43	13.5	0.5	5.3
CSV (%)	126	36	1	398	62
Max	141.6	0.87	15.3	16.5	70.1
Min	0.0	0.14	13.0	0.0	0.3
	Spatial variation of daily event on 28 May 2002 (E3)				
Mean	5.1	0.34	16.7	0.4	3.2
CSV (%)	163	46	15.0	443	94
Max	52.2	0.84	19.7	17	32.7
Min	0.0	0.11	6.4	0.0	0.0

[a]: Mean, Max and Min were the average, maximum and minimum of daily N_2O emission in all grid cells in the four sun sites.
[b]: CSV was the coefficient of spatial variation of daily N_2O emissions in all grid cells across these four sub sites.
[c]: RWFP was the relative water-filled porosity in the upper 20 cm soil zone.

During E3, with no precipitation for a long time prior to the event, the modeled RWFP was lower than 0.4 at most grid cells in the landscape, and lower at upper slopes than at lower slopes (Fig. 3.9c, f, i and l). Modeled N_2O emissions varied from 0 to 53 mg N m^{-2} d^{-1} with a coefficient of spatial variation of 163% which was larger than that during E1 and E2 (Table 3.4). Modeled daily N_2O emissions were higher at lower slopes than at upper slopes (Fig. 3.10c, f, i and l), especially at the "hot spot" ("2" in Fig. 3.10f, i and l). The spatial variation of modeled RWFP increased from 9% on rainy days, through 36% in three days after a large rainfall, to 46% in a dry period, and enhanced the spatial variations of NH_4^+ and NO_3^- contents (Table 3.4).

Spatial variation of modeled soil temperature (ST) in the upper 20 cm soil zone was smaller than 15%, and increased from E1 to E3 (Table 3.4). Due to the large heat capacity of water, wet soils tended to uniform soil temperatures in the landscape, so that

the spatial variation in E1 and E2 were smaller than 2%. Modeled RWFP, ST, and NH_4^+ and NO_3^- contents explained 32%, 49%, 27% and 56% of the spatial variation in modeled daily N_2O emissions, respectively. However, the spatial variations of ST, NH_4^+ and NO_3^- contents resulted partially from the spatial differences of water. Therefore, the spatial variation of water was the key cause of spatial variations in daily N_2O emissions in the landscape as well as in the hill slope transect (see 3.6.3.1).

3.6.3.3 Spatial variation of modeled annual N_2O emissions

Modeled annual N_2O emission varied from 0.01 g N m^{-2} to 7.3 g N m^{-2} in the hummocky agricultural landscape (Table 3.5). The coefficient of spatial variation (CSV – the percentage of standard deviation to mean of annual N_2O emissions over the landscape) varied from 58% to 367% in the four sub sites (F1, F2, F3 and F4, Fig. 3.2) in 2000, 2001 and 2002. The CSVs were doubled from the wet year (2000), through the normal year (2001) to the dry year (2002) (Table 3.5). CSVs were markedly different among these four sub sites. Sub site F4 had the highest annual emission and the largest CSV, because of its internal watershed and complex topography. The annual N_2O emissions of sub site F3 were similar to the sub sites F1 and F2, but the CSVs were lower because of its smooth slopes with water outlets. The complex spatial heterogeneities in topography, soil properties and soil water content resulted in the large spatial variation and the large differences in CSV of annual N_2O emission among these four sub sites.

For these four sub sites (895 grid cells), annual N_2O emissions were generally larger than 0.4 g N m^{-2} in the wet year, and were generally larger at upper slopes than at lower slopes (Fig. 3.11a, d, g and j). In the normal year, annual N_2O emissions were between 0.1 g N m^{-2} and 0.4 g N m^{-2} at most landscape positions, the emissions on slopes were uniform, and very high emissions occurred at foot slopes, water flow paths and depressions (Fig. 3.11b, e, h and k). In the dry year, annual emissions were generally lower than 0.1 g N m^{-2} (Fig. 3.11c, f, i and l). The largest annual N_2O emission always occurred in the "hot spot" at foot slopes and depressions (position "2" in Fig. 3.11), where it could be more than 10 times higher than at upper slopes and tops (position "2" in Fig. 3.11b, c, e, f, k and l). At "cold spots" ("1" in Fig. 3.11), the annual N_2O emissions were always the lowest because the RWFPs were too high (e.g. > 0.7, position "1" in Fig.

3.9) to generate less than 0.1 mg N m^{-2} d^{-1} (position "1" in Fig. 3.11) at most times during the year. However, the "hot spots" could switch to "cold spots" if RWFPs rose enough (position "2" in Fig. 3.11j, k and l).

Table 3.5: Spatial variation of annual N_2O emission in the four sub sites (F1, F2, F3 and F4) in the hummocky agricultural landscape at Viking, Alberta, Canada, in 2000, 2001 and 2002.

Sub Site	Item	2000	2001	2002
F1	Mean (g N m^{-2} y^{-1})	0.52	0.40	0.15
	CSV (%)	61	154	214
	Max (g N m^{-2} y^{-1})	3.36	4.66	3.48
	Min (g N m^{-2} y^{-1})	0.04	0.03	0.02
F2	Mean (g N m^{-2} y^{-1})	0.56	0.31	0.12
	CSV (%)	58	105	163
	Max (g N m^{-2} y^{-1})	2.79	2.16	1.93
	Min (g N m^{-2} y^{-1})	0.09	0.08	0.01
F3	Mean (g N m^{-2} y^{-1})	0.55	0.36	0.16
	CSV (%)	41	77	109
	Max (g N m^{-2} y^{-1})	1.52	1.30	0.70
	Min (g N m^{-2} y^{-1})	0.12	0.09	0.02
F4	Mean (g N m^{-2} y^{-1})	0.63	0.45	0.29
	CSV (%)	122	210	367
	Max (g N m^{-2} y^{-1})	7.09	6.67	7.30
	Min (g N m^{-2} y^{-1})	0.06	0.07	0.02
ALL sub sites	Mean (g N m^{-2} y^{-1})	0.57	0.39	0.19
	CSV (%)	88	170	341
	Max (g N m^{-2} y^{-1})	7.09	6.67	7.30
	Min (g N m^{-2} y^{-1})	0.04	0.03	0.01

3.6.4 The relationship between modeled N_2O emissions and terrain attributes

Terrain attributes, which indicated the topographic characteristics, were significantly related to soil properties, and directly influenced redistribution of water, sediment and solutes (see Chapter 2). Therefore, terrain attributes (TAs) may also be predictors of N_2O emissions. Annual N_2O emissions were significantly and negatively related to the slope gradient (SP), special catchment area (SCA), and stream power index (SPI) of the landscape (Table 3.6). Profile curvature (PFC), plan curvature (PLC), total upslope length

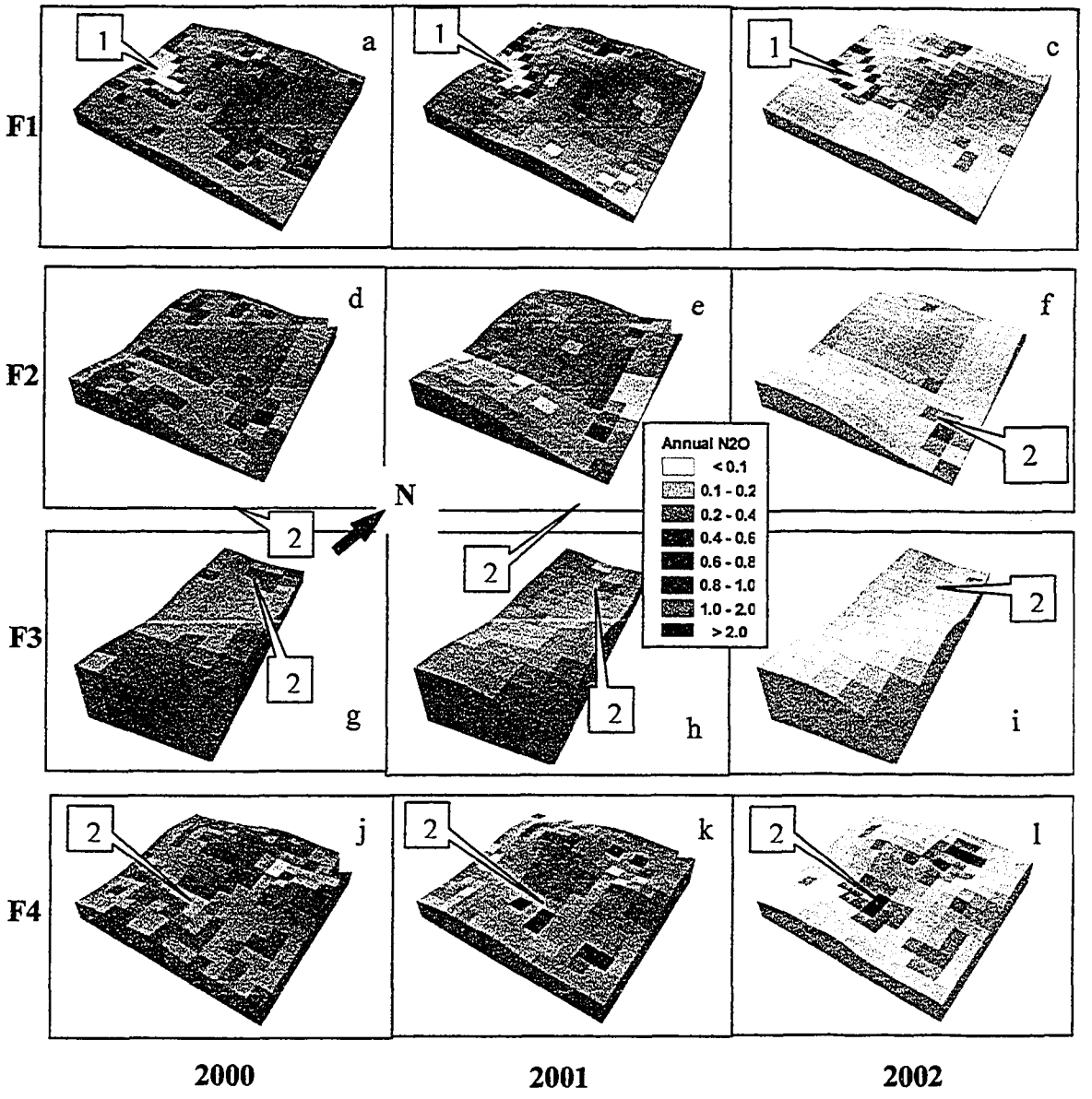

Figure 3.11: The annual N_2O emissions (g N m^{-2}) in the four sub sites (F1, F2, F3 and F4) in the hummocky agricultural landscape at Viking, Alberta, Canada, in 2000, 2001 and 2002. 1 indicates a grid cell with continuously low emission ("cold spot"). 2 indicates a grid cell that changed between low and high emissions ("cold spot" or "hot spot").

(TUL), topographic complex index (TCI), and catchment area (CA) significantly affected the annual N_2O emissions, but the relationships were dependent on precipitation. In the wet and normal year (2000 and 2001), effective rainfall events (Fig. 3.3a and e) caused active surface and subsurface water movement and solute translocation (Fig. 3.8). Water accumulated at concavities (PFC < 0), lower landscape positions (RE < 0), gilgai depressions (TCI > 0), and at grid cells which had large catchment areas (large CA or longer TUL). More water infiltrated at slope divergences (PLC > 0) than at convergences (PLC < 0) because of reduction in velocity of surface flow. As a result, these locations maintained high soil water contents for long periods, causing a sustained deficiencies of electron acceptors (R_e and R_{en}, Eqs. A3.17 and A3.26) due to reduced O_2 supply (U_{gk}, R_{O2} and R_{O2n}, Eqs. A3.8, A3.17 and A3.25). As a result, less N_2O was emitted in the model because N_2O was converted to N_2 (Eq. A3.21). Therefore, N_2O emissions were positively related to PFC and RE, and negatively related to PLC, TUL, TCI and CA in the wet and normal years. In the dry year, water and solute redistribution did not effectively happen with very low precipitation, especially during the main emission period (May to July, Fig. 3.5a). With generally lower soil water contents over the landscape in the dry year than in the wet and normal years (Fig. 3.9), soil water contents at the locations of water accumulation were high enough to cause active N_2O emission. Therefore, N_2O emissions were negatively related to PFC and RE, and positively related to PLC, TUL, TCI and CA.

However, the total N_2O emissions over two and three years (multiple-year periods) had consistently significant relationships with terrain attributes. The effects of annual precipitation on annual N_2O emissions was eliminated because of the long-term N_2O emissions reflected the average effect of precipitation over long-term period. In summary, terrain attributes could be used to estimate spatial N_2O emissions, but estimations would be more reliable for long term (multiple years) N_2O emissions than for annual N_2O emissions. The terrain attributes that were the best predictors for annual N_2O emissions were different for different years. The PFC, RE, LUL, SPI, SP, SCA were the best predictors to estimate long-term (multiple-year) N_2O emissions.

In addition, some terrain attributes such as SPI and SCA were highly related to N_2O emissions, but were not related to soil properties. The terrain attribute affected soil properties at either positively or negatively, but affected N_2O emissions at both direction.

Table 3.6: The Pearson correlation (R) between annual N_2O emissions and terrain attributes[†] in the hummocky agricultural landscape at Viking, Alberta, Canada in 2000, 2001, 2002.

Item	Annual N_2O emission			Multiple year N_2O emission		
Year	2000	2001	2002	00-02[‡]	00-01[§]	01-02[¶]
Profile curvature (PFC)	0.14	0.24	-0.15	0.13	0.15	0.15
Plan curvature (PLC)	-0.14	-0.08	0.1	-0.07	-0.08	-0.02
Relative elevation (RE)	0.23	0.28	-0.02	0.27	0.27	0.22
Aspects (AS)	0.07	0.05	-0.04	0.05	0.07	0.02
Total upslope length (TUL)	-0.07	-0.12	0.09	-0.06	-0.07	-0.06
Longest upslope length (LUL)	-0.05	-0.13	0.08	-0.07	-0.08	-0.08
Topographic complex index (TCI)	-0.16	-0.14	0.16	-0.1	-0.11	-0.07
Stream power index (SPI)	-0.22	-0.42	-0.24	-0.38	-0.33	-0.4
Inverse wetness index (IWI)	0.06	0.01	-0.25	-0.05	0	-0.06
Special catchment area (SCA)	-0.22	-0.36	-0.13	-0.32	-0.29	-0.31
Catchment area (CA)	-0.07	-0.11	0.09	-0.06	-0.07	-0.06
Slope gradient (SP)	-0.17	-0.42	-0.34	-0.38	-0.31	-0.43

Note: Correlation coefficient ≥ 0.07 at significance level 0.05, and ≥ 0.09 at significance level 0.01 with n = 895. [†]: The terrain attributes were defined at Chapter 2. [‡]: The total N_2O emission from 2000 to 2002. [§]: The total N_2O emission of 2000 and 2001; [¶]: The total N_2O emission of 2001 and 2002.

3.7 Discussion

3.7.1 The reliability of modeled N_2O fluxes

Measured N_2O fluxes did not show the large short-term fluctuations apparent in the modeled fluxes (Figs. 3.3 to 3.6). In the *3D-Ecosys-GIS* model, the functions of soil water (gas diffusivity, Eq. A3.10) and temperature (Arrhenius, Eq. A3.21) in N_2O emissions promoted rapid changes of N_2O fluxes (Figs. 3.3 to 3.6). This large temporal variation had been found in measurements elsewhere. Thornton et al. (1996) found that N_2O fluxes measured with chamber in 3 minute intervals had a coefficient of temporal variation larger than 200% in a fertilized maize field. Continuous measurements have shown that the diurnal changes of N_2O fluxes could be as much as 2500 μg N m^{-2} h^{-1}, and often more than 720 μg N m^{-2} h^{-1} in a fertilized maize field (by micrometeorological method, Laville et al., 1999), and as much as 1200 mg N m^{-2} h^{-1} in a fertilized grassland in silty clay loam soil (by automated chamber, Thornton et al., 1998). Research with a continuous automated chamber, conducted in a potato field north of Munich in Germany,

showed that N_2O fluxes could change between ~0 μg N m^{-2} h^{-1} and ~1200 μg N m^{-2} h^{-1} with a change of less than 0.05 in soil water-filled porosity over 2 to 5 days (Flessa et al., 2002). At the same site, Flessa and Dörsch (1995) found that N_2O fluxes measured by chamber ranged from 0 to 2700 μg N m^{-2} h^{-1} over about 5 days in a spring barley field fertilized with 50 kg N ha^{-1}. Lemke et al. (1999) measured N_2O fluxes up to 1400 μg N m^{-2} h^{-1} by chamber near Edmonton, Alberta, where soil and soil management were similar to those in this study. In this study, the non-continuous chamber measurements (8, 9 and 11 measured events in 2000, 2001 and 2002, respectively. Fig. 3.3) might not have recorded short-term changes in emissions. Laville et al. (1999) found that non-continuous chamber measurements did not show the large diurnal variation of N_2O fluxes measured by micrometeorological methods. In addition, modeled peak N_2O fluxes occurred during the late afternoon to early night following diurnal variation in soil temperature in the upper 20 cm soil zone (Fig. 3.6). Measurements taken with a continuous monitoring flow-through system on grassland demonstrated that the peak N_2O fluxes occur in the late afternoon and diurnal changes followed soil temperature at 10 cm depth (Williams et al., 1999). The chamber measurements in this study were performed between 13:00 and 14:00 of local daylight saving time, perhaps too early to measure peak N_2O emissions.

The modeled N_2O fluxes explained a significant fraction of the variation in measured N_2O fluxes, although these fractions were lower in the normal (2001) and dry (2002) years (Table 3.1). The ratio of standard differences between modeled and measured N_2O fluxes to the mean of measured values (RSD: 123% to 169% in Table 3.1) were comparable to variation of replicated chamber measurements measured elsewhere. Kaiser et al. (1998) reported that the coefficients of variation among repeated chamber measurements varied between 149% and 161% with an average of 154% in a fertilized sugar beet field at Lower Saxony, Germany. Folorunso and Rolston (1984) reported that the differences of measured N_2O fluxes might be 282% to 379% at chamber locations 1 to 2 meters apart of in a sorghum field (alluvial soil) at California, USA. Coefficients of variation among measured N_2O fluxes from four chambers located in a 2×3 m grid in a fertilized spring wheat field of clay-loamy soil with slight slope (≈ 2%) varied between 11% and 976% with an average of 173% (Metivier et al. 2003, unpublished data). Comparison of variation in measured and modeled fluxes was complicated by their

different spatial scales. Measured N_2O fluxes represented emission from 0.1 m^2 flux chambers while modeled results represented emissions from a 100 m^2 grid cell. The RSDs were comparable with variation measured over a 100 m^2 area (123% ~ 169% in Table 3.1 vs. 31% ~ 168% in 100 m^2 in Matthias et al. (1980)).

In summary, measuring frequency may have been too low to follow the large temporal variations of modeled N_2O emission, and would have to be increased for well-constrained model validation and better estimates of N_2O emissions. Continuous data from automated chambers or micrometeorological methods would be much better than those from manual chambers in representing the large temporal variation of N_2O fluxes and for validating simulation results. Measuring time in this study (13:00 to 14:00 of local daylight saving time) did not coincide with the peak time of modeled N_2O emissions, and should have been delayed to the late afternoon to try to capture peak emissions. However, modeled N_2O fluxes appeared to reproduce measured N_2O fluxes, with differences between measured and modeled N_2O fluxes being comparable to uncertainty of chamber measurements caused by temporal and spatial differences.

3.7.2 Temporal variation of modeled N_2O emissions

The large temporal variation in N_2O fluxes (Table 3.3) resulted from the functions of soil water and temperature used to calculate N_2O emissions in the *3D-Ecosys-GIS* (Eqs. A3.7 to A3.27). These strong effects of soil water and temperature on N_2O emissions as described in section 3.6.1 have been demonstrated in other field measurements. The coefficients of temporal variation in hourly N_2O fluxes modeled in this study were lower than that in measurements of Flessa and Dörsch (1995) (73 to 97% vs. 143 to 233%), and consistent with the temporal variations of N_2O fluxes measured in other arable soils (Sehy et al., 2003; Flessa et al., 2002; Chao et al., 2000).

The differences in annual precipitation from 2000 to 2002 resulted in differences from 1 to 10 times in averaged hourly N_2O emissions, and differences of 2 to 3 times in annual N_2O emissions. These differences suggested that (1) the CTV in N_2O emission was likely independent of site conditions such as crop, soil and management, and likely determined by short-term changes of soil water content and temperature; (2) the differences in length of main emission periods resulted in large differences in total N_2O emissions (i.e. peak

emissions may be similar, but duration of emission events may be longer with wetter or warmer conditions); and (3) current N_2O emission inventory for provincial and national scales (IPCC guidelines, 1997) that does not account for temporal variation could generate large uncertainty in estimates of N_2O emissions.

3.7.3 Spatial variations of modeled N_2O emission

The spatial variation in modeled N_2O emissions resulted from the redistribution of soil water, NH_4^+ and NO_3^- through surface and subsurface flows (Eqs. A3.1 to A3.6; Figs. 3.8, 3.9, 3.10 and 3.11; Tables, 3.3, 3.4 and 3.5). Generally, the higher water, NH_4^+ and NO_3^- at lower landscape positions caused higher N_2O emissions (Eqs. A3.7, A3.10, A3.17 to A3.20). This result was consistent with research conducted by Corre et al. (1996), van Kessel et al. (1993) and Pennock et al. (1992) in agricultural fields of glacial till landscapes at central Saskatchewan, Canada, and by Weitz et al. (2001) in loam and clay soils with annual (maize and taro) and perennial (papaya, balsa) crops in Costa Rica. The CSV in modeled annual N_2O emissions varied between 61% and 367% with differences in curvatures, catchment areas and slope gradients among four sub sites and in annual precipitation (Table 3.5; Fig. 3.8 to 3.11). The CSVs were similar to the measured spatial variability in a permanent pasture of UK (21% to 287%, Williams et al. 1999), and consistent with the measured spatial variation elsewhere (100% to 500%, Röver et al., 1999; Kaiser et al., 1996; Myrold, 1988; Folorunso and Rolston, 1984).

Modeled daily and annual N_2O emissions were lower at foot slopes and depressions, especially the "cold spots" indicated as "1" (Figs. 3.10a and j, 3.11a, d, g and j) if the RWFP was consistently higher than 0.6 – 0.7 (Figs. 3.8c, 3.9a and j). When RWFPs were lower than 0.6 over the landscape (Fig. 3.9), N_2O emissions were higher at the lower slopes than those at the upper slopes, and the "cold spots" switched to "hot spots" ("2" in Figs. 3.10 and 3.11). Davidson (1991) predicted maximum N_2O fluxes would occur when RWFP was about 0.6. Weitz et al. (2001) measured decreasing N_2O fluxes when RWFP exceeded 0.7 in annual and perennial crop fields in tropical lowland of Costa Rica, and Crill et al. (2000) reported evidence of decreasing N_2O fluxes when RWFP exceeded 0.8 in a loamy land under annual cropping. However, this study found that there were no

fixed RWFP threshold values at which N_2O emission increased or decreased (Fig. 3.6). The thresholds likely became lower at higher temperatures.

In summary, modeled N_2O emission in the hummocky agricultural landscape showed a similar spatial variation to that measured elsewhere. The large spatial variation meant measurements taken at a few locations could not represent the N_2O emissions for the entire landscape. The aggregated N_2O emissions from grid cell (100 m^{-2}) in a watershed could represent landscape effects on N_2O emissions at small watershed scales. The results could then be scaled up to larger areas. It would be helpful to reduce uncertainty in current N_2O inventory (IPCC guidelines) by accounting for the large spatial variation of N_2O emissions.

3.7.4 Relation of temporal and spatial variation in N_2O emissions to N_2O inventory

The temporal and spatial changes of soil water and solute contents, and soil temperature caused temporal and spatial variation in N_2O emissions (>70%, Table 3.3, 3.4, and 3.5). In particular, annual N_2O emissions were 1 to 3 times different due to differences in precipitation, and more than 10 times different between upper and lower slopes due to topographic differences (Table 3.5, Figs. 3.10 and 3.11). Therefore, measurements taken at a lower frequency or at a few locations would not likely represent N_2O emissions at larger temporal and spatial scales. Flessa et al. (2002) and Scott et al. (1999) have demonstrated that large temporal and spatial variations of N_2O fluxes were a main source of error in estimating cumulative N_2O fluxes from cultivated soils. Crill et al. (2000), Flessa et al. (2002), Scott et al. (1999) and Brumme and Beese (1992) reported that the differences of cumulative N_2O emissions estimated from higher (2 to 5 measurement per day) and from lower (1 measurement per day to month) measurement frequencies were 6% – 56%. Alternation between "hot spots" and "cold spots" ("2" in Figs. 3.10 and 3.11) would cause large uncertainty in estimated N_2O emissions if a few measurement sites were located at these spots. Denmead et al. (2000) found differences of about 360% in averaged N_2O emissions estimated at 0.05 ha., 5 km^2 and 100 km^2 spatial scales regardless of spatial variation. Current N_2O inventory (IPCC guidelines, 1997), which do not consider the large temporal and spatial variation of N_2O emissions,

would generate large errors in the estimates of N_2O emissions, probably larger than 62% (Brown et al. 2001).

This variation could be represented by ecosystem simulation models such as *3D-Ecosys-GIS*. N_2O emissions for the entire study field could be estimated from modeled results for the four sub sites. Uncertainty of total N_2O emissions could then be reduced with full consideration of the temporal and spatial variability at field scale. However, the performance limitation of current computers made it difficult to simulate the N_2O emissions for more than 100 hectares in tens of meters resolution. Fortunately, there were correlations between terrain attributes and N_2O emissions (Table 3.6). Although these correlations were weak, the relationship function could be built by using the simulation results for N_2O emission from pilot sub sites and terrain attributes derived from DEM. The DEM can be easily obtained from GIS. Therefore, N_2O emission at coarse scales, such as provincial and national scales, could be estimated with consideration of this large temporal and spatial variation. At the least, the results from this method could be used to improve confidence in the estimate of N_2O emissions from IPCC guidelines.

3.8 Conclusions

The modeled N_2O fluxes were comparable with the measured fluxes during measured emission events. Due to the low measuring frequency and the brief measuring time, measurements did not catch the large temporal variability that exists in most agroecosystems. Variability in the modeled results was consistent with continuous chamber and micrometeorological measurements conducted in similar agroecosystems elsewhere. However, frequent or continuous measurements are still necessary for well-constrained model validation.

By analyzing the modeled outputs, the coefficients of temporal variation were found to be 83%, 99%, and 51% for hourly, seasonal and annual N_2O emissions, respectively. Dry climate enlarged the temporal variations, and shortened the main emitting season. More than 60% of N_2O was emitted during the period of crop vegetation development. Emissions were lower in fall, winter, and early spring. Fall fertilizer did not produce noticeable N_2O emissions after application in this hummocky agricultural landscape. The

annual N_2O emission in the dry year was only one-third of that in the wet year with lower peak emissions and shorter emission season.

In the hummocky agricultural landscape, coefficients of spatial variation increased from 88% in the wet year, through 170% in the normal year, to 341% in the dry year. The spatial heterogeneities of RWFP and soil temperature in the upper 20 cm soil zone caused the large spatial variability of N_2O emission. N_2O emissions were higher at upper slopes than at lower slopes during rainy period and in the wet year, but they were lower at upper slopes than at lower slopes during dry period and in the normal and dry years.

Landscape modeling methods that fully represent the large temporal and spatial variation of N_2O emissions could improve confidence in the N_2O inventory, and provide more realistic estimates of N_2O emissions.

References

Brown, L., Brown, S.A., Jarvis, S.C., Syed, B., Goulding, K.W.T., Phillips, V.R., Sneath, R.W., Pain, B.F., 2001. An inventory of nitrous oxide emissions from agriculture in the UK using the IPCC methodology: emission estimate, uncertainty and sensitivity analysis. Atmospheric Environment. 35(8):1439–1449

Brumme, R. and Beese, F., 1992. Effect of liming and nitrogen fertilization on emissions of CO_2 and N_2O from a temperate forest. J. Geophys. Res. 97:12851–12858.

Chao, C.C., Young, C.C., Wang, Y.P., Chao, W.L., 2000. Daily and seasonal nitrous oxide fluxes in soils from hardwood forest and different agroecosystems of Taiwan. Chemosphere: Global Change Science. 2:77–84.

Choudhary, M.A., Akramkhanov, A., Saggar, S., 2002. Nitrous oxide emission from a New Zealand cropped soil: tillage effects, spatial and seasonal variability. Agric. Ecosys. Environ. 93:33–43.

Corre, M.D., Pennock, D.J., Van Kessel, C., Elliott, D.K., 1999. Estimation of annual nitrous oxide emissions from a transitional grassland-forest region in Saskatchewan, Canada. Biogeochemistry. 44(1):29-49.

Corre, M.D., Van Kessel, C., Pennock, D.J., 1996. Landscape and seasonal patterns of nitrous oxide emissions in a semiarid region. Soil Sci. Soc. Am. J. 60:1806–1815.

Cousin, I., Porion,P., Renault, P., and Levitz, P., 1999. Gas diffusion in a silty-clay soil: experimental study on an undisturbed soil core and simulation in its three-dimensional reconstruction. European Journal and Soil Science. 50:249–259.

Crill, P.M., Keller, M., Weitz, A.M., Grauel, W.T., Veldkamp, E., 2000. Intensive field measurements of nitrous oxide emissions from tropical agricultural soils. Global Biogeochemical Cycles. 14:85–95.

Davidson, E.A., 1991. Fluxes of nitrous oxide and nitric oxide from terrestrial ecosystems. In: Rogers, J.E. and Whitman, W.B. (Eds.). Microbial Production and Consumption of greenhouse Gases: Methane, Nitrogen Oxides, and Halomethane. American Society for Microbiology, Washington, pp. 219–235.

Denmead, O.T., Leuning, R., Jamie, I., Griffith, D.W.T., 2000. Nitrous oxide emissions from grazed pastures: measurements at different scales. Chemosphere – Global Change Science. 2:301–312.

El-Sadek, A., de Vos, J., Feyen, J., Ducheyne, S., 1999. Analysis of the nitrate leaching to surface water using a simplified and detiled model approach. In: Feyen J. and Wiyo K. (Eds). Modelling of transport processes in soils. Wageningen Press, Wageningen, The Netherlands. pp.569–579.

Flessa, H. and Dörsch, P., 1995. Seasonal Variation of N_2O and CH_4 fluxes in differently managed arable soils in southern Germany. J. Geoph. Res. 100(D11):23115–23124.

Flessa, H., Ruser, R., Schilling, R., Loftfield, N., Munch, J.C., Kaiser, E.A., Beese, F., 2002. N_2O and CH_4 fluxes in potato fields: automated measurement, management effects and temporal variation. Geoderma. 105(3-4):307–325.

Folorunso, O.A. and Rolston, D.E., 1984. Spatial variability of field measured denitrification gas fluxes. Soil Science Society of America Journal. 48:1214–1219.

Grant, R.F. 1998. Simulation in ecosys of root growth response to contrasting soil water and nitrogen. Ecol. Modelling. 107:237–264.

Grant, R.F. and Nalder, I.A., 2000. Climate change effects on net carbon exchange of a boreal aspen-hazelnut forest: estimates from the ecosystem model ecosys. Global Change Biology. 6(2):183–200.

Grant, R.F. and Pattey, E., 2003. Modelling variability in N_2O emissions from fertilized agricultural fields. Soil Biol. Biochem. 35(2):225–243.

Grant, R.F., 1995. Dynamics of energy, water, carbon and nitrogen in agricultural ecosystems: simulation and experimental validation. Ecol. Modeling. 81(1–3): 169–181.

Grant, R.F., 1995b. Mathematical modelling of nitrous oxide evolution during nitrification. Soil Biol. Biochem. 27:1117–1125.

Grant, R.F., 1997. Changes in soil organic matter under different tillage and rotation: mathematical modeling in ECOSYS. Soil Sci. Soc. Am. J. 61(4): 1159-1175.

Grant, R.F., 1999. Simulation of methanotrophy in the mathematical model *ecosys*. Soil Biol. Biochem. 31:287–297.

Grant, R.F. 2001. A review of the Canadian ecosystem model ecosys. Chapter 6. In: Shaffer, M.J., Ma, L.W. and Hansen, S. (Eds). Modeling Transformations of Soil Organic Carbon And Nitrogen At Differing Scales Of Complexity. CRC Press. pp. 173–273.

Grant, R.F., Black, T.A., Hartog, G. den, Berry, J.A., Neumann, H.H., Blanken, P.D., Yang, P.C., Russell, C., Nalder, I.A., den Hartog, G., 1999a. Diurnal and annual exchanges of mass and energy between an aspen-hazelnut forest and the atmosphere: testing the mathematical model ECOSYS with data from the BOREAS experiment. J. Geoph. Res. 104(D22):27699–27717.

Grant, R.F., Izaurralde, R.C., Chanasyk, D.S., 1995b. Soil temperature under different surface managements: testing a simulation model. Agric. For. Meteorol. 73:89–113.

Grant, R.F., Jarvis, P.G., Massheder, J.M., Hale, S.E., Moncrieff, J.B., Rayment, M., Scott, S.L., Berry, J.A., 2001a. Controls on carbon and energy exchange by a black spruce-moss ecosystem: testing the mathematical model Ecosys with data from the BOREAS experiment. Glob. Biogeochem. Cycles. 15(1):129–147.

Grant, R.F., Juma N.G., Robertson, J.A., Izaurralde, R.C., McGill, W.B., 2001b. Long-term changes in soil carbon under different fertilizer, manure, and rotation: testing the mathematical model ecosys with data from the Breton plots. Soil Sci. Soc. Am. j. 65(1):205–214.

Grant, R.F., Kimball, B.A., Brooks, T.J., Wall, G.W., Pinter, P.J.Jr, Hunsaker, D., Adamsen, F.J., Lamorte, R.L., Leavitt, S.W., Thompson, T.L., Matthias, A.D., 2001c. Modeling Interactions among carbon dioxide, nitrogen, and climate on energy

exchange of wheat in a free air carbon dioxide experiment. Agronomy Journal. 93:638–649.

Grant, R.F., Nyborg, M., Laidlaw, J., 1993a. Evolution of nitrous oxide from soil: I. Model development. Soil Sci. 156:259–265.

Grant, R.F., Nyborg, M., Laidlaw, J., 1993b. Evolution of nitrous oxide from soil: II. Experimental results and model testing. Soil Sci. 156:266–277.

Grant, R.F., Izaurralde, R.C., Nyborg, M., Malhi, S.S., Solberg, E.D, Jans-Hammermeister, D., Stewart, B.A., 1998. Modeling tillage and surface residue effects on soil C storage under ambient vs. elevated CO2 and temperature in ECOSYS. In: Ed. Lal, R., Kimble, J.M., Follett, R.F. (Eds). Soil processes and the carbon cycle. CRC Press Inc. Boca Raton; USA. Pp. 527-547.

Grant, R.F., Garcia, R.L., Pinter, P.J, Hunsker, D.J.Jr, Wall, G.W et al., 1995a. Interaction between atmospheric CO_2 concentration and water deficit on gas exchange and crop growth: Testing of ecosys with data from the Free Air CO_2 Enrichment (FACE) experiment. Global Change Biol. 1: 443-454.

Grant, R.F., Wall, G.W., Kimball B.A., Frumau, K.F.A., Pinter, P.J.Jr, Hunsaker, D.J., Lamorte, R.L., 1999b. Crop water relations under different CO_2 and irrigation: testing of ECOSYS with the free air CO_2 enrichment (FACE) experiment. Agric. For. Meteorol. 95:27–51.

Intergovernmental Panel on Climate Change (IPCC), Climate Change 2001: The Scientific Basis: Contribution of Working Group I to the Third Assessment Report of the Intergovernmental Panel on Climate Change, 881 pp., Cambridge Univ. Press, New York, 2001.

Intergovernmental Panel on Climate Change (IPCC), Organization for Economic Cooperation and Development (OECD) and International Energy Agency (IEA), Revised 1996 IPCC Guidelines for National Greenhouse Gas Inventories, Organ. for Econ. Coop. Dev., Paris, 1997.

Kaiser, E.A., Kohrs, K., Küchke, E., Schnug, E., Heinemeyer, O., Munch, J.C., 1998. Nitrous oxide release from arable soil: importance of N fertilization, crops and temporal variation. Soil Biol. Biochem. 30(12):1553–1563.

Kaiser, E.A., Munch, J.C., Heinemeyer, O., 1996. Importance of soil cover box area for the determination of N2O emissions from arable soils. Plant and Soil. 181:185–192.

Kasteel, R., Vogel, H.J., Roth, K., 2000. From local hydraulic properties to effective transport in soil. European Journal of Soil Science. 51:81–91.

Kutilek, M.; and Nielsen, D.R., 1994: Soil hydraology. Catena Verlag, Cremilingen Destedt, Germany. 87–116.

Laville, P., Jambert, C., Cellier, P., Delmas, R., 1999. Nitrous oxide fluxes from a fertilized maize crop using micrometeorological and chamber methods. Agric. For. Meteorol. 96:19–38.

Lemke, R.L., Izaurralde, R.C., Malhi, S.S., Arshad, M.A., Nyborg, M., 1998. Nitrous oxide emission from agricultural soils of the Boreal and parkland regions of Allberta. Soil Sci. Soc., Am. J. 62:1096–1102.

Lemke, R.L., Izaurralde, R.C., Nyborg, M., Solberg, E.D., 1999. Tillage and N source influnce soil-emitted nitrous oxide in the Alberta Parkland region. Canadian Journal of Soil Science. 79(1):15–24.

Li, T., Grant, R.F, Flanagan, L.B., 2004. Climate impact on net ecosystem productivity of a semi-arid natural grassland: modeling and measurement. Agric. For. Meteorol. 126:99–116.

Lim, B. Boileau, P., Bonduki, Y., van Amstel, A.R., Janssen, L.H.J.M., Olivier, J.G.J, Kroeze, C., 1999. Improving then quality of national greenhouse gas inventories. Environmental Science and Policy. 2:335–346.

Matthias, A.D., Blackmer, A.M., Brenmner, J.M., 1980. A simple chamber technique for field measurement of emission of nitrous-oxide from soils. J. Environ. Qual. 9(2):251–256.

Morgan, R.P.C., Quinton, J.N., Smith, R.E., Govers, G., Poesen, J.W.A., Auerswald, K., Chisci, G., Torri, D. and Styczen, M.E. 1998a. The European Soil Erosion Model (EUROSEM): a dynamic approach for predicting sediment transport from fields and small catchments. Earth Surface Processes and Landforms. 23:527–544.

Morgan, R.P.C., Quinton, J.N., Smith, R.E., Govers, G., Poesen, J.W.A., Auerswald, K., Chisci, G., Torri, D., Styczen, M.E. and Folly, A.J.V. 1998b. The European Soil

Erosion Model (EUROSEM): documentation and user guide v. 3.6. Silsoe College, Cranfield University, Silsoe, Bedford, U.K.

Myrold, D.D., 1988. Denitrification in rye-grass and winter wheat cropping systems of western Oregon. Soil Sci. Soc. Am. J. 52: 412–416.

Olsen, K., Wellisch, M., Bioleau, P., Blain, D., et al., 2003. Canada's greenhouse gas inventory (1990 – 2001). ISBN 0-662-35106-1, Environment Canada.

Paul, E.A. and Clark, F.E., 1996. Soil microbiology and biochemistry. Second edition, Academic Press.

Pennock, D.J. and M.D. Corre, 2001. Development and application of landform segmentation procedures. Soil and Tillage Research. 58:151–162.

Pennock, D.J., van Kessel, C., Farrell, R.E., Sutherland, R.A., 1992. Landscape-scale variations in denitrifcation. Soil Sci. Soc. Am. J. 56:770–776.

Röver, M., Heinemeyer, O., Munch, J.C., Kaiser, E.A., 1999. Spatial heterogeneity within the plough layer: high variability of N_2O emission rates. Soil Biol. Biochem. 31(2):167–173.

Scott, A., Crichton, I., Ball, B.C., 1999. Long-term monitoring of soil gas fluxes with closed chambers using automated and manual systems. J. Environ. Qual. 28:1637–1643.

Sehy, U., Ruser, R., Munch, C., 2003. Nitrous oxide fluxes from maize fields: relationship to yield, site-specific fertilization, and soil conditions. Agric. Ecosys. Environ. 99(1-3):97–111.

Shaffer, M.J. and Larson, W.E., 1987. NTRM, a soil-crop simulation model for nitrogen, tillage and crop-residue management. USDA Conservation Research Report 34-1. National Technical Information Service, Springfield, Virginia.

Sharma, M.L., Luxmoore, R.J., R., DeAngelis, R.C., Ward, and G.T., Yeh, 1987. Subsurface water flow simulated for hillslope with spatially dependent soil hydraulic characteristics. Water Resour. Res. 23(8):1523–1530.

Somma, E., Hopmans, J.W., Clausniter, V., 1998. Transient three-dimensional modeling of soil water and solute transport with simultaneous root growth, root water and nutrient uptake. Plant and Soil. 202:281–293.

Sprout, C. and Goddard, T, 2003. Documentation of Sampling Protocols and Materials for the Green House Gas Projects at the Three Hills Long-Term Plots and other Sites in Alberta. Farm Resource Conservation Unit, Conservation and Development Branch, AAFRD. Document. Edmonton, Alberta, Canada.

Su, Ninghu, 1997. Extension of the Feller-Fokker-Planck equation to two and three dimensions for modelling solute transport in fractal propous media. Water Resour. Res. 33(5):1195-1197.

Thornton, F.C., Bock, B.R., Tyler, D.D., 1996. Soil emissions of nitric oxide and nitrous oxide from injectd anhydrous ammonium and urea. J. Environ. Qual. 25:1378–1384.

Thornton, F.C., Shurpall, N.J., Bock, B.R., Reddy, K.C., 1998. N_2O and NO emissions from poultry litter and urea applications to Bermuda grass. Atmosph. Environ. 32(9):1632–1630.

Van Kessel, C., Pennock, D.J., Farell, R.E., 1993. Seasonal variations in denitrifcation and nitrous-oxide evolution at the landscape scale. Soil Sci. Soc. Am. J. 57:988-995.

Weitz, A.M., Linder, E., Frolking, S., Crill, P.M., Keller, M., 2001. N_2O emissions from humid tropical agricultural soils: effects of soil moisture, texture and nitrogen availability. Soil Biol. Biochem. 33(7-8):1077–1093.

Williams, D.Li., Ineson, P., Coward, P.A., 1999. Temporal variations in nitrous oxide fluxes from urine-affected grassland. Soil Biol. Biochem. 31(5):779–788.

Yang, J.Z.; Zhang, R.D.; Wu, J.Q., 1997. Stochastic analysis of adsorbing solute transport in three-dimensional, heterogeneous, unsaturated soils. Water Resour. Res. 33(8):1947–1956.

Appendix 3.1: The main equations and variables for simulating of landscape N_2O emissions in the *3D-Ecosys-GIS*

Subscripts:

i: The direction in x (W–E) or y (N–S) in each landscape position (, i is the direction in x, y, z in subsurface).
j: The solute (j = 1, 2, 3, n).
k: Gas.
x: Landscape position increasing from west to east.
y: Landscape position increasing from north to south.
z: Landscape position increasing with depth.

Variables:

$[W_C]$: Concentration of soluble hydrolysis products of soil carbon in soil solution (g C m^{-3}).
$[CO_{2s}]$: CO_2 concentration in soil solution (g C m^{-3}).
$[O_{2h}]$: O_2 concentration at heterotroph surfaces (g O_2 m^{-3}).
$[O_{2n}]$: O_2 concentration at ammonia oxidizer surfaces (g O_2 m^{-3}).
a: Air-water interface area.
A_k and B_k: Empirical parameter to solve the solubility of gas k at 30 °C.
C_j: Concentration of j as solute (g m^{-3}).
C_j: The concentration of solute j in water phase (g m^{-3}).
d: Depth of mobile surface water per unit area (m).
D: The dispersivity-diffusivity coefficient (m^2 h^{-1}).
D'_g: Gaseous diffusivity at 30 °C (m^2 h^{-1}).
D_{wk}: Aqueous diffusivity of gas k in water at 30 °C (m^2 h^{-1}).
D_g: Gaseous diffusivity of gas k (m^2 h^{-1}).
D_{sk}: Volatilization-dissolution transfer coefficient of gas k (m h^{-1}).
D_{wk}: Aqueous dispersivity-diffusivity of gas k (m^2 h^{-1}).
E: Activation energy (cal mol^{-1}).
E_k: Gas exchange of gas k between gaseous and aqueous phases (g m^{-3}).
f_e: The fraction of transferred electrons based on the ratio of denitrifer growth rates under anaerobic vs. aerobic conditions (Koike and Hattori, 1975).
f_{sk}: Temperature function on solubility of gas k.
f_t: Soil temperature function (dimensionless).
G_{gk}: The concentration of gas k in soil air (g m^{-3}).
G_{wk}: The concentration of gas k in aqueous phases (g m^{-3}).
$K(\theta)$: A spatially dependent unsaturated hydraulic conductivity (m h^{-1}) at landscape position x, y, z.
K_{NH4}: Michaelis-Menten constant for oxidation of NH_4^+ by M_{na} (g N m^{-3}).
K_{NO2}: Michaelis-Menten constant for reduction of NO_2^- by ammonia oxidizers (g N m^{-3}).
K_{NO3} , K_{NO2} and K_{N2O} are Michaelis-Menten constant for reduction of NO_3^-, NO_2^- and N_2O by heterotrophic denitrifiers (g N m^{-3}).

K_{O2h}: Michaelis-Menten constant for reduction of O_2 in soil solution by heterotrophs (0.032 g O_2 m^{-3}).
K_{O2n}: Michaelis-Menten constant for reduction of O_2 in soil solution by ammonia oxidizers (0.32 g O_2 m^{-3}).
K_{Rh}: Michaelis-Menten constant for respiration of W_C by heterotrophs (35 g C m^{-3}).
L: Width of flow paths (m).
L_x: Width of water flow path in x direction (grid cell size) (m).
L_y: Width of water flow path in y direction (grid cell size) (m).
M_{ha}; Active biomass of heterotrophs (g C m^{-2}).
M_j: Mass of solute j (g).
M_{na}: Active biomass of NH_4^+ oxidizers (g C m^{-2})
n: Manning's surface roughness coefficient ($m^{5/3}$ h).
Q_{sj}: Solute flow of solute j (g m^{-2} h^{-1}).
Q_w: Water flow (m^3 m^{-2} h^{-1}).
Q_{wi}: The ith (i = 1, 2, 3 in x, y, or z direction) component of water flux density (m^3 m^{-2} h^{-1}).
R: Gas constant (cal mol^{-1} k^{-1}).
r: Hydraulic radius is the rate of area flow cross-section to wet perimeter (m).
R'_{O2}: O_2 reduction by heterotrophs under saturating soil [O_2] (g O_2 m^{-2} h^{-1}).
R'_{O2n}: Rate of soil solution O_2 reduction by ammonia oxidizers under non-limiting soil solution O_2 (g O_2 m^{-2} h^{-1});
R_e: Electron transfer to N oxides by denitrifiers (mol e^- m^{-2} h^{-1}).
R_{en}: Electron transfer to N reduced by nitrifiers (mol e^- m^{-2} h^{-1}).
R_{NO3}, R_{N2O} and R_{N2O}: NO_3^-, NO_2^- and N_2O reduction by heterotrophic denitrifiers (g N m^{-2} h^{-1}).
R_{O2}: O_2 reduction by heterotrophs under ambient soil [O_2] (g O_2 m^{-2} h^{-1}).
R_{O2c}: Respiratory quotient for reduction of O_2 coupled to oxidation of C (2.67 g O_2 g^{-1} C)
R_{O2n}: Rate of soil solution O_2 reduction by ammonia oxidizers under ambient soil solution O_2 (g O_2 m^{-2} h^{-1});
r_{O2n}:Respiratory quotient for reduction O_2 coupled to oxidation of NH_4^+ (3.43 g O_2 g^{-1} N).
S: Slope (m m^{-1}).
S_k: Ostwald solubility coefficient of gas k at 30 °C (m^3 air m^{-3} water).
s_r: Slope of channel side during surface flow (m m^{-1}).
T: Soil temperature (°C).
T: The temperature of soil (°C).
U_{gk}: The uptake (negative value) or production (positive value) of microbial and plant in gas O_2 or N_2O (g m^{-3} h^{-1}).
U_{gO2}: O_2 reduction by heterotrophs under ambient soil [O_2] (g O_2 m^{-2} h^{-1}).
U_n: Added or removed solute (g m^{-3} h^{-1}).
U_w: Root water uptake (m^3 m^{-3} h^{-1}).
W: Soil water mass (m^3).
X'_C: Specific oxidation of W_C by heterotrophs at saturating [W_C] and 30°C (0.2 g C g C^{-1} h^{-1}. Ridge, 1976; Shields et al., 1974).
X'_{NH4}: Specific rate of NH_4^+ oxidation of by M_{na} under non-limiting [O_{2n}] at 30°C (g N g^{-1} M_{na} h^{-1}).

X_C: Oxidation of W_C coupled to reduction of O_2 by heterotrophis under saturating [O_2] (g C m^{-2} h^{-1}).
X_{NH4}: Oxidation of NH_4^+ coupled to reduction of O_2 by M_{na} under non-limiting [O_{2n}] at the surface of nitrifiers (NH_4^+ oxidizers) (g N m^{-2} h^{-1}).
Z_{di}: Distance in i^{th} directions (m, i=1, 2, 3 in x, y, and z directions).
Ψ: Soil water potential (MPa; time 100 using in A3.3).
α: Frequency factor.
λ: Hydrodynamic dispersion coefficient (0.04 m, Bresler, 1973).
θ: Volumetric water content (m^3 m^{-3}).
θ_g: Air-filled porosity (m^3 m^{-3}).
θ_s: Total porosity (m^3 m^{-3}).
θ_w: Aqueous gas content (m^3 m^{-3}).
τ: Tortuosity coefficient for aqueous diffusion. (0.2).

Equations:

Water translocation

Surface water flow

$$Q_{wi} = \frac{r^{2/3} S_i^{1/2} d\, L_i}{n} \tag{A3.1}$$

$$r = \frac{s_r d}{2(s_r^2+1)^{0.5}} \tag{A3.2}$$

Subsurface water flow

$$\frac{\partial\theta}{\partial t} = \sum_{i=1}^{3} \frac{\partial Q_{wi}}{\partial Z_{di}} - U_w = \sum_{i=1}^{3} \frac{\partial}{\partial Z_{di}}[K(\theta)\frac{\partial \Psi_i}{\partial Z_{di}}] - U_w \tag{A3.3}$$

Solute transport

Surface solute transport

$$Q_{sji} = Q_{wi} C_j \tag{A3.4}$$

$$C_j = M_j / (W + dL_x L_y) \tag{A3.5}$$

Subsurface transport

$$\frac{\partial(\theta C_j)}{\partial t} = \sum_{i=1}^{3} [\frac{\partial}{\partial Z_{di}}(\theta D \frac{\partial C_{ji}}{\partial Z_{di}}) - \frac{\partial(Q_{wi} C_{ji})}{\partial Z_{di}}] - U_n \tag{A3.6}$$

Gas Flux

$$\frac{\partial(\theta_g G_{gk})}{\partial t} = \sum_{i=1}^{3} [\frac{\partial}{\partial X_i}(D_{gk} \frac{\partial G_{gki}}{\partial X_i})] \tag{A3.7}$$

$$\frac{\partial(\theta_w G_{wk})}{\partial t} = \sum_{i=1}^{3} [\frac{\partial(Q_{wi} G_{wki})}{\partial X_i} - \frac{\partial}{\partial X_i}(D_{wk} \frac{\partial G_{wk}}{\partial X_i})] - U_{gk} \tag{A3.8}$$

$$E_k = aD_{sk}(S_k f_{sk} G_{gk} - G_{wk}) \tag{A3.9}$$

$$D_{gk} = D'_{gk} f_g \theta_g^{3.33} / \theta_s^2 \tag{A3.10}$$

$$D_{wk} = \lambda |Q_w| + D'_{wk} f_w \tau\theta \tag{A3.11}$$

$$f_{sk} = e^{(A_k - B_k T)} \quad \text{(A3.12)}$$

$$f_g = \left(\frac{T+273.15}{273.15}\right)^6 \quad \text{(A3.13)}$$

$$f_w = \left(\frac{T+273.15}{273.15}\right)^{1.75} \quad \text{(A3.14)}$$

N_2O production

Denitrification

$$X_C = \{X'_C M_{ha}[W_C]/(K_{Rh} + [W_C])\} f_t \quad \text{(A3.15)}$$

$$R'_{O2} = R_{O2c} X_C \quad \text{(A3.16)}$$

$$R_{O2} = R'_{O2}[O_{2h}]/([O_{2h}] + K_{O2h}]) \quad \text{(A3.17)}$$

$$R_e = 0.125 f_e (R'_{O2} - R_{O2}) \quad \text{(A3.18)}$$

$$R_{NO3} = 7 R_e [NO_3^-]/([NO_3^-] + K_{NO3}) \quad \text{(A3.19)}$$

$$R_{NO2} = (7 R_e - R_{NO3}) [NO_2^-]/([NO_2^-] + K_{NO2}) \quad \text{(A3.20)}$$

$$R_{N2O} = 2 (7 R_e - R_{NO3} - R_{NO2}) [N_2O]/([N_2O] + K_{N2O}) \quad \text{(A3.21)}$$

$$f_t = \alpha e^{-\frac{E}{R(273.15+T)}} \quad \text{(A3.22)}$$

Nitrification

$$X_{NH4} = \{X'_{NH4} M_{na}[NH_4^+]/([NH_4^+] + K_{NH4})\}\{[CO_{2s}]/([CO_{2s}] + K_{CO2})\} f_t \quad \text{(A3.23)}$$

$$R'_{O2n} = r_{O2n} X_{NH4} \quad \text{(A3.24)}$$

$$R_{O2n} = R'_{O2n}([O_{2n}]/([O_{2n}] + K_{O2n}) \quad \text{(A3.25)}$$

$$R_{en} = 0.125 f_e (R'_{O2n} - R_{O2n}) \quad \text{(A3.26)}$$

$$R_{N2On} = 7 R_{en} \{[CO_{2s}]/([CO_{2s}] + K_{CO2})\} \{[NO_2^-]/([NO_2^-] + K_{NO2n})\} \quad \text{(A3.27)}$$

Appendix 3.2: The interface of *3D-Ecosys-GIS*

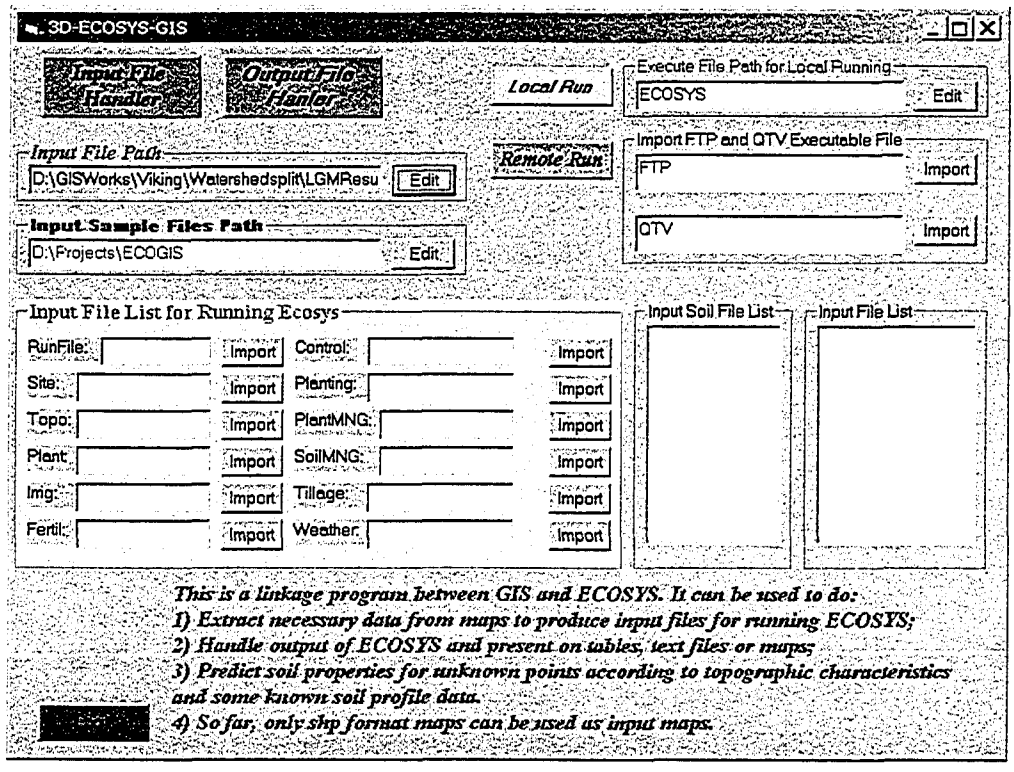

Appendix 3.2A: The main interface of 3D-ECOSYS-GIS model.

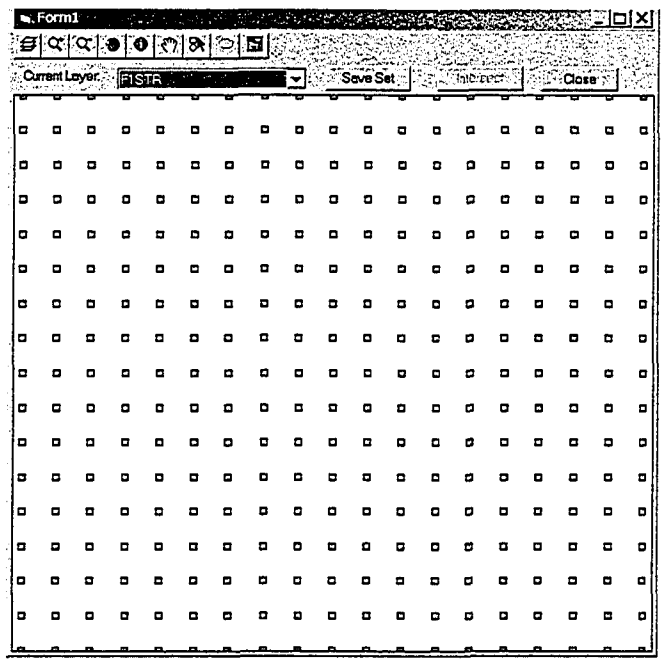

Appendix 3.2B: The sub interface for selecting data maps.

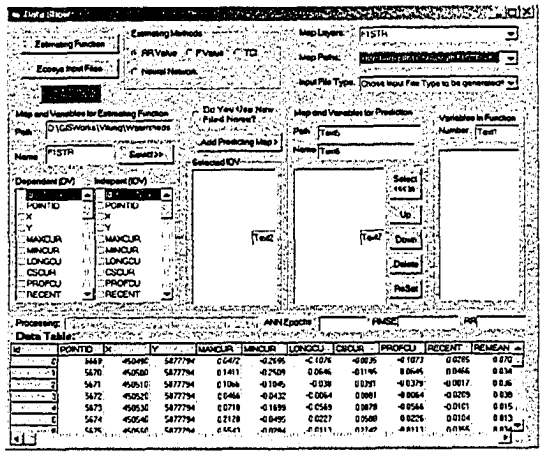

Appendix3.2C: The sub interface for estimating soil properties from terrain attributes and handling the input files of ecosys.

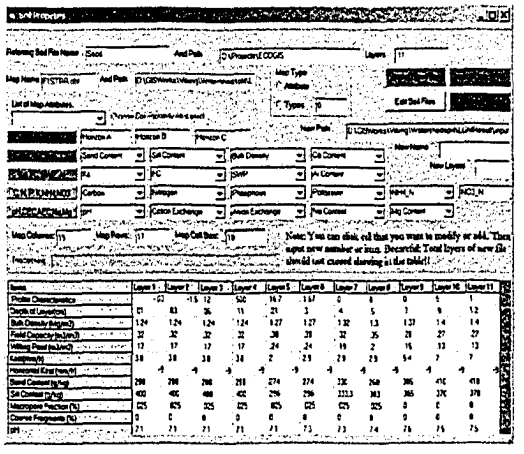

Appendix 3.2D: The sample of sub interface to handle input files of ecosys (This was used for handling soil data input file).

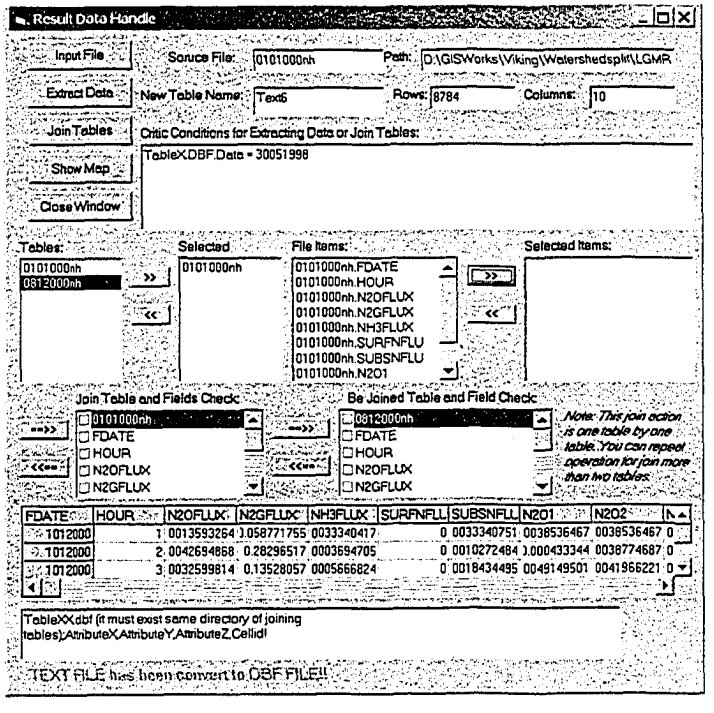

Appendix 3.2E: The interface to handle outputs.

Chapter 4: The Effects of Land and Cropping Management on N_2O Emissions in a Hummocky Agricultural Landscape

4.1 Introduction

Agriculture is the main anthropogenic source of N_2O (Choudhary et al., 2002), perhaps as much as 80% of all anthropogenic sources (Beauchamp, 1997). In Canada, N_2O emission accounts for 60% of the agricultural greenhouse gas effect. How to reduce N_2O emissions by changes in agricultural practices is still a crucial question. The amount of N_2O emission depends on complex interactions among agricultural practices, climatic factors, soil properties, soil water content, soil temperature, and microbial biomass (Scott et al. 2002; Akiyama et al., 2000; Kaiser and Ruser, 2000; Frolking et al., 1998; Kaiser et al., 1998; Smith et al., 1998; Minami, 1997; Qian et al., 1997; Matson and Vitousek, 1990; Cicrone, 1989; Cates and Keeney, 1987; Cates and Keeney, 1986; Goodroad and Keeney, 1984; Smith et al., 1983). Among these factors, agricultural practices are the easiest ones to change. Appropriate agricultural practices, such as tillage, fertilizer, and crop rotation can reduce N_2O emission from agricultural land.

Tillage affects N_2O emissions. Aulakh et al. (1984) found that N_2O emissions with no-tillage were two times that with conventional tillage in a wheat field in Saskatchewan, Canada. Reduced aerobic conditions and higher denitrifier populations contributed to the higher N_2O emissions. Ball et al. (1999) measured 2 to 10 times higher N_2O emissions by automated chambers in a no-tillage than in a conventionally tilled spring barley in an imperfectly drained loamy soil. Choudhary et al. (2002) found that N_2O emissions were slightly higher in a no-tillage than in a conventional tillage field, but the differences were not significant. However, Lemke et al. (1999) measured that N_2O emissions were generally lower in a no-tillage than in a conventional (intensive) tillage field, and higher in a fallow field than in a crop field in the Alberta parkland region, Canada.

Fertilizer applications increase N_2O emissions, but the effects depend on fertilizer types. In a permanent grassland on a sandy loam soil, cow slurry resulted in 8 times as much N_2O emissions as did NH_4NO_3 fertilizer with doubled N input (Christensen, 1983). A crop field fertilized by farmyard manure (93 kg N ha^{-1} y^{-1}) emitted twice as much N_2O

as one fertilized by cattle slurry (333 kg N ha^{-1} y^{-1}) in a sandy soil in northern Germany because of higher microbial biomass and approximately neutral pH in the farmyard manure field (Mogge et al., 1999). Harrison and Webb (2001) reviewed the effects of N fertilizer types on N_2O emission. They found that nitrate fertilizer caused greater N_2O emissions than did ammonium sulfate under wet conditions, and that urea generally caused greater N_2O emissions than did ammonium and ammonia fertilizers unless soil was dry and soil temperature was low. Lemke et al. (1999) estimated lower N_2O emissions in a manured field (total N 90 kg ha^{-1} and C:N $\approx$ 24:1) than in a urea fertilized field (56 kg N ha^{-1}) according to chamber measurements from a Black Chernozemic soil at Ellerslie, Alberta, Canada.

Crop rotation also affects soil N_2O emissions. The soil in the corn phase of a corn-oat-alfalfa-alfalfa rotation emitted 2.5 times more N_2O than did the soil of a continuous corn in a laboratory anaerobic incubation experiment (Drury et al., 2004). Field chamber measurements showed that N_2O emissions were respectively 50% and 23% higher in a continuous corn (fertilizer 180 kg N ha^{-1} y^{-1}) and corn-soybean (150 kg N ha^{-1} in corn year) rotations than in a corn-soybean/wheat-hairy vetch (130 kg N ha^{-1} in corn year) rotation in fine loamy and silt soil at Piketon, OH, USA (Jacinthe and Dick, 1997). Kaiser et al. (1998) summarized three years of field chamber measurements to estimate the effects of crops on N_2O emissions in a loamy silt luvisol soil in southern Germany. They found that the N_2O emission factors in sugar beet fields were the highest followed by those in winter rape, winter barley and winter wheat fields, and that the carbon to nitrogen ratio (C:N) of crop residues contributed to the differences in N_2O emissions. N_2O emissions of grasslands were always lower than those of crop fields with and without fertilizer in a sandy soil in northern Germany (Mogge et al., 1999) and a silt loamy soil in New Zealand (Choudhary e al., 2002).

In summary, the N_2O emissions in arable soils were site specific, and the effects of agricultural practices on N_2O emissions were inconsistent. No-till resulted in higher N_2O emissions in poorer drained or wetter ecosystems, but it might reduce N_2O emissions in well-drained or dry ecosystems when O_2 supply is adequate. With same fertilizer rates, N_2O emissions were higher in wetter or poorer drained ecosystems. Under the same crop rotations, differences in fertilizer rates or C:N of crop residue resulted in different N_2O

emissions. Therefore, the influence of agricultural practices on N_2O emissions still needs to be carefully investigated in future studies. The great spatial and temporal variability of N_2O emissions (Choudhary et al., 2002; Kaiser et al., 1998) make these attempts more difficult.

The accurately measuring or estimating N_2O emissions at landscape, field, regional, provincial and national scales is difficult because of the large spatial and temporal variability of those emissions (Choudhary et al., 2002; Kaiser et al., 1998; Chapter 3), the heterogeneities of soil properties over landscapes (Chapter 2), and the limitations of current measuring methods (Laville et al., 1999; Chapter 1). Nowadays, national and provincial N_2O emissions are estimated by using the IPCC guidelines (Olsen et al. 2003; Mosier et al., 1998). The factors in the IPCC guidelines were summarized from numerous experiments and observations, and are for all agricultural soils, regardless of variations in soil, cropping and climates. However, uncertainties in the estimates of N_2O emissions were 70 to 80% for agricultural soils (Lim et al., 1999).

Instead of IPCC, other methods have been tested to reduce the uncertainty in estimates of N_2O emissions in provincial, national and continental scales. Sozanska et al. (2002) used field measurements to establish a multiple regression model between N_2O emissions and factors affecting them. This model was coupled with a GIS framework to estimate regional and national N_2O emissions. This model accounted for effects of land use, soil temperature, soil water content, soil carbon content and nitrogen input on N_2O emissions. It offered a simple method for producing a spatial and temporal inventory of N_2O emissions, but it was also constrained by the accuracy of model inputs for soil temperature and soil water content that varied with landscape position. Bouwman et al. (1993) had earlier proved that this kind of regression has potential problems because minor differences in N_2O emission or factors at only one of the measurement sites used in model calibration could cause major shifts in model parameterization. Freibauer (2003) reported that errors in N_2O emissions estimated by regression models, which were used to estimate regional to continental N_2O emissions from agricultural soils in Europe, were 30 to 100%. Li et al. (2001) used the denitrification-decomposition (DNDC) model to estimate national N_2O emission using a county as a single plot. They found the uncertainty of this estimates would be ±50%. However, they did not account for the great

variation in topography, landscape, soil properties and land uses within a county, resulting in uncertainty similar to that of the IPCC method. The problem in scaling measurements and modeling results of N_2O emissions from soils was related to their extreme spatial and temporal heterogeneity (Bouwman et al., 2002). So far, the crucial problem of scaling up N_2O emissions from the micro-site or plot scales (those of chamber and micrometeorological measurements, and model outputs) to large scales (landscape, field, regional, provincial and national scales) remains unsolved.

Modeling can provide well-constrained tests of the effects of agricultural practices on N_2O emission because all factors that affect N_2O emissions can be easily constrained, except for the one being tested. *Ecosys*, which is the core of *3D-Ecosys-GIS* (Chapter 3), has the capability to represent the effects of cropping and soil management on the productivity, CO_2, N_2O and CH_4 emission, water and energy exchange of ecosystems (Grant et al., 2004, 2001; Grant, 2004, 1999, 1998; Li et al., 2004; Grant and Pattey, 2003, 1999). *3D-Ecosys-GIS* can be used to investigate the effects of agricultural practices on N_2O emissions. The combination of modeling results of *3D-Ecosys-GIS* and terrain attributes that are easily derived from elevation maps (Chapters 2 and 3) may provide a good way to estimate N_2O emissions at large scales, because *3D-Ecosys-GIS* can simulate landscape N_2O emissions in three dimensions to represent the large temporal and spatial variation of N_2O emissions (Chapter 3).

The objectives of this study were (1) to use modeling to investigate the effects of tillage, rotation and fertilizer on N_2O emissions at a landscape scale, and (2) to test scaling up methods for improving current N_2O inventory methodology.

4.2 Methods

4.2.1 Study site

The study site (Fig. 4.1) is a 76.6 hectare field representative of the black soil region in the aspen parkland eco-region in east central Alberta, at

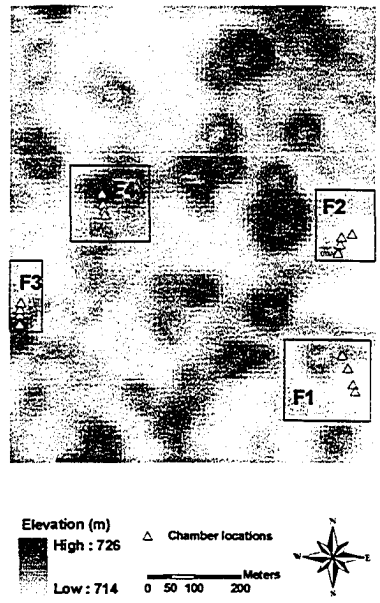

Figure 4.1: The study site, chamber locations and sub sites at Viking, Alberta, Canada (53°05'N, 111°47'W).

Viking, Alberta, Canada. It has a hummocky topography with moderate slope (10-13%). Elevation varies from 714 m to 726 m above sea level. The field is dominated by black chernozemic soils. The field is under conventional cultivation with a wheat, barley and canola crop rotation fertilized with 86, 13, 76 kg N ha^{-1}, respectively, and management using precision agriculture. Average annual precipitation from 1997 to 2002 was 359 mm, and average air temperature was 2.8 °C. Four sub sites described in Chapter 3 (F1, F2, F3, F4 in Fig. 4.1) were used to simulate N_2O emissions in *3D-Ecosys-GIS*.

4.2.2 Land and cropping management scenarios

This study was designed to test the effects of tillage, fertilizer and rotation on N_2O emissions. The interacting effects of these three factors were not considered in this study. The land use practices that were tested in this study are widely used currently or have potential to reduce N_2O emissions. Table 4.1 presents all tested land use scenarios and their crop and soil management. The current crop rotation (wheat-barley-canola (WBC)) and soil management (chemical fertilizer (CF) and conventional tillage (CT)) in the study site are used as a check scenario for all other scenarios. Except for the management practice being tested, all other management was same among scenarios in each of following three testing groups:

1. The tillage group included three scenarios: conventional tillage (CT), reduced tillage (RT) and no-tillage (NT). The CT scenario had two tillage events in spring and fall. The spring tillage was implemented with a heavy harrow one-half month before seeding. The fall tillage was implemented with a cultivator one-half or one month after harvest. In *3D-Ecosys-GIS*, the effect of tillage is represented as an implement-specific tillage coefficient that incorporates surface crop residue, changes the land surface roughness, and mixes soil material to a specified depth. (Grant et al., 2004, 2001). This incorporation affects surface energy exchange and soil heating, and also spatial relations between microbial population and soil organic matter, thereby affecting decomposition, respiration, mineralization, nitrification and denitrification.
2. The fertilizer group involved four scenarios: chemical fertilizer (CF), cattle manure (MF), no-fertilizer (NF) and double chemical fertilizer (DCF). In the MF scenario,

the total amount of nitrogen input for each crop was same as that in the CF scenario, 10% and 30% of total nitrogen in MF were NH_4^+-N and urea, and the total C to total N ratio was 24:1. The spring fertilizer was banded in 23 cm rows at 3.8 cm depth at seeding, and the fall fertilizer was injected to 9 cm depth in rows 30 cm apart in the middle of October. For CF, the amount of nitrogen fertilizer was 86, 13 and 76 kg N ha^{-1} in 2000, 2001 and 2002, respectively. In *ecosys*, products of fertilizer solubilization and manure mineralization are added to mineral N pools (NH_3, NH_4^+ and NO_3^-) in the zone of incorporation, thereby altering N transformation kinetics (Appendix 3.1: Eqs. A3.7 to A3.27).

Table 4.1: The scenarios and their cropping, tillage and fertilizer managements for which N_2O emissions were simulated in the hummocky agricultural landscape at Viking, Alberta, Canada.

Group	Scenario	Crop			Tillage			Fertilizer		
		2000	2001	2002	2000	2001	2002	2000	2001	2002
Check	Wheat-barley-canola (WBC)	Wheat	Barley	Canola	CT	CT	CT	CF00‡	CF01‡	CF02‡
Tillage	Reduced tillage (RT)	Wheat	Barley	Canola	RT	RT	RT	CF00	CF01	CF02
	No-tillage (NT)	Wheat	Barley	Canola	NT	NT	NT	CF00	CF01	CF02
Fertilizer	Manure fertilizer (MF)	Wheat	Barley	Canola	CT	CT	CT	MF	MF	MF
	Double chemical fertilizer (DCF)	Wheat	Barley	Canola	CT	CT	CT	2× CF00	2× CF01	2× CF02
	No-fertilizer (NF)	Wheat	Barley	Canola	CT	CT	CT	NF	NF	NF
Rotation	Continuous wheat (CW)	Wheat	Wheat	Wheat	CT	CT	CT	CF00	CF01	CF02
	Continuous hay (CH)	Grass	Grass	Grass	NT	NT	NT	CF00	CF01	CF02
	Wheat-fallow (WF)	Wheat	Fallow	Wheat	CT	CT	CT	CF00	NF	CF02
	Wheat-wheat-fallow (WWF)	Wheat	Wheat	Fallow	CT	CT	CT	CF00	CF01	NF
	Hay-hay-hay-wheat-wheat-wheat (HHHWWW)	Wheat	Wheat	Wheat	CT	CT	CT	CF00	CF01	CF02

‡: CF00, CF01, CF02 indicate the chemical fertilizer in 2000, 2001 and 2002. In 2000, spring and fall fertilizer were 14 (40% urea + 60% NH_4^+) and 72 (93% urea + 7% NH_4^+) kg N ha^{-1} respectively. In 2001, spring and fall fertilizer were 10 (100% urea) and 3 (100% urea) kg N ha^{-1}. In 2002, spring and fall fertilizer were 14 (40% urea + 60% NH_4^+) and 62 (95% urea + 5% NH_4^+) kg N ha^{-1}.

3. The crop rotation group included six scenarios: wheat-barley-canola (WBC), continuous wheat (CW), continuous hay (CH) harvested twice a year on July 15 and September 15, wheat-fallow (WF), wheat-wheat-fallow (WWF), and hay-hay-hay-wheat-wheat-wheat (HHHWWW). In HHHWWW, hay was harvested once on August 30 in the first year of hay, and twice on July 15 and September 15 in the second and third years. Hay land was plowed at 20 cm depth one-half month after the second harvest in the third year. The amount and date of fertilizers in the three years of hay in this rotation corresponded to those of WBC banded at 5 cm depth in rows 30 cm apart. In *ecosys*, key functional characteristics of each crop species (e.g. photosynthetic type, growth habit, N_2-fixing capability, maturity group and others) direct the model to simulate its biological behavior during its phase in the modeled rotation.

4.2.3 Scaling up N_2O emissions to field scale

In order to estimate the total N_2O emission in the entire study site, four scaling up methods were calculated using N_2O emissions calculated from the check scenario (same as measurement conditions) in the first part of the modeling experiment.

1. Scaling up of measured results (MeM): The total emission of the entire study site was the product of the total area of the entire study field multiplied by the average of annual N_2O emissions estimated from field measurements. The estimated annual N_2O emissions at 16 chamber measurement locations (Fig. 4.1) were derived by linear interpolation from 8, 9 and 11 measured events in 2000, 2001 and 2002, respectively. These 16 locations represented the depressions, footslopes, midslopes and tops in the hummocky agricultural landscape.
2. Scaling up of modeling results (MoM): the total N_2O emission of the entire site was the product of the field area and the average of annual N_2O emissions aggregated from model outputs (Fig. 3.11) for each sub site (F1, F2, F3 and F4 in Fig. 4.1) on per unit area.
3. IPCC method: The total N_2O emission of the entire study site was estimated by using 1997 IPCC guidelines given by equations in Appendix 4.1 (Eqs. A4.1 – A4.4) (Eqs. A3-12 to A3-19 in Olsen et al., 2003). The N_2O emission from chemical fertilizer

applications was calculated by Eqs. A4.2 and A4.3. The N_2O emission from crop residues was calculated by Eq. A4.4 (Eqs. A3-19, Olsen et al., 2003).

4. Relationship of terrain attributes to N_2O emissions (TAR): A regression function was developed by stepwise multiple linear regression based on the modeled N_2O emissions and terrain attributes in the four sub sites (F1, F2, F3 and F4, Fig. 4.1). Terrain attributes were derived in Chapter 2, and used in the regression function to estimate N_2O emissions for each grid cell. The total emission of entire study site was the sum of N_2O emissions in all grid cells.

4.2.4 Model runs and evaluation

The *3D-ECOSYS-GIS* model (Chapter 3) was used to simulate N_2O emissions from the different scenarios for tillage, fertilizer and rotation in Table 4.1. To reduce computation time required to run the three dimensional model for the entire study site that included 7663 grid cells at 10×10 meter resolution, four sub sites (F1, F2, F3 and F4 in Fig. 4.1) were selected from the entire study field and used to formulate four simulation runs for each scenario. Each sub site included one mini-watershed to represent distribution of tops, midslopes, foot slopes and depressions in the hummocky agricultural landscape. Simulations were started on a model date of 1 January 1997 and ended on 31 December 2002, using hourly weather data from the meteorological station at Viking nearest the study field (about 10 km away) provided by Len Kryzanowski (Alberta Agriculture, Food and Rural Development, Edmonton, Alberta, Canada). Crop and soil management practices, except for those being tested, were same as those in the check scenario (WBC). The model was initialized with 1235 g C m^{-2} of residue carbon (i.e. the sum of accumulative crop and microbial residues) with a C:N of 12.4:1 (Chapter 3). Topographically referenced soil properties were those derived in Chapter 2 by a stepwise multiple linear regression (SMLR) method in the landscape soil property predictor (LSPP).

The modeled annual N_2O emissions in 2000, 2001 and 2002, and the total of the three years were used to examine the effects of cropping system, tillage and fertilizer on N_2O emissions.

4.3 Results and discussion

4.3.1 Effects of tillage on N_2O emissions

Simulation data showed that no-tillage (NT) reduced total N_2O emission by 19% and 38% during 2000 to 2002 in the hummocky agricultural landscape in comparison with reduced (RT) and conventional tillage (CT), respectively (Table 4.2). RT decreased total N_2O emission during the three years by 23% in comparison with CT. In the normal year (2001, precip. 332 mm ≈ average precip. 359 mm), annual N_2O emissions across the landscape under NT were not remarkably different from those under RT, but were lower than those under CT. In the wet (2000, precip. = 451 mm >> average precip.) and dry (2002, precip. = 221 mm << average precip.) years, reduced tillage lowered the annual N_2O emissions. As the climate changed from the wet to dry year, annual N_2O emissions declined by 67% under CT, 76% under RT and 81% under NT. Reduced tillage caused a larger relative decline in N_2O emissions during dry versus wet weather.

Table 4.2: Annual N_2O emissions and spatial variations under different tillage management at the hummocky agricultural landscape at Viking, Alberta, Canada, in 2000, 2001 and 2002.

Values across 4 sub sites	Tillage	2000	2001	2002	Total
Mean emission over landscape (g N m^{-2})	CT	0.57	0.39	0.19	1.14
	RT	0.55	0.20	0.13	0.88
	NT	0.43	0.21	0.08	0.71
Coefficient of spatial variation in N_2O emission (CSV, %)	CT	88	170	341	116
	RT	82	136	201	86
	NT	114	292	496	168

Lower N_2O emissions were modeled under NT because crop residue was not incorporated into soil. Consequently, surface residue was much larger under NT than under RT or CT (Table 4.3), so that less N was mineralized, reducing mineral N in soil. As a result, NO_3^- concentration was lower under NT than under RT and CT in 2000, especially during the main emission period (May to July, Chapter 3), although not in 2001 and 2002 (Fig. 4.2b). The accumulation of surface reside lowered soil temperature under NT, so that carbon oxidation declined from CT, through RT, to NT (Table 4.3), reducing the demand for O_2 (Eqs. A3.15, A3.16, A3.23 and A3.24), while increasing O_2 solubility and hence supply of O_2 (Eqs. A3.9 and A3.12). In the *3D-Ecosys-GIS*, soil was less aerobic when the respiration coefficient (the ratio of O_2 taken up to CO_2 evolved

from soil) was lower than 2.67 g O_2 g^{-1} C, indicating higher relative water-filled porosity (RWFP) (Fig. 4.2c). The days with lower respiration coefficient were more frequent under NT than under RT and CT, especially in the wet year (2000) (Table 4.3). The higher modeled RWFP under NT also indicated less aerobic soil (Fig. 4.2c), decreasing the supply of O_2 (Eqs. A3.7 and A3.10). However, the decreased O_2 demand plus higher O_2 solubility with lower NO_3^- more than offset the decreased O_2 supply due to higher RWFP, resulting in lower N_2O emission (Eqs. A3.15 to A3.27; Fig. 4.2d).

Table 4.3: The key factors explaining differences in N_2O emissions among conventional (CT), reduced (RT) and no (NT) tillage.

Year	Scenario	Surface residue at the end of calendar year (g C m^{-2})	Annual average soil temperature in upper 10 cm (°C)	Soil carbon oxidation (g C m^{-2} y^{-1})	Days for respiration coefficient[§] < 2.67
	CT	355	5.6 ± 7.5	310	133
2000	RT	550	5.4 ± 7.2	278	163
	NT	648	5.1 ± 6.6	257	193
	CT	278	6.2 ± 8.4	287	125
2001	RT	548	5.8 ± 7.9	242	127
	NT	702	5.4 ± 7.2	224	130
	CT	225	4.6 ± 9.7	228	130
2002	RT	514	4.4 ± 8.9	183	132
	NT	694	3.9 ± 7.9	175	133

[§]: Respiration coefficient is the ratio of O_2 uptake to carbon released through soil respiration.

However, the simulation results also showed that N_2O emissions were higher under RT and NT than under CT during selected periods, for example, after day 180 in 2000 (Fig. 4.3). In *3D-Ecosys-GIS*, large precipitation (130 mm, 29% of annual precipitation) during this period caused soil water contents (0–2.5 cm) to be frequently higher under NT (modeled daily RWFP = 0.59 ± 0.18) and RT (0.57 ± 0.17) than under CT (0.49 ± 0.15), resulting more frequent temporary surface blockage of gas exchange, although the modeled RWFPs in upper 20 cm soil zone were similar (Fig. 4.2c). As a result, gas diffusivity was sharply decreased after rainfall under RT and NT (Eq. A3.10), rapidly reducing the supply of O_2 (Eqs. A3.7 to A3.9, A3.17 and A3.25), so that the deficiency of electron acceptors increased greatly (Eqs. A3.18 and A3.26), leading to the increase of N_2O emission (Eqs. A3.19 to A3.21 and A3.27).

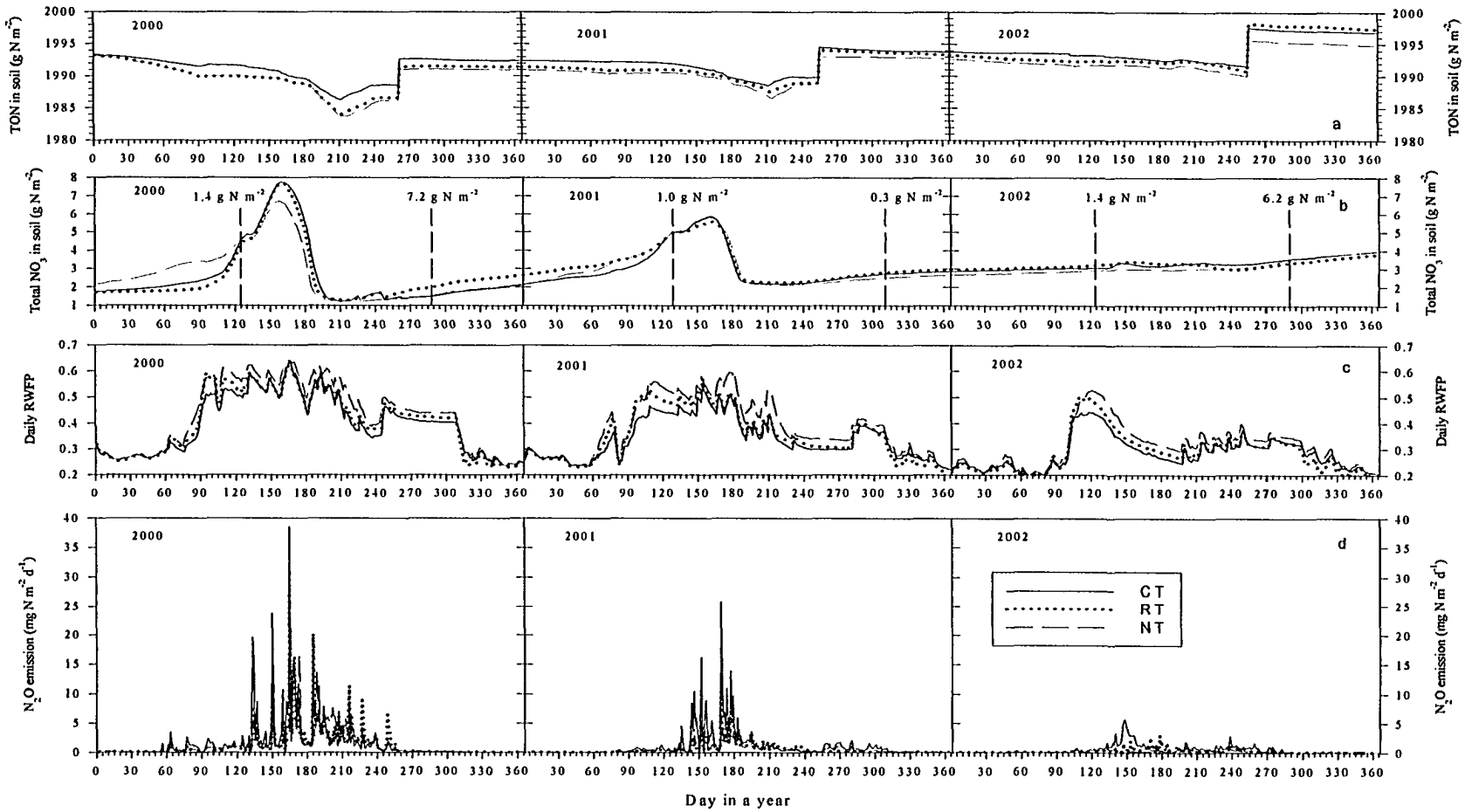

Figure 4.2: The dynamics of soil total organic nitrogen (TON) and NO_3^- contents, daily RWFP in upper 20 cm soil zone and N_2O emissions under conventional tillage (CT), reduced tillage (RT) and no-tillage (NT) in the hummocky-agricultural landscape at Viking, Alberta, Canada, in 200, 2001, 2002.

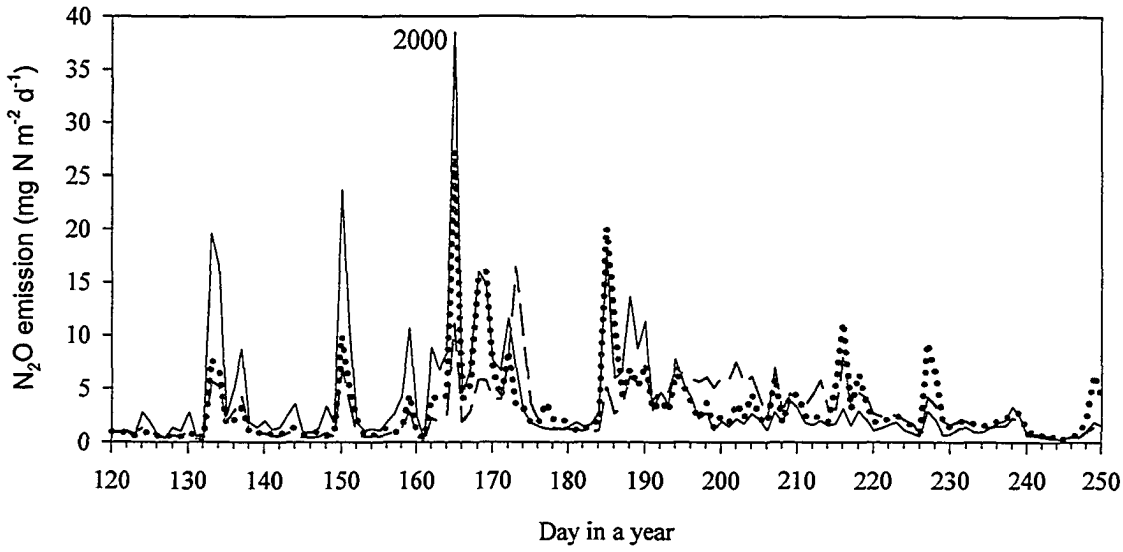

Figure 4.3: An expanded graph from Fig. 4.2d to show the differences of N_2O emission in a period of 2000 under conventional (CT, black solid line), reduced (RT, dots) and no (NT, long dash line) tillage.

Lower N_2O emissions modeled under NT and RT than under CT disagreed with results of chamber measurements by Choudhary et al. (2002), Ball et al. (1999) and Aulakh et al. (1984). Aulakh et al. (1984) found that less aerobic conditions and higher denitrifier population contributed to the higher N_2O emissions under NT soil than under CT soil in Saskatchewan, Canada. On the other hand, some field measurements supported the modeled results. Lemke et al. (1999) measured N_2O emissions that were generally lower, but occasionally higher, in NT than in CT at Ellerslie, Alberta, Canada, where the soil was similar to the soil in this study. The following reasons may explain the conflicting results. Measurements taken over short periods, such as shown in Fig. 4.3, might lead to the conclusion that N_2O emission was higher in NT and RT than in CT. Under certain conditions, small spatial variation in topography and soil properties could cause large differences in measurements of N_2O emissions (20% to 500%) (Chapter 3; Williams et al., 1999; Röver et al., 1999; Kaiser et al., 1996; Folorunso and Rolston, 1984; Myrold, 1988). Spatial variation in soil properties and topography between field plots under NT and CT might also cause differences in measurements of N_2O emissions. The simulation tests ensured that all conditions, except for tillage, were the same across landscape for different tillage scenarios, so that the differences of modeled N_2O emissions came only

from tillage. Model results suggested that tillage effects on N_2O emissions may be seasonal.

The coefficients of spatial variation (CSV) in annual N_2O emissions ranged between 81% and 496% in three tillage scenarios in 2000, 2001 and 2002 (Table 4.2). RT decreased the spatial variations in N_2O emission, but NT increased them. Guzha (2004) measured that roughness and infiltration under NT were significantly lower than under CT. Different tillages in the model caused differences in surface roughness under NT, RT and CT (additional surface roughness was 0 cm for NT and 4 cm for RT and CT, the storage capacity of surface residue in water did not account for in the model currently). As a result, with the same amount of rainfall, more runoff was generated under NT than under RT and CT, so that more water could accumulate at lower landscape positions and less water would infiltrate at upper landscape positions, enlarging the spatial differences of soil water content. Therefore, spatial variations of N_2O emissions were larger under NT than under RT and CT. Because the differences in surface roughness and infiltration between RT and CT were small or even non-existent, the differences in the coefficients of spatial variations in N_2O emissions were also small. In addition, annual N_2O emissions decreased sharply with the decreases of annual precipitation from the wet to dry year, enlarging CSV.

In summary, tillage increased N_2O emissions, but decreased spatial variation. In addition, there was large temporal variation of annual N_2O emission. Therefore, the current N_2O inventory, which does not account for the effects of tillage on N_2O emissions, and on their temporal and spatial variations, could have a large uncertainty.

4.3.2 Effects of fertilizer on N_2O emissions

Simulated annual N_2O emissions across the landscape were significantly different under different fertilizer management (Table 4.4). Doubling current chemical fertilizer rates (DCF) raised N_2O emissions by 108% in the normal year (2001), by 47% in the wet year (2000), and by 32% in the dry year (2002) in comparison with current chemical fertilizer rates (CF) (8.6 g N m^{-2} y^{-1} in 2000, 1.3 g N m^{-2} y^{-1} in 2001, 7.6 g N m^{-2} y^{-1} in 2002) (Table 4.4). Total N_2O emission from CF during three years was respectively 1.7 and 2.5 times those from cattle manure (MF) and no-fertilizer (NF). Over three years,

fertilizer emission factors evaluated from the emissions during the 12 months period following fall application (mid-Sept. – mid-Sept.) were different. Therefore, was no relationship was found between N input and N_2O emissions under CF, DCF and MF. This result agreed with the conclusion of Kaiser and Ruser (2000) from numerous field measurements in different arable soils in Germany.

Table 4.4: Annual N_2O emissions, spatial variations and emission factors under chemical (CF), manure (MF), double chemical (DCF) and no (NF) fertilizer management in the hummocky agricultural landscape at Viking, Alberta, Canada, in 2000, 2001 and 2002.

Values across 4 sub sites	Fertilizer	2000	2001	2002	Total
Mean emission over landscape (g N m^{-2})	CF	0.57	0.39	0.19	1.14
	DCF	0.84	0.81	0.45	2.10
	MF	0.34	0.27	0.08	0.68
	NF	0.22	0.18	0.06	0.46
Mean emission factor over landscape (%)‡	CF	4.6	2.6	7.6	3.9
	DCF	4.1	3.8	5.6	4.1
	MF	1.6	1.1	1.2	1.3
Coefficient of spatial variation in N_2O emission (CSV, %)	CF	88	170	341	116
	DCF	74	124	140	80
	MF	181	266	621	212
	NF	149	227	456	177

‡: The emission factor was calculated from period between fall fertilizer applications.

In *3D-Ecosys-GIS*, additional N (mostly urea) increased NH_4^+ under DCF. Part of the increased NH_4^+ was oxidized, increasing soil NO_3^- content (Fig. 4.4b) and raising O_2 demand (Eqs. A3.23 and A3.24). Under less aerobic soil, this demand rapidly increased deficiency of electron acceptors for nitrification (Eqs. A3.25 and A3.26), leading to more N_2O production (Eq. A3.27; Fig. 4.4d; Table 4.4). Higher NO_3^- (Fig. 4.4b) provided more substrate for denitrification, thereby raising N_2O emissions under anaerobic soil (Eqs. A3.19 to A3.21; Fig. 4.4d, Table 4.4). The additional N under DCF was partially taken up by the crop, increasing crop productivity (net primary productivity (NPP) = 1402 g C m^{-2} y^{-1} under DCF vs. 1152 g C m^{-2} y^{-1} under CF in three years). The organic nitrogen returned from residue in DCF was higher than those in CF, NF and MF, leading to the accumulation of organic carbon and nitrogen in soil (Fig. 4.4a). Therefore, more rapid carbon oxidation (988g C m^{-2} y^{-1} under DCF vs. 825 g C m^{-2} y^{-1} under CF in three years) increased O_2 demand, raising N_2O emissions (Eqs. A3.15 to A3.21).

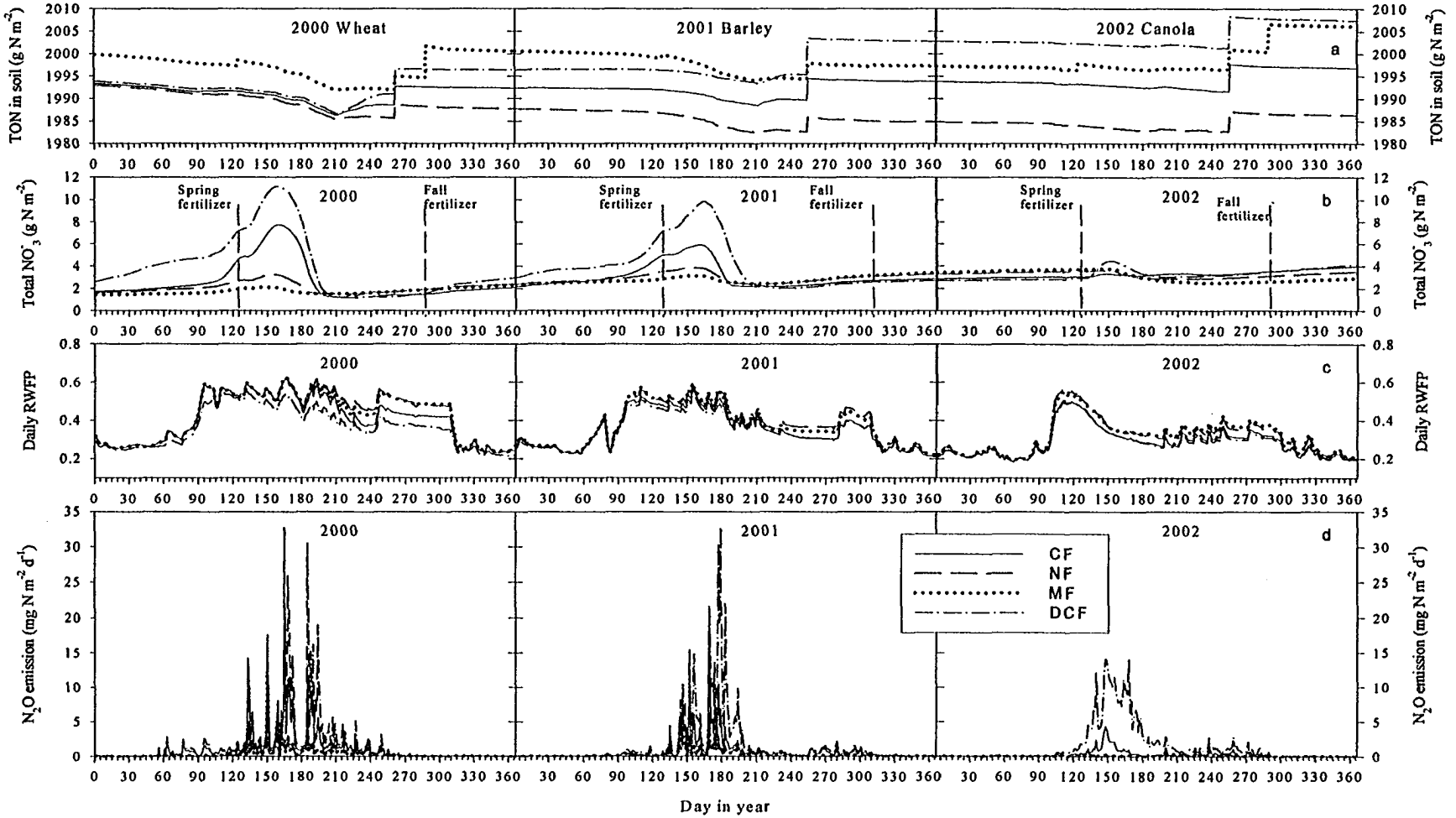

Figure 4.4: The dynamics of soil total organic nitrogen (TON) and NO_3^- contents, daily RWFP and daily N_2O emissions under chemical fertilizer (CF), double chemical fertilizer (DCF), no-fertilizer (NF) and cattle manure (MF) in the hummocky agricultural landscape at Viking, Alberta, Canada, in 2000, 2001, 2002.

The N_2O emissions in MF were 42% to 62% of those in CF from the wet to the dry years with same total nitrogen fertilizer rates. The total organic nitrogen was higher in MF than in CF (Fig. 4.4a) because 60% of nitrogen in manure was organic nitrogen rather than 100% inorganic nitrogen as in chemical fertilizers. The organic nitrogen was available for nitrification only after it had been mineralized, and for denitrification only if NH_4^+ had been nitrified. In the simulation, the total C to total N ratio was assigned as 24:1 for cattle manure. The higher organic C:N ratio (e.g. 36:1 for organic C to organic N) reduced net mineralization rate and sources of nitrification, resulting in lower substrate (NO_3^-, Fig. 4.4b) for denitrification, and hence lower N_2O emission (Fig. 4.4d) under similar soil water conditions (Fig. 4.4c). In contrast, CF provided more direct sources of nitrification and denitrification than did manure fertilizer under the same nitrogen application (Fig. 4.4b). In the model, higher nitrification substrate developed higher O_2 demand (Eqs. A3.23 and A3.24), resulting higher N_2O emission from nitrification process under less aerobic soil (Eqs. A3.25 to A3.27). Therefore, greater proportion of urea in chemical fertilizer (60% to 97% of input N) also increased N_2O emissions more than ammonium and ammonia-nitrogen fertilizers (Harrison and Webb, 2001), and the additional high soil nitrate favored high N_2O emissions through denitrification (Sehy et al, 2003).

The lower N_2O emissions modeled in MF disagreed with most field research. Kaiser and Ruser (2000), Mogge et al (1999), Eichner (1990) and Bouwmam (1990) found that N_2O emissions were larger in the arable soils that received organic fertilizers than those that received chemical fertilizers, because the more easily mineralizable organic matter in organic fertilizers might increase microbial biomass and O_2 consumption, thereby elevating N_2O emissions (Flessa and Beese, 1995). On the other hand, lower N_2O emissions modeled in MF were consisted with other field measurements. Paul and Zebarth (1997) found that the N_2O production was lower with manure than with chemical fertilizer in a laboratory incubation study of the soils of south coastal British Columbia, Canada. Through a field experiment on an andisol soil at Tsukuba, Japan, Hiroko and Haruo (2003) found that N_2O emissions were lower with cattle manure than with urea fertilizer under the same N inputs. They thought that the reason for this was that the high C:N ratio (24:1) reduced the NO_3^- in soil, leading to the lower N_2O emissions, although

the differences were not significant. Lemke et al. (1999) also measured significantly higher N_2O emissions with chemical fertilizer than with manure fertilizer at Ellerslie, Alberta, Canada, where the soil was similar to the soil in this study, even though N input with organic manure was much higher than that with chemical fertilizer (90 vs. 65 kg N ha^{-1}).

The simulation results showed that both CF and MF increased soil nitrogen content (Fig. 4.4a) resulting in higher N_2O emissions than those under NF (Fig. 4.4d). With the lower N_2O emissions, emission factors of N_2O were consistently lower under MF than under CF in the three years.

The emission factors and CSVs in annual N_2O emissions changed with the amount and types of fertilizer, and climate. There were no consistent relationships between N_2O emission, its CSV, and the amount and type of fertilizer. In addition, the differences of annual precipitation caused large differences in N_2O emissions. Therefore, current N_2O inventory (Olsen et al., 2003; IPCC guidelines, 1997), in which N_2O emission is estimated from a constant emission factor regardless of the effects of fertilizer types, amount, climate (e.g. precipitation) and spatial variation, would be unlikely to allow accurate estimates of N_2O emissions.

4.3.3 Effects of rotation on N_2O emissions

In the hummocky agricultural landscape, cropping systems strongly influenced N_2O emissions (Table 4.5). Among the six rotations, total N_2O emissions modeled during three years varied from 0.7 to 1.3 g N m^{-2} and were significantly different among the cropping systems, except for the total N_2O emissions between CW and WBC. The total N_2O emission was the highest in hay-hay-hay-wheat-wheat-wheat (HHHWWW) (i.e. emissions under wheat following conversion from grassland), followed by WBC, CW, WWF, CH and WF. For the total N_2O emissions during the three years, CSV decreased from 116% to 63% in the order of WBC, CH, WF, CW, WWF and HHHWWW. The spatial variations were reduced when grass and fallow were included in rotation systems. Annual N_2O emissions declined with declining precipitation in 2000, 2001 and 2002 (Table 4.5). Therefore, the effects of crop rotation and climate on soil N_2O emissions, and

on their temporal and spatial variations must be accounted in current N_2O inventory methods to reduce the uncertainties of estimations.

4.3.3.1 Effects of conversion from grassland to cropping on N_2O emissions

The conversion from grassland to cropland increased N_2O emissions in cropland phase by 18% in comparison with CW, especially N_2O emission was 49% higher during the first crop year after the third hay year than in CW (Table 4.5). In the model, plowing mixed a large amount of residue into the soil, accelerating carbon oxidation (325 g C m^{-2} y^{-1} in HHHWWW vs. 298 g C m^{-2} y^{-1} in CW during 2000) and nitrogen mineralization, thereby raising NO_3^- (Fig. 4.5d). More rapid oxidation of carbon and NH_4^+ elevated the demand for O_2, raising N_2O emissions (Table 4.5; Eqs. A3.15 to A3.27). However, the conversion effects on N_2O emissions were not apparent in 2001 and 2002 (Table 4.5). Field measurements are consistent with simulation results. Flessa and Beese (1995) and Kasier et al. (1998) found residue incorporation in soil increased O_2 consumption and elevated N_2O emission. Mosier et al. (1997) also found that conversion from grassland to cropland increased N_2O emission from the shortgrass steppe at Fort Collins, Colorado, USA.

Table 4.5: Annual N_2O emissions and spatial variations under wheat-barley-canola (WBC), wheat-fallow (WF), wheat-wheat-fallow (WWF), continuous wheat (CW), continuous hay (CH) and hay-hay-hay-wheat-wheat-wheat (HHHWWW) in the hummocky agricultural landscape at Viking, Alberta, Canada, in 2000, 2001 and 2002.

Values across 4 sub sites	Cropping system	2000	2001	2002	Total
Mean emission over landscape (g N m^{-2})	WBC	0.57	0.39	0.19	1.14
	WF	0.55	0.09	0.07	0.70
	WWF	0.55	0.25	0.13	0.93
	CW	0.53	0.31	0.27	1.11
	CH	0.46	0.18	0.12	0.76
	HHHWWW	0.79	0.28	0.18	1.31
Coefficient of spatial variation in N_2O emission (CSV, %)	WBC	88	170	341	116
	WF	69	251	338	86
	WWF	69	159	209	78
	CW	96	140	87	82
	CH	91	205	247	109
	HHHWWW	69	143	109	63

Note: See the crops in 2000, 2001 and 2002 in Table 4.1.

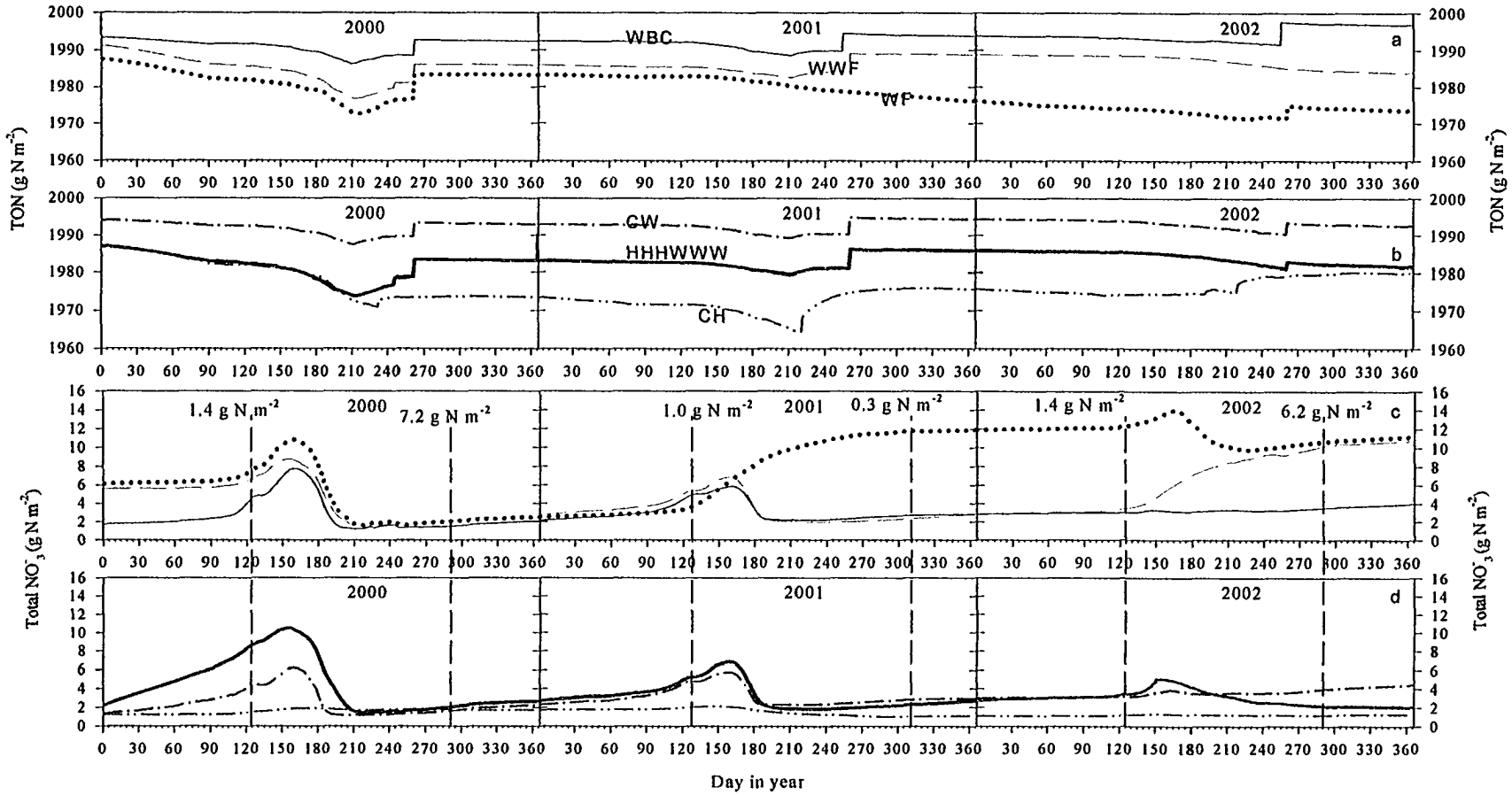

(Continued on next page)

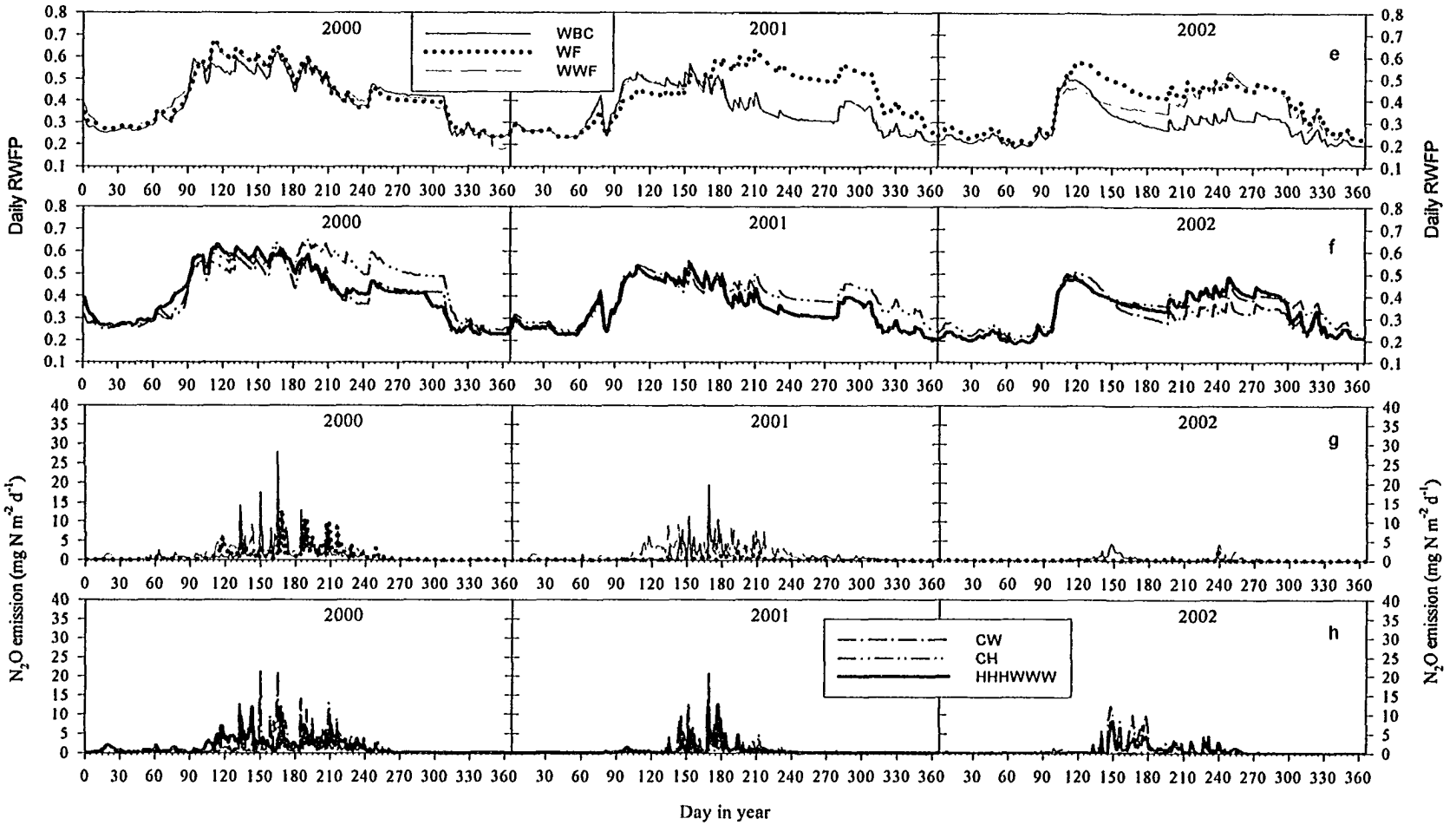

Figure 4.5: The dynamics of soil total organic nitrogen (TON) and NO_3^- contents, daily RWFP and daily N_2O emissions under wheat-barley-canola (WBC), wheat-wheat-fallow (WWF), wheat-fallow (WF), continuous wheat (CW), hay-hay-hay-wheat-wheat-wheat (HHHWWW) and continuous hay (CH) in the hummocky agricultural landscape at Viking, Alberta, Canada, in 200, 2001, 2002.

4.3.3.2 Effects of fallow on N_2O emissions

The simulation results showed that annual N_2O emissions in the fallow year of WF and WWF were lower than those in the cropped year of WBC, CW and HHHWWW, and comparable with those of CH (Table 4.5). In model, much lower CO_2 effluxes modeled in fallow years [201 g C m^{-2} y^{-1} in fallow year of WF (2001) and 159 g C m^{-2} y^{-1} in fallow year of WWF (2002) vs. 276 g C m^{-2} y^{-1} and 239 g C m^{-2} y^{-1} in CW in 2001 and 2002] indicated much lower O_2 demand (Eq. A3.16). The reason for the lower carbon oxidation under fallow in the model was the lower microbial actovoty, as has been found in field measurements (Mosier et al., 1997). Modeled accumulation of NO_3^- in fallow years (Fig. 4.5c) provided more alternative electron acceptors for carbon oxidation. The conversion of NO_3^- to NO_2^- would meet most of the limited demand for electron acceptors, so that less NO_2^- was converted into N_2O, resulting in less N_2O emission (Eqs. A3.19 to A3.21), even though higher RWFP in fallow years (Fig. 4.5e) reduced O_2 supply (Eqs. A3.7 to A3.14). Therefore, small demand for, and large supply of electron acceptors would suppress N_2O production (Fig. 4.5g; Cooper and Smith, 1963). The lower N_2O emissions modeled in fallow years conflicted with field measurements (Mosier et al. 1996, 1997). They found that the high soil water content (e.g. Fig. 4.5e) and mineral nitrogen content in fallow periods (e.g. Fig. 4.5c) contributed to high N_2O emissions.

4.3.3.3 Effects of continuous grassland versus cropping on N_2O emissions

CH reduced N_2O emissions by 35% in comparison with those from CW and WBC (Table 4.5). In the simulation, soil organic carbon and nitrogen in CH were decreased because of heavy mowing while they were unchanged or increased in CW and WBC (Fig. 4.5a and b). The much lower NO_3^- content in soil under CH provided little substrate for denitrification (Fig. 4.5d), resulting in low N_2O emissions (Fig. 4.5h). The lower N_2O emissions modeled under CH were consistent with field measurements elsewhere. Choudhary et al. (2002) and Mogge et al. (1999) found that N_2O emissions were lower in permanent grassland than in cropland.

4.3.4 Scaling N_2O emission up to field scale

Four scaling up methods were used to estimate N_2O emissions in WBC for the entire site (76.6 ha) over the three years. These estimates varied between 359 kg N and 873 kg N over the field during three years (Table 4.6).

The MeM method using field chamber measurements derived the lowest N_2O emissions (Table 4.6). The annual N_2O emission in 2000 was only one-fifth to one-third of that estimated by other three methods, leading to a low total N_2O emission over the three years. Field studies have demonstrated that estimates of N_2O emissions aggregated from low frequency measurements have large uncertainties. Brumme and Beese (1992) used an automated gas sampling chamber and analysis system to measure N_2O emissions from a beech stand. They found that weekly measurements resulted in a mean overestimation of 21% of emissions aggregated from continuous measurements during 6 months. Scott et al. (1999) reported that cumulative emissions from continuous measurements over a sewage sludge-amended grassland were underestimated by about 40% when aggregated from measurements twice a week by chamber. Flessa et al. (2002) reported that over-estimates of cumulative fluxes from a potato field based on weekly measurements could be reduced from 48% to 15% with additional measurements after rainfall events. Crill et al. (2000) reported that total N_2O emissions estimated from 1 measurement per day or per 2.5 days were 20% and 40% higher respectively than that from 5 measurements per day. In this study, the number of chamber measurements from each of 16 locations was 8 in 2000, 9 in 2001, and 11 in 2002. The low frequency of measurements led to large uncertainty in the estimations of annual N_2O emissions. For example, although the precipitation was highest in 2000, the estimated annual N_2O emission linearly interpolated from 8 measurements was lower than that in 2001 and close to that in 2002. As discussed in chapter 3, spatial variation of annual N_2O emissions were larger than 200% in the hummocky agricultural landscape. Measurements were done at 16 locations that represented the depressions, foot-slopes, midslopes and tops. These measurements did not represent the diversity of N_2O emissions in the hummocky agricultural landscape. Therefore, MeM would have a larger uncertainty (likely underestimated) in the total N_2O emission for the entire field than that reported by Flessa et al. (2002), Crill et al. (2000), Scott et al. (1999) and Brumme and Beese (1992).

Unfortunately, continuous measurement covering the entire field was not practical, so that the error was impossible to identify.

Table 4.6: Total N_2O emissions in the entire study field (76.6 ha) derived by different scaling up methods.

Scaling up methods‡	2000	2001	2002	Total
	For entire study field (kg N_2O-N)			
MeM	95.3	186.7	76.8	358.9
IPCC	308.2	257.2	204.9	770.3
MoM	433.2	296.9	143.1	873.1
TAR¶	298.9	219.8	112.4	631.1
	For unit area (kg N_2O-N ha^{-1})			
MeM§	1.2	2.4	1.0	4.7
IPCC	4.0	3.4	2.7	10.1
MoM	5.7	3.9	1.9	11.4
TAR	3.9	2.9	1.5	8.2

‡: For descriptions, see section 4.2.3. §: Provided by Tom W. Goddard. ¶: Terrain attributes explained 42% to 57% of the variation of N_2O emissions.

N_2O emissions estimated by the IPPC method from fertilizer rate and crop production were 22% and 115% higher than those estimated from terrain attributes (TAR) and directly from the model (MeM), but 9% lower than that derived from field measurements (MoM). Webster et al. (2002) reported that global estimations of N_2O emissions based on six N_2O IPCC emission scenarios had at least 67% uncertainty. The estimation of N_2O emission from the UK, using the IPCC default values for all emission factors and parameters, had an overall uncertainty of 62% (Brown et al., 2001). N_2O emissions had great temporal and spatial variability in the hummocky agricultural landscape (Chapter 3). The simulation results of *3D-Ecosys-GIS* showed that tillage, fertilizer and crop rotation changed the N_2O emission as well as spatial variation. Akiyama et al (2000) found that the fertilizer types strongly affected N_2O emission factors. Kaiser and Ruser (2000) found that soil properties, crops and cropping management affected N_2O emissions. IPCC methods did not account for the temporal and spatial variations that resulted from heterogeneities of soil properties, microtopography, fertilizer types, soil and cropping management, and climate. In this study, in comparison with three other scaling up methods, uncertainty similar to that reported by Brown et al (2001) might

exist, and the IPCC method would likely overestimate the N_2O emissions for the hummocky agricultural landscape.

The scaled up N_2O emissions from TAR (Appendix 4.2) were higher than those from MeM, but lower than those from IPCC and MoM (Table 4.6). Terrain attributes indicated the characteristics of microtopography that are related to soil properties, and to the redistribution of water, solute and sediment (Chapter 2), that affect N_2O emissions (see Chapter 3 for key terrain attributes). Through simulations of *3D-Ecosys-GIS* and TAR functions, this method accounted for the effects of climate, and spatial variability of microtopography, soil properties, soil water content and crop growth on N_2O emission during scaling up. Therefore, this method would eliminate the uncertainties generated by temporal and spatial variability. However, the accuracy of the TAR in the estimation of N_2O emission was limited by (1) the accuracy of the mathematical model used to represent the soil N_2O emission; (2) the accuracy and precision of the digital elevation map (DEM) that determined the accuracy of terrain attributes; and (3) the error generated by the function relating N_2O emission to terrain attributes. In this study, the modeled N_2O fluxes were validated by measurement data in Chapter 3 (Tables 3.1 and 3.2, Fig. 3.3 to 3.7). The modeled N_2O emissions represented the temporal and spatial variation in N_2O emissions in the hummocky agricultural landscape in as much as differences between modeled and measured N_2O fluxes were within the range of uncertainty of chamber measurements. The DEM was generated from intensive field data (1 measurement per 10 to 12 m^2 area) measured by a global positioning system (GPS). Therefore, the uncertainty in the TAR would mainly come from error in the function relating N_2O emission to terrain attributes. Unfortunately, the uncertainty in the TAR method could not be evaluated because of total N_2O emission could not be measured at entire field.

The MoM method derived the highest N_2O emissions (Table 4.6). The estimated annual N_2O emissions were 27% to 45% higher, although the grid cell emissions were the same as those used in the TAR method. Differing proportions of landscape positions in the four sub sites and the entire study site resulted in differences in N_2O emissions. For example, the proportion of concavities (profile curvature <= 0 associated with the higher N_2O emissions) and convexities (profile curvature > 0 associated with the lower N_2O emissions) were 54% and 46% in the four sub sites as opposed to 50% and 50% in the

entire field. Moreover, the proportion of micro-depressions associated with higher N_2O emissions and micro-mounds associated with lower N_2O emissions were 53% and 47% in the four sub sites rather than 50% and 50% in the entire field. As discussed in Chapter 3, the differences between lower and higher N_2O emissions across the landscape were 80% to 250% if soil water content was high enough for generation of N_2O. The higher proportion of locations associated with higher N_2O emissions in the sub sites resulted in a bias to higher N_2O emissions for the entire site.

4.4 Conclusions

Modeled total N_2O loss from NT in three years was 81% of that from RT and 62% of that from CT, and the emissions of N_2O from RT was 77% of that from CT. NT increased spatial variation of N_2O emissions in comparison with that from CT. Lower emissions modeled under NT were caused by reduced residue incorporation. MF reduced total N_2O emissions by 40%, and fertilizer emission factors by two-third during the three years in comparison with CF under same N input. However, MF showed higher spatial variation of N_2O emissions in the hummocky agricultural landscape. Doubled chemical fertilizer resulted in 67% increase of total N_2O emission during three years in comparison with CF. The conversion from grassland to cropping led to a increase in N_2O emissions of 15% to 87% in comparison with continuous cropping or permanent grassland. However, the spatial variation of N_2O emissions under conversion was lower. Crop rotation that included fallow and permanent hay lowered N_2O emissions and their spatial variation.

The total N_2O loss over the entire study site during three years may have been underestimated from the field chamber measurements, because the measuring frequency was too low and the peak fluxes may not have been measured (Fig. 3.3 to 3.6 in Chapter 3). IPCC methods may have overestimated the total N_2O loss for the hummocky agricultural landscape because they did not account for site and climate effects, and large temporal and spatial variation in N_2O emissions. MoM may have overestimated N_2O emissions because of the higher proportions of landscape positions associated with higher N_2O emissions in four pilot sub sites. The TAR accounted for the effects of soil heterogeneities, the redistribution of water and solute, site and management specification on N_2O emissions. Therefore, it could estimate the total N_2O emissions at the field scale

more realistically. This method estimated that total N_2O loss from the 76.6 ha hummock agricultural landscape during three years was 631 kg N_2O-N (2.7 kg N_2O-N ha^{-1} y^{-1}). However, further research is needed for this method because terrain attributes can only explain 40% to 60% of the variation of N_2O emissions.

References

Akiyama, H., Tsuruta, H., Watanabe, T., 2000. N_2O and NO emissions from soil after the application of different chemical fertilizers. Chemosphere – Global Change Sciences. 2:313–320.

Aslam, T., Choudhary, M.A., Saggar, S., 1999. Tillage impacts on soil microbial biomass C, N and P, earthworms and agronomy after two years of cropping following permanent pasture in New Zealand. Soil & Tillage Research. 51(1-2):103–111.

Aulakh, M.S. and Rennie, D.A., 1984. Nitrogen transformations with special reference to gaseous N losses from zero-tilled soils of Saskatchewan, Canada. Soil and Tillage Research. 7(1-2):157–171.

Ball, B.C., Scott, A., Parker, J.P., 1999. Field N_2O, CO_2 and CH_4 fluxes in relation to tillage compaction and soil quality in Scotland. Soil & Tillage Research. 53:29–39.

Beauchamp, E.G., 1997. Nitrous oxide emission from agricultural soils. Canadian Journal of Soil Science. 77 (2):113–123.

Bouwman, A.F., 1990. Exchange of greenhouse gases between terrestrial ecosystems and the atmosphere. In Bouwman A.F.: Soils and the greenhouse effect. John Wiley, Chichester, pp 61–127.

Bouwman, A.F., Boumans, L.J.M., Batjes, N.H., 2002. Modelling global annual N_2O and NO emissions from fertilized fields. Global Biogeochemical Cycles. 16(4):1980–1091.

Bouwman, A.F., Fung, I., Matthews, E., John, J., 1993. Global analysis of the potential for N_2O production in natural soils. Global Biogeochemical Cycles. 7:557–597.

Brown, L., Brown, S.A., Jarvis, S.C., Syed, B., Goulding, K.W.T., Phillips, V.R., Sneath, R.W., Pain, B.F., 2001. An inventory of nitrous oxide emissions from agriculture in the UK using the IPCC methodology: emission estimate, uncertainty and sensitivity analysis. Atmospheric Environment. 35(8):1439–1449.

Brumme, R. and Beese, F., 1992. Effect of liming and nitrogen fertilization on emissions of CO_2 and N_2O from a temperate forest. J. Geophys. Res. 97:12851–12858.

Cates, R.L. and Keeney, D.R., 1986. Nitrous oxide emissions from native and established prairies in southern Wisconsin. American Midland Naturalist. 117:35–42.

Cates, R.L. and Keeney, D.R., 1987. Nitrous oxide production throughout the year from fertilized and manured maize fields. J. Environ. Qual. 16:443–447.

Choudhary, M.A., Akramkhanov, A. Saggar, S., 2002. Nitrous oxide emissions from a New Zealand effects, spatial and seasonal variability. Agriculture, Ecosystems and Environement. 93:33–43.

Christensen, S., 1983. Nitrous oxide emission from soil under permanent grass: seasonal and diurnal functions as influenced by manuring and fertilization. Soil Biol. Biochem. 15(5):531–536.

Cicerone, R.J., 1989. Analysis of source and sinks of atmospheric nitrous oxide (N_2O). J. Geophs. Res. 94:18265–18271.

Cooper, G.S. and Smith, R.L., 1963. Sequence of products pormed during denitrification in some diverse western soils. Soil Science Society Proceedings. 27:659–662.

Crill, P.M., Keller, M., Weitz, A., Grauel, B., Veldkamp, E., 2000. Intensive field measurements of nitrous oxide emissions from a tropical agricultural soil. Global Biogeochemical Cycles. 14(1):85–95.

Drury, C.F., Yang, X.M., Reynolds, W.D., Tan, C.S., 2004. Influence of crop rotation and aggregate size on carbon dioxide production and denitrification. Soil & Tillage Research. 79(1):87–100.

Eichner, M.J.M, 1990. Nitrous oxide emissions from fertilized soils: Summary of available data. Journal of Environmental Quality. 19:272–280.

Flessa, H. and Beese, F., 1995. Effects of sugar beet residues on soil redox potential and nitrous oxide emissions. Soil Sci. Soc. Am. J. 59:1044–1051.

Flessa, H., Ruser, R., Schilling, R., Loftfield, N., Munch, J.C., Kaiser, E.A., Beese, F., 2002. N_2O and CH_4 fluxes in potato fields: automated measurement, management effects and temporal variation. Geoderma. 105(3-4):307–325.

Folorunso, O.A. and Rolston, D.E., 1984. Spatial variability of field measured denitrification gas fluxes. Soil Science Society of America Journal. 48:1214 –1219.

Freibauer, A., 2003. Regionalised inventory of biogenic greenhouse gas emissions from European agriculture, Europ. J. Agronomy. 19:135–160.

Frolking, S.E., Mosier, A.R., Ojima, D.S., Li, C., Parton, W.J., Potter, C.S., Priesack, E., Stenger, R., Haberbosch, C., Dorsch, P., Flessa, H., Smith, K.A., 1998. Comparison of N2O emissions from soils at three temperate agricultural Sites:simulation s of year-round measurements by four models. Nutrient Cycling in Agroecosystems. 52:77–105.

Goodroad, L.L and Keeney, D.R., 1984. Nitrous oxide production in aerobic soils under varying pH, temperature and water content. Soil Biol. Biochem. 16(1):39–43.

Grant, R.F., Armani, M., Heaney, D.J., Wright, R., Zhang, M., 2004. Mathematical modeling of phosphorus losses from land application of hog and cattle manure. Journal of Environmental Quality. 33(1):210–231.

Grant, R.F., 2004. Modeling topographic effects on net ecosystem productivity of boreal black spruce forests. Tree physiology. 24(1):1–18.

Grant, R.F., 1999. Simulation of methanotrophy in the mathematical model ecosys. Soil Biology & Biochemistry. 31(2):287–297.

Grant, R.F., 1998. Simulation of methanotrophy in the mathematical model ecosys. Soil Biology & Biochemistry. 30(7):883–896.

Grant, R.F., Juma, N.G., Robertson, J.A., Izaurralde, R.C., McGill, W.B., 2001. Long-Term Changes in Soil Carbon under Different Fertilizer, Manure, and Rotation: Testing the Mathematical Model *ecosys* with Data from the Breton Plots. Soil Sci. Soc. Am. J. 65:205–214

Grant, R. F. and Pattey, E., 2003. Modelling variability in N_2O emissions from fertilized agricultural fields. Soil Biology and Biochemistry. 35(2):225–243.

Grant, R.F. and Pattey, E., 1999. Mathematical modeling of nitrous oxide emissions from an agricultural field during spring thaw. Global Biogeochemical Cycles. 13(2):679–694.

Guzha, A.C., 2004. Effects of tillage on soil microrelief, surface depression storage and soil water storage. Soil and Tillage Research. 76(2):105–114.

Harrison, R. and Webb, J., 2001. A review of the effect of N fertilizer type on gaseous emissions. Advances in Agronomy. 73:65–108.

Hiroko, A. and Haruo, T., 2003. Effect of organic matter application on N_2O, NO, and NO_2 fluxes from an Andisol field. Global Biogeochem. Cycles. 17(4):1100–1116.

Intergovernmental Panel on Climate Change (IPCC), Climate Change 2001: The Scientific Basis: Contribution of Working Group I to the Third Assessment Report of the Intergovernmental Panel on Climate Change, 881 pp., Cambridge Univ. Press, New York, 2001.

Intergovernmental Panel on Climate Change (IPCC), Organization for Economic Cooperation and Development (OECD) and International Energy Agency (IEA), Revised 1996 IPCC Guidelines for National Greenhouse Gas Inventories, Organ. for Econ. Coop. Dev., Paris, 1997.

Jacinthe, P.A. and Dick, W.A., 1997. Soil management and nitrous oxide emissions from cultivated fields in southern Ohio. Soil and Tillage Research. 41(3-4):221–235.

Kaiser, E.A. and Ruser, R., 2000. Nitrouxs oxide emissions from arable soils in Germany – an evaluation of six long-term field experiments. Journal of Plant Nutrient and Soil Science (J. Plant Nutr. Soil Sci.), 163:249–260.

Kaiser, E.A., Kohrs, K., Kucke, M., Schnug, E., Heinemeyer, O., Munch, J.C., 1998. Nitrous oxide release from arable soil: importance of N-fertilizztion, crop and temporal variation. Soil Biology and Biochemistry, 30(12):1553–1563.

Kaiser, E.A., Munch, J.C., Heinemeyer, O., 1996. Importance of soil cover box area for the determination of N2O emissions from arable soils. Plant and Soil. 181:185–192.

Laville, P., Jambert, C., Cellier P., Delmas, R., 1999. Nitrous oxide fluxes from a fertilised maize crop using micrometeorological and chamber methods, Agricultural and Forest Meteorology, 96(1-3):19–38.

Lemke, R.L., Izaurralde, R.C., Nyborg, M., Solberg, E.D., 1999. Tillage and N source influnce soil-emitted nitrous oxide in the Alberta Parkland region. Canadian Journal of Soil Science. 79(1):15–24.

Li, C.S., Zhuang, Y.H., Cao, M.Q., Crill, P., Dai, Z.H., Frolking, S., Moore III, B., Salas, W., Song, W.Z., Wang, X.K., 2001. Comparing a process-based agro-ecosystem model to the IPCC methodology for developing a national inventory of N_2O emissions from arable lands in China. Nutrient Cycling in Agroecosystems. 60:159–175.

Lim, B., Boileau, P., Bonduki, Y., van Amstel, A.R., Janssen, L.H.J.M., Olivier, J.G.J., Kroeze, C., 1999. Improving the quality of national greenhouse gas inventories. Environmental Science & Policy. 2(3):335–346.

Li, T., Grant, R.F., Flanagan, L.B., 2004. Climate impact on net ecosystem productivity of a semi-arid natural grassland: modeling and measurement. Agricultural and Forest Meteorology. 126:99–116.

Matson, P.A. and Viousek, P.M., 1990. Ecosystem approach to a global nitrous oxide budget. BioSci. 40:667–672.

Minami, K., 1997. Atmospheric methane and nitrous oxide: sources, sinks and strategies for reducing agricutltural emissions. Nutrient Cysling in Agroecosystems. 49(1-3): 203–211.

Mogge, B., Kaiser, E.A., Munch, J.C., 1999. Nitrous oxide emissions and denitrification N-losses from agricultural soils in the Bornhoved Lake region: influence of organic fertilizers and land-use. Soil Boilogy and Biochemistry. 31:1245–1252.

Mosier, A., Kroeze, C., Nevison, C., Oenema, O., Seitzinger, S., van Cleemput, O., 1998. Closing the global N_2O buget: nitrous oxide emissions through the agricultural nitrogen cycle – OECD/IPCC/IEP phase II development of IPCC guidelines for national greenhouse gas inventory methodology. Nutrient Cycling in Agroecosystems. 52(2-3):225–248.

Mosier, A.R, Parton, W.J., Valentine, D.W., Ojima, D.S., Schimel, D.S., Heinemeyer, O., 1997. CH4 and N2O fluxes in the Colorado shortgrass steppe. 2. Long-term impact of land use change. Global Biogeochemical Cycles. 11:29–42.

Mosier, A.R, Parton, W.J., Valentine, D.W., Ojima, D.S., Schimel, D.S., Delgado, J.A., 1996. CH4 and N2O fluxes in the Colorado shortgrass steppe. 1. Impact of landscape and nitrogen addition. Global Biogeochemical Cycles. 10:387–399.

Myrold, D.D., 1988. Denitrification in rye-grass and winter wheat cropping systems of western Oregon. Soil Science Society of America Journal. 52:412–416.

Olsen, K., Wellisch, M., Bioleau, P., Blain, D., et al., 2003. Canada's greenhouse gas inventory (1990 – 2001). ISBN 0-662-35106-1, Environment Canada.

Paul, J.W. and Zebarth, B.J., 1997. Denitrification and nitrate leaching during the fall and winter following dairy cattle slurry application. Can. J. Soil. Sci. 77:231–240.

Qian, J.H., Doran, J.W., Weier, K.L., Mosier, A.R., Peterson, T.A., Power, J.F., 1997. Soil denitrification and nitrous oxide losses under corn irrigated with high-nitrate groundwater. J. Environ. Qual. 26(2):348–360.

Röver, M., Heinemeyer, O., Munch, J.C., Kaiser, E.A., 1999. Spatial heterogeneity within the plough layer: high variability of N_2O emission rates. Soil Biology and Biochemistry. 31(2):167–173.

Scott, A., Crichton, I., Ball, B.C., 1999. Long-term monitoring of soil gas fluxes with closed chambers using automated and manual systems. J. Environ. Qual. 28:1637–1643.

Scott, M.J., Sands, R.D., Rosenberg, N.J., Izaurralde, R.C., 2002. Future N_2O from US agriculture: projecting effects of changing land use, agricultural technology, and climate on N_2O emissions. Global Environmental Change. 12(2):105–115.

Sehy, U., Ruser, R., Munch, J.C, 2003. Nitrous oxide fluxes from maize fields: relationship to yield, site-specific fertilization, and soil conditions. Agriculture, Ecosystems & Environment. 99(1-3):97–111.

Smith, K.A., Thomson, P.E., Clayton, H., McTaggart, I.P., Conen, F., 1998. Effects of temperature, water content and nitrogen fertilization on emissions of nitrous oxide by soils. Atmos. Environ. 32:3301–3309.

Smith, C.J., Wright, M.F., Patrick Jr., W.H., 1983. The effect of soil redox potential and pH on the reduction and production of nitrous oxide. J. Environ. Qual. 12:186–188.

Sozanska, M., Skiba, U., Metcalfe, S., 2002. Developing an inventory of N_2O emissions from British soils. Atmospheric Environment. 36(6):987–998.

Webster, M.D., Babiker, M., Mayer, M., Reilly, J.M., Harnisch, J., Hyman, R., Sarofim M.C., Wang, C., 2002. Uncertainty in emissions projections for climate models. Atmospheric Environment. 36(22):3659–3670.

Williams, D.Li., Ineson, P., Coward, P.A., 1999. Temporal variations in nitrous oxide fluxes from urine-affected grassland. Soil Biology and Biochemistry. 31(5):1999, 779 – 788.

Appendix 4.1: Equation for estimates of N_2O emissions by IPCC method

Variables:

E_{N_2O} : Total N_2O emission from crop land (kg N ha^{-1} y^{-1}).

CF_{N_2O} : The emission from chemical fertilizer (kg N ha^{-1} y^{-1}).

CR_{N_2O} : Total emission from crop residue (kg N ha^{-1} y^{-1}).

SF_t: fertilizer application (kg N ha^{-1} y^{-1}).

F_{ASN}: the fraction of chemical nitrogen fertilizer available for nitrification and denitrification process.

$F_{racGASN}$: the fraction of chemical nitrogen fertilizer applied to soil that volatilizes as NH_3 and NO_x (used 0.1 kg (NH_3-N + NO_x-N) kg^{-1} N, IPCC, 1997).

F_A: the fraction of nitrogen available for nitrification/denitrification processes due to animal waste applied as fertilizers.

$EF1$: the emission factors for fraction of nitrogen input (0.0125 kg N_2O-N kg^{-1} N, IPCC, 1997).

C_{TCR}: Total crop production (kg ha^{-1}).

DMF_T: Specific dry matter fraction (0.8).

F_N: Fraction of nitrogen in dry mass (0.3 kg N kg^{-1} dry mass. IPCC, 1997).

F_R: Fraction of crop mass removed from fields (0.45, Canada's Greenhouse Gases Inventory, 2003).

Equations:

$$E_{N_2O} = CF_{N_2O} + CR_{N_2O} \quad \text{(A4.1)}$$

$$CF_{N_2O} = SF_t \times F_{ASN} EF1 \quad \text{(A4.2)}$$

$$F_{ASN} = 1 - F_{racGASN} \quad \text{(A4.3)}$$

$$CR_{N_2O} = 2[C_{TCR} \times F_N \times DMF_T \times (1 - F_R) \times EF1] \quad \text{(A4.4)}$$

Appendix 4.2: The annual N_2O emissions in the entire study site estimated by the regression function of terrain attributes and modeled N_2O emissions of four sub sites.

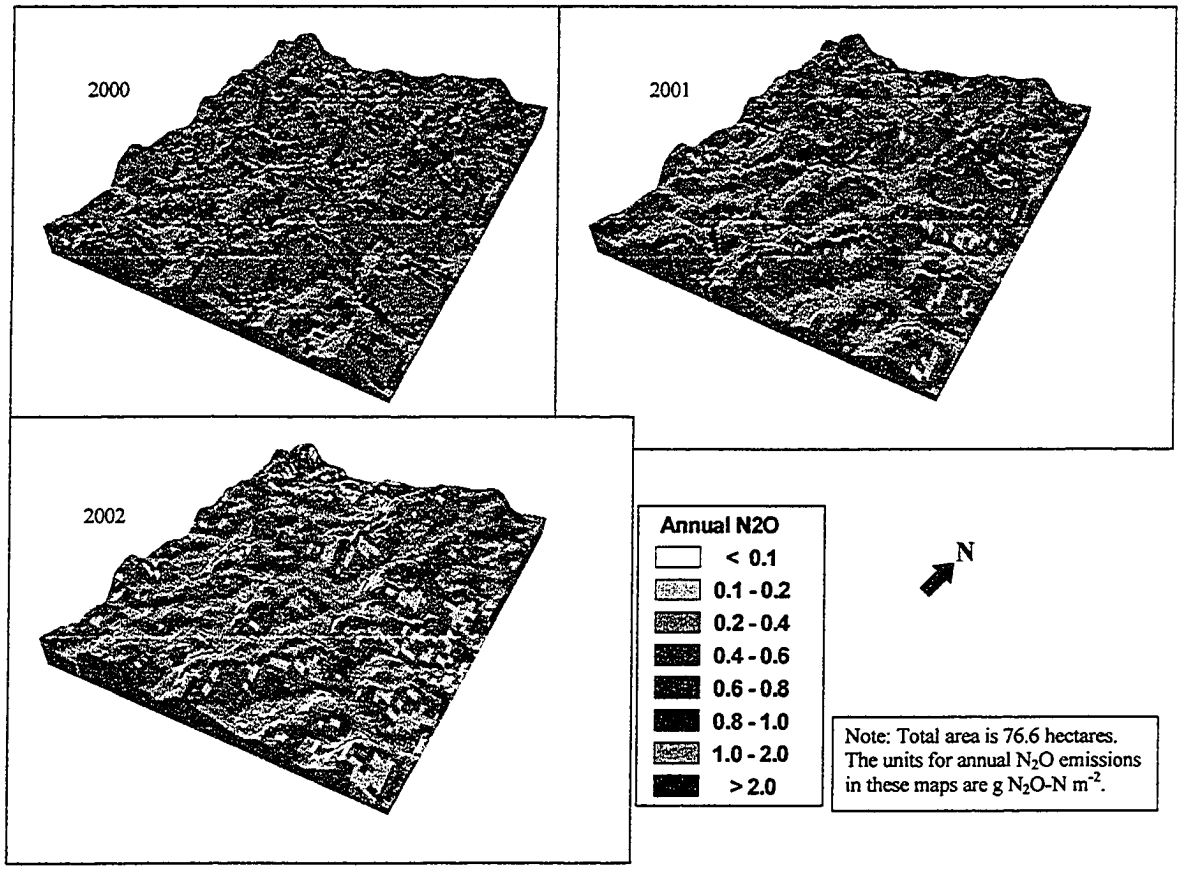

Chapter 5: Climate Impact on Net Ecosystem Productivity of a Semi-arid Natural Grassland: Modeling and Measurement

5.1 Introduction

Grasslands are important primary producers, and store substantial amounts of carbon. Thuille et al. (2000) used radiocarbon dating to show that grassland after deforestation in the Southern Alps, Italy, gained an average of 15 g C m^{-2} y^{-1} between 1740 and 1935. Anderson (1977) reported that dry grassland in a cool temperate steppe of southern Saskatchewan gained 28 ± 4 g C m^{-2} y^{-1} organic carbon. The impact of climate change on these gains is of concern because of the large areas occupied by grasslands. Melillo et al. (1996) used CENTURY to model climate perturbations for more than 31 grassland sites representing more than 7 ecoregions of the world in which annual precipitation ranged from 220 mm to over 1500 mm. Their results showed that global grasslands would lose 1 to 2×10^{15} g C after 50 years of climate change.

Rising atmospheric CO_2 concentration (C_a) and temperature hypothesized during climate change exert interactive effects on net ecosystem productivity (NEP). Elevated C_a often stimulates gross primary productivity (GPP), and improves the efficiency of plant water use, causing substantial increases of NEP (Hu et al., 1999; Cao and Woodward, 1998; Thornley and Cannell, 1997). On the other hand, rising air temperature can reduce NEP (Coughenour and Chen, 1997) by raising heterotrophic respiration (R_h) more than net primary productivity (NPP) (Thornley and Cannell, 1997), especially if water deficits are aggravated (Arneth et al., 1998). The magnitude and direction of changes in grassland NEP during climate change will be determined by the balance between positive and negative impacts of changes in C_a, temperature and water status.

The impacts of climate on CO_2 and energy exchange of ecosystems including grasslands is currently studied at a number of locations using the eddy covariance technique as part of international networks, for example Euroflux and FLUXNET (Aubinet et al., 2000, Running et al., 1999). Because eddy covariance captures these impacts on the diurnal time scales at which they occur, this technique has become an important means of measuring seasonal and annual variation in ecosystem carbon

budgets (Flanagan et al., 2002; Saigusa et al., 1998), and of measuring environmental and biological controls on CO_2 exchange processes (Valentini et al., 2000; Baldocchi and Meyers 1998).

However the eddy covariance technique has some CO_2 and energy flux loss (Massman, 2000) caused by separation of the sampling tubes for CO_2 and water vapour measurements, loss of turbulent structure during gas flow in sampling tubes, and limitation in the response time of sensors and data acquisition hardware to changes in vertical wind speed measured by the sonic anemometer (Moncrieff et al., 2000). This loss causes incomplete retrieval of input energy as sensible (H) and latent (LE) heat. In inter-comparisons of different eddy covariance systems over grassland, Twine et al. (2000) observed a systematic lack of closure in surface energy budgets between 10% and 30%, and standard deviation (SD) of latent heat fluxes (LE) between 17 W m^{-2} and 48 W m^{-2}. They also observed that CO_2 fluxes were underestimated by the same factor as eddy covariance LE measurements when energy balance closure was not achieved. Although transfer functions could be used to account for these losses, underestimation of CO_2 and energy flux occurs, particularly of nighttime effluxes. Flanagan (2002) showed that LE plus H measured by eddy covariance over a grassland accounted for 87% to 90% of net radiation minus soil heat flux.

In spite of these losses, CO_2 and energy fluxes measured by eddy covariance are extremely important in testing mathematical models of ecosystem CO_2 and energy exchange. These models can in turn provide estimates of these fluxes when measured values are missing or inaccurate, and also under future climate scenarios. **Ecosys** is one such model used to estimate energy, CO_2, N_2O, CH_4, and nutrient exchange under current or projected climates (Grant, 1999, 1997, 1995a, 1995b; Grant et al., 2003, 2001a, 2001b, 2000, 1999, 1998). This model uses several basic hypotheses described below to simulate effects of CO_2, temperature and water stress on carbon and energy exchange of terrestrial ecosystems (Grant et al. 1995a, 1995b, 1998, 1999, 2001c). By testing these effects with eddy covariance measurements recorded during soil drying, we can obtain a degree of constraint to hypothesis testing not accomplished in earlier modelling studies.

The objectives of this study are to (1) test hypotheses of how current climate affects ecosystem energy and CO_2 exchange over a semiarid grassland near Lethbridge, Alberta,

Canada using eddy covariance measurements, and (2) predict how CO_2 exchange of this grassland will be affected by projections of climate change during the next 100 years.

5.2 Methods

5.2.1 Model Description

Ecosys is a general model of terrestrial ecosystems, which can simulate the dynamics of carbon, nitrogen, phosphorus, heat and water, and the effects of management practices such as tillage methods, fertilizer and irrigation on these dynamics (Grant et al., 2001b). Hypotheses and algorithms of *ecosys* relevant to the objectives of this study are described below with reference to equations published in earlier articles.

5.2.1.1 Energy exchange

First-order closures of energy balances are used to calculate hourly energy exchange between the atmosphere and grassland canopy, residue, soil and snow surfaces (Grant, 2001, Eqs. A1-A16) (Grant et al. 1999a, 1999b, 1995a, 1995b, 1993a, 1992). Surface energy exchanges are coupled to subsurface conductive, convective and latent heat transfers using a forward differencing scheme with heat capacities and thermal conductivities calculated from De Vries (1963) (Grant, 2001, Eqs. A18, A26, A27). If intercepted precipitation is present on leaf or stem surfaces, latent heat flux is calculated from evaporation caused by canopy-atmosphere vapor density gradients and aerodynamic conductance (Grant, 2001, Eq. A4). If intercepted precipitation is not present, latent heat flux is calculated from transpiration which is also controlled by stomatal conductance (Grant, 2001, Eqs. A3, A13, A14).

5.2.1.2 Water Relations

Soil-plant and plant-atmosphere water transfers are coupled through an hourly two-stage convergence solution for the transfer of water and heat through a multi-layered, multi-population soil-root-canopy-atmosphere system. The first stage of this solution requires convergence to a canopy temperature for each plant population at which the first-order closure of the canopy energy balance is achieved. In the second stage, a canopy water potential is sought at which the difference between canopy transpiration

from the energy balance and total water uptake from all rooted soil layers (Grant, 2001, Eqs. B9, B10) equals the difference between canopy water contents from the previous and current hours. The canopy water potential determines transpiration by setting the osmotic potential (Grant, 2001, Eq. B2) and hence turgor potential (Grant, 2001, Eq. B1) which, with leaf carboxylation rate described under ***CO_2 fixation*** below, determines stomatal conductance. Canopy and root water potentials (Grant, 2001, Eq. B15) also determine water uptake in each rooted soil layer by setting the soil-root-canopy potential gradients (Grant, 2001, Eqs. B9, B10) used to calculate total water uptake (Grant et al., 1999). Changes in canopy water potential also determine changes in canopy water content according to plant water potential–water content relationships. Soil-root resistances are the sum of radial hydraulic resistances to water uptake from each soil layer (Grant, 2001, Eq. B11), and of radial + axial hydraulic resistances of primary and secondary root systems (Grant, 2001, Eqs. B12, B13, B14). Root lengths and surface areas used in calculating these resistances are provided by a root system submodel driven by shoot-root C transfers and by root C oxidation and growth (Grant, 1993a, 1993b, 1998; Grant and Robertson, 1997).

5.2.1.3 CO_2 fixation

NEP is the difference between gross CO_2 fixation (GPP) and autotrophic (R_a) plus heterotrophic respiration. CO_2 fixation is calculated in *ecosys* from coupled algorithms for carboxylation and diffusion (Grant, 2001, Eq. C10). Carboxylation rates are calculated for each leaf surface of multispecific plant canopies as the lesser (Grant, 2001, Eqs. C1, C6, C10) of dark and light (Grant, 2001, Eqs. C2, C3, C5, C7, C8, C9) reaction rates according to Farquhar et al. (1980) (Grant et al., 1999). These rates are driven by absorbed irradiance, canopy temperature and C_a. Maximum dark or light reaction rates used in these functions are determined by specific activities and surficial concentrations of rubisco (Grant, 2001, Eq. C3) or chlorophyll (Grant, 2001, Eq. C8) respectively. These activities and concentrations are determined by N and P uptake and assimilation during leaf growth as described in Grant et al. (2001c, 1989).

CO_2 diffusion rates are calculated for each leaf surface by first calculating the leaf stomatal conductance required to maintain a set CO_2 concentration in leaf (C_i) to C_a ratio

according to the leaf carboxylation rate and the CO_2 concentration difference between the canopy atmosphere and the mesophyll at zero canopy water potential (Grant, 2001, Eq. C11). This conductance is then reduced according to an exponential function of canopy turgor (Grant, 2001, Eq. C13) generated from the convergence solution for canopy water potential described above. A convergence solution is then sought for C_i and its aqueous equivalent at which diffusion equals carboxylation (Grant, 2001, Eq. C14).

5.2.1.4 Autotrophic respiration

Total R_a is the sum of maintenance, growth and senescence (if any) respiration. R_a is driven by the oxidation of non-structural C products of GPP in each tiller and root layer as determined by the size of the non-structural C pool, temperature, and O_2 uptake (roots) (Grant et al., 1999, Eq. A26). R_a is divided into maintenance and growth components. Maintenance respiration is calculated from the N content of each tiller and root layer (Grant et al., 1999, Eq. A27), and an exponential function of canopy or soil temperature. If oxidation of non-structural C is less than maintenance respiration, the difference is made up from respiration of remobilizable C (assumed to be protein C) in leaves and supporting organs (Grant et al., 1999, Eq. A29), causing senescence and litterfall of associated non-remobilizable C. Non-structural C oxidized in excess of maintenance respiration requirements is used as growth respiration (Grant et al., 1999, Eq. A28) that drives the formation of new phytomass.

5.2.1.5 Heterotrophic respiration

5.2.1.5.1 Decomposition

Soil organic matter in *ecosys* is resolved into four substrate-microbe complexes (plant residue, animal manure, particulate organic matter and non-particulate organic matter) within each of which C, N and P may move among five organic states: solid substrate, absorbed substrate, soluble hydrolysis products, microbial communities, and microbial residues (Grant, 1999). Each organic state in each complex is resolved into structural components of differing vulnerability to hydrolysis and further resolved into elemental fractions C, N and P within each structural component. Microbial communities are also resolved into functional type including obligate aerobes, facultative anaerobes

(denitrifiers), obligate anaerobes (fermenters), methanogens, diazotrophs (N fixers) and autotrophs (nitrifiers and CH_4 oxidizers).

Litterfall described in ***Autotrophic Respiration*** above is added to the plant residue complex and partitioned into carbohydrate, protein, cellulose and lignin components. Rates of component hydrolysis are the product of the active biomass and specific activity of each microbial functional type within each complex (Grant, 2001, Eq. E1) (Grant and Rochette, 1994; Grant et al., 1993b), and by temperatures of surface residue and a spatially resolved soil profile (Grant *et al.*, 1998; Grant, 1997; Grant and Rochette, 1994). Biomass growth of each functional type is driven by its growth respiration described in *Microbial Growth* below. Specific microbial activity is determined by substrate-microbe density relationships affected by soil water content (Grant, 2001, Eq. E3) (Grant and Rochette, 1994; Grant et al., 1993a). A fraction of the hydrolysis products from lignin (*j=lignin* in Grant, 2001, Eqs. E1, E3) are coupled with those from protein and carbohydrate according to the stoichiometry proposed by Schulten and Schnitzer (1997), and the resulting compound is transferred to the particulate organic matter complex. Rates of particulate organic matter formation are thus determined by substrate lignin content and heterotrophic microbial activity. All remaining hydrolysis products are added to soluble pools which drive microbial respiration and growth.

5.2.1.5.2 Microbial growth

The concentration of the soluble hydrolysis products in *Decomposition* above determines rates of C oxidation by each heterotrophic population in each complex (Grant, 2001, Eq. E11), the total of which drives CO_2 emission from the soil surface. This oxidation is coupled to the reduction of O_2 by all heterotrophic aerobic populations (Grant, 2001, Eq. E13) (Grant et al., 1993a, 1993b; Grant and Rochette, 1994), to the sequential reduction of NO_3^-, NO_2^- and N_2O by heterotrophic denitrifiers (Grant et al., 1993c, 1993d) and to the reduction of organic C by fermenters and of their acetate product by heterotrophic methanogens (Grant, 1999). Some of the C oxidation is required for maintenance respiration as determined from microbial N and soil temperature (Grant, 2001, Eq. E18), and the remainder is used for growth respiration that drives biosynthesis (Grant, 2001, Eq. E20) (Grant and Rochette, 1994). The energy yields of these oxidation-

reduction reactions vs. energy requirements for biosynthesis determine microbial growth and hence active biomass of each heterotrophic functional type from which its decomposer activity is calculated as described in *Decomposition* above. In addition, autotrophic nitrifiers conduct NH_4^+ and NO_2^- oxidation and N_2O evolution (Grant, 1995), autotrophic methanogens conduct H_2 oxidation, and autotrophic methanotrophs conduct CH_4 oxidation (Grant, 1999), the energy yields from which determine autotrophic growth and hence biomass and activity. Microbial populations in the model seek to maintain steady-state ratios of biomass C:N:P by mineralizing or immobilizing NH_4^+, NO_3^- and $H_2PO_4^-$, thereby regulating solution concentrations that drive N and P uptake by roots and mycorrhizae. Microbial populations undergo first order decomposition, products of which are partitioned between microbial residues within the same substrate-microbe complex, and the solid substrate of the non-particulate organic matter complex according to soil clay content (Grant *et al.*, 1993a,b). Rates of non-particulate organic matter formation are thus determined by rates of microbial decay and by soil clay content.

5.2.2 Field Experiment

5.2.2.1 Description of study site

The data used to validate *ecosys* were from a research project established in June 1998 on a prairie grassland site at Lethbridge as part of the Ameriflux network (Flanagan et al., 2002; Running et al 1999). The study site was approximately 1.5 km west of Lethbridge, Alberta, Canada (Latitude: N49.43°, Longitude: W112.56°, Altitude: 951 m), on 64 ha of an uncultivated, mixed grass prairie (slopes equal to or less than 2%). The soils were Orthic Dark-Brown Chernozems with a clay loam A horizon (0.09 m, 29% sand, 40% silt, and 31% clay) and a clay B horizon (0.16 m, 27% sand, 30% silt, and 43% clay). Mean daily temperature for January and July were –8.6°C and 18°C, respectively. The long-term mean annual precipitation (1908 to 1999) was 401.5 mm. There was often a single peak in precipitation early in the summer followed by moderate to severe drought. Average pan evaporation (Class A) normally exceeded the average precipitation by at least 200% and often 300% in the summer months.

5.2.2.2 Measurement energy and CO_2 fluxes

The eddy covariance technique was used to measure the fluxes of water vapor, CO_2 and sensible heat on a continuous basis from June 19, 1998 to December 31, 2000. A three dimensional ultrasonic anemometer (Solent 1012, Gill Instruments Ltd., Lymington, England) was mounted on a one meter boom placed on top of a 6 meter tower and oriented in the prevalent wind direction (west) to measure wind speed, direction and air temperature. Changes in CO_2 and water vapor concentration were measured with a closed path, fast response infrared gas analyzer (IRGA) (LI-6262, LI-COR Inc., Lincoln, Nebraska) housed in an insulated instrument hut. Air for CO_2 and water vapor measurements was drawn at 8 L min^{-1} through 15 m of tubing (3 mm inner diameter Bev-A-Line IV Tubing, LABCOR, Concord, Ontario) by a diaphragm pump (Capex V2X 12 VDC, Charles Austen Pumps Ltd., Surrey, England, or KNF UN828 KNI, KNF Neuberger Inc, Trenton, New Jersey) placed downstream from the IRGA. Fluxes of water vapor, CO_2, and sensible heat were computed using the University of Edinburgh EdiSol software (Moncrieff et al., 1997). Transfer functions were used to correct for a high frequency component of the flux that was missing from the measurements (Moncrieff et al., 1997).

Along with the eddy flux instrumentation, a weather station was established to provide meteorological data. Net radiation and photosynthetic photon flux density (PPFD, 400-700 nm wave band) were measured by a net radiometer (REBS Q*7.1, Radiation Energy Balance System, Seattle, Washington) and a LI-COR Quantum Sensor (LI-190SA, LI-COR, Lincoln, Nebraska) mounted on a nearby 3 m tower. Relative humidity and air temperature were measured using a shielded thermistor and a capacitance humidity probe (207 Temperature and Relative Humidity Probe, Campbell Scientific Ltd., Edmonton, Alberta) placed 2 meters above the ground. Mean soil heat flux was calculated from two soil heat flux transducers (REBS HFT-3.1, Radiation Energy Balance System, Seattle, Washington), placed about 2 cm below the soil surface. Total precipitation was recorded in 15-minute intervals by a tipping bucket rain gauge (TE525, Texas Electronics, Inc., Dallas, Texas) positioned 1 meter above ground approximately 6 m from the eddy covariance tower. All data other than precipitation were recorded as half-hourly averages on dataloggers (CR10 and CR10X, Campbell Scientific Ltd., Edmonton, Alberta).

Because we were not equipped to measure precipitation in the form of snow, precipitation data from the Lethbridge Research Centre (LRC) of Agriculture and Agri-Food Canada about 10 km away were used from October 1 to April 30. Data from the RLC were also used when meteorological data from the site were missing.

Soil samples (0 to 10 cm depth for 1998 and 0 to 15 cm for 1999 and 2000) were collected for water content measurements on a weekly basis using a soil corer. Six replicates were selected using a stratified random method. The known volume of soil was weighed, dried at 105°C for 24 hours, and then re-weighed. The gravimetric moisture content was converted into volumetric measurement using the bulk density of the soil

5.2.3 Model Experiment

5.2.3.1 Testing CO_2 and energy fluxes under current climate

Hourly climate data from 1990 to 1997 and during non-measurement periods from 1998 to 2000 were obtained from the LRC about 10 km away from the study site. These data were combined with those recorded at the study site during eddy covariance measurements to construct continuous hourly (1990-1997) and half-hourly (1998-2000) meteorological files of incoming shortwave radiation, air temperature, relative humidity, wind speed and precipitation used to simulate surface boundary conditions in *ecosys*. The model was initialized with the physical properties of the Orthic Dark-Brown Chernozem (Table 5.1). Soil texture, pH and organic carbon and nitrogen contents of A and B horizons were measured at the field site, and those of deeper horizons up to 120 cm were extracted from Agricultural Region of Alberta Soil Inventory Database (AGRASID, Nikiforuk et al., 1998). Field capacity (θ_{FC}), permanent wilting point (θ_{WP}), bulk density (ρ_b) and saturated hydraulic conductivity (K_{sat}) were calculated from soil texture according to Saxton et al. (1986). The model was also initialized with the biological properties of grass (Grant et al., 2001b) which was seeded onto bare soil during the first year of the model run. The model was then run for 110 years by repeating the climate record from 1991 to 2000 eleven times. Average annual precipitation during this run was 94% of the mean annual value recorded from 1908 to 1999 (375.9 mm vs. 401.5 mm).

Table 5.1: Properties of the Orthic Brown Chernozem at Lethbridge, Alberta. Soil texture, organic matter content and pH of A (0 to 9 cm) and B horizons (9 to 25 cm) were measured at the field site, and those of lower layers were extracted from AGRASID (http://www.agric.gov.ab.ca/agdex/000/agrasid.html). θ_{FC}, θ_{WP}, ρ_b and K_{sat} were calculated from soil texture (Saxton et al., 1986).

Depth of layers (m)	0.01	0.03	0.05	0.11	0.21	0.3	0.4	0.5	0.7	0.9	1.2
ρ_b (Mg m^{-3})	1.24	1.24	1.24	1.24	1.27	1.27	1.32	1.3	1.37	1.4	1.4
θ_{FC} (m^3 m^{-3})	0.32	0.32	0.32	0.32	0.38	0.38	0.32	0.35	0.28	0.27	0.27
θ_{WP} (m^3 m^{-3})	0.17	0.17	0.17	0.17	0.24	0.24	0.19	0.2	0.15	0.13	0.13
K_{sat} (mm h^{-1})	3.8	3.8	3.8	3.8	2.0	2.0	2.9	2.9	5.4	7.0	7.0
Sand content (g kg^{-1})	288	288	288	288	274	274	330	260	385	410	410
Silt content (g kg^{-1})	400	400	400	400	296	296	333	383	365	370	370
pH	7.1	7.1	7.1	7.1	7.3	7.3	7.4	7.4	7.6	7.5	7.5
Organic C (g C kg^{-1})	61.1	47.2	31.1	19.2	14.4	3.2	3.0	2.1	1.4	0.7	0
Organic N (g N Mg^{-1})	4800	3800	2600	1600	1100	287	275	187	125	63	0

During the 78th, 79th and 80th year of the 110 year model run, in which climate data from 1998, 1999 and 2000 respectively were used, CO_2 and energy fluxes calculated by the model were compared with those measured by eddy covariance during 1998, 1999 and 2000. Diurnal variation in modeled vs. measured fluxes was compared during two 5 day periods in each of the three years, the first in late June (Day 177-182) under cooler, wetter conditions, and the second in mid-August (Day 225-230) under warmer, drier conditions. Agreement between modeled vs. measured fluxes was examined by regressing modeled hourly fluxes on hourly averages of measured half-hourly fluxes for each yearly dataset. Daily and annual totals of CO_2 exchange in the model were then compared with those estimated from measured CO_2 fluxes. These model tests were intended to establish confidence in model projections of NEP during a long-term climate change scenario.

5.2.3.2 Predicting changes in NEP during climate change

A climate change scenario was developed from the results of CRCM-II (Canadian Regional Climate Model) under the IS92a emissions scenario in which C_a was assumed to double in 100 years (Table 5.2). This rise in C_a caused rises in seasonal temperatures that varied from 1.5°C (October to December) to 4.1°C (January to March), and changes in seasonal precipitation that varied from –17.2% (July to September) to +22.7% (April to June). Relative humidity did not change, and wind speed decreased by 9.5% only

during October to December but otherwise did not change. Because changes in precipitation and humidity were predicted with less confidence than were those in air temperature, a second climate change scenario was run with the same rises in C_a and temperature but without changes in precipitation and humidity. Changes were implemented hourly to create gradual climate change during ten cycles of 1991-2000 climate data in a 110 year model run. Results for NPP and NEP of wet and dry years and for long-term soil C storage were compared with those modeled during 110 years under unchanged 1991 to 2000 climate. The possibility that climate-induced changes in NEP were an artifact of model parameterization was tested by conducting a Monte Carlo simulation of variation in NEP caused by variation in selected key parameters that regulate soil-plant-atmosphere water transfer in the model.

Table 5.2: The climate change scenario developed from results of the Canadian Regional Climate Model (CRCM-II) for the Lethbridge area.

Period	Δ Maximum temperature ($^oC\ y^{-1}$)	Δ Minimum temperature ($^oC\ y^{-1}$)	Δ Precipitation (y^{-1})	Δ Wind speed (y^{-1})	Δ CO_2 concentration (y^{-1})
Jan.—March	0.039	0.041	1.000	1.000	1.007
April—June	0.032	0.031	1.002	1.000	1.007
July—Sep.	0.031	0.038	0.998	1.000	1.007
Oct.—Dec.	0.028	0.015	1.001	0.999	1.007

5.3 Results

5.3.1 Soil Water Content

Declining annual precipitation from 1998 (466 mm) through 1999 (363 mm) to 2000 (276 mm) caused the onset of soil drying (soil water content θ declined to θ_{WP}) in the both the model and the field to advance from the end of August in 1998 to the end of July in 1999 and to the end of June in 2000 (Fig. 5.1). Lower θ modeled during spring 1998 was caused by the appearance of only 72 mm precipitation in the weather data between mid-April and mid-June which was insufficient to maintain higher θ in the model.

5.3.2 Diurnal Variation in Energy and CO_2 Fluxes

5.3.2.1 Energy Fluxes

The model accurately simulated the change in energy balance from H being similar to LE during June and August 1998 and June 1999 (Fig. 5.2) when θ was higher than θ_{WP} (0 to 15 cm soil layer) (Fig. 5.1), to H being larger than LE during August 1999 and June 2000 when θ was close to θ_{WP}, and to H being much larger than LE during August 2000 when θ was lower than θ_{WP}.

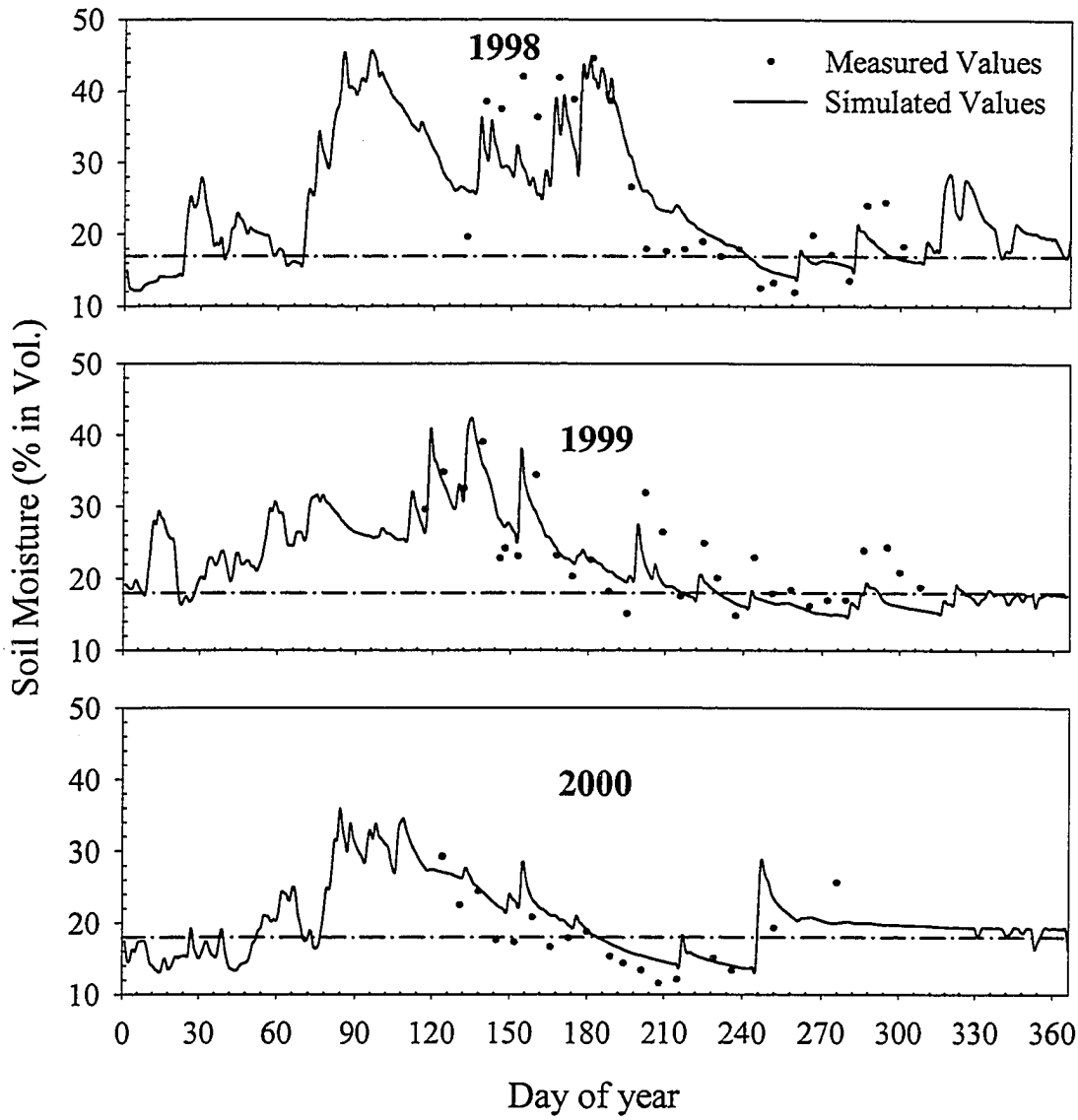

Figure 5.1: Measured (symbol) and modelled (line) soil moistures. Dash dot line indicates the permanent wilting point (17 % in vol. in 1998, 18% in 1999 and 2000). The depths for comparing measured and simulated data were 10 cm in 1998, 15 cm in 1999 and 2000.

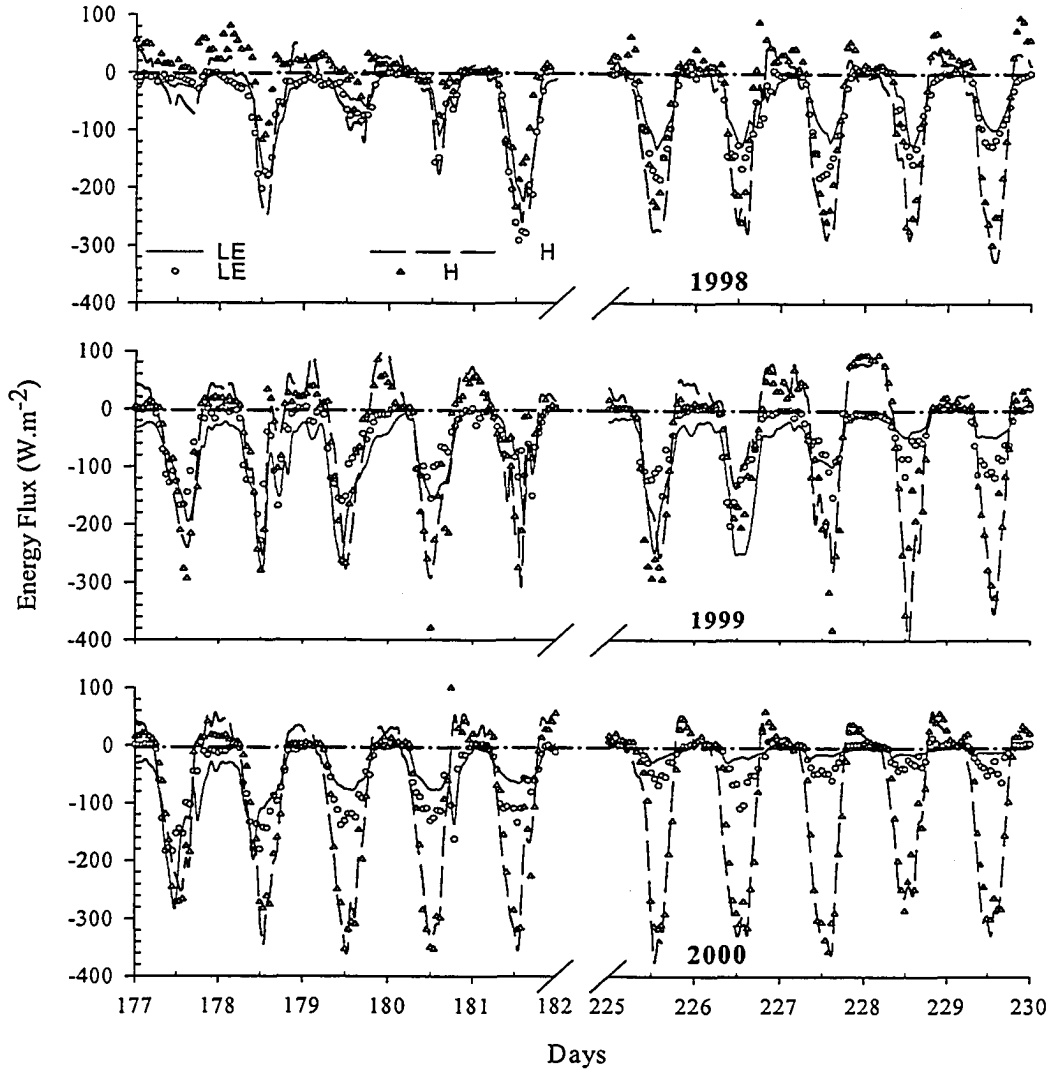

Figure 5.2: Measured (symbols) and modelled (lines) latent heat flux (LE) and sensible heat flux (H) from days 177 to 182 and 225 to 230 during 1998 to 2000. Negative values indicate upward fluxes.

Changes in modelled H and LE were determined by relationships among equations for energy exchange (Grant, 2001, Eqs. A1-A27) and water relations (Grant, 2001, Eqs. B1-B15). During soil drying (Fig. 5.1), declining hydraulic conductivity caused soil-root resistances to rise (Grant, 2001, Eq. B11). In combination with declining soil water potential, these rises forced declines in root and canopy water potentials (Grant, 2001, Eq. B15) and hence turgor (Grant, 2001, Eq. B1), which forced rises in canopy stomatal

resistance (Grant, 2001, Eqs. A13, A14) that reduced LE (Grant, 2001, Eq. A3) and raised H (Grant, 2001, Eq. A1).

5.3.2.2 CO_2 Fluxes

Both modelled and measured influxes and effluxes of CO_2 declined from June and August 1998 and June 1999 when θ was higher than θ_{WP} (Fig. 5.1) through August 1999 and June 2000 when θ was close to θ_{WP} to August 2000 when θ was lower than θ_{WP} (Fig. 5.3). Modeled effluxes of CO_2 were frequently larger than those measured, notably during 1998 when θ was higher.

During soil drying, the rise in canopy stomatal resistance to water vapor (Grant, 2001, Eqs. A13, A14) and hence leaf resistance to CO_2 (Grant, 2001, Eqs. C13, C14) caused a decline in CO_2 diffusion in the model (Grant, 2001, Eq. C11) and hence in GPP (Grant, 2001, Eq. C10) and NPP. Soil drying also increased the aqueous concentration of microbes, and thereby decreased rates of heterotrophic decomposition (Grant, 2001, Eqs. E1, E3), and hence microbial respiration (Grant, 2001, Eqs. E11, E13). Declines with θ in R_h were less than those in NPP, causing NEP also to decline with θ (Fig. 5.3).

Modeled and measured fluxes indicated that the grassland at Lethbridge was a net sink during June and August 1998 and June 1999 when θ was higher than θ_{WP}, neither a sink nor a source during June 2000 and August 1999 when θ was close to θ_{WP}, and a source during August 2000 when θ was lower than θ_{WP}.

5.3.3 Modeled vs. Measured Energy and CO_2 Fluxes

5.3.3.1 Energy Fluxes

Modeled and measured H were well correlated (R^2 was greater than 0.8) and unbiased (slope *b* close to one, intercept *a* close to zero) during 1998, 1999 and 2000 (Table 5.3). Modeled LE was close to measured LE (*b* was close to 1) during 1999, and smaller (*b* was less than 1) during 1998 and during 2000 when variation in both modelled and measured fluxes was limited by water stress (Fig. 5.2). Standard differences (SD) between modelled and measured H and LE were not higher than 42 W m^{-2} and 23 W m^{-2} respectively during the 3 years of the study.

Table 5.3: Regression of modeled on measured hourly energy and CO_2 fluxes in 1998, 1999 and 2000. Model outputs in the 58th, 59th and 60th year of a 110 year model run were used in the regression analysis.

Item	Year	1998	1999	2000
H	R^2	0.90	0.91	0.91
	$b \pm$ SE	1.00 ± 0.02	0.86 ± 0.01	0.98 ± 0.01
	$a \pm$ SE (W m^{-2})	-11 ± 1	3 ± 1	-2 ± 1
	SD (W m^{-2})	38	37	42
LE	R^2	0.82	0.83	0.72
	$b \pm$ SE	0.74 ± 0.01	0.98 ± 0.01	0.68 ± 0.01
	$a \pm$ SE (W m^{-2})	-11 ± 1	-11 ± 0	-11 ± 0
	SD (W.m^{-2})	23	21	22
C	R^2	0.81	0.79	0.68
	$b \pm$ SE	0.79 ± 0.02	1.00 ± 0.01	0.61 ± 0.01
	$a \pm$ SE (μmol m^{-2} s^{-1})	-0.5 ± 0.0	-0.2 ± 0.0	-0.1 ± 0.0
	SD (μmol m^{-2} s^{-1})	1.3	1.0	0.8
n		995	3207	3300

b = slope. *a* = intercept. SD = standard difference between modelled and measured values

5.3.3.2 CO_2 Fluxes

Correlation between measured and modeled CO_2 fluxes was greater than 0.6 (Table 5.3). Modeled fluxes were similar to measured fluxes in 1999 (*b* was 1) and smaller in 1998 and 2000 (*b* was smaller than 1). The negative bias in the modeled fluxes (*a* was negative) was caused by frequently larger modelled vs. measured effluxes (Fig. 5.3). SD between measured and modeled fluxes averaged 1.0 μmol m^{-2} s^{-1} during the 3 years of the study.

5.3.4 Daily Net Ecosystem Productivity

Seasonal changes in modeled vs. measured daily NEP were examined during 1998 to 2000. Modeled and measured NEP rose during late April and May to maximum values in late May and early June and then declined during July and August (Fig. 5.4). Daily NEP rose less and declined earlier with declining precipitation from 1998 to 2000. The earlier rise of NEP measured in 2000 vs. 1999 was not simulated from air temperatures measured in 2000 vs. 1999, indicating a need to improve the timing of modeled leafout. This earlier rise reduced correlations between modeled vs. measured LE and CO_2 fluxes in 2000 (Table 5.3). After early June, NEP declined with soil drying (Fig. 5.1), reaching zero when θ was lower than θ_{WP} in late August 1998, late July 1999 and late June 2000,

and remaining below zero thereafter. Measured NEP followed similar annual time courses. Rainfall events during August and September 2000 caused brief CO_2 emission events to be modelled and measured (Fig. 5.4).

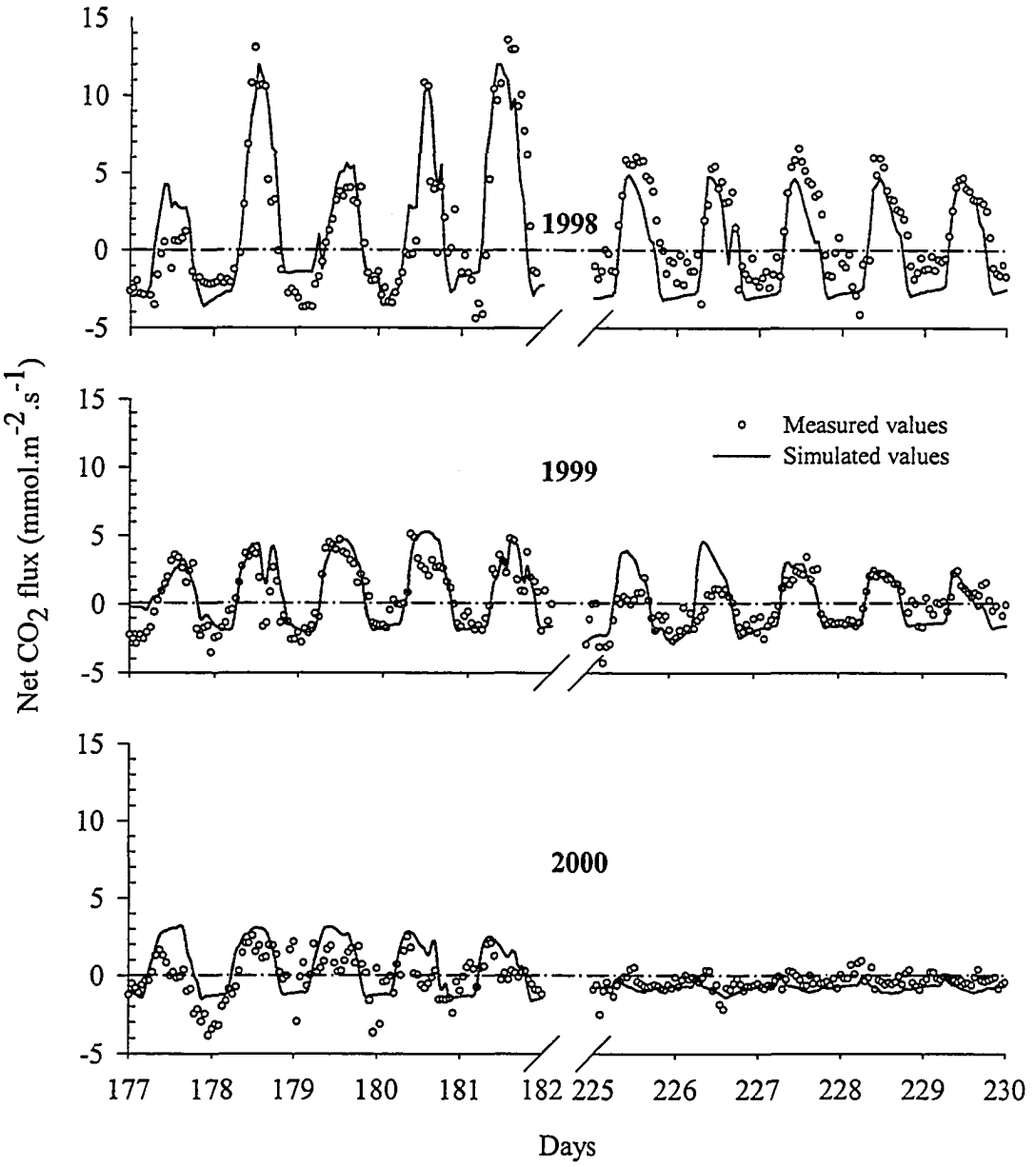

Figure 5.3: Measured (symbol) and modeled (line) net ecosystem CO_2 flux from days 177 to 182 and 225 to 230 during 1998 to 2000. Negative values indicate upward fluxes.

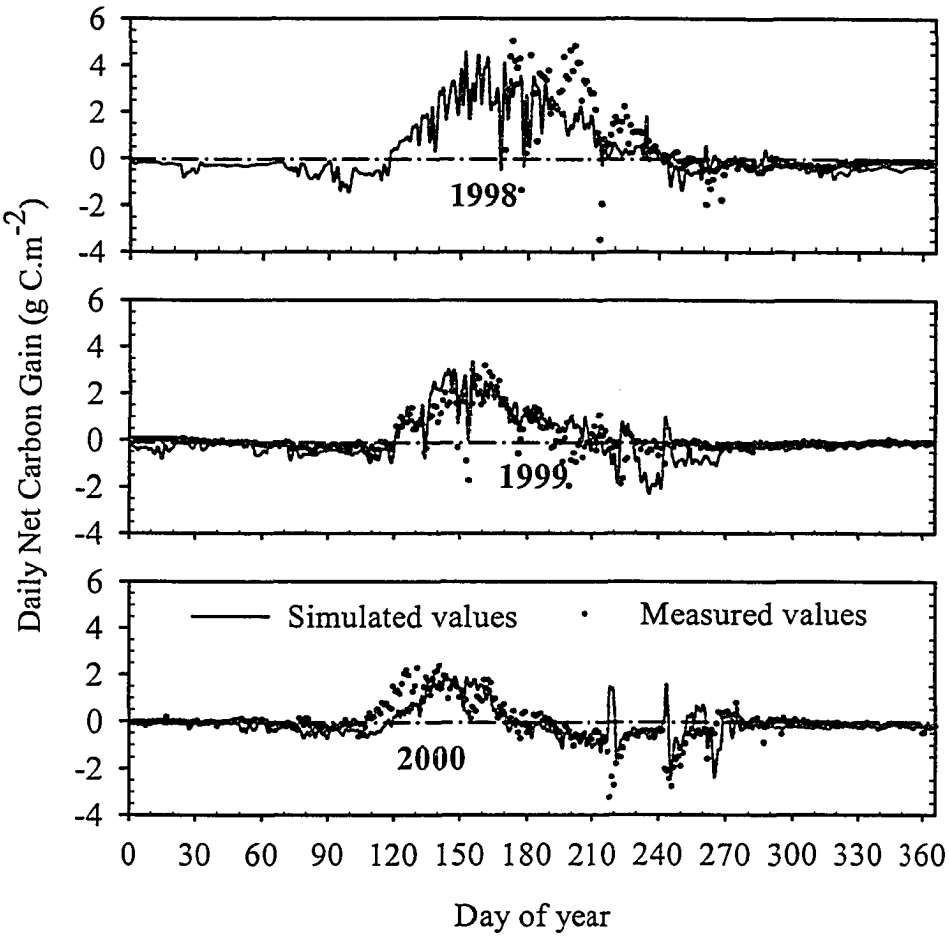

Figure 5.4: Measured (symbol) and modeled (line) daily net carbon exchange during 1998 to 2000. Negative values indicate C loss.

5.3.5 Annual Net Ecosystem Productivity

Annual GPP of the modelled grassland decreased with annual precipitation from 627 g C m^{-2} in 1998 through 384 g C m^{-2} in 1999 to 227 g C m^{-2} in 2000 (Table 5.4). The fraction of R_a modelled in the roots to total R_a rose with declining precipitation from lower than 0.5 in 1998 to higher than 0.5 in 1999 and 2000. In the model this rise was driven by greater constraints on shoot vs. root growth respiration (R_g, Grant, et al., 1999, Eq. A28) imposed by lower shoot vs. root turgor generated from lower shoot vs. root water potentials during water uptake (Grant, 2001, Eq. B15). Modeled NPP declined from 372 g C m^{-2} in 1998 through 200 g C m^{-2} in 1999 to 92 g C m^{-2} in 2000. Greater root vs. shoot R_g (Grant, et al., 1999, Eq. A28) caused modeled root NPP to increase from less than 0.7 of total NPP in 1998 to more than 0.7 in 1999 and 2000, thereby simulating

the rise in the allocation of plant C to root growth commonly found in plants growing under water stress (Derner et al., 2001). Annual R_h decreased with precipitation through decreased specific microbial decomposition caused by higher aqueous microbial concentrations (Grant, 2001, Eq. E1) (Grant and Rochette, 1994; Stott, et al., 1986). McGinn and Akinremi (2001) measured similar declines in soil respiration from fallow fields at Lethbridge in drier vs. wetter years. In the model the decrease in annual R_h was comparatively less than that in NPP, so that NEP declined from +59 g C m^{-2} (C sink) in 1998 through +5 g C m^{-2} in 1999 to -33 g C m^{-2} (C source) in 2000.

Table 5.4: The C balance of grassland calculated from gap-filled eddy covariance fluxes and modelled in 1998, 1999 and 2000. Positive values indicate C gain from atmosphere, negative values indicate C loss to atmosphere.

Items	1998		1999		2000	
Precipitation (mm)	466		363		276	
	Calculated	Modeled	Calculated	Modeled	Calculated	Modeled
	g C m^{-2} y^{-1}					
GPP (Total C Fixation)	373†	627	287	384	272	227
Autotrophic respiration		255		184		135
Shoot		141		91		66
Root		114		93		69
NPP		372		200		92
Shoot		184		78		35
Root		188		122		57
PAGB‡	95	79	53	52	41	36
Heterotrophic respiration		313		195		125
TER	264†	568	266	379	290	260
NEP	109†	59	21	5	-18	-33

† calculated GPP, TER and NEP in 1998 were from 120 days of data during June 24 to June 30 and August 4 to December 10.
‡ Peak above-ground biomass without litterfall.

Above-ground NPP (ANPP) of 184 g C m^{-2} (Table 5.4) modelled in 1998 under 466 mm of precipitation was close to the 168 g C m^{-2} found by Epstein et al. (1996) to correspond to the ANPP of North American grasslands with a mean annual temperature of 5°C and a mean annual precipitation of 400 mm to 450 mm as at Lethbridge. Modeled ANPP declined sharply with precipitation below 400 mm as found in other temperate

grasslands by Epstein et al. (1996). The modeled and measured peak above-ground biomass declined with annual precipitation from 1998 to 2000 (Table 5.3) (Fig. 5.5).

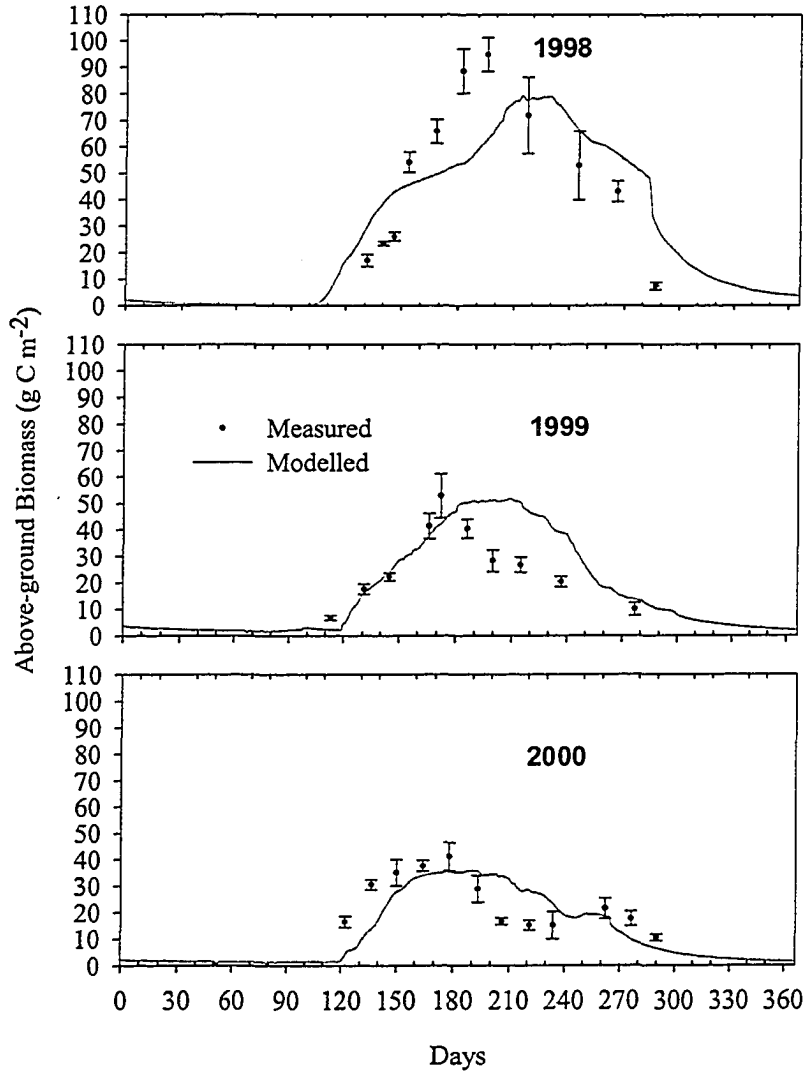

Figure 5.5: Measured (symbol) and modelled (line) above-ground C during 1998 to 2000.

Annual GPP and total ecosystem respiration (TER) were estimated from eddy covariance fluxes as described by Flanagan et al. (2002) who showed that this grassland was a net C sink in 1998 and 1999 and a source in 2000. These estimates were lower than GPP and TER modelled in 1998 and 1999, but were slightly higher than those modelled in 2000. NEP estimated from eddy covariance fluxes was larger than that modelled in 1998 (109 g C m^{-2} estimated from 20 June to 31 Dec. in 1998 vs. 59 g C m^{-2} modelled

during the entire year), but was close in 1999 (21 g C m^{-2} estimated vs. 5 g C m^{-2} modelled) and in 2000 (-18 g C m^{-2} measured vs. –33 g C m^{-2} modelled). The lower modeled vs. estimated values of annual NEP were attributed to larger TER calculated from modeled vs. measured CO_2 effluxes (Fig. 5.3).

5.3.6 Century-Scale Net Ecosystem Productivity

Changes in soil C modelled during 110 years after grassland seeding are shown in Fig. 5.6. The decline in soil C modelled during the first 10 years occurred while grass C stocks were being rebuilt after seeding, and was thus a transient disturbance effect. During the following 100 years under current climate, the semiarid ungrazed grassland at Lethbridge was modelled to gain an average of 26 g C m^{-2} y^{-1} (Fig. 5.6). In this water-limited ecosystem, modelled gains in soil C tended to be larger during wetter years as shown in Table 5.4. Greatest gains in soil C were modelled during years with average or above average precipitation that followed years with below-average precipitation. For example, soil carbon gained more than 60 g C m^{-2} y^{-1} under 1997 weather with 370 mm annual precipitation following 1996 weather with 237 mm, and less than 30 g C m^{-2} y^{-1} under 1993 weather with 506 mm annual precipitation following 1992 weather with 361 mm. Under these conditions NPP rose more rapidly with precipitation than did R_h because active litter C had been depleted by low litterfall from the previous year. Greatest losses of soil C were modelled during years with below-average precipitation that followed years with average or above-average precipitation. For example, soil C lost more than 30 g C m^{-2} y^{-1} under 2000 weather with 276 mm following 1999 weather with 363 mm (Table 5.4), and more than 30 g C m^{-2} y^{-1} under 1996 weather with 237 mm following 1995 weather with 459 mm. Under these conditions NPP declined more rapidly with precipitation than did R_h, which was partly sustained by high litterfall from the previous year. There was thus no unique relationship in the model between annual precipitation and NEP.

During 100 years under the climate change scenario described in Table 5.2, the average modelled gain in soil C rose from 26 to 28 g C m^{-2} y^{-1} so that after 100 years soil C was 159 g C m^{-2} greater than that modelled under current climate (Fig. 5.6). Modeled gains in soil C were little affected by uncertainty about changes in precipitation or

humidity predicted under climate change. Averages GPP of grassland modelled under climate change rose by 20% after 100 years (Table 5.5), because (1) elevated C_a raised CO_2 fixation (Grant, 2001, Eqs. C1, C6, C10), although this rise was partially offset by reduced leaf nitrogen concentration (Grant, 2001, Eq. C3) (Grant et al., 2001c), (2) elevated C_a reduced stomatal conductance (Grant, 2001, Eq. A14) and hence transpiration (Grant, 2001, Eq. A3) (Grant et al., 2001c), and so delayed onset of water stress (Volk et al., 2000), (3) elevated temperature increased CO_2 fixation (Grant, 2001, Eq. C3), and (4) elevated temperature increased rates of soil N mineralization (Grant, 2001, Eqs. E1, E3), biological N fixation and plant N uptake, partially offsetting the reduction in leaf nitrogen concentration modelled under elevated C_a. An increase in the ratio of shoot to root NPP modelled under the climate change scenario was caused by improved plant water status. This improvement occurred because rises in transpiration under higher air temperatures were offset by declines in transpiration under higher C_a, so that higher precipitation (Table 5.2) contributed to higher soil water content. R_h modelled after 100 years of climate change rose almost as much as did NPP, so that NEP was little changed.

Table 5.5. Average annual C transfers during last ten years following 100 years under current (1991-2000) vs. changed (Table 5.2) climates. Sd is standard deviation of annual values.

	Current climate		Climate change	
Year	Average	Sd	Average	Sd
Annual precipitation (mm)	372	84	395	89
	g C m^{-2} y^{-1}			
GPP	428	104	512	91
Autotrophic respiration	180	29	208	22
Above ground	91	20	111	11
Root	89	13	97	21
NPP	248	78	304	73
Heterotrophic respiration	222	53	278	49
NEP	26	30	26	37

In all the long-term model runs, maximum NEP was attained 30 to 80 years after seeding, after which NEP declined (Fig. 5.6), indicating that modelled soil C would eventually reach a maximum (Dugas et al., 1999).

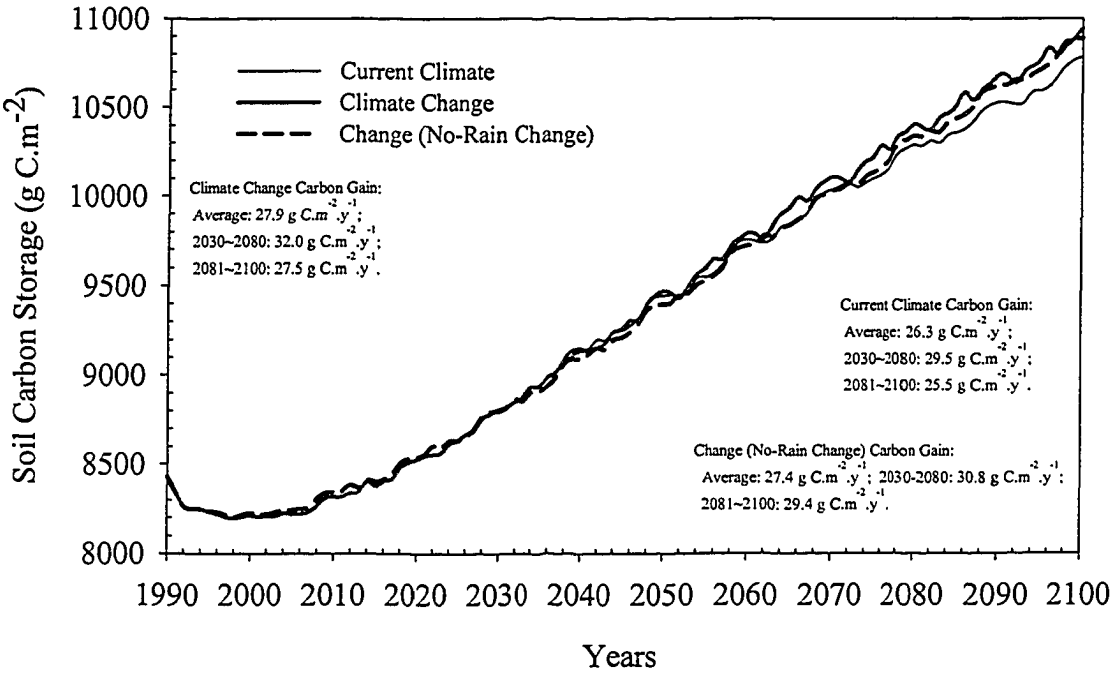

Figure 5.6: Soil carbon change under current climate and climate change scenarios. The climate change scenarios were developed from the results of the Canadian Regional Climate Model (CRCM-II V3.5) nested with CGCM2 outputs from the GHG+A transient simulation under scenario "IS92a".

5.4 Discussion

Correlation coefficients relating modelled to measured energy and CO_2 fluxes during the three years of this study were 0.7 to 0.8 (Figs. 2 and 3; Table 5.3). Because eddy covariance flux measurements were unreplicated, differences between modelled and measured fluxes must be assessed from comparisons with estimates of uncertainty in the measured fluxes. Although modelled LE was less than measured LE in 1998 and 2000 (Table 5.3), standard differences (SD) between modelled and measured values (22 W m^{-2}) were smaller than standard errors for LE measured over grassland with different eddy covariance systems when regressed on LE measured by a common standard system by Twine et al. (2000) (38 W m^{-2}). Twine et al. (2000) also reported that uncertainty in CO_2

flux measurement by eddy covariance varied between 10% and 30% over grassland. These uncertainties, if applicable to this site, are as great as the differences in modelled vs. measured hourly CO_2 fluxes (Table 5.3) and annual NEP (Table 5.4) except for NEP in 1998 when the measured value was estimated from about 120 days of eddy covariance data.

The differences between modelled and measured annual C balances may be attributed to larger TER modelled vs. measured during 1998 and 1999 (Table 5.4). These larger modelled values were apparent in the larger nighttime CO_2 effluxes frequently modelled vs. measured during the flux comparison periods (Fig. 5.3). In the model, CO_2 effluxes were closely coupled to CO_2 influxes because R_a and R_h were calculated from well-established coefficients applied to products of CO_2 fixation, either plant non-structural C, the substrate for R_a, or soil litter C, the main substrate for R_h. TER measured by eddy covariance has been found to be about 30% less than that estimated by scaling up chamber measurements under well-mixed conditions in forests (Lavigne et al., 1997), although the difference may be smaller in grassland. Modeled TER and GPP were partly affected by the timing of leafout and leaf fall (Fig. 5.4), controls on which remain unclear.

Our modelled long-term gain of 26 g C m^{-2} y^{-1} in a cool, semi-arid grassland under current climate was less than one of 33 g C m^{-2} y^{-1} for cool, temperate, and subtropical grassland following conversion from agriculture summarized from the literature by Post and Kwon (2000), greater than one of 15 g C m^{-2} y^{-1} in dry natural grassland during more than 100 years following forest in the Italian Alps measured with radiocarbon dating by Thuille et al (2000), and close to one of 28 ± 4 g C m^{-2} y^{-1} in a cool temperate dry natural grassland (Anderson, 1977).

The further gain of about 2 g C m^{-2} y^{-1} modelled in this grassland under changing vs. current climate differed from the small net loss (1 to 2×10^{15} g C from global grasslands after 50 years of climate change) simulated by the CENTURY model (Melillo et al, 1996). However, modelling and experimental results have indicated that elevated C_a and temperature can raise grassland NPP and C storage. The increases in NPP of the cool semi-arid grassland modelled here after 100 years (average 23%, Table 5.5) was within the range of 20% to 30% simulated by Coughenour and Chen (1997) for a warmer semi-

arid grassland in Colorado under higher vs. lower precipitation, a 3 °C rise in temperature and doubled C_a. Our modelled increase in NPP was slightly lower than ones in ANPP of 26% to 47% measured in open-top chambers by Morgan et al. (2001) over a semiarid grassland under doubled C_a which they attributed to more rapid CO_2 fixation and improved water status. The long-term increase in grassland NEP under climate change of about 2 g C m^{-2} y^{-1} modelled here was close to one of about 4 g C m^{-2} y^{-1} modelled by Cao and Woodward (1998) for global terrestrial ecosystems under doubled C_a, and smaller than one of about 8 g C m^{-2} y^{-1} modelled for semi-arid grasslands by Coughenour and Chen (1997) under a 20% increase in precipitation, a 3°C rise in temperature and doubled C_a.

Questions have been raised about the effects of uncertainty in poorly constrained model parameters on model results. In *ecosys*, three key parameters regulating soil-plant-atmosphere water transfer that are poorly constrained (in that experimental research into their values has given variable results) are: the stomatal resistance shape parameter (Grant, 2001, Eqs. A13, C13), root radial resistivity (Grant, 2001, Eq. B13) and root axial resistivity (Grant, 2001. Eq. B12). Monte Carlo error analysis showed that random variation in these parameters within 20% of their set values in the model caused variation of less than 2% in long-term average grassland NEP under current climate. This small variation in modelled NEP occurred because other processes in the model responded to the perturbation in the test parameter by offsetting its effect on NEP. For example, reducing the shape parameter for stomatal resistance initially lowered stomatal resistance and raised transpiration, thereby lowering both soil and canopy water potentials. Lower canopy potential forced lower canopy turger and hence higher stomatal resistance, thereby offsetting the effect of the reduced shape parameter. Similar offsetting responses to perturbation occurred with the other test parameters. The modelled increase in NEP under climate change was less than the 2 g C m^{-2} y^{-1} or 7% gain in long-term NEP under climate change, indicating that this gain was unlikely to be an artifact of uncertainty in model parameterization. However this gain is small, and indicates that no substantial change in NEP is likely to occur under the hypothesized climate scenario.

Concern has been expressed that rising temperatures predicted under most climate change scenarios (e.g. Table 5.2) will lead to soil drying during summer in northern

continental land areas (Boer et al., 1992). In the model, the assumption that ratio of C_i to C_a is conserved (but not constant) caused rising C_a to reduce transpiration even when accompanied by rising temperature. The modelled reduction in transpiration was greater under N-limited conditions as such as those in natural grasslands. In a free air CO_2 enrichment experiment under 1.5 time ambient C_a, Kimball et al. (1999) measured, and Grant et al. (2001c) modelled (with *ecosys*), reductions in wheat evapotranspiration of 19% and 16% respectively under low N fertilization, but reductions of only 7% and 9% respectively under high N fertilization. In sensitivity tests of the model at the grassland site, doubling C_a over 100 years with no change in temperature and precipitation reduced average annual evapotranspiration by 32% after 100 years, and raising air temperature by 3 °C over 100 years without raising C_a increased annual evapotranspiration by 26%. This increase in evapotranspiration modelled under higher temperature did not entirely offset the decrease in transpiration modelled under doubled C_a. The combined effects of rising C_a, temperature and precipitation during climate change in the model were such that soil water content increased slightly from that modelled under current climate. Therefore current climate change scenarios are not predicted to cause soil drying in semi-arid grassland unless they include substantial reductions in precipitation.

5.5 Conclusions

Ecosys was able to simulate energy and carbon fluxes over a temperate semi-arid grassland within the precision of eddy covariance measurements, although further research is needed to reconcile modelled vs. measured ecosystem respiration. These simulations indicated that grassland was a carbon source when near-surface soil water content was lower than wilting point, and a carbon sink when it was higher than wilting point. The eddy covariance measurements provided a well-constrained test of *ecosys* which improved confidence in model predictions that the grassland would gain 26 g C m^{-2} y^{-1} and 28 g C m^{-2} y^{-1} during next 100 years under current climate and a climate change scenario developed from CRCM-II under IS92a. Gains in soil C were predicted to increase slightly under climate change because increases in GPP from rising air temperature, precipitation and C_a offset increases in respiration from rising air temperature.

REFERENCES

Anderson, D.W., 1977. Early stage of soil formation on glacial till mine spoils in a semi-arid climate. Geoderma. 19:11–19.

Arneth, A., Kelliher, F.M., McSeveny, T.M., Byers, J.N., 1998. Net ecosystem productivity, net primary productivity and ecosystem carbon sequestration in a Pinus radiata plantation subject to soil water deficit. Tree Physiol. 18:785–793.

Aubinet, M., Grelle, A., Ibrom, A, Rannik, U., Moncrieff, J, Foken, T, Kowalski, A.S., Martin, P.H., Berbigier, P., Bernholfer, C., Clement, R., Elbers, J., Granier, A., Grunwald, T., Morgenstern, K., Pilegaard, K., Rebmann, C., Snijders, W., Valentini, R., Vesala, T., 2000. Estimates of the annual net carbon and water exchange of forests: the EUROFLUX methodology. Advances in Ecological Res. 30:114–175.

Baldocchi, D.D. and Meyers, T., 1998. On using eco-physiological, micrometeorological and biogeochemical theory to evaluate carbon dioxide, water vapor and trace gas fluxes over vegetation: a perspective. Agric. For. Meteorol. 90:1–25.

Boer, G.J., McFarlane, N.A., Lazare, M., 1992. Greenhouse gas-induced climate change simulated with the CCC second-generation general circulation model. J. Climate. 5:1045–1077.

Cao, M., Woodward, F.I., (998. Net primary and ecosystem production and carbon stocks of terrestrial ecosystems and their responses to climate change. Global. Change Biol. 4:185–198.

Coughenour, M.B. and Chen, D.X., 1997. Assessment of grassland ecosystem responses to atmospheric change using linked plant–soil process models. Ecolog. Appl. 7:802–827.

De Vries, D.A., 1963. Thermal properties of soils. In: van Wijk R. (Ed.), Physics of Plant Environment.. North Holland Publishing, Amsterdam, The Netherlands, pp. 210-235.

Derner, J.D., Polley, H.W., Johnson, H.B., Tischler, C.R., 2001. Root system response of C4 grass seedlings to CO2 and soil water. Plant and Soil. 231:97–104.

Dugas, W.A., Heuer, M.L., Mayeux, H.S., 1999. Carbon dioxide fluxes over bermudagrass, native prairie, and sorghum. Agricul. For. Meteorol. 93:121–139.

Epstein. H.E., Lauenroth, W.K., Burke, I.C., Coffin, D.P., 1996. Ecological responses of dominant grasses along two climatic gradients in the Great Plains of the United States. J. Veg. Sci. 75:777–788.

Farquhar, G.D., Caemmerer, S.-von, Berry, J.A., 1980. A biochemical model of photosynthetic CO_2 assimilation in leaves of C_3 species. Planta. 149:78–90.

Flanagan, L.B., Wever, L.A., Carlson, P.J., 2002. Seasonal and interannual variation in carbon dioxide exchange and carbon balance in a northern temperate grassland. Global. Change Biol. 8:599–615.

Grant, R.F. and Baldocchi, D.D., 1992. Energy transfer over crop canopies: simulation and experimental verification. Agricul. For. Meteorol. 61:129–149.

Grant, R.F. and Pattey, E., 2003. Modelling variability in N_2O emission from fertilized agricultural field. Soil Biol. Biochem. 35:225–243.

Grant, R.F. and Rochette, P., 1994. Soil microbial respiration at different water potentials and temperatures: theory and mathematical modeling. Soil Sci. Soc. Am. J. 58:1681–1690.

Grant, R.F., 1993a. Simulation model of soil compaction and root growth. I. Model development. Plant and Soil. 150:1–14.

Grant, R.F., 1993b. Simulation model of soil compaction and root growth. II. Model development. Plant and Soil. 150:15–24.

Grant, R.F., 1995a. Dynamics of energy, water, carbon and nitrogen in agricultural ecosystems: simulation and experimental validation. Ecological Modeling. 81:169–181.

Grant, R.F., 1995b. Mathematical modelling of nitrous oxide evolution during denitrification. Soil Biol. Biochem. 27:1117–1125.

Grant, R.F., 1997. Changes in soil organic matter under different tillage and rotation: mathematical modeling in ECOSYS. Soil Sci. Soc. Am. J. 61:1159–1175.

Grant, R.F., 1998. Simulation in ecosys of root growth response to contrasting soil water and nitrogen. Ecological Modelling. 107:237–264.

Grant, R.F., 1999. Simulation of methanotrophy in the mathematical model ecosys. Soil Biol. Biochem. 31:287–297.

Grant, R.F., 2001. A review of the Canadian Ecosystem model – ecosys. In: Shaffer, M.J., Ma L.W., Hansen, S. (Eds.), Modeling Carbon and Nitrogen Dynamics for Soil Management. CRC Press LLC, pp. 173–264.

Grant, R.F. and Robertson, J.A., 1997. Phosphorus uptake by root systems: mathematical modeling in ecosys. Plant and Soil. 188:279–297.

Grant, R.F., Izaurralde, R.C., Chanasyk, D.S., 1995b. Soil temperature under different surface managements: testing a simulation model. Agricul. For. Meteorol. 3:89–113.

Grant, R.F., Izaurralde, R.C., Nyborg, M., Malhi, S.S., Solberg, E.D, Jans-Hammermeister, D., Lal, R., Kimble, J.M., Follett, R.F., Stewart, B.A., 1998. Modeling tillage and surface residue effects on soil C storage under ambient vs. elevated CO2 and temperature in ECOSYS. In: Lal, R., Kimble, J.M., Follett, R.F., Stewart, B.A. (Eds.), Soil Processes and the Carbon Cycle. CRC Press Inc., Boca Raton, USA, pp. 527–547.

Grant, R.F., Jarvis, P.G., Massheder, J.M., Hale, S.E., Moncrieff, J.B., Rayment, M., Scott, S.L., Berry, J.A., 2001a. Controls on carbon and energy exchange by a black spruce-moss ecosystem: testing the mathematical model **Ecosys** with data from the BOREAS experiment. Global. Biogeochem. Cycles. 15:129–147.

Grant, R.F., Juma N.G., Robertson, J.A., Izaurralde, R.C., McGill, W.B., 2001b. Long-term changes in soil carbon under different fertilizer, manure, and rotation: testing the mathematical model ecosys with data from the Breton plots. Soil Sci. Soc. Am. J. 65: 205–214.

Grant, R.F., Juma, N.G., McGill, W.B., 1993b. Simulation of carbon and nitrogen transformation in soils. Microbial biomass and metabolic products. Soil Biol. Biochem. 27:1331–1338.

Grant, R.F., Kimball, B.A., Brooks, T.J, Wall, G.W., Pinter, P.J. Jr., Hunsaker, D.J., Adamsen, F.J., Lamorte, R.L., Leavitt, S.W., Thompson, T.L., Matthias, A.D., 2001c. Modeling interactions among carbon dioxide, nitrogen, and climate on energy exchange of wheat in a free air carbon dioxide experiment. Agronomy J. 93:638–649.

Grant, R.F., Kimball, B.A., Pinter, P.J.J., Wall, G.W., Garcia, R.L., La Morte, R.L., Hunsaker, D.J., 1995a. Carbon dioxide effects on crop energy balance: testing ecosys with a the Free Air CO_2 Enrichment (FACE) experiment. Agronomy J. 87:446–457.

Grant, R.F. and Nalder, I.A., 2000. Climate change effects on net carbon exchange of a boreal aspen-hazelnut forest: estimates from the ecosystem model ecosys. Glob. Change Biol. 6:183–200.

Grant, R.F., Nyborg, M., Laidlaw, J.W., 1993c. Evolution of nitrous oxide from soil. I. Model development. Soil Science. 156:259–265.

Grant, R.F., Nyborg, M., Laidlaw, J.W., 1993d. Evolution of nitrous oxide from soil. II. Experimental results and model testing. Soil Science. 156:266–277.

Grant, R.F., Peters, D.B., Larson, E.M., Huck, M.G., 1989. Simulation of canopy photosynthesis in maize and soybean. Agricul. For. Meteorol. 48:75–92.

Grant, R.F., Rochette, P., Desjardins, R.L., 1993a. Energy exchange and water use efficiency of field crops: validation of a simulation model. Agronomy J. 85:916–928.

Grant, R.F., Wall, G.W., Kimball, B.A., Frumau, K.F.A., Pinter, P.J. Jr., Hunsaker, D.J., Lamorte, R.L., 1999. Crop water relations under different CO_2 and irrigation: testing of ECOSYS with the free air CO_2 enrichment (FACE) experiment. Agricul. For. Meteorol. 95:27–51.

Hu, S., Firestone, M.K, Chapin, F.S., 1999. Soil microbial feedbacks to atmospheric CO2 enrichment. Trends in Ecology and Evolution. 14:433–437.

Kimball, B.A., LaMorte, R.L., Pinter, P.J., Wall, G.W., Hunsaker, D.J., Adamsen, F.J., Leavitt, S.W., Thompson, T.L., Matthias, A.D., Brooks, T.J., 1999. Free-air CO2 enrichment and soil nitrogen effects on energy balance and evapotranspiration of wheat. Water Resources Res. 35:1179–1190.

Lavigne, M.B., Ryan, M.G., Anderson, D.E., Baldocchi, D.D., Grill, P.M., 1997. Comparing nocturnal eddy covariance measurements to estimates of ecosystem respiration made by scaling chamber measurements at six coniferous boreal sites. J. Geophys. Res. 102(D24):28977–28985.

Massman, W.J., 2000. A simple method for estimating frequency response corrections for eddy covariance systems. Agricul. For. Meteorol. 104:185–198.

McGinn, S.M. and Akinremi, O.O., 2001. Carbon dioxide balance of a crop-fallow rotation in western Canada. Can. J. Soil Sci. 81:121–127.

Melillo, J.M., Hall, D.O., Agren, G.I., 1996. Executive Summary. In: Breymeyer, A.I., Hall, D.O., Melillo, J.M., Agren G.I. (Eds.), Global Change: Effects on Coniferous Forests and Grasslands. John Willey & Sons Ltd, England, pp. 9–11.

Moncrieff, J.B., Jarvis, P.G., Valentini, R., 2000. Canopy Fluxes. In: Sala, O.E., Jackson, R.B., Mooney, H.A., Howarth, R.W. (Eds.), Methods in Ecosystem Science. Springer Verlag, New York, pp. 161–180.

Moncrieff, J.B., Massheder, J.M., Bruin, H. de, Elbersm J., Friborg, T., Heusinkveld, B., Kabat, P., Scott, S., Soegaard, H., Verhoef, A., De Bruin, H., 1997. A system to measure surface fluxes of momentum, sensible heat, water vapour and carbon dioxide. J. Hydrol. 188–189:589–611.

Morgan, J.A., LeCain, D.R., Mosier, A.R., Milchunas, D.G., 2001. Elevated CO_2 enhances water relations and productivity and affects gas exchange in C3 and C4 grasses of the Colorado shortgrass steppe. Global. Change Biol. 7:451–466.

Nikiforuk, W. L., Abramenko, J., Archibald, H., Boon, S., Brierley, T., 1998. Agricultural Region of Alberta Soil Inventory Database. SLRI Consultants Limited. (Wensie: http://www.agric.gov.ab.ca/agdex/000/agrasid.html).

Post, W.M. and Kwon, K.C., 2000. Soil carbon sequestration and land-use change: processes and potential. Global. Change Biol. 6:317–327.

Running, S.W., Baldocchi, D.D., Turner, D.P., Gower, S.T., Bakwin, P.S., Hibbard, K.A., 1999. A global terrestrial monitoring network integrating tower fluxes, flask sampling, ecosystem modeling and EOS satellite data. Remote Sensing of Environ. 70:108–127.

Saigusa, N., Oikawa, T., Liu, S., 1998. Seasonal variations of the exchange of CO_2 and H_2O between grassland and the atmosphere: an experimental study. Agricul. For. Meteorol. 89:131–139.

Saxton K. E., W.J. Rawls, J.S. Romberger, R. I. Papendick, 1986. Estimating generalized soil-water characteristics from texture. Soil Sci. Soc. Am. J. 50:1031–1036.

Schulten, H.R., Schnitzer, M., 1997. Chemical model structures for soil organic matter and soils. Soil Sciences. 162:115–130.

Stott, D.E., Elliott, L.F., Papendick, R.I., Campbell, G.S., 1986. Low temperature or low water potential effects on the microbial decomposition of wheat residue. Soil Biol. Biochem. 18:577–582

Thornley, J.H.M., Cannell, M.G.R., 1997. Temperate grassland responses to climate change, an analysis using the Hurley Pasture Model. Annual of Botany. 80:205–221.

Thuille, A., Buchmann, N., Schulze, E.D., 2000. Carbon stocks and soil respiration rates during deforestation, grassland use and subsequent Norway spruce afforestation in the Southern Alps, Italy. Tree Physiol. 20:849–857.

Twine, T.E., Kustas, W.P., Norman, J.M., Cook, D.R., Houser, P.R., Meyers, T.P., Prueger, J.H., Starks, P.J., Wesely, M.L., 2000. Correcting eddy-covariance flux underestimates over a grassland. Agricul. For. Meteorol. 103:279–300.

Valentini, R., Matteucci, G., Dolman, A.J., Schulze E.D., Robmann, C., 2000. Respiration as the main determinant of carbon balance in European forests. Nature. 404:861-865.

Volk, M., Niklaus, P.A., Korner, C., 2000. Soil moisture effects determine CO2 responses of grassland pecies. Oecologia .125:380–388.

Chapter 6: Overview, Discussion and General Conclusions

Large temporal and spatial variations in N_2O emissions, which result from site specific conditions, are key impediments to estimating regional emissions of N_2O emissions in national greenhouse gas (GHG) inventories. This study is intended to develop a scientifically defensible methodology to account for these variations under diverse agricultural practices. This methodology will contribute to needs of IPCC Tier 2 methodology for assessing GHG emissions. IPCC Tier 2 will eventually replace IPCC Tier 1 methodology (IPCC guidelines, 1997) to improve estimates of national GHG emissions. By using a constant ratio between N input and N_2O emissions, IPCC Tier 1 does not account for following factors which are known to affect the N_2O emissions.

(1) Changes of air temperature and precipitation result in the temporal variation of soil temperature and soil water content, which strongly affect N_2O emissions (Flessa et al. 2002). N_2O emissions increase greatly when the climate changes from dry to wet or from cold to warm (Kaiser and Ruser, 2000; Röver et al., 1998).

(2) Heterogeneity in soil texture and nutrient content causes differences in soil hydraulic properties and in available substrate for carbon oxidation, mineralization, nitrification and denitrification, causing differences in N_2O emissions (Bouwman and Boumans, 2002; Skiba et al., 1997; Remde et al., 1993; Davidson, 1991).

(3) Topography affects the redistribution of soil water and solutes, and translocation of sediment in a given landscape (Morgan et al., 1998a and 1998b), strongly affecting N_2O emissions (Choudhary et al, 2002; Corre et al., 1996).

(4) Agricultural practices such as tillage, fertilizer application and cropping system also strongly change N_2O emissions (Choudhary et al., 2002; Ball et al., 1999; Lemke et al., 1999; Mogge et al., 1999; Kaiser et al., 1998; Jacinthe and Dick, 1997; Eichner, 1990).

The complex interactions of above factors cause the large temporal and spatial variations in N_2O emissions which are the sources of uncertainty in the estimate of N_2O emission using IPCC Tier 1 methodology. Because this uncertainty is larger than 62% in

agricultural soils (Brown et al., 2002; Lim et al., 1999), the effects of the above factors on N_2O emissions must be involved in the IPCC Tier 2 methodology.

Currently, chamber measurement methods can address spatial variation of N_2O emissions while micrometeorological methods can only detect the temporal variation at fine scale. No measurement method can address both temporal and spatial variation simultaneously (Chapter 1). Modeling is the potential method to address all factors and their interactions that affect N_2O emissions (Grant and Pattey, 2003). However, the model must have the ability to simulate biological, physical and chemical processes of N_2O emission, to calculate water, solute and gas exchanges in three dimensions, and to represent the effects of climate and agricultural practices on N_2O emissions at fine scale. *Ecosys* is the only terrestrial ecosystem model which can match these requirements (Li et al., 2004; Grant 2001, 1999, 1997, 1995a, 1995b; Grant and Nalder, 2000; Grant and Pattey, 2003, 1999; Grant et al., 2001a, 2001b, 2001, 1999a, 1999b, 1998, 1993a, 1993b, 1993c), but it does not have the ability to manage large amount of inputs and outputs for complex landscapes. Therefore, *ecosys* was integrated into a geographic information system (GIS) framework to be a new version of *ecosys* for landscape scale modeling which was entitled *3D-Ecosys-GIS* in this study.

With the *3D-Ecosys-GIS*, site-specific N_2O emissions and their temporal and spatial variations were evaluated at a full landscape (or mini-watershed) scale. In *3D-Ecosys-GIS*, the cycling of carbon and nitrogen, and the three-dimensional transport of water, solute and gas (Eqs. A3.1 to A3.14) were computed at a time-step of seconds to hours and at a spatial scale of meters. The sensitivities of cycling and transport to soil water and temperature were also considered (Eqs. A3.9 to A3.27). These greatly detailed calculations allowed the effects of diverse soils, crops, climates, agricultural practices and topography to be reflected in landscape-scale estimates of N_2O emissions. The inadequacies of IPCC Tier 1 methodology discussed earlier have been addressed as following in this study:

(1) Modeled results of 3D-Ecosys-GIS clearly showed the effects of precipitation and air temperature on N_2O emissions. Annual N_2O emission decreased by 67% as precipitation declined by 51% from wet through normal to dry years (Tables 4.2, 4.4 and 4.5). The field chamber measurements (4 times per week) conducted by

Hellebrand et al. (2003) showed that annual N_2O emissions decreased by 29% as annual precipitation declined by 30% in a fertilized biofuel field at Postdam in Germany.

The changed dynamics of soil water and temperature resulting from the changes of precipitation and air temperature were the main causes of large temporal variations in hourly and seasonal N_2O emissions (Figs. 3.3 to 3.6). These temporal variations of N_2O emissions in the hummocky agricultural landscape (73% – 99%, Table 3.3) were consistent with field measurements elsewhere (36% – 131% in Sehy et al., 2003; Flessa et al., 2002 and Chao et al., 2000). As a result, emission factors for a given N input varied with changes of climate (Table 4.4) as also found by Hellebrand et al. (2003). Therefore, estimates of annual emissions using IPCC Tier 1 with a fixed emission factor (0.0125 kg N kg^{-1} N input, Olsen et al., 2003) are not likely to be accurate if the effects of air temperature and precipitation are not accounted for. Estimates of emissions linearly interpolated from infrequent chamber measurements are also not likely to be accurate because these measurements cannot represent the temporal variation of N_2O emissions, so that (Flessa et al., 2002).

Other modeled results in this study showed the strong effects of climate on CO_2 exchange after a well-constrained validation by highly frequent eddy covariance measurement data. The natural grassland at Lethbridge was modeled and measured to be carbon sink under higher precipitation and a carbon source under lower precipitation (Figs. 5.3 and 5.4, Tables 5.4 and 5.5).

(2) Landscape Soil Property Predictor (LSPP), a sub-model of *3D-Ecosys-GIS*, represented spatial heterogeneity in key soil properties related to N_2O emissions over the hummocky agricultural landscape (Fig. 2.8). Modeled results of *3D-Ecosys-GIS* successfully addressed the effects of soil heterogeneity on N_2O emissions. As soil texture changed from coarse to fine, and total organic carbon and nitrogen contents increased from upper to lower slopes (Fig. 2.8), annual N_2O emissions increased (Fig. 3.11; Appendix 4.2) which was consistent with results summarized from a large number of field measurements (Table 5 in Bouwman and Boumans, 2002). Therefore, estimates of N_2O emissions must involve the

effect of soil properties on N_2O emissions, although this is not done in IPCC Tier 1.

(3) Modeled results also demonstrated the strong effects of topography on the spatial variation of N_2O emissions (Table 3.5, Figs. 3.10 and 3.11). The N_2O emissions increased from upper to lower slopes under dry conditions, but decreased under wet conditions. Such large spatial variation (88% to 341% in Table 3.5) has been measured in comparable studies elsewhere (Choudhary et al., 2002; Corre et al., 1996), but the complexity in spatial variation could not be measured by current methods (i.e. chamber and micrometeorological methods).

Modeled results showed that the positions of "hot spots" (localized sites with very high N_2O emission) and "cold spots" (localized sites with very low N_2O emission) could alternate while relative soil water-filled porosity changed around 0.6–0.7 in the hummocky agricultural landscape (Figs. 3.8 to 3.11; Sehy et al. 2003). The detailed identification of "hot spots" and "cold spots" are useful for more accurate estimates of N_2O emissions, but current field measurements and IPCC Tier 1 cannot identify those spots at landscape scale, and may not account for the contribution of rapid emission from "hot spots" to total emission over a landscape. Moreover, the spatial complexity of N_2O emissions must be considered when evaluating the effects of agricultural practices on N_2O emissions at a full landscape scale.

(4) With *3D-Ecosys-GIS*, the effects of agricultural practices on N_2O emission were evaluated at a full landscape scale. Modeled results showed the effects of agricultural practices on N_2O emissions. N_2O emission was 38% lower under zero-tillage than under conventional tillage (Table 4.2). Lower N_2O emission under zero-tillage was measured by Lemke et al. (1999) on a similar soil to that of this study, and also in some other field studies (Kaharabata et al., 2003; Choudhary et al., 2002; Yamulki and Jarvis, 2002; Jacinthe and Dick, 1997), but Baggs et al. (2003), Röver et al. (1999) and Williams et al. (1999) measured higher N_2O emissions in zero-tillage fields. Manure fertilizer lowered N_2O emission in the model by 40% in comparison with chemical fertilizer under the same N input (Table 4.4). Such a reduction was apparent in the field

measurements of Hiroko and Haruo (2003) and Lemke et al. (1999), but was contradicted by field measurements of Kaiser and Ruser (2000) and Mogge et al. (1999). Conversion from cropland to grassland in the model also lowered N_2O emission (Table 4.5) as has been measured elsewhere (Choudhary et al, 2002). Fallow decreased N_2O loss by 48% to 75% (Table 4.5). Lower N_2O emission was measured by Lemke et al. (1999) in fallow field on a similar soil to that of this study, but Mosier et al. (1997) measured higher N_2O emission. In contrast, increasing chemical fertilizer rate and conversion from grassland to cropland increased N_2O loss from the hummocky agricultural landscape (Tables 4.4 and 4.5). These results were consistent with field measurements (Bouwman and Boumans, 2002; Mosier et al., 1997). The conflicting conclusions about the effects of agricultural practices on N_2O emissions might result from large spatial variation of emissions. These conflicts must be reconciled before definitive statements can be made about how agricultural practices affect N_2O emission.

Above advances addressed in this study will contribute to the needs of IPCC Tier 2. As the large temporal and spatial variation under various agricultural practices become fully accounted for, the total N_2O emission aggregated from modeled outputs of meter scale grid cells at hourly time intervals may replace those calculated from a fixed annual emission factor (0.0125 kg N kg^{-1} N input, Olsen et al., 2003) or linearly interpolated from a few localized measurements.

However, the conflicting conclusions from modeled results and some field measurements weakened the reliability of modeled results. Furthermore, the degree to which modeled results were corroborated by field measurements was limited by measurement methodology. There was some difficulty in the validation of model outputs for N_2O emissions with low frequency field chamber measurements in this study. This difficulty highlighted the need for more and better datasets, particularly with more frequent field measurements of N_2O, likely using automated chambers. This study also identified a requirement for more measurements during large emission events, main emission periods and at particular landscape locations. In contrast, the highly frequent eddy covariance measurements provided well-constrained model validation which increased the reliability of modeled results in the study of CO_2 exchange in a semi-arid

natural grassland at Lethbridge. Such measurements of N_2O emissions could make an important contribution to testing modeled N_2O estimates in future studies.

References

Baggs, E.M., Stevenson, M., Pihlatie, M., Regar, A., Cook, H., Cadisch, G., 2003. Nitrous oxide emissions following application of residues and fertilizer under zer and conventional tillage. Plant Soil. 254:361–370.

Ball, B.C., Scott, A., Parker, J.P., 1999. Field N_2O, CO_2 and CH_4 fluxes in relation to tillage compaction and soil quality in Scotland. Soil & Tillage Research. 53(1):29–39.

Bouwman, A.F. and Boumans, L.J.M., 2002. Emissions of N_2O and NO from fertilized fields: Summary of available measurement data. Global Biogeochimical Cycles. 16(4):1058.

Brown, L., Syed,B., Jarvis, S. C., Sneath, R. W., Phillips, V. R., Goulding, K. W. T., Li., C., 2002. Development and application of a mechanistic model to estimate emission of nitrous oxide from UK agriculture. Atmospheric Environmen. 36(6):917–928.

Chao, C.C., Young, C.C., Wang, Y.P., Chao, W.L., 2000. Daily and seasonal nitrous oxide fluxes in soils from hardwood forest and different agroecosystems of Taiwan. Chemosphere: Global Change Science. 2:77–84.

Choudhary, M.A., Akramkhanov, A., Saggar, S., 2002. Nitrous oxide emission from a New Zealand cropped soil: tillage effects, spatial and seasonal variability. Agriculture, Ecosystems and Environment. 93:33–43.

Corre, M.D.; Van Kessel, C.; Pennock, D.J., 1996. Landscape and seasonal patterns of nitrous oxide emissions in a semiarid region. Soil Sci. Soc. Am. J. 60:1806–1815.

Davidson, E.A., 1991. Fluxes of nitrous oxide and nitric oxide from terrestrial ecosystems. In: Rogers, J.E. and Whitman, W.B. (Eds.). Microbial Production and Consumption of greenhouse Gases: Methane, Nitrogen Oxides, and Halomethane. American Society for Microbiology, Washington, pp. 219–235.

Eichner, M.J.M, 1990. Nitrous oxide emissions from fertilized soils: Summary of available data. Journal of Environmental Quality. 19:272–280.

Flessa, H., Ruser, R., Schilling, R., Loftfield, N., Munch, J.C., Kaiser, E.A., Beese, F., 2002. N_2O and CH_4 fluxes in potato fields: automated measurement, management effects and temporal variation. Geoderma. 105(3-4):307–325.

Grant, R. F. and Pattey, E., 2003. Modelling variability in N_2O emissions from fertilized agricultural fields. Soil Biology and Biochemistry. 35(2):225–243.

Grant, R.F., 2001. A review of the Canadian ecosystem model ecosys. In: Shaffer, M., (Ed.), Modeling Carbon and Nitrogen Dynamics for Soil Management. CRC Press, Boca Raton, 175–264.

Grant, R.F., Jarvis, P.G., Massheder, J.M., Hale, S.E., Moncrieff, J.B., Rayment, M., Scott, S.L., Berry, J.A., 2001a. Controls on carbon and energy exchange by a black spruce-moss ecosystem: testing the mathematical model Ecosys with data from the BOREAS experiment. Glob. Biogeochem. cycles. 15(1):129–147.

Grant, R.F., Juma N.G., Robertson, J.A., Izaurralde, R.C., McGill, W.B., 2001b. Long-term changes in soil carbon under different fertilizer, manure, and rotation: testing the mathematical model ecosys with data from the Breton plots. Soil Sci. Soc. Am. j. 65(1):205–214.

Grant, R.F., Kimball, B.A., Brooks, T.J, Wall, G.W., Pinter Jr, P.J., Hunsaker, D.J., Adamsen, F.J., Lamorte, R.L., Leavitt, S.W., Thompson, T.L., Matthias, A.D., 2001c. Modeling Interactions among carbon dioxide, nitrogen, and climate on energy exchange of wheat in a free air carbon dioxide experiment. Agronomy Journal. 93: 638–649.

Grant, R.F. and Nalder, I.A., 2000. Climate change effects on net carbon exchange of a boreal aspen-hazelnut forest: estimates from the ecosystem model ecosys. Global Change Biology. 6(2):183–200.

Grant, R.F., 1999. Simulation of methanotrophy in the mathematical model ecosys. Soil Biol. Biochem. 31:287–297.

Grant, R.F. and Pattey, E., 1999. Mathematical modelling of nitrous oxide emissions from an agricultural field during spring thaw. Global Biogeochemical Cycles. 13:679–694.

Grant, R.F., Black, T.A., Hartog, G. den, Berry, J.A., Neumann, H.H., Blanken, P.D., Yang, P.C., Russell, C., Nalder, I.A., den Hartog, G., 1999a. Diurnal and annual

exchanges of mass and energy between an aspen-hazelnut forest and the atmosphere: testing the mathematical model ECOSYS with data from the BOREAS experiment. Journal of Geophysical Research. 104(D22):27699–27717.

Grant, R.F., Wall, G.W., Kimball, B.A., Frumau, K.F.A., Pinter, P.J.Jr, Hunsaker, D.J., Lamorte, R.L., 1999b. Crop water relations under different CO_2 and irrigation: testing of ECOSYS with the free air CO_2 enrichment (FACE) experiment. Agricultural and Forest Meteorology. 95:27–51.

Grant, R.F., Izaurralde, R.C., Nyborg, M., Malhi, S.S., Solberg, E.D, Jans-Hammermeister, D., Stewart, B.A., 1998. Modeling tillage and surface residue effects on soil C storage under ambient vs. elevated CO2 and temperature in ECOSYS. In: Soil processes and the carbon cycle. (Ed. Lal, R., Kimble, J.M., Follett, R.F.). CRC Press Inc.; Boca Raton; USA. 527-547.

Grant, R.F., 1997. Changes in soil organic matter under different tillage and rotation: mathematical modeling in ECOSYS. Soil Science Society of America Journal. 61(4): 1159–1175.

Grant, R.F., 1995a. Dynamics of energy, water, carbon and nitrogen in agricultural ecosystems: simulation and experimental validation. Ecological Modeling. 81(1-3): 169–181.

Grant, R.F., 1995b. Mathematical modelling of nitrous oxide evolution during nitrification. Soil Biol. Biochem. 27:1117–1125.

Grant, R.F., Nyborg, M., Laidlaw, J., 1993a. Evolution of nitrous oxide from soil: I. Model development. Soil Sci. 156:259–265.

Grant, R.F., Nyborg, M., Laidlaw, J., 1993b. Evolution of nitrous oxide from soil: II. Experimental results and model testing. Soil Sci. 156:266–277.

Grant, R.F., Juma, N.G., McGill, W.B., 1993c. Simulation of carbon and nitrogen transformations in soils. I: mineralization. Soil Biology & Biochemistry. 25:1317–1329.

Hellebrand, H.J., Kern, J. Scholz V., 2003. Long-term studies on greenhouse gas fluxes during cultivation of energy crops on sandy soils. Atmospheric Environment. 37(12): 1635-1644.

Hiroko, A. and Haruo, T., 2003. Effect of organic matter application on N_2O, NO, and NO_2 fluxes from an Andisol field. Global Biogeochem. Cycles. 17(4):1100–1116.

Intergovernmental Panel on Climate Change (IPCC), Organization for Economic Cooperation and Development (OECD) and International Energy Agency (IEA), Revised 1996 IPCC Guidelines for National Greenhouse Gas Inventories, Organ. for Econ. Coop. Dev., Paris, 1997.

Jacinthe, P.A. and Dick, W.A., 1997. Soil management and nitrous oxide emissions from cultivated fields in southern Ohio. Soil and Tillage Research. 41(3-4):221–235.

Kaharabata, S.K., Drury, C.F., Priesack, E., Desjardins, R.L., McKenney, D.J., Tan, C.S., Reynolds, D., 2003. Comparing measured and expert-N predicted N_2O emissions from conventional till and no till corn treatments. Nutrient Cycle of Agroecosystem. 66:107–118.

Kaiser, E.A. and Ruser, R., 2000. Nitrous oxide emissions from arable soils in Germany: An evaluation of six long-term field experiments. J. Plant Nutr. Soil Sci. 163:249–259.

Kaiser, E.A., Kohrs, K., Küchke, E., Schnug, E., Heinemeyer, O., Munch, J.C., 1998. Nitrous oxide release from arable soil: importance of N fertilization, crops and temporal variation. Soil Biol. Biochem. 30(12):1553–1563.

Lemke, R.L., Izaurralde, R.C., Nyborg, M., Solberg, E.D., 1999. Tillage and N source influnce soil-emitted nitrous oxide in the Alberta Parkland region. Canadian Journal of Soil Science. 79(1):15–24.

Li, T., Grant, R.F., Flanagan, L.B., 2004. Climate impact on net ecosystem productivity of a semi-arid natural grassland: modeling and measurement. Agricultural and Forest Meteorology. 126:99–116.

Lim, B., Bioleau, P., Bonduki, Y., van Amstel, A.R., Janssen, L.H.J.M., Olivier, J.G.J., Kroeze, C., 1999. Improving the quality of national greenhouse gas inventories. Environmental Sciences and Policy. 2:335–346.

Mogge, B., Kaiser, E.A., Munch, J.C., 1999. Nitrous oxide emissions and denitrification N-losses from agricultural soils in the Bornhoved Lake region: influence of organic fertilizers and land-use. Soil Boilogy and Biochemistry. 31:1245–1252.

Morgan, R.P.C., Quinton, J.N., Smith, R.E., Govers, G., Poesen, J.W.A., Auerswald, K., Chisci, G., Torri, D. and Styczen, M.E. 1998a. The European Soil Erosion Model

(EUROSEM): a dynamic approach for predicting sediment transport from fields and small catchments. Earth Surface Processes and Landforms. 23:527–544.

Morgan, R.P.C., Quinton, J.N., Smith, R.E., Govers, G., Poesen, J.W.A., Auerswald, K., Chisci, G., Torri, D., Styczen, M.E. and Folly, A.J.V. 1998b. The European Soil Erosion Model (EUROSEM): documentation and user guide v. 3.6. Silsoe College, Cranfield University, Silsoe, Bedford, U.K.

Mosier, A.R, Parton, W.J., Valentine, D.W., Ojima, D.S., Schimel, D.S., Heinemeyer, O., 1997. CH4 and N2O fluxes in the Colorado shortgrass steppe. 2. Long-term impact of land use change. Global Biogeochemical Cycles. 11:29–42.

Olsen, K., Wellisch, M., Bioleau, P., Blain, D., et al., 2003. Canada's greenhouse gas inventory (1990 – 2001). ISBN 0-662-35106-1, Environment Canada.

Remde, A., Ludwig, J., Meixner, F., Conrad, R., 1993. A study to explain the emission of nitric oxide from a marsh soil. J. Atmos. Chem. 17:249–275.

Röver, M., Heinemeyer, O., Munch, J.C., Kaiser, E.A., 1999. Spatial heterogeneity within the plough layer: high variability of N_2O emission rates. Soil Biology and Biochemistry. 31(2):167–173.

Röver, M., Heinemeyer, O., Kaiser, E.A., 1998. Microbial induced nitrous oxide emissions from an arable soil during winter. Soil Biol. Biochem. 30:1859–1865.

Sehy, U., Ruser, R., Munch, C., 2003. Nitrous oxide fluxes from maize fields: relationship to yield, site-specific fertilization, and soil conditions. Agriculture, Ecosystems & Environment. 99(1-3):97–111.

Skiba, U., Fowler, D., Smith, K.A., 1997. Nitric oxide missions from agricultural soils in temperate and tropical climates: sources, controls and mitigation options. Nutr. Cycling Agroecosyst. 48:139–153.

Williams, D.Li., Ineson, P., Coward, P.A., 1999. Temporal variations in nitrous oxide fluxes from urine-affected grassland. Soil Biology and Biochemistry. 31(5):1999, 779 – 788.

Yamulki, S. and Jarvis, S.C., 2002. Short-term effects of tillage and compaction on nitrous oxide, nitric oxide, nitrogen dioxide, methane and carbon dioxide fluxes from grassland. Biol. Fertil. Soils. 36:224–231.